Surface Crack Growth in Metallic Pipes Reinforced with Composite Repair System

Li, Z.

DOI
10.4233/uuid:efb18518-074f-4159-880b-0eb6cbc88ff3

Publication date
2021

Document Version
Final published version

Citation (APA)
Li, Z. (2021). *Surface Crack Growth in Metallic Pipes Reinforced with Composite Repair System* (T2021/8 ed.). [Dissertation (TU Delft), Delft University of Technology]. TRAIL Research School. https://doi.org/10.4233/uuid:efb18518-074f-4159-880b-0eb6cbc88ff3

Surface Crack Growth in Metallic Pipes Reinforced with Composite Repair System

Zongchen LI

Delft University of Technology

Surface Crack Growth in Metallic Pipes Reinforced with Composite Repair System

Proefschrift

ter verkrijging van de graad van doctor
aan de Technische Universiteit Delft,
op gezag van de Rector Magnificus Prof.dr.ir. T.H.J.J. van der Hagen,
voorzitter van het College voor Promoties,
in het openbaar te verdedigen op woensdag 20 Januari 2021 om 10:00 uur

door

Zongchen LI
Master of Science in Mechanical Engineering,
Wuhan University of Technology, China,
geboren te Rizhao, Shandong, China.

Dit proefschrift is goedgekeurd door de:
Prof. ir. J.J. Hopman
Dr. ir. X. Jiang

Samenstelling van de promotiecommissie:

Rector Magnificus	chairperson
Prof. ir. J.J. Hopman	Technische Universiteit Delft, promotor
Dr. ir. X. Jiang	Technische Universiteit Delft, copromotor

Onafhankelijke leden:

Prof. dr. C.G. Soares	Técnico Lisboa, Portugal
Prof. dr. M. Veljkovic	CiTG, Technische Universiteit Delft
Prof. dr. C. Bisagni	LR, Technische Universiteit Delft
Prof. dr. L. Zhu	Wuhan University of Technology, China
Dr. C.L. Walters	3ME, Technische Universiteit Delft

This research was funded by Delft University of Technology (TU Delft) and China Scholarship Council (CSC) under grant: 201606950024. The experimental studies were funded by the '111 Project' of State Administration of Foreign Experts Affairs under grant: 444110356 and the Department of Maritime and Transport Technology, TU Delft.

TRAIL Thesis Series no. T2021/8, the Netherlands Research School TRAIL

TRAIL
P.O. Box 5017
2600 GA Delft
The Netherlands
E-mail: info@rsTRAIL.nl

ISBN: 978-90-5584-283-4

Printed in the Netherlands.

Dedicated to

My wife Bing and my parents

Preface

When my life was jammed with issues and plans, I gradually developed a habit of going straightforward and seldom looking back. While at this moment, this cosy early-winter afternoon is dragging me back into my memories. Four years is long enough to add meaningful and colourful pigment into the painting of my life. I see houses and sailboats reflecting in canals, I see cows and sheep lying in pastures, I see rabbits and pheasants shuttling in the mountain bike trails. But the most notable drawing, belongs to the amazing, delightful, brilliant, and different people that I have met. At present, I feel so pleased to express my appreciations.

To begin with, my great appreciation goes to my promoter, Prof. Hans Hopman. Although having a huge amount of responsibilities, Hans was always approachable, kind, and generous. His rich knowledge and experience offered clear guidance throughout my Ph.D. journey. His encouragement and support played a key role, in terms of gaining confidence and seeking potential opportunities of my research. For instance, he offered the opportunities to visit potential collaborative partners, in particular for my experimental study. He also encouraged me to present my progress in a variety of international conferences and seminars, for exchanging the latest development and building networks.

Then, I would like to express my sincere gratitude to my co-promoter/daily supervisor, Dr. Xiaoli Jiang. Dear Xiaoli, thank you for your support throughout my Ph.D. research. You were always deeply concerning my research details, shaping my research approaches. Your timely feedback, detailed comments, and valuable discussions are crucial for my academic achievements. Your rigorous academic quality and experienced insights pushed me to jump

out of my comfort zone and continuously breaking my limits. Your trust and support motived me to rise from the valley bottom to the peak. Particular, I would like to thank you for your support on my experimental investigations. You have played the key role of bringing my experimental research to the right track and fulfilling my experimental plans to reality. In addition, thank you very much for encouraging me to share my research in international conferences and seminars, and introducing me to senior researchers and peers.

I would like to express my gratitude to my master daily supervisor, Prof. LIU Zhiping, who introduced me to the academic world. Dear Zhiping, I appreciate your concern and support during my postgraduate study, and you had set a good example in academia. Thank you very much for supporting me to apply for the Ph.D. position and the related scholarship. Also appreciation to the concern and support on my Ph.D. research and our fruitful collaborations.

Great appreciation to my committee members. Dear Prof. Carlos Guedes Soares, Prof. Milan Veljkovic, Prof. Chiara Bisagni, Prof. ZHU Ling, and Dr. Carey Walters, thank you very much for the time and efforts that you devoted to reviewing and commenting on my draft thesis. I am looking forward to our discussions during the defence ceremony. In addition, I would like to thank Dr. Sape Miedema as a committee member for my Go/No go meeting.

Sincere appreciation to the China Scholarship Council for supporting my living expense during the oversea study, which also offered me an opportunity of exploring the western world, as well as additional potential possibilities. Also appreciation to Prof. Gabriël Lodewijks for inviting me to conduct my Ph.D. research in the department of Maritime and Transport Technology (MTT). Great thanks to Overseas Expertise Introduction Project for Discipline Innovation–111 project of Chinese Ministry of Education and State Administration of Foreign Experts Affair of P. R. China for supporting my experimental investigations. Also great thanks to the department of Maritime and Transport Technology of Delft University of Technology (TU Delft) for supporting my travelling and living expense during the experimental investigation in Wuhan, China. Appreciation to the School of Transportation, Wuhan University of Technology (WUT) for offering the facilities and technical supports during the experimental investigation.

I would like to express my appreciation to the vice president of WUT, Prof. LIU Zuyuan, for offering the opportunity of conducting the experimental research under the 111 grant. Great appreciation to the dean of School of Transportation of WUT, Prof. ZHU Ling, for offering the facilities and support for conducting the research in the Key Laboratory of High Performance Ship Structure of the Chinese Ministry of Education. In addition, I would like to thank vice deans of School of Logistics of WUT, Prof. LI Wenfeng and Prof. LIU Zhiping, for your supports on my experimental research. Your generous help had made considerable effects on putting my research onto the right track for the collaboration between TU Delft and WUT. Special thanks to Mr. TANG Weiguo for technical supports during my experimental investigation. Appreciation to Mr. SUN Wen, Ms. ZHU Fengna, Dr. CHANG, Mr. HUANG Chuanhai, and Mr. WANG Xiangui for your support during my experimental investigation.

Many thanks to the director of CSSC-branch, Mr. HU Ting and the manager of Zhongfu Shenying Carbon Co., Ltd., Mr. ZHANG Xu and engineer Mr. YANG Zhiwei for the technical support and manufacturing regarding the metal specimens &components and composite reinforcement. I would like to thank Dr. Michael Janssen from LR, TU Delft, and Ing. Jeroen Koning from DEMO, TU Delft, for giving me the advice considering the specimen manufacturing and fatigue test.

Appreciation to the Laboratory for Mechanical Systems of Engineering of Swiss Federal Laboratory of Material Science and Technology (Empa) for the Postdoctoral Scientist position in Switzerland. Special thanks to Prof. Giovanni Terrasi and Mr. Christian Affolter for offering the job and letting me start my work before my Ph.D. defence ceremony. Also, thanks to Dr. Bernhard Weisse, Dr. Barbezat Michel, Ms. Patricia Nitzsche, Ms. Evelyne Aerne, and Mr. Patrick Alpiger for the interview and concern.

Thanks to the talent senior researchers and peers that I met during the international conferences. Special thanks to Dr. WU Guiyi, Dr. Carol Johnston, and Dr. ZHANG Yanhui from TWI, UK and Ms. Agnes Marie Horn from DNVGL, Norway, and Dr. Mamdouh Salama from ConocoPhillips, US, and Dr. DONG Yan from CENTEC. Thank you for our interesting discussions and your interests, concern & help in or to my research. I would like to express my appreciation to the reviewers of my journal publications. It was a bit strange but a blessing of me to meet you anonymously, yet your encouragement throughout your comments and suggestions let me gained a huge amount of knowledge and taught me how to be a responsible researcher in the future.

I would like to express my thanks to the Education Department of the Chinese Embassy in the Kingdom of the Netherlands for your care and support during my oversea research. Special thanks to the counsellor, Mr. MENG Qingyu and the general secretary, Mr. WANG Yiwei, for your concern about my research and living in the Netherlands, as well as your great support to the development of Association of Chinese Student and Scholars in the Netherlands-Delft Branch (ACSSNL-Delft) during my term of office. Appreciation to the ASCCNL which offered me a platform to develop my management capability and to know such many talented students and scholars in the Netherlands, as well as offering the best stages for being the chief emcee for the Chinese New Year Galas in the Netherlands. Great thanks to every board members of ACSSNL-Delft and ACSSNL Domain during my term of office. It is a pleasure for me as the president of ACSSNL-Delft, while it is more of a fortune to work with you. Your great enthusiasm had brought our Chinese culture to the land of the Netherlands, and your amazing work had fulfilled our ambitious goals. Special thanks to the three vice presidents of ACSSNL-Delft, Ms. WANG Mengran, Mr. SONG Yan and Mr. WANG Youwei.

Appreciation to the people of 3ME Ph.D. council, it was a pleasure to work with you as a board member, to the well-being of the Ph.D. students in our faculty. During my term of office, I enjoyed working with our colleagues and I learned a lot in terms of the working and thinking style from different backgrounds. Special thanks to Ms. Mascha Toppenberg for

taking me in the Ph.D. council and to all board members for the interesting and meaningful discussions & activities.

I would like to express my gratitude to all of my colleagues and friends in the department of MTT and TU Delft in general. Dear Dr. LIU Xiangwei, Dr. CAI Jie, Dr. LIU Jialun and Dr. LI Shijie, Dr. HU Qu, Dr. Elena Rogova, Dr. ZENG Qingsong, Dr. CHEN Lianying, Dr. ZENG Qinqin and Dr. PANG Yunsong, thank you for your concern and help for my research and living in Delft. Dear Alina Colling, LI Xiao, Hamid Gilvari, Javad Mohajeri, Carmen Kooij, Vittorio Garofano, WANG Kai, Breno Alves Beirigo, CHEN Pengfei, Kartika Nurhayati, GUO Wenjing, thank you for the interesting discussions. I learned a lot through the cross-culture communication and your opinions from different perspectives. Thanks to the junior Ph.D. candidate DENG Zhikang, ZHANG Min, Marc Fransen, LI Mingxin, FANG Pan, YAN Yunpeng, TAN Jian, DU Zhe, ZHANG Yimeng, Nikos Vasilikis. Success with your research. Special thanks to Dick Mensch for translating my thesis summary into the Dutch version. Many thanks to our secretaries Patty, Anouk, Pauline, and Monique for always being kind and helpful during my Ph.D. journey.

Taking this opportunity, I would like to express my gratitude to my friends both in China and in the Netherlands. Appreciation to my friends LIU Jialun's couple, PANG Libao's couple, ZOU Sheng's couple and SUN Zhenning's couple. Dear Jialun and Shijie, thank you for your hosting when I was travelling in Wuhan, as well as your concern on my research. Dear Libao, thank you for lending your car and bicycle to me when I was doing my experimental research in Wuhan, which made a great convenience to me. Dear Sheng, thank you for your warm accommodation in Wuhan, I will definitely come to your place the next time. Dear Zhenning, you did not offer physical assistance due to the long-distance, but I could feel your spiritual wishes. Also appreciation to my friends in the Netherlands for our entertainment and sports, such as mountain biking, bouldering, and basketball. Special thanks to ZHANG Jian, LIU Xiangwei, Alina Colling, PIAO Longjian, WEI Xuanzi.

Finally, I would like to express my sincere appreciation to my family. Dear father and mother, thank you so much for all the love, concern and support during all those years. Time has taught me how perfect parents you were, and how great examples you have set for me. From now on, it is my honour and responsibility to take care of our family. Dear Bing, my love and soul mate, thank you so much for your accompany, that we experienced ups and downs in our lives together. I could not imagine what my life would be if without you. Meeting you is predetermination and getting to know you is an expedition journey for fortune. Let us create a better future together!

The year 2020 is extraordinary. The pandemic of Covid-19 has shown me the truth of the world, both of the bright side and the seamy side. Taking this opportunity, I wish the world peace!

Zongchen (Darren) Li
Zürich, December 2020

Contents

List of Symbols

A	crack length
a	crack depth of surface cracks
a_0	notch depth
a/c	aspect ratio of surface cracks
a/t	normalized crack depth
b	plate width
C	the Paris' law constants
C_a	Paris' law constant for the deepest point
C_c	Paris' law constant for the surface point
c	half-length of surface cracks
c_0	half-length of notches
D	external diameter of pipes
d	internal diameter of pipes
$\mathrm{d}a/dN$	crack growth rate along the depth direction
dc/dN	crack growth rate along the length direction
E_i	elastic modulus along i direction
F	boundary correction factor
f	normalized SIF
f_c	geometry correction factor of circumferential surface cracked pipes
f_{ci}	geometry correction factor of internal surface cracked pipes
f_{ce}	geometry correction factor of external surface cracked pipes

f_φ	the correction factor of the eccentric angle of a surface crack
G	bending correction factor by considering stress gradient effect
G_{ij}	shear modulus
g	correction factor of a/t, a/c and φ
H	bending correction factor for flat plate
L	pipe length
L_e	external span of the four-point bending test
L_i	inner span of the four-point bending test
M	bending moment
m	the Paris' law constants
M_1, M_2, M_3	correction factor for the semi-elliptical shape of the crack
N	cyclic index
Nu	Poisson's ratio
Q	an approximation factor
T	tensile strength
t	thickness of the pipe/plate
R	stress ratio
R_i	inner radius of a steel pipe
σ	normal stress
σ_t	normal tensile stress
σ_b	maximum of the bending nominal stress
K_I	Mode-I of SIF
K_{nor}	normalised SIF
K_{Ic}	the SIF of the deepest point of the surface crack
$K_{I,FE}$	SIF calculated by finite element method
ΔK_{Ia}	the range of SIFs of the deepest point
ΔK_{Ic}	the range of SIFs of the surface point

φ	the eccentric angle of surface cracks
φ_c	the eccentric angle for the surface point

List of Acronyms and Abbreviations

API	American Petroleum Institute
ASME	American Society of Mechanical Engineers
ASTM	American Society for Testing and Materials
ACPD	alternating current potential drop
BM	beach mark
BS	British Standards
COA	crack opening area
COD	Crack Opening Displacement
CFRP	Carbon Fibre Reinforced Polymer
CRS	Composite Repair System
CTOA	crack tip opening angle
DNVGL	Det Norske Veritas
EDM	electric-discharging machining
EPD	Electric Potential Drop
FCGR	fatigue crack growth rate
FE	finite element
FEA	finite element analysis
FEM	finite element method
FRP	Fibre Reinforced Polymer
GFRP	Glass Fibre Reinforced Polymer

ISO	International Organization for Standardization
RP	Recommended Practice
SIF	Stress Intensity Factor
X-FEM	extended FEM

List of Standards and Recommended Practices

API 570	Piping inspection code
API 579-1/ASME FFS-1	Fitness-for-service
API SPEL 5L	Specification for Line Pipe
API RP 1111	Design, Construction, Operation, and Maintenance of Offshore Hydrocarbon Pipelines
ASME B31.4	Pipeline Transportation Systems for Liquids and Slurries
ASME PCC-2	Repair of Pressure Equipment and Piping
ASME Section XI	American Society of Mechanical Engineers
ASTM E2899	Standard Test Method for Measurement of Initiation Toughness in Surface Cracks Under Tension and Bending
ASTM E647	Standard Test Method for Measurement of Fatigue Crack Growth Rates
ASTM E740	Standard Practice for Fracture Testing with Surface-Crack Tension Specimens
BS 7910	Guide to methods for assessing the acceptability of flaws in metallic structures
ISO 24817	Petroleum, petrochemical and natural gas industries-Composite repairs for pipework-Qualification and design, installation, testing and inspection
DNVGL-OS-F201	Dynamic Risers
DNVGL-RP-C205	Environmental Conditions and Environmental Loads
DNVGL-RP-F206	Riser Integrity Management
DNVGL-RP-F108	Assessment of flaws in pipeline and riser girth welds

DNVGL-RP-F113	Pipeline Subsea Repair
DNVGL-RP-F204	Riser fatigue
GJB 6055-2007	Specification for 907A prefiled of military ship

Chapter 1 Introduction

Surface crack growth is a major threat to the structural integrity of offshore metallic pipes. Preventing leakage due to crack penetration through the pipe wall has been one of the main tasks for offshore practitioners and academics. Composite repairing is an efficient method on damaged metallic structures, which has a promising prospect on cracked metallic pipes. This dissertation focuses on the mechanism of surface crack growth reinforced with composite repair system (CRS), in order to develop/improve the associated CRS standards. In this chapter, the research background, research questions, methodology, contribution, and research scope are introduced successively. The outline of this dissertation is described at the end.

1.1 Background

Generally, offshore metallic pipes are employed for transporting oil and natural gas. They have been widely applied in offshore operation and transmission industries due to their advantages of structure simplicity, cost-effective and easy installation & maintenance. In recent years, the increasing demand for energy and natural resources has led a development trend of offshore oil and gas production and transmission activities, where offshore metallic pipelines have an extensive application prospect [1, 2].

Offshore metallic pipes may fail in different ways and the main failure modes of concern include the fatigue cracking [3, 4]; metal loss caused by corrosion [5]; buckling induced by overloaded bending during installation or by operational errors [6]. Among these failure modes, fatigue cracking failure is a prime one [7-9]. In the marine environment, metallic pipes bear dynamic tensile and bending loads continuously, generated by wave, current, wind [9, 10], and 2nd order floater motions [11-13]. The cyclic bending and tension loads, as dominant load cases, commonly applied on critical zones such as hang-off zone, sag bend, arch bend and the touch-down zone [14], as shown in Figure 1.1. Meanwhile, circumferential

surface cracks often appear on the surface of the steel pipes initiate from corrosion pitting or girth weld defects [15-17]. Under this circumstance, surface cracks might continually propagate to through-thickness cracks, resulting in leakage or collapse eventually.

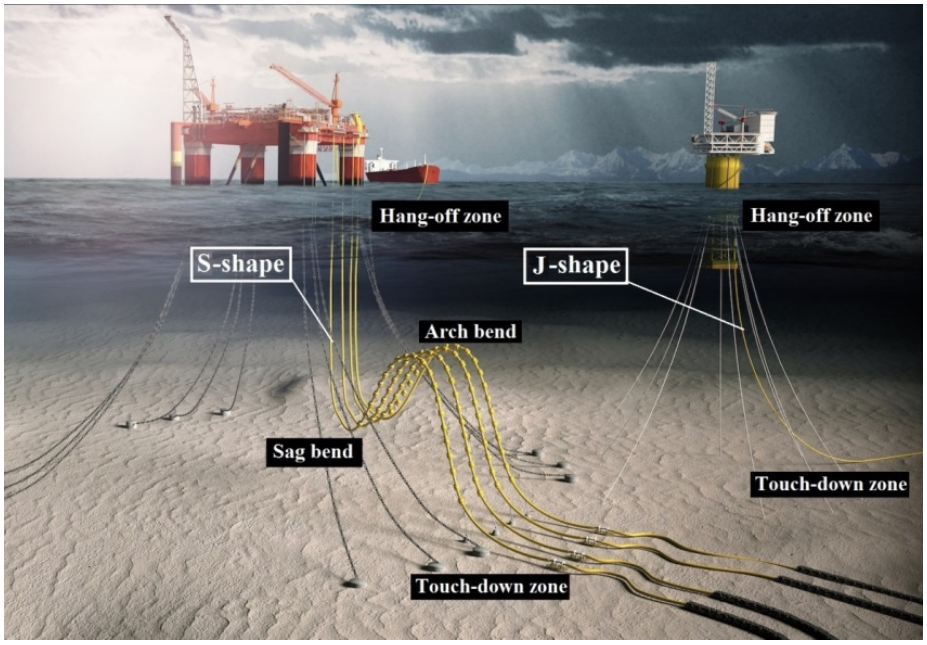

Figure 1.1. Critical fatigue zones of J-Shape and S-Shape offshore metallic pipelines

Surface cracks in offshore steel pipes with critical size need to be repaired instantly to avoid oil and gas leakage. Generally, cracks in offshore metallic pipes are detected by periodic in-service inspection [18] with the assistance of non-destructive automatic detection device and intelligent pig. After that, pipe maintenance will be implemented [19, 20].

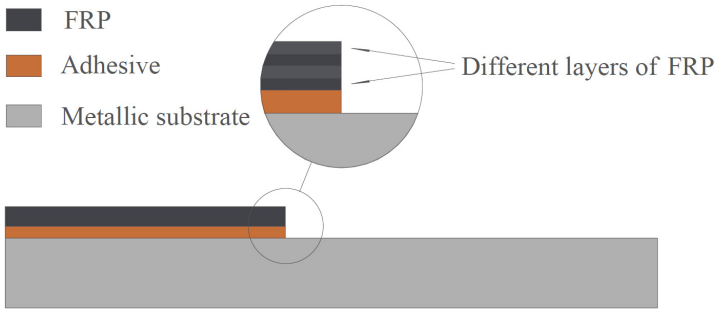

Figure 1.2. Metallic structure reinforced with Fibre Reinforced Polymer (FRP)

The CRS is an advanced maintenance technique in the pipeline industry as a representative application case of composite reinforcement on metallic structures [21-25], which has been widely used in metallic structures (see in Figure 1.2). Compared to the traditional methods, CRS has a favourable prospect in piping maintenance, on account of its prominent advantages [26]:

- Cost-effective: needless to suspend operation during maintenance;
- Time-saving: quick reinforcement;

- Lightweight: less dead load;
- Avoiding secondary damage to the substrate pipeline: non-destructive;
- Corrosion resistance;
- Easy installation underwater employing ROV and automatic wrapping machine.

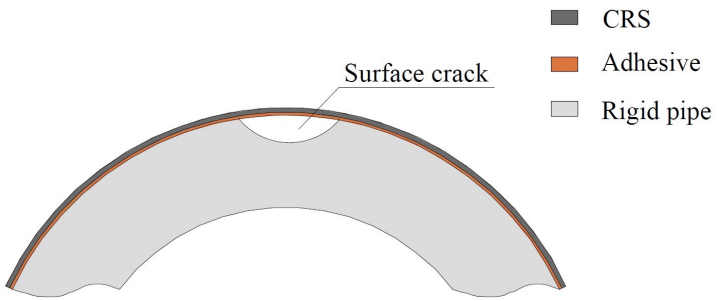

Figure 1.3. CRS on a surface cracked pipe

Generally, the hoop-wrapped CRS is employed to restore the integrity of offshore pipe structures [27-36], as shown in Figure 1.3. At present, composite repair on cracked metallic pipes conforms to standards based on either the rule of thumb [37] or strength-based approach [38], aiming to rehabilitate the load-bearing capacity of damaged steel pipes rather than decreasing the fatigue crack growth rate (FCGR). The method of evaluating surface crack growth reinforced with CRS is absent from open documents. It has resulted in a lack of confidence in the system, which seriously restricted the application and development of CRS.

1.2 Research questions

The objective of this research is to reveal the mechanism of surface crack growth in metallic pipes reinforced with CRS, in order to develop/improve the associated CRS standards. To achieve this, the main research questions of this dissertation are:

- **What is the mechanism of CRS on decreasing the surface crack growth in metallic pipes subjected to cyclic bending/tension loads?**

To answer the main research question, the following sub-questions are addressed:

1) *What are the available methods of evaluating the Stress Intensity Factor (SIF) of circumferential surface cracks in pipes subjected to bending/tension?*

2) *What are the key influential parameters in a prediction method of evaluating the surface crack growth in different scenarios?*

3) *What are the research gaps of using composite reinforcement on the surface cracked metallic pipes?*

4) *What are the differences of using composite reinforcement on surface cracked pipes and on surface cracked plate under tension?*

5) *What is the difference between employing composite reinforcement on the internal surface crack and the external surface crack of metallic pipes?*

6) *What are the possible failure modes of composite reinforced surface cracked metallic pipes, and how would they influence the crack growth behaviour?*

7) *How to appropriately reinforce the surface cracked metallic pipes, in order to achieve the desired reinforcement effect?*

1.3 Methodology

For the purpose of addressing the research questions, two approaches are employed throughout this dissertation, which are the experimental investigation and the finite element analysis (FEA). Finally, an analytical method is proposed to evaluate the SIF of the surface crack in metallic pipes.

The *three-dimensional FEA* is the well-recognised method owing to its accuracy, efficiency, reliable characteristics. It is capable of accurately evaluating the SIF along the surface crack front, as well as simulating the mechanical response of the composite reinforced steel structure system. The FEA is a significant tool to understand the mechanism by demonstrating the mechanical transmission in a sub-structural level. Besides, the influential factors can be further identified by the parametric study using the FEA.

The experimental investigation is an essential component in this research in regards to the various uncertainties, such as the unclear failure modes and the mechanical response of the composite reinforced surface cracked metallic pipes. The experimental investigation is of great value in terms of guiding the finite element (FE) modelling, validating the corresponding numerical and analytical methods. In this dissertation, the experimental investigation contains two parts: *composite reinforced surface cracked steel plates subjected to tension*, and *the composite reinforced surface cracked steel pipes subjected to bending*. The investigation on steel plate is conducted as the basics of the investigation on steel pipe, owing to the relatively simpler geometry and load case.

The analytical method has a unique value in practical application. The purpose of proposing the analytical method is to provide an efficient method to evaluate the SIF of surface cracks on the composite reinforced metallic pipes. In this dissertation, the analytical method for circumferential surface cracks in metallic pipes subjected to cyclic bending/tension is proposed at the first. Then on account of it, the analytical method on the composite reinforced surface crack in metallic pipes is proposed by considering the reinforcement effects and the key influential parameters.

1.4 Research scope

The research boundary is needed to be clearly identified. First of all, since the design and manufacturing of pipelines follows different standards in the global market, the geometry of the metallic pipes in this research cannot cover the various pipelines in offshore industry in terms of material properties and dimension. In this research, the commonly used API 5L X65 pipes for offshore scenarios conforming to the API SPEC 5L code [39] have been studied. At present, it is one of the most widely used offshore pipelines worldwide, which has a minimal yield strength of 448 MPa. The pipe in this research has a dimension of D = 168.3 mm and t = 12.7 mm, which has been investigated by the experimental method. Then on this basis, a variety of pipe dimensions are investigated through the FEA.

Second, this research focuses on *the circumferential surface crack growth subjected to tensile and bending loads*. In another word, other scenarios (e.g., longitudinal surface crack growth to internal pressure, inclined cracks subjected to torsion, combined loads, multi-crack growth) are excluded. Nevertheless, the research in this dissertation might share similar interests within these excluded research scenarios, or some of these research items (e.g., combined load cases, multi-crack growth) can be conducted as further research objectives.

Third, this research focuses on *the mechanism of composite reinforcement on surface crack growth in the base material of the metallic pipes*. Although in many cases, surface cracks initiate around the girth welding zone and its propagation might be affected by the welding residual stress, such discussions are excluded. The welding effect can be regarded as an influence factor and in the common case it is introduced as an influential parameter into the analytical prediction method.

Fourth, *the influence from the marine environmental are excluded in this research, such as temperature, humidity, corrosion-cracking, and the durability of the CRS.* Although it is believed that these factors are of great importance especially from the application perspective, they can refer to relevant studies such as crack growth or CRS durability problems influenced by marine environment.

1.5 Contribution

The contributions of this dissertation are listed below:

1) The contribution on the state-of-art: this dissertation overviews the achievements of the available literature on surface crack growth in metallic pipes and the composite reinforcement on metallic pipes, which facilitates the peers obtaining knowledge of the existing methods and identifies the research gaps, in order to pave the way of improving the crack growth prediction methods on bare pipes and the composite reinforced pipes.

2) The contribution to the understanding the mechanism of crack growth in composite reinforced surface cracked pipes: this dissertation identifies the possible failure modes of

using CRS to reinforce the surface cracked metallic pipes. Therewith, the mechanism of composite reinforcement on surface cracked metallic pipe is further understood, which further gives rise to the prediction methods on the SIF of the composite reinforced surface cracks.

3) The contribution on the application of composite reinforcement: the study on the optimization design of the composite reinforcement and the prediction on the surface crack growth provides considerable confidence from the application perspective. Besides, the reinforcement method and its evaluation criterion in this dissertation provide a stepping stone to develop/improve the associate CRS standards.

1.6 Outline of the dissertation

The structure of this dissertation is shown in Figure 1.4.

In **Chapter 2**, the literature review on surface cracked metallic pipes and composite reinforcement on pipes is documented. On account of the limited investigations of surface crack growth in metallic pipes reinforced with CRS from open documents, the literature review is divided into two parts: surface crack growth in metallic pipes, and composite reinforcement on metallic pipes. This chapter identifies the research gaps, as well as answering the research questions of the state-of-art.

In **Chapter 3**, the research focuses on the fundamental problem—circumferential surface crack growth in metallic pipes subjected to bending/tension—which paves the way for further investigations. In this chapter, an analytical method of evaluating the SIF of circumferential surface cracks in metallic pipes is proposed. In light of pipe geometry and bending load case, the analytical formula is raised by introducing new bending correction factors and new geometry correction factors on the basis of the Newman-Raju's method. Owing to a large data set requirement by the parametric studies, three-dimensional FE models of evaluating SIFs of circumferential surface cracks are developed. The FE method (FEM) is validated to ensure that it could provide accurate SIF estimations. Analytical verification is conducted which shows that the SIF evaluated by the proposed analytical method match well with the results evaluated by the recommended analytical method. Then experimental investigations and FEA studies are implemented to further validate the analytical method of predicting surface crack growth rate.

In **Chapter 4**, the surface crack growth in composite reinforced metallic plates subjected to cyclic tension is investigated. The purpose of applying composite reinforcement on this primary structure under tension is try to simplify the reinforcement system in order to better understand the mechanism by eliminating potential influences from the pipe geometry and the bending load. In this chapter, experimental investigations are first conducted to identify the failure modes. Then the possible interfacial failures and interfacial stiffness degradation are analysed using the cohesive zone modelling. After that, the FE model of composite reinforced surface cracked metallic plate is developed and validated by the experimental results. Through

the FE models, different reinforcement methods and the optimum reinforcement design has been discussed.

In light of the difference of the bond behaviour between the CRS and the metallic substrate—whether the surface crack contact with the CRS, the study is divided into two parts: (1) internal surface cracked metallic pipes reinforced with CRS, and (2) external surface cracked metallic pipes reinforced with CRS. These two parts are discussed in two chapters respectively. Therefore first in **Chapter 5**, the composite reinforcement on internal surface cracked metallic pipes is first investigated. In Section 5.1, the FE model is developed and then it is successively validated with available experimental results from literature. Then using the FEA, the effectiveness on a certain cracked pipe as a case study is analysed in Section 5.2. Later on in Section 5.3, a parametric study has been carried out to indicate the influential factors on the reinforcement effectiveness from the composite reinforcement method, material properties, pipe dimension, and crack dimension perspectives. In Section 5.4, an analytical method of evaluating the SIF of the internal surface crack in metallic pipes reinforced with CRS is proposed. Finally, the conclusions of this chapter are drawn in Section 5.5.

Following Chapter 5, the composite reinforcement on external surface cracked metallic pipes is investigated in **Chapter 6**. In Section 6.1, the experimental investigations on external surfaced cracked metallic pipes subjected to bending are first conducted, in order to analyse the mechanical response and identify the possible failure modes during the fatigue test. Then in Section 6.2, the FE model of composite reinforced external surface cracked pipe is developed on the basis of the FE models in Chapters 2 to 4 and Section 5.1. Thereafter, the FEM is validated by the experimental data. In Section 6.3, a parametric study has been conducted to identify the influential factors on the composite reinforcement on external surface cracked pipes. Then an analytical method is proposed to evaluate the SIF of the external surface crack reinforced with CRS. Finally, the conclusions of this chapter are drawn in Section 6.5.

In **Chapter 7**, the conclusions and the answers to the research question in Section 1.2 are drawn in Section 7.1. The recommendations for future studies are provided in Section 7.2.

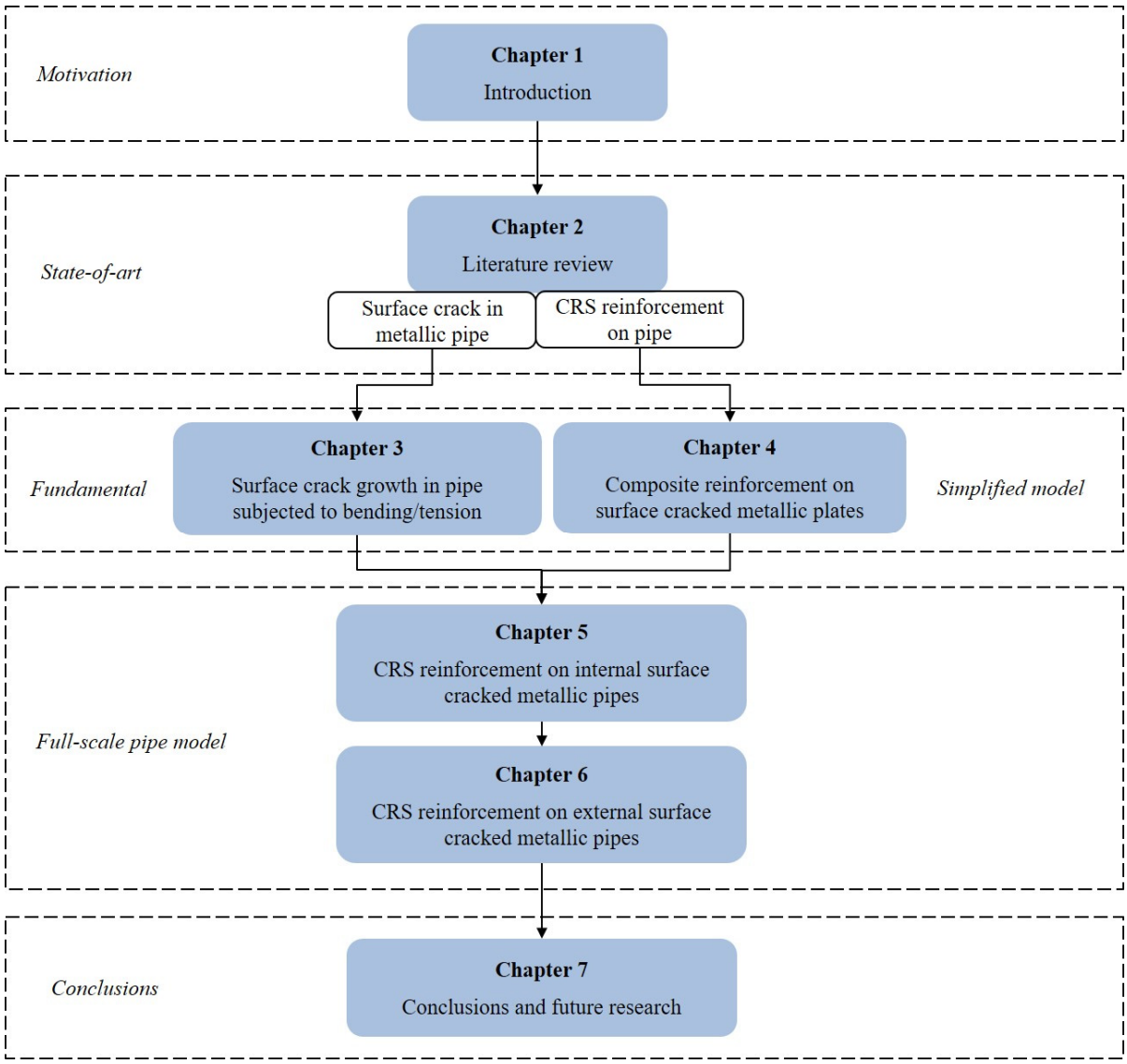

Figure 1.4. Outline of the dissertation

Chapter 2 Literature Review*

This chapter reviews existing investigations related to the topic on surface crack growth in offshore metallic pipes reinforced with CRS. The findings and conclusions of this chapter pave a way to the following chapters. In regards to the very limited number of investigations, the literature review is divided into two constitute parts: surface crack growth in offshore metallic pipes, and composite reinforcement on metallic pipes. These two parts are able to provide fundamental knowledge for this topic. Section 2.1 reviews the state-of-art of surface crack growth in offshore metallic pipes from the fracture mechanics perspective, in order to identify targeting problem and explicit the research methods in terms of experimental, numerical and analytical approaches; Section 2.2 conducts a survey on the composite reinforcement on metallic pipes from the composite repairing and failure mechanics aspects, to identify the research questions including the composite reinforcement schemes, repairing effectiveness, composite failure modes. Conclusions of this chapter regarding the two reviews are provided in Section 2.3.

* This chapter is based on the published journal article—[40] Z. Li, X. Jiang, H. Hopman, and Engineering, "Surface Crack Growth in Offshore Metallic Pipes under Cyclic Loads: A Literature Review," *Journal of Marine Science and Engineering,* vol. 8, no. 5, p. 339, 2020., and the draft journal article – Li, Z., Jiang, X. and Hopman, H., 2020. Composite Repair System on metallic circular hollow section structures: A literature review., submitted to a journal.

2.1 A literature review on surface crack growth in offshore metallic pipes

2.1.1 Introduction

Surface cracks, in most cases as a semi-elliptical shape [41] (see in Figure 2.1), frequently initiate and propagate in these critical areas. They may initiate from surface defects or corrosion pits on the base material or at weld toes [17], appearing on either the internal or the external surface. Under dynamic loads of combined tensile and bending loads (e.g., the hang-off zone), or high magnitude bending moment (e.g., the touch-down zone, sag bend, and arch bend), in combination with the internal pressure, surface cracks may continually propagate, and finally cause leakage or collapse. For instance, a report by Petroleum Safety Authority Norway indicated that between 1975 and 2018, 140 out of around 930 total anomalies were due to cracks, accounting for around 15% [42].

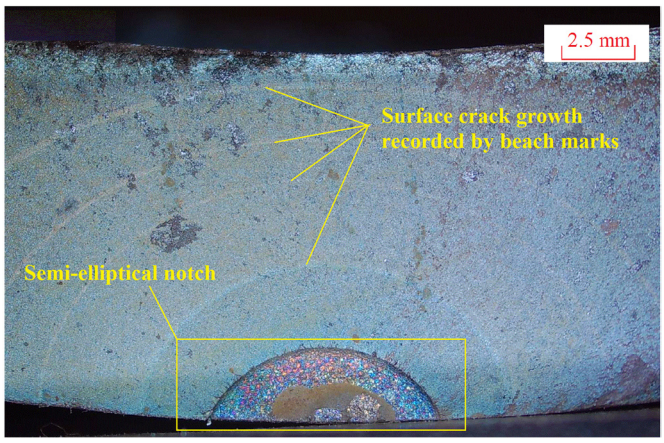

Figure 2.1. Circumferential semi-elliptical surface crack in metallic pipes [43]

Particularly, besides the internal pressure which is the principle load case for transportation pipelines, cyclic bending is a dominate load case on the offshore pipes. In addition, the offshore metallic pipelines in practical situations are connected by standardised pipes through girth welding, which is the hotbed for crack initiation [17]. In a DNVGL's report, the failure data of 1,719 fatigued metallic pipe specimens was collected, where 445 pipes failed due to circumferential surface crack growth, accounting for 25.89% [44].

Hence, surface crack growth is a huge threat to the structural integrity of metallic pipes, which drawn a wide attention from the offshore industry and academia. In our review effort, searching the SCOPUS and Google Scholar using "surface crack" or "part through crack", and "pipe", as well as their synonyms, as key terms, plus applying the forward and backward snowballing techniques, the related topics regarding the issue of surface crack growth in metallic pipe structures were selected. Figure 2.2 shows the research statue on different surface cracked structures, where 60% of the research is on the cracked plate. The research on pipe structures (including pressure vessels) accounts for 40% is the second biggest research hotspot.

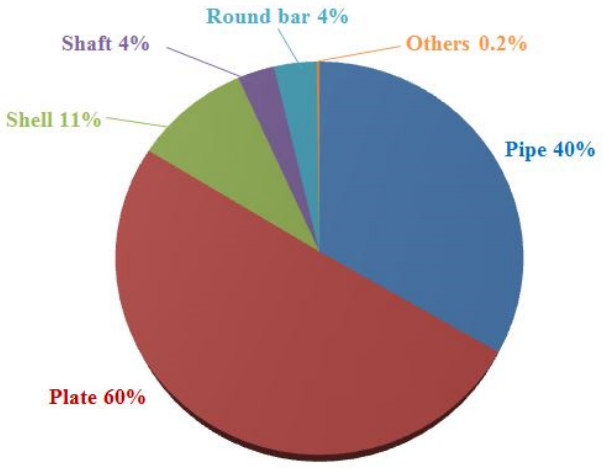

Figure 2.2. Research status of surface crack growth in different structures [40]

In the past few decades, researchers reviewed the surface crack problem from different perspectives. The surface crack growth and the SIF evaluation methods were reviewed by Newman and Raju [45] in 1979, Scott and Thorpe [46] in 1981, Parks [47] in 1990, and Pang [48] in 1990. These studies reviews majorly focused on the surface crack growth and its analytical evaluation methods in plate structures, while issues such as longitudinal surface cracked pipes, surface crack in fillet weld toes have been discussed in some reviews as well. In recent years, Brighenti and Carpinteri [16] reviewed the general problems of the surface crack growth, where typical structural components with surface cracks have been overviewed, and the part-through-crack shell has been analysed as a case study. Along with the development of the three-dimensional FEM, Branco, et al. [49] reviewed the re-meshing technique on simulating the surface crack growth, as well as the research progress of such technique applied on different situations from geometry, and load case perspectives.

For the sake of identifying the research gaps and providing guidelines for the following research, the latest research was reviewed by analysing the state-of-art of existing evaluation methods on the surface crack growth in pipe structures from the fracture mechanics perspective. Sub-section 2.1.2 overviews he research progress from experimental, numerical, and analytical perspectives respectively. Then in Sub-section 2.1.3, the state-of-the-art of the research status was analysed and the insufficiencies of the available literature were discussed. The conclusions of Section 2.1 are addressed in Sub-section 2.1.4.

2.1.2 Overview of the research on surface crack growth in metallic pipes

Surface crack growth in metallic pipes is investigated in the past decades. Generally, as shown in Figure 2.3, the scenarios of surface crack growth in metallic pipes are including circumferential external (a) and internal (b) surface cracks, longitudinal external (c) and internal (d) surface cracks, and the inclined surface crack (e). In this section, the research progress of these scenarios is overviewed from experimental, numerical, and analytical perspectives.

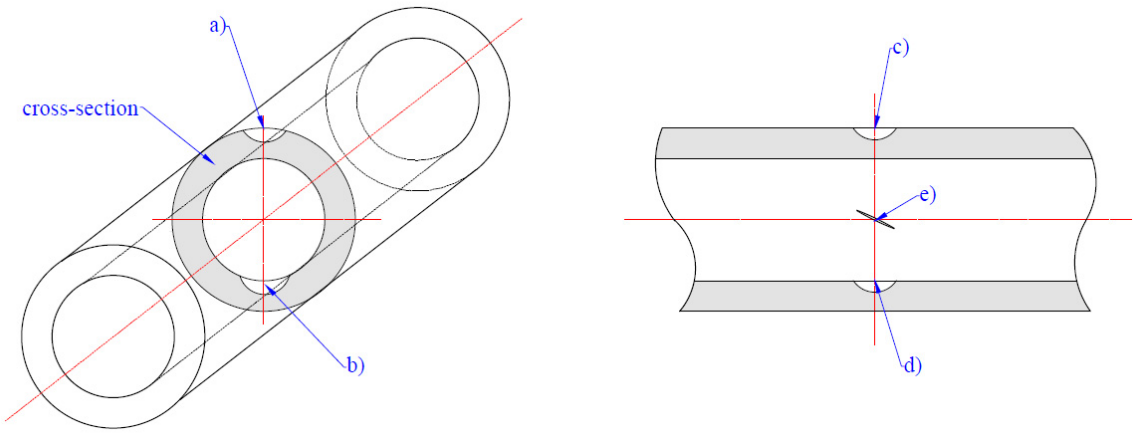

Figure 2.3. Research status of surface crack growth in different structures

2.1.2.1. Experimental research

Experimental research is a reliable and important approach in terms of understanding the mechanism, calibrating and validating relevant numerical and analytical methods. In the past decades, researchers have conducted a series of experimental studies on surface cracked metallic pipes subjected to cyclic loads, as listed in Table 2.1.

Table 2.1. The available experimental studies of surface crack growth in metallic pipes

Scenarios	Authors	Year	Material	Crack shape	Load type	Load ratio	Crack detection method
Circumferential external surface crack	Shimakawa, et al. [50]	1993	304 Stainless steel	Semi-elliptical	Bending	\	\
Longitudinal internal and external surface cracks	Zhu, et al. [51]	1998	AISI4340H II steel	Semi-elliptical	Internal pressure	0	BM
Circumferential internal surface crack	Yoo and Ando [52]	2000	STS370 carbon steel	Semi-elliptical	Bending	0.1	BM
Circumferential external surface crack	Singh, et al. [53]	2003	SA333 seamless steel	Rectangular machined notch propagated to semi-elliptical cracks	Bending	0.1, 0.3, 0.5.	ACPD
Circumferential external surface crack	Arora, et al. [54]	2011	Stainless SA312 type 304LN steel	Semi-elliptical	Bending	0.1	BM, ACPD
Circumferential external surface crack	Sahu, et al. [55]	2017	Stainless steel TP316L	Notch with a straight line at the bottom propagated to semi-elliptical cracks	Bending	0.1	COD
Circumferential external surface crack	Shlyannikov, et al. [56]	2018	Aluminium alloy	Semi-elliptical	Tension	0.1	BM

- Experimental procedures and methods

A rational experimental scheme of surface crack growth under cyclic loading is vital for data acquisition. Thus it is important to follow the relevant fatigue test codes (e.g., ASTM E647 [57]). The manufacturing of semi-elliptical shaped notches is more complicated than making through-thickness notches. The recommended notch making methods can be referred to ASTM E2899 [58] and ASTM E740 [59]. Micro electric-discharging machining (micro-EDM) is recommended for obtaining a user defined shape and size of a semi-elliptical notch, as well as avoiding the heat effect. Other machining techniques such as conventional machining techniques (e.g., mill, grind) and laser cutting might be used effectively as well [57]. The machined notch size design, fatigue test parameters should be identified based on both of the standard's requirement and the practical condition (e.g., critical size of surface crack in offshore metallic pipes [17], load amplitude and load ratio of bending applied on the pipes). Among these experimental studies, the majority of machined notches were semi-elliptical shaped, except Ref. [53] which adopted rectangular machined notch and Ref. [55] which adopted the notch with a straight bottom, as shown in Figure 2.4. However, these notches soon propagated to semi-elliptical shape and then continually grew in this shape till the end of the fatigue test.

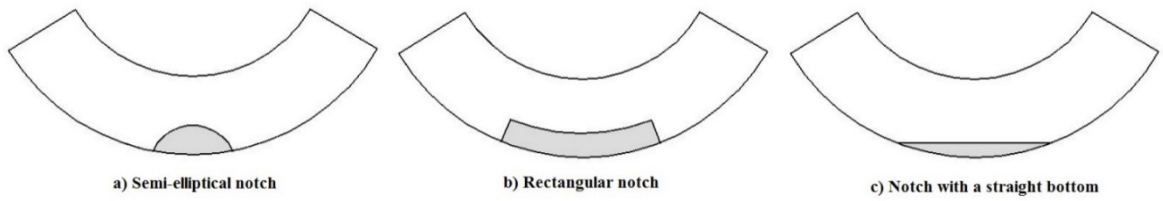

Figure 2.4. Notch type: a) semi-elliptical notch; b) rectangular notch [53]; c) notch with a straight bottom [55]

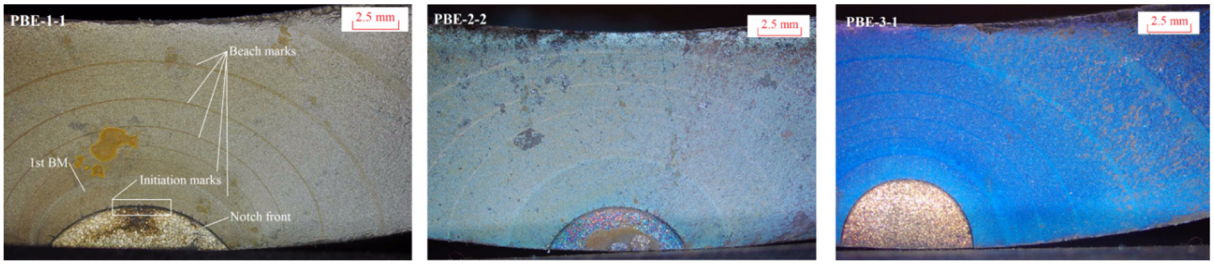

Figure 2.5. Photographs of surface crack growth in metallic pipes marked by BM technique [43]

Before the fatigue crack test, a pre-cracking procedure should be implemented in order to generate the fatigue crack from the manual notch. The pre-cracking procedure should follow the relevant standards such as ASTM E647 [57], which regulate the pre-cracking steps, the load amplitude of each step, cyclic index, the minimum propagation length of each step. After the pre-cracking procedure, the specimen can be ready for the fatigue crack growth test.

Crack growth detection and measurement approaches are significant to acquire valid crack growth data. The beach mark (BM) technique, which might be the most reliable and efficient

method of tracing the surface crack growth, has been widely adopted, as indicated in Table 2.1. The BMs, which usually obtained through changing the stress amplitude or load ratio, can be reserved permanently on the surface crack cross-section plain, as shown in Figure 2.5. In addition, the BMs are not influenced by the covering on metallic pipes (e.g., coating, composite repair), which widens its application scope. The Electric Potential Drop (EPD), particularly the Alternating Current Potential Drop (ACPD), was adopted in Ref. [53, 54] as well. This method is efficient, while measurement errors still existed, which can be used as an alternative or a supplementary detection method.

- Crack orientation, and load cases

Most of the experimental studies on surface cracked pipes focused on the Mode-I crack growth where surface cracks propagate perpendicular to the normal stress. Among those studies, the majority were conducted under cyclic bending loads. In these cases, four-point bending set-up is adopted in order to generate a pure bending moment on the middle part of pipe specimens, as shown in Figure 2.6a. The longitudinal surface crack growth subjected to cyclic loads, as a common case for transportation pipelines, has been studied as well. In addition to longitudinal normal stress, the circumferential tensile force induced by the cyclic internal pressure is the driving factor of the crack propagation, as shown in Figure 2.6b. Zhu, et al. [51] investigated the longitudinal surface crack growth subjected to cyclic internal pressure with the range of 0 to 294 MPa. The external surface cracked circular hollow sections subjected to tension [56], which usually exists in the hang-off zone, was investigated as well. The set-up of pipe subjected to tension is shown in Figure 2.6c.

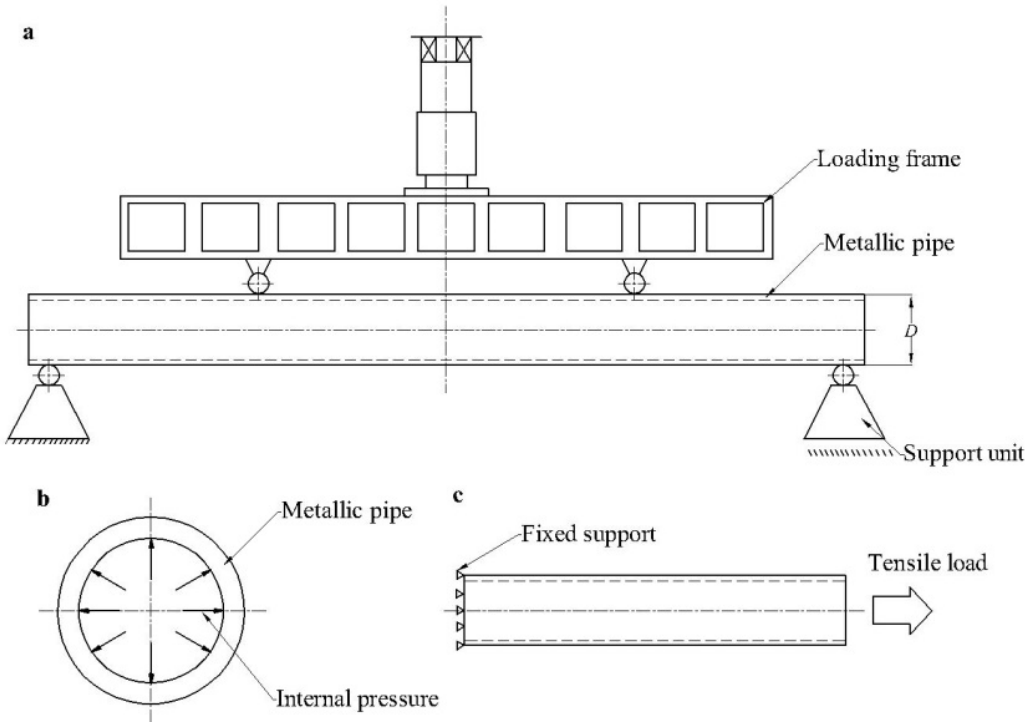

Figure 2.6. Test set-up and load cases: a) 4-point bending, b) internal pressure, and c) tension

- Load ratio and the Paris' constants

The load ratio equals to 0.1 was commonly adopted for the fatigue tests. In the area along offshore pipes such as the sag bend and arch bend, load ratio equals to 0.5 is a more practical case [60]. The surface crack growth in metallic pipes under bending with stress ratio of 0.1, 0.3 and 0.5 were investigated, indicating that for a given crack depth, the number of cycles required for initiation increased within the increase of the load ratio. This can be explained by the fact that the mechanism of initiation requires development of slip planes in the material, which coincide with maximum shear stress, and becomes sites for crack initiation. The development of the slip bands depends on the magnitude of stress range at the notch tip [53]. In addition, the load ratio can affect the crack growth rate as well, because the load stress changed the range of the SIF – ΔK. Load ratio has a minor influence on the Paris' constants values as well, which can be obtained from crack growth assessment codes (e.g., BS 7910 [20], ASME Section XI [61]) or calibrate from fatigue crack growth tests [53, 54]. Singh, et al. [53] also found that the Paris constants for predicting crack growth along depth direction and along length direction were the same. However, this had a contradiction with the experimental observation by Corn [62], whom claim that the Paris constant C at the deepest point and surface point were not equal, due to the difference of plane stress and plain strain from the surface point to the deepest point of surface cracks.

2.1.2.2. Numerical simulation of predicting surface crack growth in metallic pipes

Although experimental research offers reliable predictions of surface crack growth in metallic pipes, the relatively high cost hinders its application. The numerical simulation, as a cost-effective alternative, has been widely applied to evaluate the fracture mechanics parameters of surface cracks, such as the SIF and J-integral. At present, it is the most common adopted approach. In the two past decades, researchers have conducted a series of numerical investigations on surface cracked metallic pipes subjected to cyclic loads, as listed in Table 2.2. In this section, the numerical studies are overviewed from different perspectives.

- FE modelling strategy

To date, the majority of numerical simulations of surface cracks in metallic pipes were conducted by FEM, as shown in Table 2.2. The implementation and accuracy of FEM are the major concerns, guaranteed by several aspects: modelling, element type choosing, meshing methods, the element size, and the solver algorithms. First, the contour numbers around the surface crack might affect the calculation results. At least two contours around the crack front are suggested in order to eliminate the errors [63]. Second, a spider web pattern of the meshing shape consisting several concentric rings around the crack front is recommended, and the minimum angular discretisation of the elements should be $30°$ [64]. Third, when using displacement matching method to estimate SIFs, the orthogonal mesh (see in Figure 2.7a) around the crack front should be adopted [65]; while if energy based method is applied, the non-orthogonal mesh (see from Figure 2.7b to 2.7e) would not affect the results [66]. Fourth, the type of element commonly adopts the iso-parametric formulation, with quadratic

shape functions [67]. The iso-parametric elements can present curved shapes with a small number of elements owing to their distorted shapes. Fifth, the element size, especially for those around the surface crack tip should be defined properly. Last but not least, the interaction angle between the crack front and the free surface of the pipe should be carefully modelled in order to ensure the square singularity at the corner point [68]. More information of three-dimensional crack modelling can be found in the review paper by Branco, et al. [49].

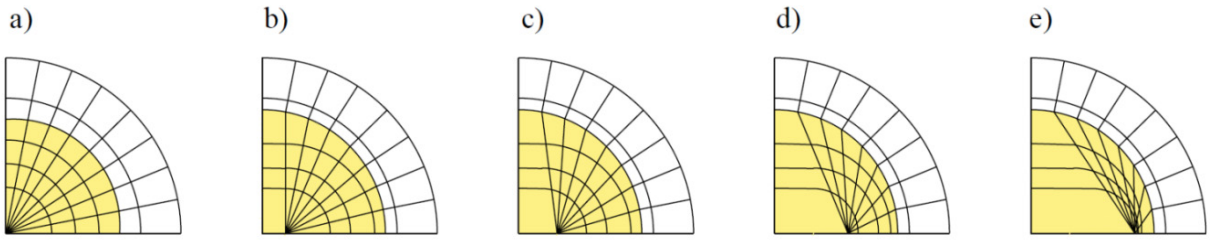

Figure 2.7. Five degrees (a-e) of mesh non-orthogonality, from an orthogonal mesh to a distorted mesh [66]

Table 2.2 Numerical simulations conducted on surface cracked metallic pipes

Scenario	Author	Year	Geometry and pipe material	Load type	*a*/*t* range	R_t/*t* range	*a*/*c* range
Longitudinal internal surface crack	Diamantoudis and Labeas [69]	2005	Steel pressure vessel	Internal pressure	\	10, 14.29, 24.92	[0.2,1.0]
	Oh, et al. [70]	2007	Pipe	Internal pressure	0.25, 0.5, 0.6, 0.75	[5, 20]	0.01
	Meshii, et al. [71],	2010	Steel pipeline	Internal pressure	0.2, 0.4, 0.5	5, 10	[0.2,1.0]
	Li and Yang [72]	2012	Cast iron sewer pipe	Internal pressure	\	\	[1.0,+∞)
	Sharma, et al. [73]	2014	Steel pipe bend	Internal pressure	\	\	\
Circumferential external surface crack	Carpinteri, et al. [74]	2003	Pipe	Tension, bending	0.2, 0.5, 0.8	1, 10	0.2, 0.6, 1.0
	Ligoria, et al. [75]	2005	Nuclear power plant piping	Bending	0.24, 0.35, 0.53,0.79	4, 6	(0,0.5]
	Kou and Burdekin [76]	2006	Steel tubular	Tension	[0.8, 1)	10, 15, 22.5	[0.4,0.8]
	Shahani and Habibi [77]	2007	Metallic hollow cylinder	Combined tension, bending, and torsion	[0.2, 0.8]	\	[0.2,1.2]
	Mechab, et al. [78]	2011	Steel pipeline	Bending	[0.2, 0.8]	[1, 80]	[0.6,0.8]
	Dao and Sellami [79]	2012	Steel pipe	Bending and tension	[0, 1]	10	0.2, 0.5, 1.0
	Predan, et al. [80]	2013	High strength steel tubular	Torsion	[0.1, 0.5]	2	[0.1,1.0]

- Crack and pipe dimensions

As long as using proper modelling and analysis methods, the FEM is a reliable and accurate approach of modelling surface cracks in metallic pipes. Table 2.2 lists the numerical studies of surface cracks in pipes. The FEM provide an efficient path to understand the mechanism of surface crack growth, such as the geometry effects (e.g., a/c, a/t and R_t/t) and load effects (e.g., internal pressure, bending, tension, and torsion) on SIF estimations. Most of the numerical studies focused on the aspect ratio (a/c) smaller than 1.0. The growth behaviour of shallow surface cracks ($a/c \leq 0.5$) were studies, which concluded that shallow cracks grew more rapidly in depth direction than in the surface direction, correspondingly the largest SIF is at the deepest point of the surface crack. While for high aspect ratio surface crack ($a/c > 1.0$) due to corrosion attacks, the maximum SIF might occur at different position along the crack front. Deep surface crack growth ($a/t > 0.8$) in pipes subjected to tension was studies [76], which indicated that the maximum and minimum SIF were always at the deepest point and the surface point respectively. The effects of the ratio between the internal radius and the pipe thickness (R_t/t) was studied as well [78], which shows that the R_t/t ratio was an independent coefficient to the a/c and a/t ratio of SIF evaluation on surface cracks in metallic pipes.

The initial crack dimensions could significantly affect the surface crack initiation and propagation. Singh, et al. [53] indicated that the surface crack initiation strongly depended on the crack depth. For a given stress range, the numbers of cycles required for crack initiation was depended on the initial crack depth, owing to the fact that the SIF was less for a shallow crack than a deep crack. In the early stage, the surface crack growth strongly depends on the initial crack shape as well. Lin and Smith [81] investigated its influence by comparing crack front of a V-notch and a U-notch respectively, demonstrated that the crack shape changed more rapidly of the V-notch than the U-notch, due to its high stress concentration along the free boundary. Later on, with the semi-elliptical surface crack profile, Couroneau and Royer [82] ascertained that the surface crack growth could be divided into two stages: the first stage is affected by the initial crack shape and size, the exponent of Paris' law, and the loading cases; while the second stage is no longer affected by the initial crack shape.

- Crack propagation evaluation

Along with crack growth model such as Paris law [83], the propagation of surface cracks can be traced. This method is generally known as the adaptive re-meshing technique, which can be summarized into five main steps [49], indicated in Figure 2.8: a) building a three-dimensional FE model; b) dividing the crack front into a certain amount of nodes; c) calculating the effective SIFs along the surface crack front; d) choosing the adequate fatigue crack growth law and calculating the crack growth; e) defining a new crack front of a new FE model. These steps are then repeated until the crack propagates to a required crack length.

2.1.2.3. Analytical methods of predicting surface crack growth in metallic pipes

Although numerical analysis is an accurate and cost-effective evaluation method, the following factor has restricted its application: the idealization of numerical modelling is inherent with numerical approaches, and the reasonability of numerical approaches relies on a large extent on the user expertise. The analytical method is an efficient alternative, which provides a rapid and user friendly assessment solution. To date, researchers have proposed a series of analytical methods to evaluate the surface crack growth in pipes under different situations.

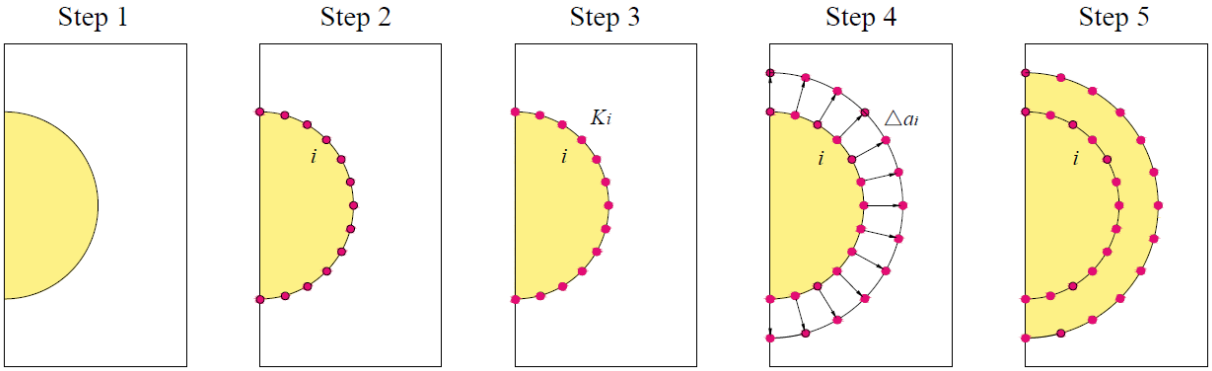

Figure 2.8. Five steps of the adaptive re-meshing technique [49]

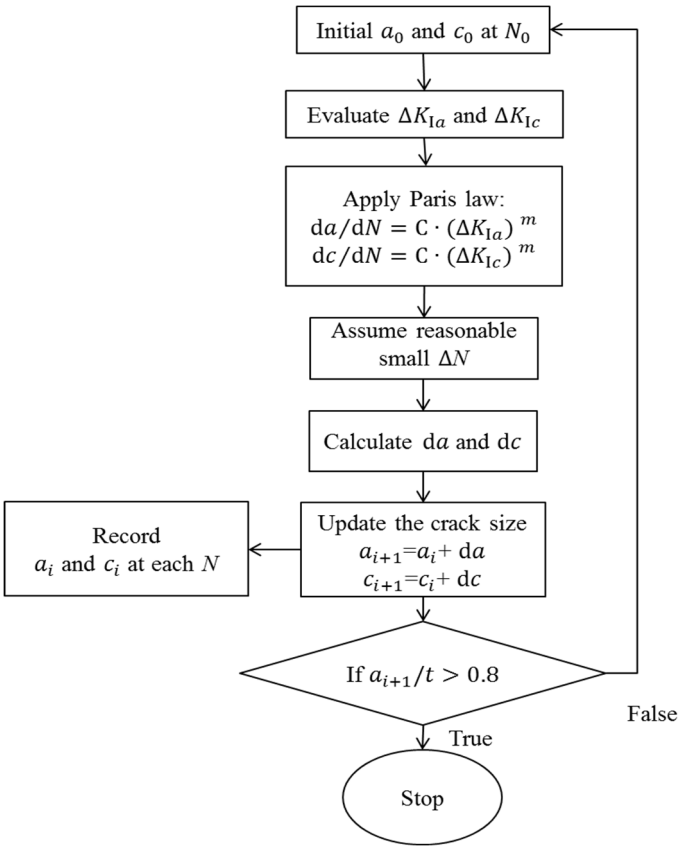

Figure 2.9. The procedure of evaluating surface crack growth

The surface point and the deepest point are the two most important points along the surface crack front. In general cases, only the crack growth along the depth and length direction are needed to be evaluated. The procedure of tracing the crack growth process along the depth direction and the length direction is shown in Figure 2.9. The $\mathrm{d}a/\mathrm{d}N$ and $\mathrm{d}c/\mathrm{d}N$ are the crack growth rate along the depth direction and along the length direction respectively, $\Delta K_{\mathrm{I}a}$ and $\Delta K_{\mathrm{I}c}$ are the range of SIFs of the deepest point and the surface point respectively, C and m are two Paris' constants. Afterwards, by assuming a small amount of cycles, the increments of the crack length and depth are calculated. Eventually, it is possible to trace the surface crack growth along the two directions.

- The foundation of evaluating surface crack growth

In general, the surface crack growth rate is evaluated by crack propagation criterion, such as the Paris' law [83] indicated in Figure 2.9, which is

$$dA/dN = C \cdot (\Delta K_{\mathrm{I}})^m, \tag{2.1}$$

where dA/dN is the crack growth rate, ΔK_{I} is the range of SIF along the surface crack front.

Evaluating the SIF along the surface crack front is the hinge of predicting the crack growth [84], on which the proposed analytical methods for surface cracked pipes are based. In light of the pipe and crack dimensions and the load cases, the geometry correction factor F and the nominal stress S are modified, mainly through two approaches: the numerical analysis method [85, 86] and the weight function method [87]. Table 2.3 lists the available analytical approaches for surface cracked metallic pipes, including the approaches recommended by relevant crack growth evaluation codes (e.g., BS 7910, and API 579-1/ASME FFS-1) and the latest proposed methods.

Table 2.3. Analytical methods of evaluating SIF of surface cracks in metallic pipes

Method	Author	Scenarios	Year	Standard
Numerical analysis method	Newman and Raju [86]	Circumferential surface cracks in plates subjected to bending	1981	BS 7910, DNVGL-RP-F108
	Raju and Newman Jr [88]	Longitudinal surface cracks in pipes subjected to internal pressure	1982	
	Raju and Newman [89]	Circumferential external surface cracks in pipe subjected to bending	1986	-
	Mechab, et al. [78]	Circumferential external surface crack in pipe subjected to bending	2011	-
	Li and Yang [72]	Longitudinal high aspect ratio surface crack in pipe subjected to internal pressure	2012	-
	Sahu, et al. [55]	Circumferential external surface cracks in pipe subjected to bending	2017	-
Weight function method	Anderson [90]	Circumferential surface crack in pipe subjected to bending; Longitudinal surface crack in pipe subjected to internal pressure	2002	API 579-1/ASME FFS-1

- The numerical analysis method—Newman-Raju's method

The numerical analysis method modifies F and S by curving fitting and engineering judgment. Easier in 1970s, Newman and Raju [91] proposed an analytical method of evaluating the SIF of semi-elliptical surface cracks in plate subjected to tension, which is a representative of the numerical analysis method. Later on, they expanded the load cases to combined tension and bending [92], which is recommended by BS 7910 [20] for estimating the SIF of circumferential external surface cracked pipes subjected to tension and bending, which is

$$K_{\mathrm{I}} = (S_{\mathrm{t}} + HS_{\mathrm{b}})\sqrt{\pi\frac{a}{Q}}F(\frac{a}{t},\frac{a}{c},\frac{c}{b},\varphi)\,, \tag{2.2}$$

where S_{t} and S_{b} represents tension stress and bending stress respectively, the boundary-correction factor F and bending correction function H were defined by curving fitting and engineering judgement [91, 93]. Q is an approximation factor [94]. With further modifications by Dedhia and Harris [95] and Bergman [96], this method was adopted by BS 7910 [20] for circumferential internal surface crack in pipe subjected to bending. While the experimental results in Ref. [52] indicated the Newman-Raju's method provided non-conservative prediction on the FCGR. Subsequently, Newman and Raju proposed the analytical method for circumferential surface cracked pipes subjected to tension and bending [89], the geometry correction factor F is tabulated from a table index. Therefore, it is infeasible to continuously evaluate the SIF during the crack propagation.

When evaluating SIF of the longitudinal surface crack in pipe subjected to internal pressure, the pipe can be regarded as a curved plate. Thus, Newman and Raju [97] proposed an analytical method for evaluating the SIF of internal surface crack in pipe subjected to internal pressure on the basis of Eq. (2.1), by modifying the load case and the geometry factors. Then they updated the equation to both longitudinal internal and external surface cracks [88], which is

$$K_{\mathrm{I}} = \frac{pR}{t}\sqrt{\pi\frac{a}{Q}}F(\frac{a}{c},\frac{a}{t},\frac{t}{R},\varphi)\,, \tag{2.3}$$

where pR/t is the average hoop stress, F is the boundary-correction factor for either internal surface cracks or external surface cracks. Research indicated that this method is appropriate for evaluating the SIF of longitudinal surface cracks subjected to internal pressure [51].

- The weight function method

In the weight function, the nominal stress is expressed as the sum of the primary stresses and the secondary stresses, which are calculated by two equations containing a series of weight functions [98-100]. When needed, the corresponding weight function can be added into the equation. Anderson [90] modified the weight function methods by a comprehensive numerical study, including of longitudinal surface crack in pipe subjected to internal pressure and circumferential surface crack in pipe subjected to bending respectively, which are recommended by API 579-1/ASME FFS-1 [19] as

i) Longitudinal internal surface crack in pipe subjected to internal pressure:

$$K_{\mathrm{I}} = \frac{pD^2}{D^2-d^2}\left[2G_0 - 2G_1\left(\frac{a}{d}\right) + 3G_2\left(\frac{a}{d}\right)^2 - 4G_3\left(\frac{a}{d}\right)^3 + 5G_4\left(\frac{a}{d}\right)^4\right]\sqrt{\pi\frac{a}{Q}}, \quad (2.4)$$

ii) Longitudinal external surface crack in pipe subjected to internal pressure:

$$K_{\mathrm{I}} = \frac{pD^2}{D^2-d^2}\left[2G_0 + 2G_1\left(\frac{a}{d}\right) + 3G_2\left(\frac{a}{d}\right)^2 + 4G_3\left(\frac{a}{d}\right)^3 + 5G_4\left(\frac{a}{d}\right)^4\right]\sqrt{\pi\frac{a}{Q}}, \quad (2.5)$$

iii) Circumferential surface crack in pipe subjected to bending:

$$K_I = F \cdot \sigma_{\mathrm{b}} \cdot \sqrt{\pi\frac{a}{Q}}, \quad (2.6)$$

where the boundary correction factor is

$$F = A_0 + A_1 \cdot \beta + A_2 \cdot \beta^2 + A_3 \cdot \beta^3 + A_4 \cdot \beta^4 + A_5 \cdot \beta^5 + A_6 \cdot \beta^6, \quad (2.7)$$

where G_0~G_4 are determined by six order polynomials. p is the pressure, p_c is the crack face pressure if the pressure is acting on the crack face. The values of A_0 to A_6 are referred to the corresponding table sorted by the value of t/R_i, a/c, and a/t.

2.1.3 Discussion

On account of the overview in Sub-section 2.1.2, in this section, the state-of-the-art of the investigations is discussed from different perspectives.

2.1.3.1. Configurations of surface cracks and pipes

In light of the overview on surface crack growth in metallic pipes, the majority of the studies focused on Mode-I surface crack growth issues, where the surface crack propagates perpendicular to the normal stress, such as the longitudinal surface crack growth under internal pressure, and the circumferential surface crack growth under bending or tension. Most of the experimental investigations were conducted under four-point bending. Internal pressure [51] and tension [56] were included in the available documents as well, and their experimental results can be used to validate the numerical and analytical methods. Compared with experimental studies, the numerical approach is more flexible in terms of realizing the surface crack growth under different load conditions, such as combined loading cases [77, 79]. The Paris' law is the most common method for crack growth evaluation. While the argument still exists on whether the Paris' constants for the surface crack growth along the depth direction and the length direction are the same. Such experimental and analytical analysis on the generally surface crack growth is necessary.

2.1.3.2. Numerical simulation

Sub-section 2.2 summarised that the majority of the numerical analysis were conducted by means of the FEM. Other numerical methods, such as extended-FEM (X-FEM) [101] and S-version FEM [102], have been developed as alternatives for handling three-dimensional

surface cracks modelling. However, such methods stays in the trail phase that they have not been widely applied.

The adaptive re-meshing technique by FEM is a powerful tool, its time consuming and complicate conformal modelling and re-meshing procedures may hinder its application. While recently, approaches of applying apply the semi-elliptical crack modelling programme to simplify the crack modelling and re-meshing using FEM, are becoming more and more popular, such as the ANSYS workbench [103] and FRANC3D [104]. These series of software provide automatic crack modelling and meshing functions, as well as ensuring the accuracy of SIF evaluation. In addition, the built-in loop program, similarly as indicated in Figure 2.9, can realize the automatic simulation of crack growth process.

2.1.3.3. Analytical evaluation

Generally, the available analytical methods were developed based on the fundamental SIF evaluation method, by modifying the correction factors of load cases, crack profiles and geometry, mainly through two approaches: the numerical analysis method—the Newman and Raju's law, and the weight function method. The advantages of the numerical analysis method are that it is convenient for usage, and the values of geometrical parameters can be consecutively input into the formula to trace the crack growth process. In addition, the prediction scope is not limited to the deepest point and the surface point, but any points along the crack front which are determined by the eccentric angle φ. To date, these analytical methods were proposed for Mode-I semi-elliptical crack growth, thus such analytical methods for mixed-mode surface crack growth, and irregular shaped surface crack are unavailable.

The advantage of the weight function method is that it has a wide range of adaptations by introducing weight functions respectively, such that influential factors like welding effects and geometry factors could be considered [105]. However, the disadvantages of weight function methods are: first, the SIFs evaluation were restricted to the surface point and the deepest point, rather than along the whole crack front; second, since F is calculated by high order polynomials within which the coefficients are determined by discrete values tabulated in a table index, it is infeasible to continuously evaluate the SIF during the crack propagation, which means it is impracticable to trace the surface crack growth.

An accurate analytical result might not be achieved by hand calculation; therefore, a rational analytical approach can be developed based on extensive numerical studies. The analytical method of evaluating the SIF of surface cracks in metallic pipes has been developed in recent years with the assistance of FEM, which might be an appropriate choice.

2.1.4 Summary

Through the literature review on the surface cracks in offshore metallic pipes from the experimental, numerical, analytical perspectives, as well as the discussion section, the conclusions of Section 2.1 can be drawn:

- In light of the experimental design, semi-elliptical notch is superior to other notch shapes, because it is in line with the reality, as well as offering a user-define notch size and crack aspect ratio. Four-point bending set-up can provide a pure bending moment on the surface cracked area, has been widely applied by previous studies. The beach marking technique is reliable and accurate to record the data of the crack size-cyclic numbers during the fatigue test, especially for the specimens attached with composite laminates.

- The FE method is the most reliable approach for SIF/J-integral evaluation. Modelling programme such as ANSYS workbench can be used to simplify the modelling process of semi-elliptical surface cracks. For the purpose of evaluating the crack growth rate by incorporating with the Paris' law, SIF is chosen as the fracture mechanics parameter. In view of the contradiction on whether the Paris' constants at the surface point and the deepest point were equal, in this dissertation, the Paris constants will be calibrate by the experimental data if needed.

- The Newman-Raju's method is superior to the weight function methods in terms of its continuity on evaluating the surface crack growth. Since an accurate analytical result might not be achieved by hand calculation, a rational analytical approach can be developed based on extensive numerical studies.

2.2 A literature review on composite reinforcement on intact and cracked metallic pipes

2.2.1 Introduction

Surface cracks need to be repaired instantly to maintain the structural integrity of the pipeline systems towards their design service lives. Currently there are four traditional maintenance methods for offshore metallic pipes: grinding, welding steel sleeve, grouted clamp and pipe replacement (see in Figure 2.10). Grinding is the most simple and cost-effective method. While, it can only be applied when the crack depth is smaller than 1/4 of the wall thickness, and it might cause secondary damages as well [37]. Welding steel sleeve is a cost-effective repair method for onshore pipes [106]; nevertheless, the following disadvantages indicate that it is not suitable for offshore pipe maintenance [21]: operation required to be shut down as welding around metallic pipes is dangerous; in addition, welding may cause secondary damage; what's more, it is also difficult and costly to conduct welding under water. Grouted clamp installation, which is a permanent repair method, has been successfully applied in the offshore industry; however, the following disadvantages restricted its application [107] grouted clamp corrosion, complicated installation, heavy dead load, and pre-design for potential damages. The last maintenance method is the pipe replacement. As the most expensive and time-consuming method, it is only acceptable when severe damages occurs [106].

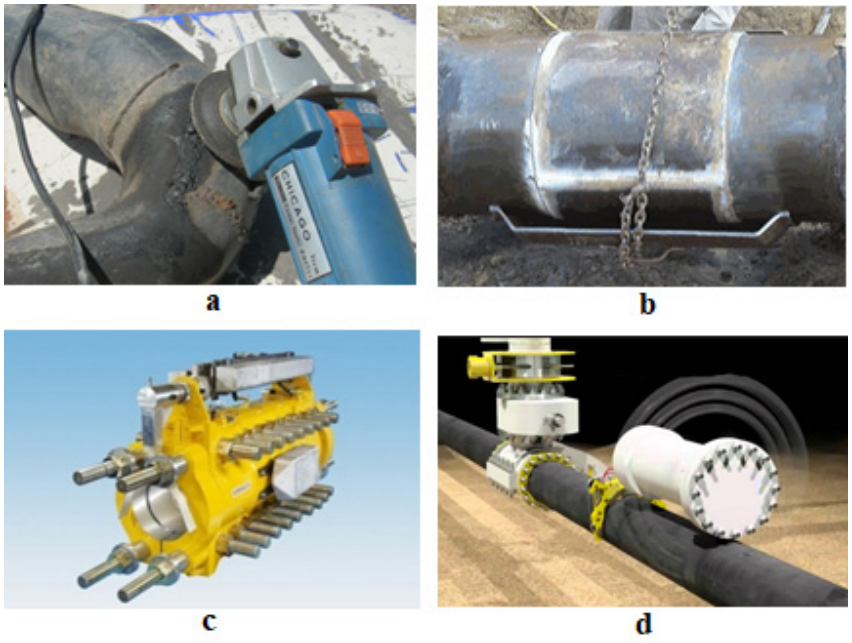

Figure 2.10. Traditional repair techniques of metallic pipelines: a) grinding; b) pipe replacement; c) grouted clamp; d) welding steel sleeve [26]

The CRS has been recognized as an efficient and advanced repairing technique in the piping industry [108]. It has been highly valued for the outstanding advantages in terms of effectiveness, time-saving, cost-effectiveness, no secondary damage and ease of installation [26]. At present, CRS on repairing cracked pipes are designed under the guidance of ISO 24817 [38] and ASME PCC-2 [109], which are based on the ultimate strength theory or the rule of thumb. Their design philosophy aims to rehabilitate the load bearing capacity rather than focusing on the FCGR. In recent years, researchers conducted studies on composite repaired fatigue cracked metallic pipes, for the purposes of identifying the repairing mechanism and its effect on the FCGR [110]. Failure modes such as crack-induced debonding and their negative effect on the reinforcement have been determined as well [111]. Those investigations raised the confidence toward the CRS application on repairing the cracked metallic pipes.

To date, the controversy on whether CRS is appropriate for repairing leaking—through-the-thickness cracked pipes still exists. The rebuttal is that leakage with high pressure will seriously damage the composite laminates. In addition, even under low pressure conditions, the leaked oil and gas might cause considerable erosion to the CRS. As a consequence, cracked metallic pipes should be repaired within the surface cracking stage, in order to prevent leakage and even collapse.

Surface cracks, however, in most cases propagating as a semi-elliptical shape, is more complex than through-thickness cracks in terms of their three-dimensional configuration. They propagate along multiple directions perpendicular to the semi-elliptical crack front, particular along the depth direction and the length direction. However, offshore metallic pipes are prone to circumferential surface cracks due to girth weld issues. The study of

circumferential surface crack growth in metallic pipes reinforced with CRS is absent from the open literature.

On account of the very limited number of investigations into the CRS repairing on surface cracked offshore metallic pipes, this section extended the research scope by conducting a survey on CRS reinforcing intact pipes and through-thickness cracked pipes. These studies shared related research interests in terms of composite reinforcing schemes, mechanical response and failure mechanism, which will facilitate the following investigations on reinforcing surface cracked metallic pipes. Sub-section 2.2.2 overviews the studies of composite reinforcement on metallic pipes. Then in Sub-section 2.2.3, the investigations of composite reinforcement on cracked metallic pipes have been overviewed. Then based on the topic of composite reinforcement on surface cracked metallic pipes, the state-of-the-art based on the available literature is discussed. A brief summary of this section was addressed in Sub-section 2.2.4.

2.2.2 An overview of composite reinforcement on metallic pipes

Table 2.4. The available studies of CRS strengthening intact metallic CHS structures

No.	Authors	Year	CHS Material	Composite material	Method	Load type	Results
1	Zeinoddini [112, 113]	2002, 2008	Steel	CFRP	Experimental, numerical	Impact	Impact damage
2	Seica and Packer [30]	2007	Steel	CFRP	Experimental	Bending	Strength, stiffness
3	Haedir, et al. [28]	2009	Steel	CFRP	Experimental	Bending	Strength, stiffness, ductility
4	Haedir, et al. [114]	2010	\	CFRP	Analytical	Bending	Ultimate strength
5	Haedir, et al. [115]	2011	\	CFRP	Analytical	Bending	Moment-curvature response
6	Haedir and Zhao [116]	2012	\	CFRP	Analytical	Bending	Load capacity
7	Mally, et al. [117]	2013	\	CFRP	Experimental	Internal pressure	Strength, underwater curing
8	Gao, et al. [118]	2013	Steel	CFRP, GFRP	Experimental	Compression	Buckling behaviour
9	Kabir, et al. [27]	2016	Steel	CFRP, GFRP	Experimental, numerical	Bending	Strength, stiffness, parametric study
10	Kumar and Senthil [32]	2016	Steel	CFRP	Experimental	Axial static and axial cyclic load	Stiffness, load bearing capacity
11	Kabir, et al. [119]	2016	Steel	CFRP, GFRP	Experimental	Bending	Durability in sea water
12	Kabir, et al. [120]	2016	Steel	CFRP, GFRP	Experimental, numerical	Bending	Durability in cold weather
13	Wu, et al. [121]	2018	Steel	CFRP, GFRP	Experimental	Torsion	Torsional capacity
14	Tafsirojjaman, et al. [122]	2019	Steel	CFRP	Experimental	Bending	Stiffness, ductility

The mechanical response and bond behaviour of intact metallic pipe reinforced with CRS have been extensively investigated. Table 2.4 lists available studies of using CRS to strengthen intact metallic CHS structures, indicating that most of the investigations were concentrating on enhancing the strength, stiffness, load bearing capacity, and ductility. The To date, the available literature of surface cracked metallic pipes reinforced with CRS is very limited; hence, the research scope broadens to composite reinforcement on cracked metallic pipes. These studies sheared similar concerns with the research of CRS on external surface crack metallic pipes, because in both cases, the adhesive layer directly contact with the crack. In such situation, interfacial failure should be concern, in case it generated a negative influence onto the composite repairing. In this sub-section, the studies of composite reinforcement on cracked metallic pipes have been overview, where the available literature has been listed in Table 2.5.

A majority of the studies were conducted by means of experimental approach. Among those studies, Carbon Fibre Reinforced Polymer (CFRP) was generally used as the reinforce material. In some studies, together with CFRP, Glass Fibre Reinforced Polymer (GFRP) has been applied for the purpose of preventing galvanic corrosion as well.

Seica and Packer [30] investigated the rehabilitation of steel pipes with CFRP, emphasising on underwater applications. Two principal performance parameters of the wrapped pipes—in-air curing versus underwater, were investigated. The results indicated that the ultimate bending strength, flexural stiffness and rotation capacity were increased owing to the reinforcement. The specimens using underwater composite and resin materials as well as curing underwater performed less effect than the specimens cured in-air. However, using a hybrid reinforcement scheme that applying a better performed composite material and underwater curing resin outperformed all other specimens, even the specimens cured in-air, indicating the selection of matrix and composite materials are of utmost importance. In addition, no serious debonding was observed in any specimens, suggesting the composite laminates bonded adequately regardless of the wrapping and curing conditions.

Haedir et. al. [28, 114-116] systematically studied composite reinforcement on metallic CHS structures by experimental and analytical approaches, including ultimate strength, stiffness, ductility, load capacity, and bucking resistance. Extensive studies have been conductd on wrapping orientations bucking resistance to achieve the optimum nominal strength gain with higher rotation ductility [28]. Thereafter, analytical approaches for calculating the ultimate strength [114], moment-curvature response [115], and capacity [116] of CFRP-reinforced steel CHS structures have been presented successively.

In recent years, Kabir, et al. [27] conduted a research on the CRS reiforcing on steel CHS structures as well, for the purpose of enhancing the strength and stiffness. Besides CFRP, a layer of GFRP as the contact inhibitor between the steel substrate and CFRP laminates has been applied to prevent the potential galvanic corrosion. Within the study, a parametric study through a validate FEM has been conducted, by which the influence from wrapping orientation, bond length, section type, tensile modulus of CFRP, thickness of adhesive, and

type of adhesive were discussed. Then, the influence of sea water environment [33] and cold weather has been discussed [123], respectively. Results indicated that failure modes, such as CFRP rupture and local bucking, were affected by environment conditions.

Tafsirojjaman, et al. [122] conducted an experimental study on composite reinforced CHS structures subjected to monotonic bending and cyclic bending. He found the cyclic loading has very little effect on both bare and CFRP strengthened CHS steel members' moment capacity, indicating the monotonic behaviour would provide sufficient envelope for hysteretic behaviour of bare and composite reinforced CHS structures. The composite reinforced CHS structures shown superior performance of moment capacity and strength over bare CHS structures under both the monotonic and cyclic bending loads. The research also pointed out that the properties of adhesive did not have much effect on the overall structural performance of CFRP strengthened CHS structures as the stiffness of the CFRP was the dominant factor of the CRS.

The composite reinforced CHS structures subjected to other load cases, such as impact loads [113], internal pressure [117], axial loads [32, 118], and torsion [121] has been investigated. The results indicated the reinforcing effectiveness on increasing load bearing capacity, stiffness, or strength. Together with the studies conducted under bending loads, the composite reinforcement has been proved as an efficient method to increase a variety of mechanical properties of metallic CHS structures.

In summary, the above studies have created the foundation for composite reinforcement on metallic pipes. A variety of general reinforcement issues have been investigated, i.e., the influence induced by the reinforcement schemes such as composite wrapping patterns, the properties of adhesive and CFRP, the thickness of adhesive and CFRP, and the influence of underwater curing. Those findings paved a way for the further investigations of composite reinforcement on cracked metallic pipes under cyclic loads.

2.2.3 An overview of composite reinforcement on cracked metallic pipes

2.2.3.1 Investigation approach

Table 2.5 clearly indicated the FEM is the main investigation approach, where SIF is the major fracture mechanics parameter. Identical to the studies on surface crack growth in metallic pipes, the fatigue life was predicted using the Paris' law. Besides, Strain energy release rate has been applied as the fracture mechanics parameter as well [124]; while for the purpose of evaluating the fatigue life, the energy release rate was eventually deduced to SIF.

Besides FEM, in recent years, X-FEM has been applied to simulate the fatigue life of the cracked metallic pipes repaired by CRS. Zarrinzadeh, et al. [125] first verified the X-FEM of simulating various cracked structures reinforced with CRS, such as plate, shell, and pipes. Then, by means of the X-FEM and the cohesive zone model, the fatigue life of a composite reinforced cracked steel pipe under axial tension was predicted [126], which agreed well with

the experimental results [127]. Such method was applied to simulate the cracked steel pipe under internal pressure reinforced with CRS as well, indicating the reinforcement decreased the crack tip opening angle (CTOA), crack opening displacement (COD) and the crack opening area (COA) [128].

Experimental approach was general adopted in several studies for validation purposes. Such method is of great importance due to the uncertainties induced by the interfacial behaviour—the occurring of crack-induced debonding during the crack process would reduce the reinforcement effectiveness on prolonging the fatigue life [126, 129]. While among most of the studies on repairing through-the-thickness cracked pipes, this issue was not considered.

Table 2.5. The available studies of CRS repairing on cracked metallic CHS pipes

No.	Authors	Year	Pipe Material	Composite material	Method	Load type	Results
1	Lam, et al. [130]	2011	Steel	CFRP	FEM	Axial tension	SIF, fatigue life
2	Ghaffari and Hosseini-Toudeshky [131]	2013	Steel	GFRP	FEM	Internal pressure	SIF
3	Chen and Pan [132]	2013	Steel	GFRP	FEM, analytical	Internal pressure	SIF
4	Benyahia, et al. [133]	2014	Steel	GFRP	FEM	Internal pressure	SIF
4	Meriem-Benziane, et al. [35]	2015	Steel	CFRP	FEM	Internal pressure	SIF, safety factor
5	Woo, et al. [124]	2016	Steel	BFRP, CFRP	FEM	Axial tension	Strain energy release rate
6	Achour, et al. [34]	2016	Steel	CFRP	FEM	Bending	SIF
7	Zarrinzadeh, et al. [125]	2016	Steel	GFRP	X-FEM	Internal pressure	Fatigue life
8	Zarrinzadeh, et al. [127]	2017	Aluminium	GFRP	Experimental and numerical	Axial tension	Fatigue life
9	Zarrinzadeh, et al. [126]	2017	Aluminium	GFRP	X-FEM	Axial tension	Fatigue life, crack-induced debonding
10	Liu, et al. [134]	2017	Aluminium	CFRP	Experimental and FEM	Axial tension	SIF, fatigue life
11	Valadi, et al. [128]	2018	Steel	CFRP/GFRP	X-FEM	Internal pressure	CTOA, COD, COA
12	Belhadri, et al. [135]	2019	Steel	GFRP	FEM	Internal pressure	SIF

2.2.3.2 Crack configurations

In general, through-the-thickness cracks repaired by CRS were studied. The crack were either along the longitudinal direction under internal pressure [128, 131], or along the circumferential direction under internal pressure [133] or axial tension [124, 127, 130, 134].

There were quite a few studies concentrated on semi-elliptical surface crack in metallic pipes reinforced with CRS. Chen and Pan [132] conducted a numerical research on using FRP

to repair axial internal surface cracked reinforced with GFRP under internal pressure, the results shown the reinforcement decreased the SIF evenly along the crack front. Belhadri, et al. [135] investigated the external surface crack in steel pipe reinforced with GFRP under internal pressure, proving the efficiency of fatigue life extension in such a case. While, possible interfacial failures were not considered.

2.2.3.3 Load cases

Load cases including axial tension and internal pressure have been extensively investigated. Those studies discussed the effectiveness of composite reinforcement on decreasing the crack growth rate and prolonging the residual fatigue life. An early study indicated that external bonded CRS were preferred when the shell is under an internal pressure while internal bonded CRS are preferred when under an external pressure [136]. For both load cases, increasing the bond thickness/layers of composite is an effective approach of improving the reinforcement. Except internal pressure and tension, bending load was investigated. Achour, et al. [34] pointed out the major disadvantage is the infeasibility of applying the internally bonded CRS to equilibrate the stress transfer between the internal and external crack tip. However, the composite reinforcement was still significant efficient to extend the lifespan of the cracked pipe.

2.2.4 Discussion

On account of the overviews in Sub-sections 2.2.2 & 2.2.3, the state-of-art is discussed based on the topic of composite reinforcement on surface crack metallic pipes. The external surface crack directly contacts with adhesive layer while the internal surface crack does not; thus, the mechanisms of reinforcing internal surface crack and external surface crack are different, the internal surface crack and external surface crack therefore are needed to be discussed respectively.

2.2.4.1 Internal surface cracked pipe reinforced with CRS

The stretch diagram of internal surface cracked pipe reinforced with CRS is shown in Figure 2.11. Basically, there are two important constituent parts of internal surface cracked pipes reinforced with CRS: the internal surface crack growth in pipe and the intact pipe reinforced with CRS. The investigation of internal surface cracked pipe reinforced with CRS can be approximately equal to the sum of these two constituent parts. The reason is that there are two main factors which dominate the reinforcement system: internal surface crack growth in metallic pipes and the bonding behaviour of intact pipe reinforced with CRS. Under such situation, the design and analysis process can refer to the related investigations on surface crack growth in metallic pipes which were reviewed in Section 2.1 and the studies on intact metallic pipes reinforced with CRS which were reviewed in Sub-section 2.2.2. For example, the SIF of the reinforced surface crack, as well the crack growth rate and the fatigue life extension can be evaluated by the similar methods proposed by investigations on surface cracked pipes. In addition, the influential parameters towards an optimum design of the

composite reinforcement on internal surface cracks can refer to the investigations on intact pipes reinforced with CRS. While whether the effectiveness of the reinforcement is derived from the enhancing of the strength and stiffness of the cracked pipes needs further investigations.

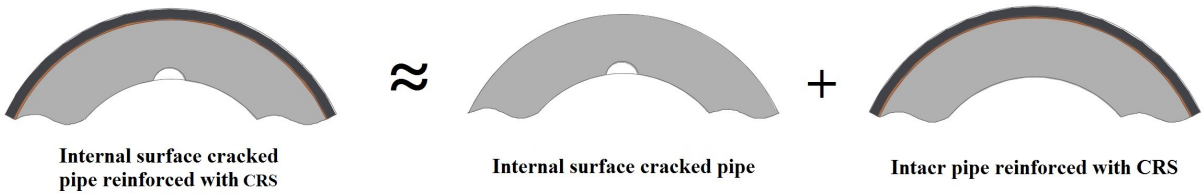

Figure 2.11. The relation between internal surface cracked pipes reinforced with CRS and its two constituent parts

2.2.4.2 External surface cracked pipe reinforced with CRS

The stretch diagram of external surface cracked pipes reinforced with CRS is shown in Figure 2.12. In such a case, the external surface cracked pipe reinforced with CRS is not equal to the sum of its two constitute parts. The first reason is when the adhesive layer directly contact with the surface crack, the crack-bridging effect owing to the composite repairing, which decreases the crack growth rate by decreasing the COD, has to be taken into consideration. Secondly, local interfacial failures might occur around the cracked area, such as crack-induced debonding, cohesive failure and delamination, as shown in Figure 2.13. These failures might induce negative effect on the composite reinforcement in return.

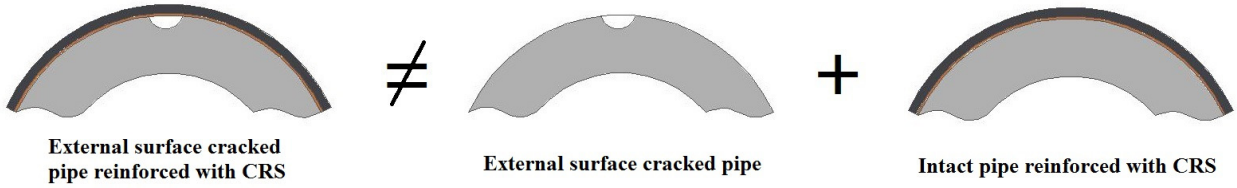

Figure 2.12. The relation between external surface cracked pipes reinforced with CRS and its two constituent parts

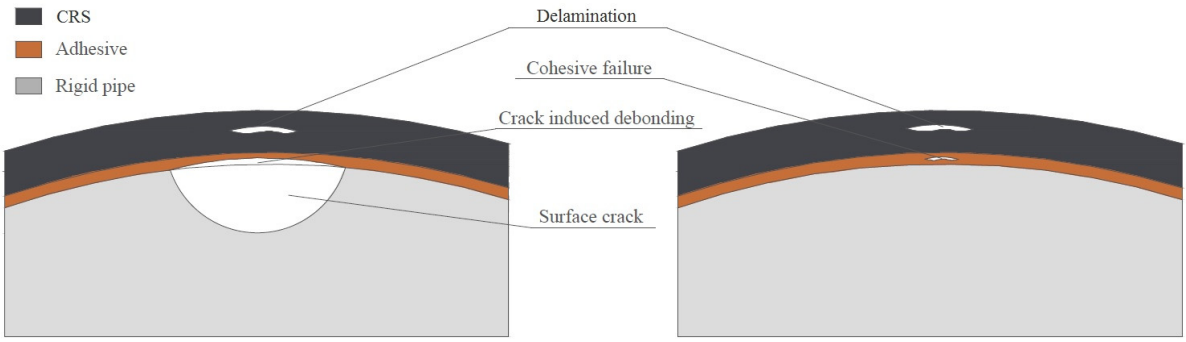

Figure 2.13. Possible failure modes of using CRS to repair external surface cracked pipes

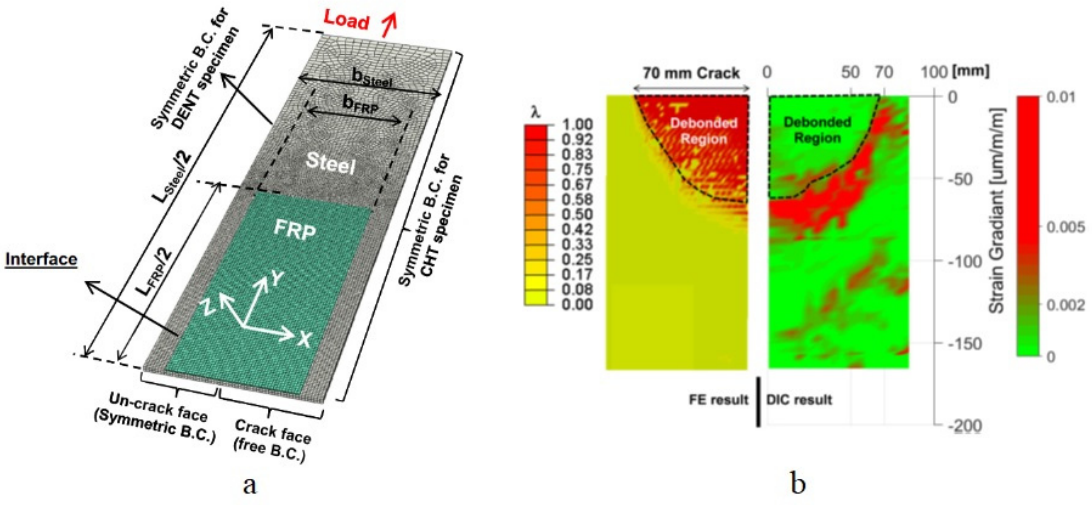

Figure 2.14. a) Half FE model of using FRP to reinforce a through-the-thickness cracked steel pipe subjected to tensile load; b) the crack-induced debonding region indicated by the numerical and experimental approaches (the other half mode to figure 2.14a) [111]

Based on the studies of composite reinforcement on through-the-thickness cracked pipes and intact pipes, the crack-induced debonding (see in Figure 2.14) [111] might occur during the surface cracking process. The λ in the figure indicates the degree of the stiffness degradation. In the region where λ equals to 1, it is considered debonded. While other failure modes including delamination, cohesive failure had small chances to occur. Therefore, the possible failure modes and their influence on the composite reinforcement need to be identified and analysed by the experimental and numerical studies.

2.2.5 Summary

In this section, available studies of composite reinforcement on intact metallic CHS structures and cracked metallic pipes are overviewed. Then a brief discussion has been made based on the topic of composite reinforcement on surface crack metallic pipes. Reinforcing the intact pipe with CRS, as a general and fundamental research issue, offered inspirations of CRS on surface cracked metallic pipes, such as the basic reinforcement method and influential parameters. These investigations, together with the investigations on surface crack growth in metallic pipes, paved a solid way to the investigation of the internal surface cracked metallic pipes reinforced with CRS. The other research topic on composite reinforcement on through-the-thickness cracked metallic pipes, laid the foundation for the investigation on external surface crack growth in metallic pipes reinforced with CRS.

2.3 Conclusion

In this chapter, the available studies on surface crack growth in metallic pipes and composite reinforcement on metallic pipes have been reviewed, respectively. The questions regarding the state-of-art, as well as the circumferential surface crack growth in metallic pipes are clarified. The conclusions of this chapter can be drawn as follows:

- To date, the weight function method is used to evaluate the SIF of the circumferential surface cracks in metallic pipe subject to bending. However, this method is infeasible to continuously evaluate the SIF during the crack growth process, such that it is impracticable to trace the surface crack growth. The Newman-Raju's method is superior to the weight function methods in terms of its continuity on evaluating the surface crack growth. Within the development of the FE modelling, a rational analytical approach can be developed based on extensive numerical studies.

- The stress gradient effect owing to the bending load case and the pipe geometry might be the hinge of proposing an analytical method to evaluating the SIF of the circumferential surface cracked pipes. In this regard, based on the methodology of the Newman-Raju's method, proposing the correction factors in regards to the load case and pipe geometry is the possible solution.

- The failure modes of using CRS to repair surface cracks might be refer to the studies of using CRS to reinforce the intact pipes, since the influence of the internal surface crack onto the reinforcement system might be negligible. However, possible failure mode such as crack-induced debonding might occur when reinforcing the external surface crack. Such issue and their effects are needed to be identified by following experimental and numerical analysis.

In the following chapters, those unsolved problems will be investigated successively. The following Chapter 3, the circumferential surface crack growth in metallic pipes is investigated via a numerical approach and an experimental validation, for the purpose of proposing an analytical method to predict the crack growth process. The methods of evaluating surface crack growth and analysis the mechanical behaviour of the pipe will be a basis for the following studies on composite reinforcement on the surface crack metallic pipes.

Chapter 3 Circumferential surface crack growth in offshore metallic pipes*

One major purpose of this chapter is to pave a way for the following research in Chapter 5 and Chapter 6 of proposing an analytical method of evaluating the SIF of the surface crack in metallic pipes reinforced with CRS. For this purpose, an analytical method on evaluating the SIF of surface cracks in pipes without composite reinforcement is proposed.

In this chapter, circumferential surface crack growth in metallic pipes subjected to fatigue tension and bending is investigated. In light of pipe geometry and bending load case, the analytical formula is raised by introducing new bending correction factors and new geometry correction factors on the basis of the Newman-Raju's method. The bending correction factors are deduced based on the bending stress gradient, while the geometry correction factors are determined by parametric studies for internal surface cracks and external surface cracks respectively. Owing to a large data set requirement by the parametric studies, three-dimensional FE models of evaluating SIFs of circumferential surface cracks are developed. The FEM is validated to ensure that it could provide accurate SIF estimations. Analytical verification is conducted which shows that the SIF evaluated by the proposed analytical method match well with the results evaluated by the recommended analytical method. Then experimental investigations of external surface crack growth in offshore metallic pipe subjected to fatigue bending are implemented to further validate the analytical method of predicting surface crack growth rate. The analytical results match well with the test results and the available experimental data from literature, indicating that the analytical method can be used for practical purposes and facilitate the crack growth evaluation and residual fatigue life prediction of cracked metallic pipes.

* This chapter is based on the published journal article—[43] Z. Li, X. Jiang, H. Hopman, L. Zhu, and Z. Liu, "An investigation on the circumferential surface crack growth in steel pipes subjected to fatigue bending," *Theoretical and Applied Fracture Mechanics,* vol. 105, p. 102403, 2020.

The structure of this chapter is assigned as follow: in Section 3.1, three-dimensional FE models of evaluating SIFs of circumferential surface cracks are first developed and validated. In Section 3.2, the analytical formula is deduced, of which its geometry correction factors are determined by means of FE-based parametric studies. In Section 3.3, the proposed analytical method of evaluating the SIF is verified by a recommended analytical method. In Section 3.4, experimental studies of circumferential external surface crack growth in metallic pipes subjected to fatigue bending are conducted. Together with available experimental data from literature, the analytical method is validated. Then in Section 3.5, the analytical method is deduced to predict the SIF of surface cracked metallic pipes subjected to bending and tension, which is further verified by the FEM. Finally the conclusions of this chapter are stated in Section 3.6.

3.1 Three-dimensional FE analysis

The three-dimensional FEM is a reliable method to evaluate SIFs of surface cracks. Rational results can be obtained through proper modelling methods [49]. In order to guarantee the accuracy of SIF evaluation, a sensitivity analysis is first conducted to determine appropriate modelling strategy (e.g., element type, meshing size, modelling contours and divisions around crack tip). Afterwards, using the modelling method, FE models of surface crack in pipe subjected to bending are developed and validated by available experimental data from literature to further ensure their feasibility for pipe scenario.

3.1.1 Surface crack modelling

The FE analysis is conducted using the commercial code ANSYS. Surface cracks are created through the *Semi-elliptical Crack* module in ANSYS workbench 19. In order to determine appropriate surface crack modelling strategy, a sensitivity analysis is carried out on a surfaced crack plate, as indicated in Figure 3.1. In order to generate ordered elements around the crack front, six contours which are concentric circles centred on the crack front with a number of divisions are modelled, as shown in Figure 3.1b. The plate is modelled using ‘solid186’ which is a high order three-dimensional 20-noded solid element that exhibits quadratic displacement behaviour. The size of the plate is 400 mm long, 60 mm wide and 10 mm thick. One edge face of the plate is fixed supported, while a pure tension is applied on the other edge face. The surface crack is located at the middle of the plate, perpendicular to the tension load. It is semi-elliptical shaped, with crack depth a = 2.0 mm, half crack length c = 4.0 mm. The area in the plate around the surface crack applies tetrahedral meshing method, while the rest parts applies the hexahedral meshing method [137]. Since the whole plate is modelled as one part, the contact between the tetrahedral mesh are and the hexahedral mesh area is not needed, and the coincident nodes are merged automatically. The surface crack uses hexahedral dominant meshing method [49]. Then the SIFs along surface cracks are evaluated through the contour integral method, and compared with the Newman-Raju’s analytical method [85], as shown in Figure 3.2 and Figure 3.3. The normalised SIF is defined as the ratio of the FE calculated SIF and the calculated SIF by Newman-Raju’s equation.

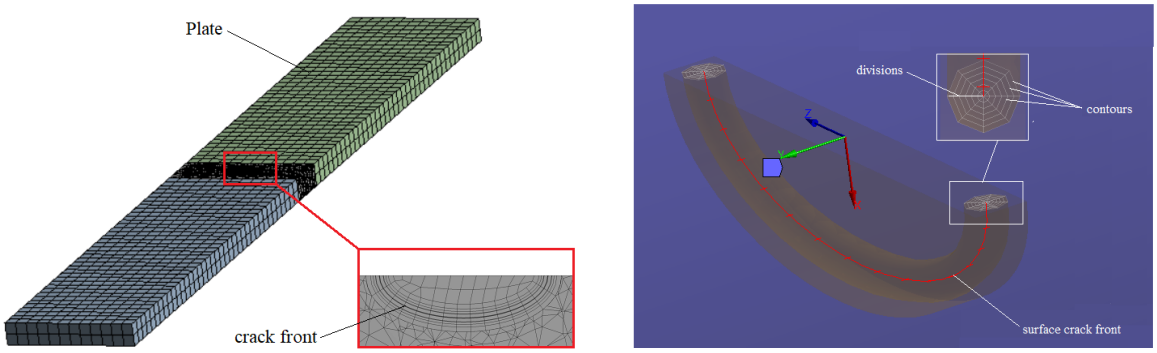

Figure 3.1. Surface cracked plate model for sensitivity analysis purpose: a) global meshing condition and local meshing condition around the surface crack; b) contours around the surface crack front and their divisions

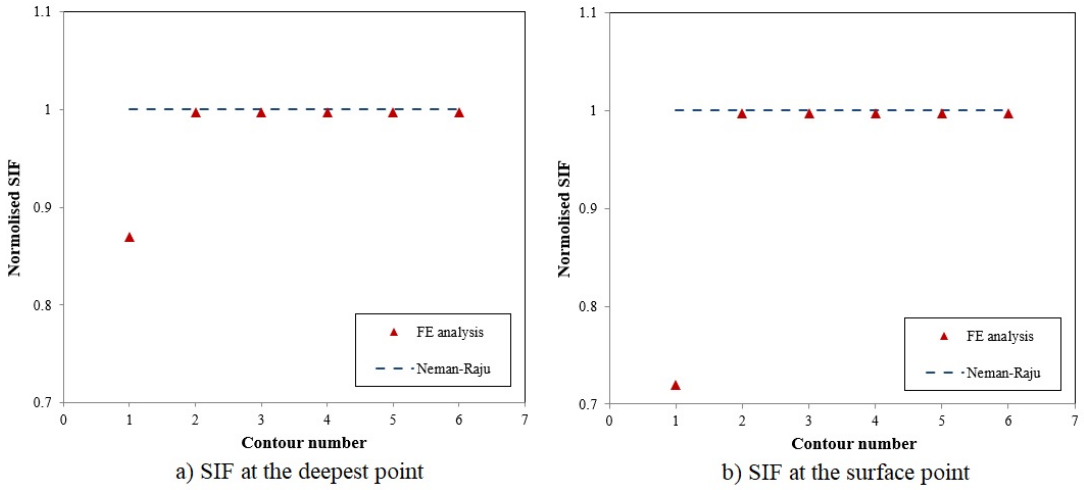

Figure 3.2. Sensitivity study of contour numbers

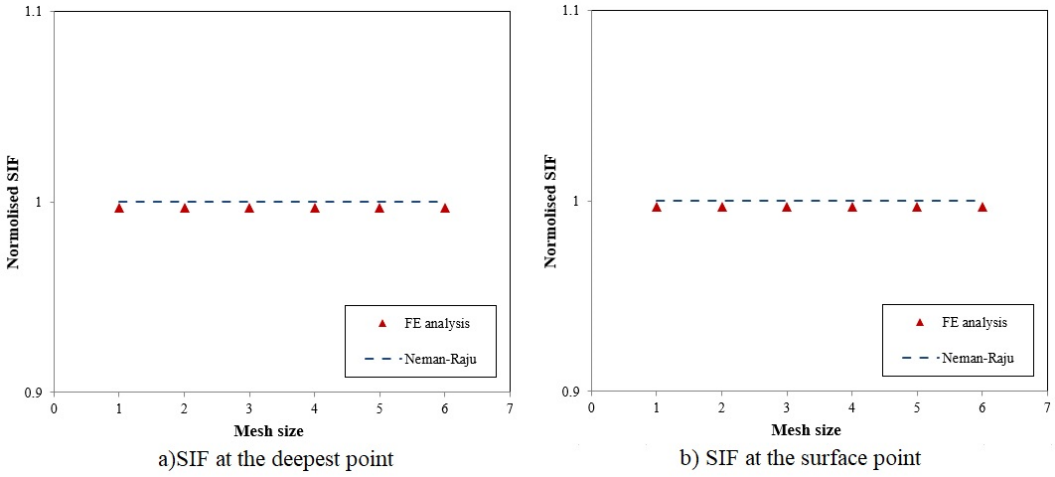

Figure 3.3. Sensitivity study of element size of the elements around the surface crack

The comparing results shown in Figure 3.2 indicated that the SIF should be obtained at least from the third contour. The mesh sensitivity study shows that the SIFs obtained from the

deepest point and the surface point using a tetrahedron meshing method has a good agreement with the Newman-Raju's method [5], whereas the mesh size of the elements around the surface crack does not significantly influence the SIFs, as shown in Figure 3.3. In this study, to ensure a robust and accurate evaluation, a 2.0 mm element size is adopted for the areas around the surface crack, and the mesh size around the surface crack front is controlled by the number of contour and their divisions (see in Figure 3.1b); while for the other area a 5.0 mm element size is used. Although the interview in sub-section 2.1.2.2 indicated the minimum angular discretisation of the elements of 30° (12 divisions around the crack contour) is recommended [64], in this study, we investigate the sensitive of the division numbers of each contour from 8 to 20, indicating the division number in this model has a negligible influence on the SIF evaluation; eventually, eight divisions of each contour are chosen.

3.1.2 The FE analysis of surface cracked metallic pipes subjected to bending

Since the surface crack modelling strategy has been determined, the modelling method is applied to the FE analysis of circumferential surface cracked metallic pipes subjected to bending. As illustrated in Figure 3.4a of the 4-point bending scenario, the pipe is positioned horizontally, supported by two support units. A pair of vertical loads are applied on the load units, generating a bending moment M onto the pipe. Therefore, the nominal bending stress σ_b can be calculated as

$$\sigma_b = \frac{M}{\frac{\pi \cdot D^3}{32} \cdot \left(1 - \frac{d^4}{D}\right)} \tag{3.1}$$

where σ_b is the maximum bending nominal stress, D and d are the external and internal diameter of the pipes respectively. The surface crack is circumferentially located in the middle of the tension side of the pipe model, either in the internal surface or the external surface, propagating in the cross-section plane, as shown in Figure 3.4b. The details and shape parameters of the surface crack is shown in Figure 3.4c. Figure 3.5 shows the metallic pipe model and the meshing conditions. The metallic pipe is created by three merged parts for different meshing purposes: required by the crack modelling method, the middle part where the surface crack is located uses tetrahedral meshing method; while the other two parts are meshed using sweep meshing method. Hexahedral dominant meshing method is adopted for the surface crack.

In order to ensure the accuracy of the pipe models, the FEM is further validated by available experimental data from literature, i.e., three sets of internal surface cracked pipes subjected to bending [52] and two sets of external surface cracked pipe subjected to bending [54]. Table 3.1 lists the five test specimens, along with the 4-point bending setup, material properties, size of the pipes, initial crack sizes, and load condition. Then the five FE models are built in the light the corresponding specimen sizes, crack dimensions and load condition. Afterwards, the SIFs of surface cracked metallic pipes subjected to bending are calculated. Then, incorporate with Paris law which is

$$\mathrm{d}a/\mathrm{d}N = C(\Delta K_{\mathrm{Ia}})^m, \tag{3.2}$$

$$\mathrm{d}c/\mathrm{d}N = C(\Delta K_{\mathrm{Ic}})^m, \tag{3.3}$$

the crack growth rate along the length direction and depth direction are estimated respectively. In Eq. (3.2) and Eq. (3.3), $\mathrm{d}a/\mathrm{d}N$ and $\mathrm{d}c/\mathrm{d}N$ are the crack growth rate along the depth direction and along the length direction respectively, ΔK_{Ia} and ΔK_{Ia} are the range of SIFs of the deepest point and the surface point respectively, C and m are two material constants which keep consistent with the referenced value, as listed in Table 3.2. Afterwards, by assuming a small amount of cycles, the increments of the crack length and depth are calculated. Eventually, it is possible to trace the surface crack growth along the two directions. The detailed procedure of evaluating surface crack growth is indicated in Figure 2.9.

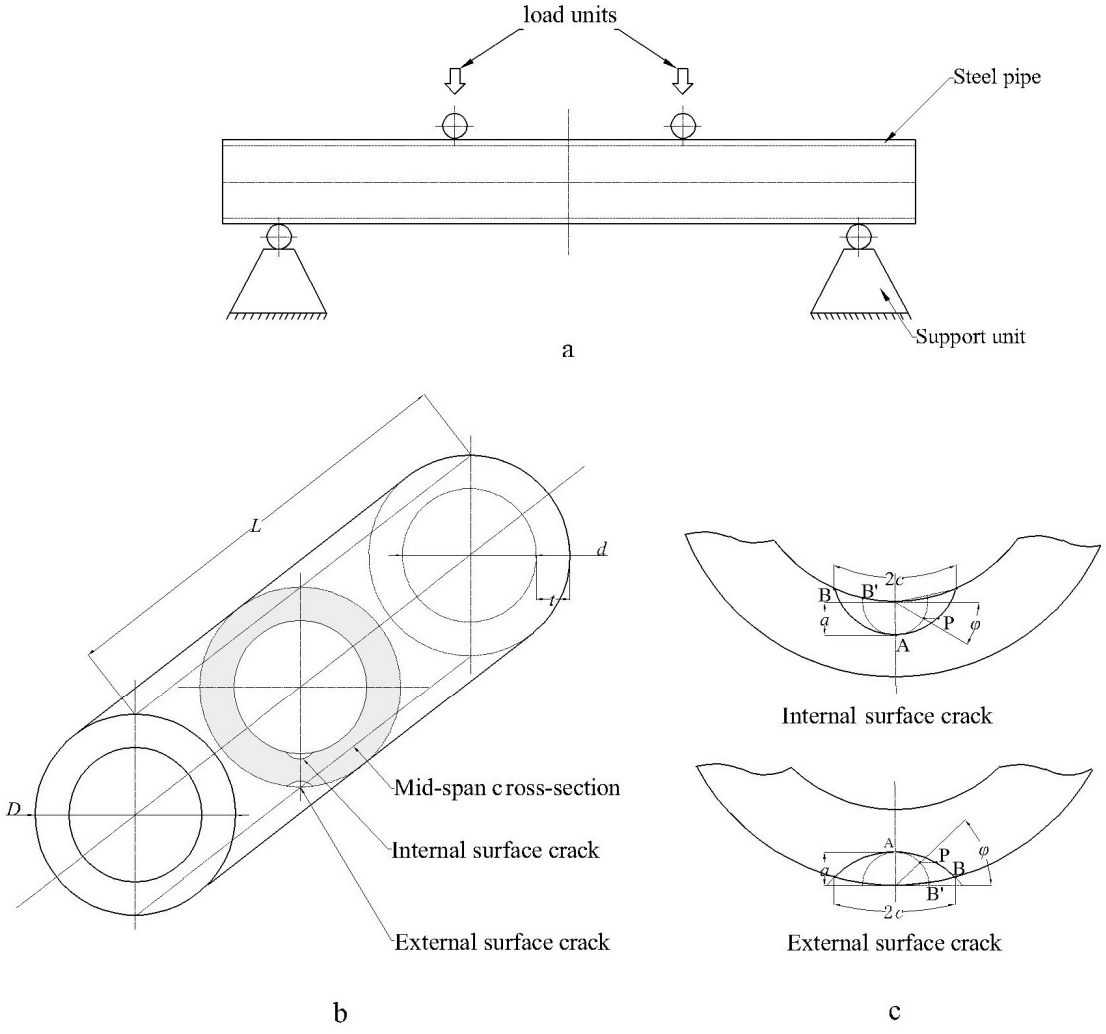

Figure 3.4. a) Schematic diagram of a surface cracked metallic pipe subjected to 4-point bending; b) the location of the internal and external surface crack; c) the dimensions of the internal and external surface crack

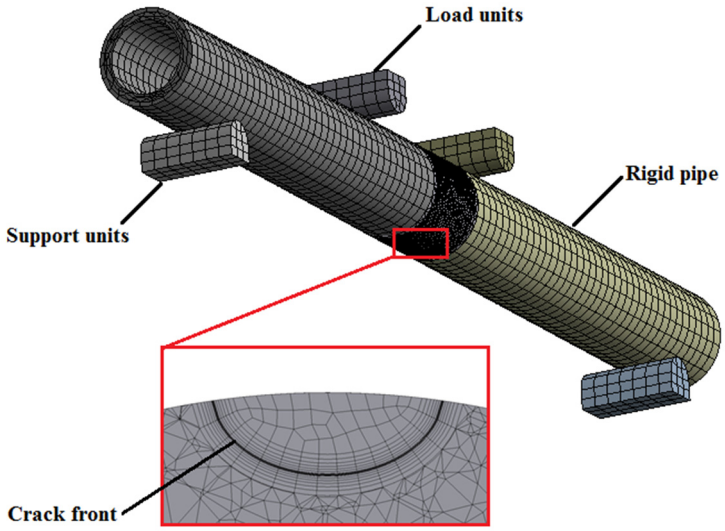

Figure 3.5. Global mesh condition of the FE model and the local meshing around the surface crack

Table 3.1. Detail information of FE models

Model index	Crack location	4-point bending set-up		Material properties		Notch and pipe size (mm)				Load condition (kN)	
		L_i (mm)	L_e (mm)	σ_y (MPa)	σ_u (MPa)	c	a	D	t	Max	Min
FI-1 [6]	Internal surface	245	1000	227	406	22.75	4.5	102	8.1	27.54	2.75
FI-2 [6]	Internal surface	245	1000	227	406	5.0	5.0	102	8.1	44.76	4.48
FI-3 [6]	Internal surface	245	1000	227	406	18.25	3.0	102	8.1	27.54	2.75
FE-1 [7]	External surface	600	1260	318	650	18.0	4.3	168	14.8	185.0	18.5
FE-2 [7]	External surface	600	4300	450	593	61.5	12.4	324	28.5	460.0	50.0

Note: L_i and L_e: internal and external span of the 4-point bending, σ_y: yield strength, σ_u: ultimate strength, c: half crack length, a: crack depth, D: external diameter of pipes, t: pipe wall thickness.

Table 3.2. The Paris constants for each specimen

Model index	Paris constant	
	C	m
FI-1 [6]	3.2×10^{-10}	3.72
FI-2 [6]	3.2×10^{-10}	3.72
FI-3 [6]	3.2×10^{-10}	3.72
FE-1 [7]	1.917×10^{-12}	3.195
FE-2 [7]	2.29×10^{-14}	4.4

Note: The Paris constant employed in crack growth calculations (in all cases examined, units for da/dN and dc/dN are mm/cycle, and the SIF in MPa/m$^{1/2}$, respectively).

The global stress distribution of FE model 'FI-2' and the local stress distribution around the internal surface crack on the internal surface are shown in Figure 3.6. Figure 3.6a shows that the stress concentrates in the mid-bottom of the pipe where the surface crack is located. More detailed, the local stress distributed around the surface crack as a butterfly shape is

shown in Figure 3.6b. Under the bending moment, the surface crack opening is observed (displayed as eleven times than the true scale).

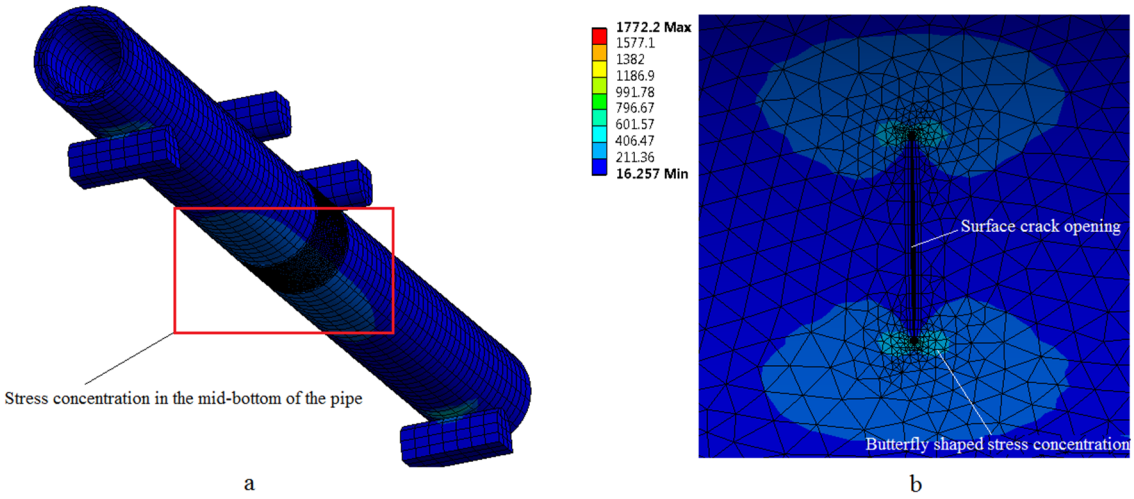

Figure 3.6. a) Global stress distribution of FE model 'FI-2'; b) local stress distribution around the internal surface crack

Figure 3.7 shows the comparison of *a*/*c* versus *a*/*t* between the FE results and the available experimental data of internal surface cracked metallic pipes. The FE results match well with the available experimental data from literature, which implies that the FEM is appropriate to evaluate the SIF of internal surface cracks. The comparisons of external surface crack growth results between the FEM and available experimental data are shown in Figure 3.8. The FE analysis gives accurate predictions of crack growth along both the depth direction and the length direction. In summary, the validations indicate that the FE analysis is suitable to evaluate the SIFs of circumferential external surface cracks in pipes subjected to bending. Note that external load cases examined here are characterized by stress ratio equal to $R = 0.1$. Then a parametric study on the basis of the FEM therefore will be implemented to determine the geometry correction factor of the analytical method in section 3.

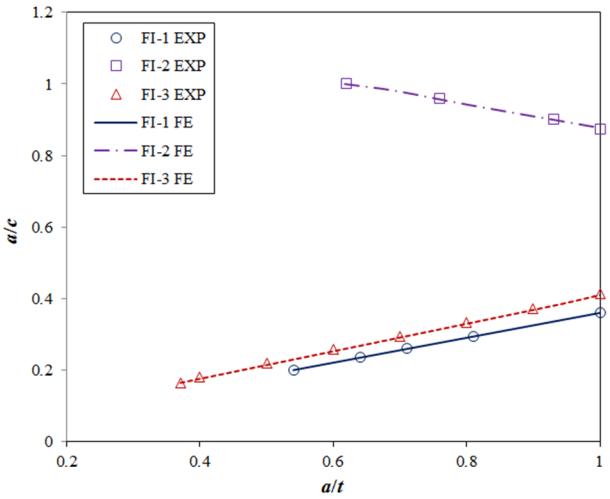

Figure 3.7. The comparison of a/c versus a/t between FE results and available experimental data of internal surface cracks [6]

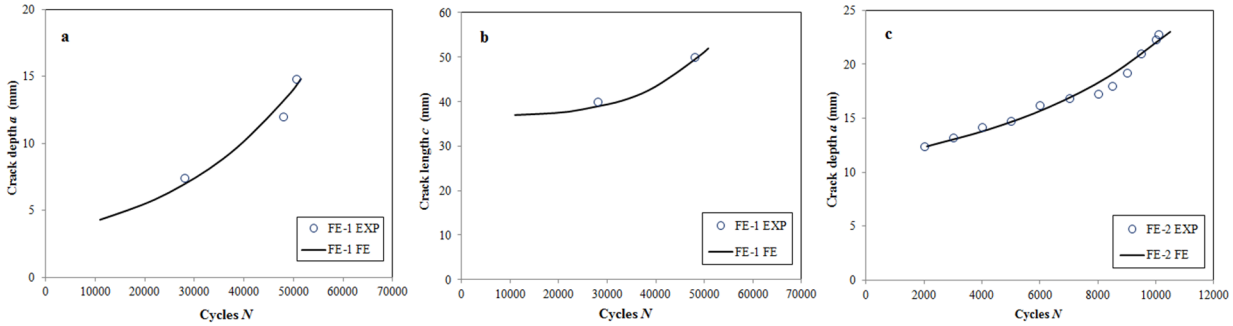

Figure 3.8. The comparison between the available experimental data and the FE results (FE-1 FE, and FE-2 FE): a) crack growth along the depth direction of FE-1; b) crack growth along length direction of FE-1; c) crack growth along depth direction *of FE-2*

3.2 The analytical method of evaluating the SIF of circumferential surface cracked metallic pipes subjected to bending

In general, surface crack growth rate is estimated by the Paris law [83], and the SIF is the assessment criteria,

$$K_{\mathrm{I}} = \sigma\sqrt{\pi A}\cdot F, \tag{3.4}$$

which is determined by the nominal stress σ, the crack dimension A, and the boundary correction factor F. In terms of surface cracks in a certain scenario, appropriate influential parameters are needed to be identified in order to give rational SIF evaluations. On this basis, researchers proposed a series of analytical methods [74, 92, 138-140].

The Newman-Raju's method, as the benchmark solution for surface cracked plane plate, is a well-recognized alternative [92]. This method is also employed in BS 7910 [20] for circumferential external surface cracks, which identifies σ and F by curving fitting and engineering judgement

$$K_{\mathrm{I}} = (\sigma_{\mathrm{t}} + H\sigma_{\mathrm{b}})\sqrt{\pi\frac{a}{Q}}F\left(\frac{a}{t},\frac{a}{c},\frac{c}{b},\varphi\right), \tag{3.5}$$

where σ_{t} and σ_{b} represents tension stress and bending stress respectively, H is a correction function for the bending nominal stress, $F(a/t, a/c, c/b, \varphi)$ is the boundary correction factor

$$F = \left[M_1 + M_2\left(\frac{a}{t}\right)^2 + M_3\left(\frac{a}{t}\right)^4\right] f_\varphi g f_w, \tag{3.6}$$

where M_1, M_2 and M_3 are the correction factor for the semi-elliptical shape of the crack, f_φ is the correction factor of the eccentric angle of surface cracks, and g can be regard as a correction factor of crack shape evolving along with crack propagation, f_w is a correction factor for the finite width of a plate geometry. The numerical method is capable to evaluate the SIFs of any stage during the crack growth process. In addition, besides the SIFs of the surface point and deepest point, the SIF of any point along the crack front is able to be

evaluated. However, Eq. (3.5) was originally proposed for flat plates, thus when applying it to cracked pipes, the SIFs are often underestimated [52, 54], leading to an overestimate prediction of the residual fatigue life, which might be dangerous for usage.

3.2.1 The bending correction factor

The bending correction factor *H* in Eq. (3.5) is developed for plate, which is inappropriate for pipe scenario. Here the new bending correction factor *G* by considering the stress gradient of pipe subjected bending is introduced, as shown in Figure 3.9.

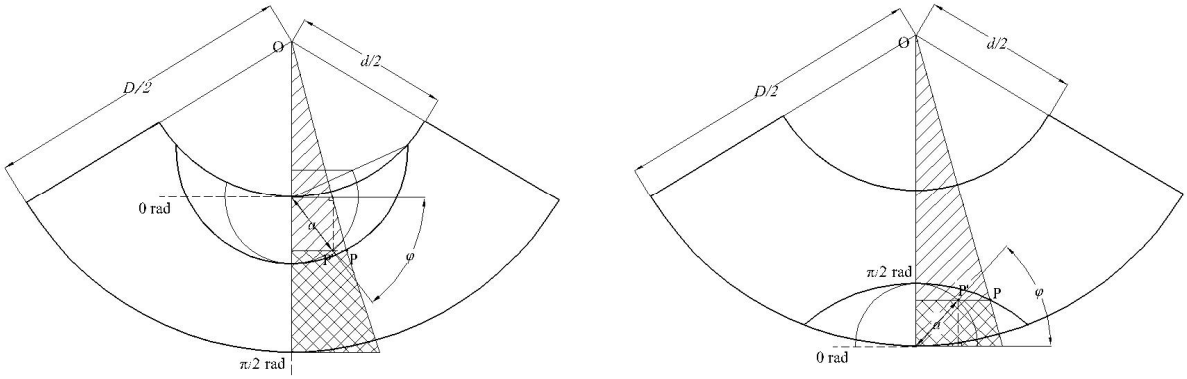

Figure 3.9. Stress gradient effect on bending nominal distribution around the surface cracks

Hence the analytical formula can be expressed as

$$K_{\mathrm{I}} = G \cdot \sigma_{\mathrm{b}} \cdot \sqrt{\pi \frac{a}{Q}} \cdot F. \tag{3.7}$$

Because the nominal stress distribution adjacent to a point "P" along the surface crack front varies in terms of its location, the bending correction factor *G* for modifying the stress distribution adjacent to 'P' therefore can be calculated by the geometrical relation shown in Figure 3.9, as:

i) for internal surface crack

$$G = \frac{2a \cdot \sin\varphi + d}{D}, \tag{3.8}$$

ii) for external surface crack

$$G = \frac{D - 2a \cdot \sin\varphi}{D}, \tag{3.9}$$

where φ is the eccentric angle of a surface crack, as shown in Figure 3.9. The eccentric angle of the deepest point equals to $\pi/2$, while the eccentric angle of the surface point φ_c is calculate as

$$\varphi_c = \frac{\pi}{2} - \frac{\pi - \frac{c}{D/2}}{2} = \frac{c}{D}. \tag{3.10}$$

Different from the plate geometry which the eccentric angle of the surface point equals to 0, $\varphi_c < 0$ for internal surface cracks while $\varphi_c > 0$ for external surface cracks, because of the curved pipe surface.

3.2.2 The parametric study to determine the geometry correction factor

The boundary correction factor of Eq. (3.6) is not developed for bending pipe scenario, further improvements are needed. In Eq. (3.6), M_1, M_2 and M_3 are the correction factor for the semi-elliptical shape of the crack, f_φ is the correction factor of the eccentric angle of surface cracks, and g can be regarded as a correction factor of crack shape evolving along with crack propagation. These coefficients aim to correct the SIFs because of the semi-elliptical shape of surface cracks. However, unlike plates, pipes are closed and curved structures; the f_w to correct the finite width of plates is inappropriate for pipes. Therefore, f_c is introduced as the geometry correction factor for circumferential surface cracked pipe subjected to bending. The boundary correction factor is then expressed as

$$F = \left[M_1 + M_2\left(\frac{a}{t}\right)^2 + M_3\left(\frac{a}{t}\right)^4\right] f_\varphi g f_c, \tag{3.11}$$

where the coefficients except f_c are keep constant with those in Eq. (3.6), which can be calculated referring to Ref. [86]. In order to determine a rational evaluation method of f_c, a FE-based parametric study is conducted. A series of FE models, which are the permutation and combination of nine sets of t/D ranging from 0.04 to 0.20 with the interval of 0.02, 19 sets of a/c with the range of [0.2, 1.0] and interval of 0.1, and seven sets of a/t of [0.2, 0.8] with the interval of 0.1, are built for internal and external surface cracked pipes respectively. Due to the FE modelling capability, the range of c/d is limited to (0, 0.8].The K_I/f_c results, which represent the SIF evaluations without considering f_c using Eq. (3.7), are analysed before the determination of f_c. The results indicate the semi-elliptical crack shape correction factors, i.e., M_1, M_2, M_3, f_φ, and g, provide an rational estimation of the SIFs distribution trend along the crack front, while the SIFs are overall deviated to the SIFs estimated by FEM. Therefore the deepest point of surface cracks is chosen to determine f_c. Then the SIFs of the deepest point of each model are calculated through the FEM, represented as $K_{\mathrm{I,FE}}$. Then f_c can be calculated through the ratio between the SIF calculated by the FEM—K_I and the rest part in Eq. (3.7), as

$$f_c = \frac{K_{\mathrm{I,FE}}}{G\cdot\sigma_\mathrm{b}\cdot\sqrt{\pi\frac{a}{Q}}\cdot\left[M_1+M_2\left(\frac{a}{t}\right)^2+M_3\left(\frac{a}{t}\right)^4\right]\cdot f_\varphi\cdot g}. \tag{3.12}$$

Figure 3.9 shows that the crack shape is influenced by the curved pipe surface, which might affect the value of f_c. In addition, the f_c for the crack on the external or internal surface also might be different. Therefore, the f_c for the internal and external surface cracks are determined respectively by the parametric study, defined as f_{ci} and f_{ce} correspondingly.

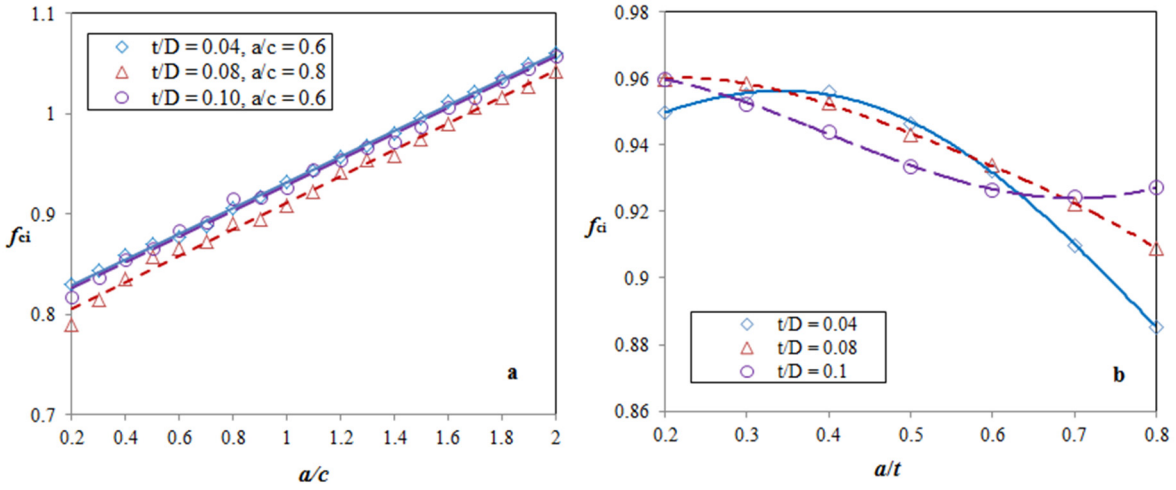

Figure 3.10. Examples of curve-fitting method of internal surface cracks: a) f_{ci}^1 as a function of t/D and a/c, b) f_{ci}^2 as a function of a/t when a/c = 1.0

When obtaining the values of f_c with their corresponding *t*/*D*, *a*/*c* and *a*/*t* ratios through Eq. (3.12), their inherent relationship is analysed, in order to proposed an analytical equation of $f_{ci} = f(t/D, a/c, a/t)$. By analysing all the data, it is found that the *a*/*c* ratio is an independent influential factor (shown in Figure 3.10a), where f_{ci} and *a*/*c* can be fitted as a linear equation with the similar gradient and y-intercept of all cases with different *t*/*D* and *a*/*t* ratio. Therefore f_{ci} can be expressed as $f_{ci} = f_{ci}^1(a/c) \cdot f_{ci}^2(a/t, t/D)$, where $f_{ci}^1(a/c)$ is

$$f_{ci}^1\left(\frac{a}{c}\right) = 0.081 \cdot \frac{a}{c} + 0.88. \tag{3.13}$$

Afterwards, the relationship between $f_{ci}^2(a/t, t/D)$ and the other two influential factors *t*/*D* and *a*/*t* is further investigated. It can be observed from Figure 3.10b that f_{ci}^2 has a non-linear relationship with the value of *a*/*t* and *t*/*D*. It should be noted that higher order polynomials might be appropriate to curve-fit f_c, which is not adopted in this study. For the purpose of simplifying calculation, a sinusoidal equation is used to curve-fit the $f_{ci}^2(a/t, t/D)$. In addition, by analyzing the calculated results, it is found that the periodicity and the phase position are influenced by *t*/*D*. The f_{ci}^2 therefore can be expressed as

$$f_{ci}^2 = \sin\left(\omega \frac{a}{t} + \varphi\right) \tag{3.14}$$

Once the value of f_{ci}^1 of different *a*/c has been determined, the relation between f_{ci}^2 and the *a*/*t* with different *t*/*D* values are obtained. Afterwards, through curve-fitting method, the corresponding values of ω and φ with different *t*/*D* ranging from 0.04 to 0.20 are calculated. The curve-fitting results show that both ω and φ have an approximately linear relation with the variation of *t*/*D* ratio, which are fit as

$$\omega = -8.36 \cdot \frac{t}{D} + 1.15, \tag{3.15}$$

$$\varphi = 5.3325 \cdot \frac{t}{D} + 1.09, \tag{3.16}$$

thus

$$f_{\mathrm{ci}} = \sin\left(\omega\frac{a}{t} + \varphi\right) \cdot \left(0.081 \cdot \frac{a}{c} + 0.88\right), \tag{3.17}$$

with its *R*-square value equals to 0.948.

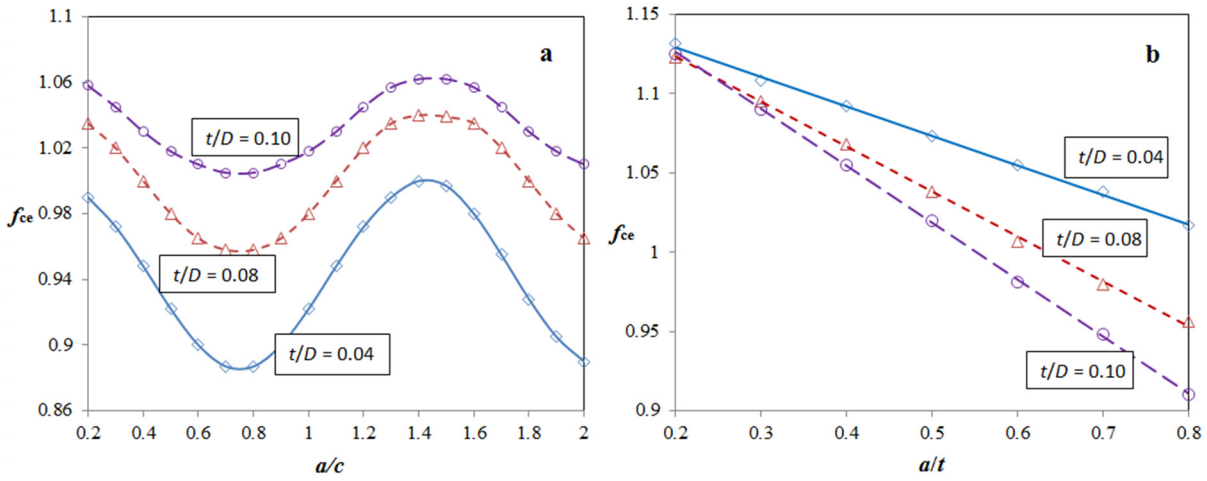

Figure 3.11. Examples of curve-fitting method of external surface cracks: a) f_{ce}^{1} as a function of t/D and a/c, b) f_{ce}^{2} as a function of t/D and a/t

The f_{ce} is identified by the same method of f_{ci}. By data analysis, it is observed that the f_{ce} presents a sinusoidal variation trend with the variation of *a*/*c* ratio, while the *t*/*D* ratio influences the amplitude value and the intercept value, as indicated in Figure 3.11a. In addition, f_{ce} has a linear relationship with *a*/*t* ratio, of which the slope value is determined by the *t*/*D* ratio, as shown in Figure 3.11b. Therefore f_{ce} can be expressed as $f_{\mathrm{ce}} = f_{ce}^{1}(a/c\,, t/D) \cdot f_{ce}^{2}(a/t\,, t/D)$, where $f_{ci}^{1}(a/t)$ is

$$f_{ce}^{1}\left(\frac{a}{c}\right) = n \cdot \sin\left(4.6 \cdot \frac{a}{c} - 5\right) + k \tag{3.18}$$

Through curve fitting, it is indicated that the value of f_{ce}^{1} is influence by *t*/*D* as an approximately sinusoidal relation (see in Figure 3.11a), where its periodicity and the phase position are influenced by *t*/*D*. Thus through curve fitting method, the '*n*' and '*k*' is fit as

$$n = -0.04 \cdot \frac{t}{D} + 0.072, \tag{3.19}$$

$$k = 1.5 \cdot \frac{t}{D} + 0.8815, \tag{3.20}$$

Similarly, f_{ce}^{2} is influenced by *t*/*D* as a linear relation (see in Figure 3.11b),

$$f_{ce}^{2}\left(\frac{a}{c}\right) = p \cdot \frac{a}{t} + q, \tag{3.21}$$

thus 'p' and 'q' is fit by curve fitting method as

$$p = -2.705 \cdot \frac{t}{D} - 0.083, \tag{3.22}$$

$$q = 0.45 \cdot \frac{t}{D} + 1.15. \tag{3.23}$$

therefore

$$f_{\mathrm{ce}} = [n \cdot \sin\left(4.6 \cdot \frac{a}{c} - 5\right) + k](p \cdot \frac{a}{t} + q), \tag{3.24}$$

which has a *R*-square value larger than 0.99.

Therefore, the geometry correction factor f_{c} can be used in Eq. (3.11) as the boundary correction factor of the proposed analytical formula of Eq. (3.7) to evaluate the SIFs of circumferential surface cracks in metallic pipes subjected to bending. The analytical formula covers a wide range of pipe geometry and surface crack shapes of $0.2 \leq a/t \leq 0.8$, $0.2 \leq a/c \leq 1.0$, $0.04 \leq t/D \leq 0.2$, $c/d \leq 0.8$, which can meet most of the conditions of offshore metallic pipes in practical situations.

3.3 Verification of the SIF evaluation of circumferential surface cracks in metallic pipes subjected to bending

In this section, the SIF evaluation by means of the proposed analytical method is compared with the weight function method recommended by API 579-1/ASME FFS-1 [19], which is

$$K_I = F_w \cdot \sigma_{\mathrm{b}} \cdot \sqrt{\pi \frac{a}{Q}}, \tag{3.25}$$

The boundary correction factor *F* evaluated by weight function is calculated by

$$F_w = A_0 + A_1 \cdot \beta + A_2 \cdot \beta^2 + A_3 \cdot \beta^3 + A_4 \cdot \beta^4 + A_5 \cdot \beta^5 + A_6 \cdot \beta^6, \tag{3.26}$$

where the value of A_0 to A_6 are referred to the corresponding table sorted by the value of t/R_{i}, a/c, and a/t. β is given as

$$\beta = 2\varphi/\pi \tag{3.27}$$

here, the range of φ is defined as [0, π]. Therefore, the eccentric angle φ for the surface point in Eq. (3.25) is defined as zero.

In this section, considering the limited tabulated values of t/R_{i}, a/c, and a/t provided by Ref. [19] as well as the common surface crack profiles and pipe dimensions (e.g., in most cases, thick-wall pipes are applied) in offshore metallic pipe scenarios, the SIF of both internal and external surface cracks within different profiles and pipe dimensions are calculated by the two analytical methods. The t/R_{i} ratio of 0.1 and 0.2, a/c ratios of 0.25, 0.5, and 1.0, a/t ranges from 0.2 to 0.8 with the interval of 0.2 are chosen for the verification. Note that other values of t/R_{i}, a/c, and a/t are impossible to be calculated by Eq. (3.26) because the corresponding values of A_0 to A_6 are not included in reference table. The comparison applied the normalized SIF to better illustrate their difference, which is defined as

$$f = \frac{K_I}{\sigma_b \cdot \sqrt{\pi \frac{a}{Q}}}. \tag{3.28}$$

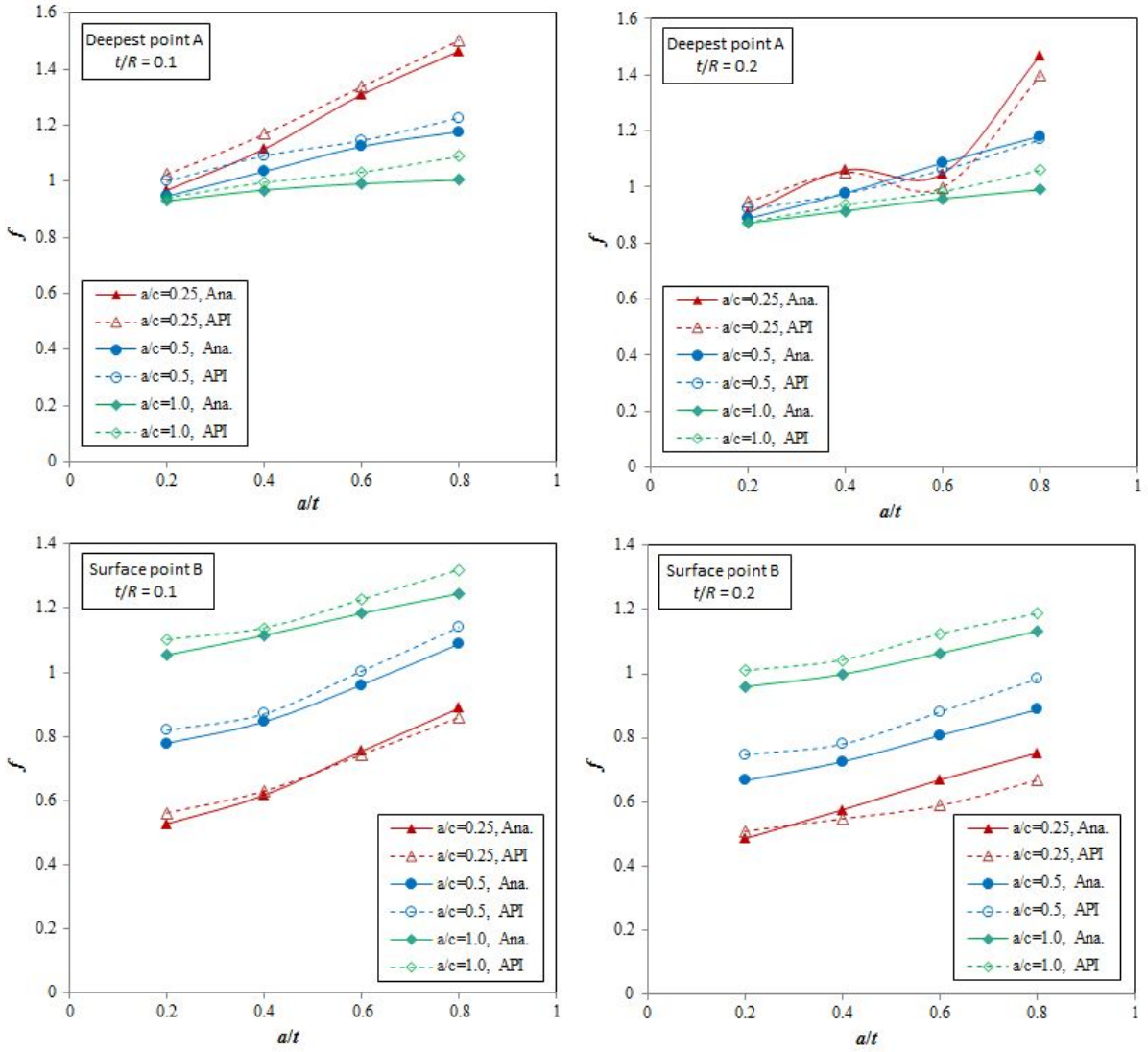

Figure 3.12. The comparison of the normalized SIF f of internal surface crack between the proposed analytical method and the API 579-1/ASME FFS-1 recommended analytical method [19]

Then the results using the proposed analytical method (results marked as 'Ana.') and the American Petroleum Institute (API) recommended analytical method (results marked as 'API') are compared. Figure 3.12 shows the result comparison of internal surface cracks in metallic pipes, which indicates that the results evaluated by the proposed analytical method match well with the results calculated by the API recommended method, with an average error of 2.6% for the deepest point, and an average error of 3.8% for the surface point. The result comparison of external surface cracks in metallic pipes are shown in Figure 3.13, the results evaluated by the proposed analytical method match well with the results from the API recommended method, with an average error of 2.3% for the surface point and an average error of 2.8% for the deepest point.

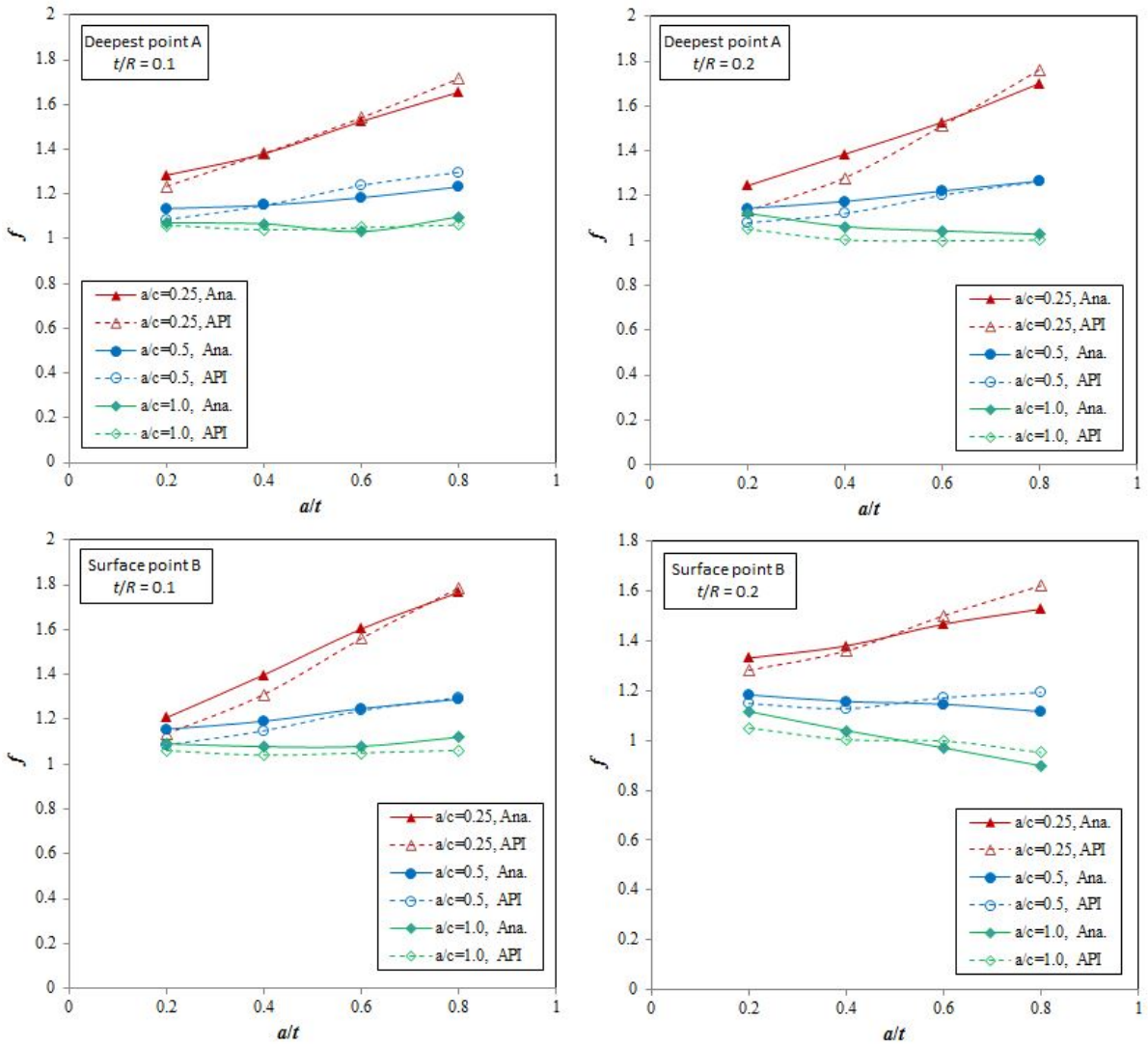

Figure 3.13. The comparison of the normalized SIF f of external surface crack between the proposed analytical method and the API 579-1/ASME FFS-1 recommended analytical method [19]

In summary, the verification by means of the API recommends method indicated that the proposed analytical method managed to accurately evaluate the SIF of the surface crack. In addition, unlike the API recommended method which is only able to calculated the SIF with limited tabulated t/R_i, a/c, and a/t ratios, the proposed analytical method is able to evaluate the SIF along the surface crack front continually during the surface crack growth process within the range of $0.2 \leq a/t \leq 0.8$, $0.2 \leq a/c \leq 1.0$, $0.04 \leq t/D \leq 0.2$, $c/d \leq 0.8$.

3.4 Experimental validation of circumferential surface cracked metallic pipes subjected to fatigue bending

Experimental studies are conducted in order to further validate the feasibility of the proposed analytical method in terms of predicting surface crack growth rate. The experimental results of crack growth rate of external surface cracks in metallic pipes subjected to bending are obtained. At the meanwhile, the analytical formula for internal surface crack in metallic pipes

subjected to bending is validated through available experimental data from literature [6]. It should be noted that three data sets different from those used for validation of FEM are utilized herein to validate the analytical method.

3.4.1 Pipe materials and specimen preparation

Offshore seamless steel pipe API 5L X65, conforming to API code [39], has been used for the experimental study. The pipes have a 168.3 mm external diameter and approximately 12.7 mm thickness. The pipe material has a yield stress of 448 MPa, and tensile stress of 530 MPa, provided by pipe manufacturer.

The detailed parameters of pipe specimens are shown in Table 3.3. Three types of semi-elliptical notches with different aspect ratio are set up in the pipe specimens. The notches are made by Micro-EDM. Each specimen category has three repetitive specimens. For instance, for specimen 'PE-1-1', 'P' means pipe, 'E' represents external surface crack, the first '1' stands for the first type of notch, and the second '1' means the No. of the repetitive specimen.

Table 3.3. Pipe specimen category and details

Specimen	*L*	*D*	*t*	*a*	*c*
PE-1(1)	2,000	168.3	12.76	2.31	4.94
PE-1(2)	2,000	168.3	12.81	2.48	5.04
PE-1(3)	2,000	168.3	12.77	2.44	4.89
PE-2(1)	2,000	168.3	12.70	2.39	3.99
PE-2(2)	2,000	168.3	12.74	2.44	3.82
PE-2(3)	2,000	168.3	12.68	2.39	3.99
PE-3(1)	2,000	168.3	12.61	3.99	4.00
PE-3(2)	2,000	168.3	12.73	3.96	3.98
PE-3(3)	2,000	168.3	12.84	3.92	3.97

Note: The parameters, i.e., *D*, *t*, *a*, *c*, are measured from each specimens, each of which is the weighted average of three measurement locations. All unit are in 'mm'.

3.4.2 The full scale pipe bending test

The fatigue tests have been carried out under constant amplitude sinusoidal cyclic loading, generated by MTS Hydraulic Actuator, which has a capacity of 1,000 kN. The schematic of test set up is shown in Figure 3.14. The load was applied in four-point bending condition to ensure a pure bending statue for the cracked location. In addition, the inner span L_i is designed more than four times larger than the pipe diameter to eliminate possible negative effects from the loading cells, which is 800 mm, while the external span L_e is 1800 mm. Therefore, the bending arm of the test is 500 mm.

Before the fatigue test, a pre-cracking procedure has been conducted to generate fatigue surface cracks initiated from the semi-elliptical notch. This procedure contains two stages of which adopt 80% yield stress and 60% yield stress respectively, as the load amplitude of the constant amplitude sinusoidal cyclic loading. Each stage conducts a certain number of cycles

until the surface crack propagate at least 1.0 mm [57]. Then the size of the surface crack after the pre-cracking procedure is regarded as the initial crack size of the surface cracked specimen, which is therefore ready for the fatigue crack growth test.

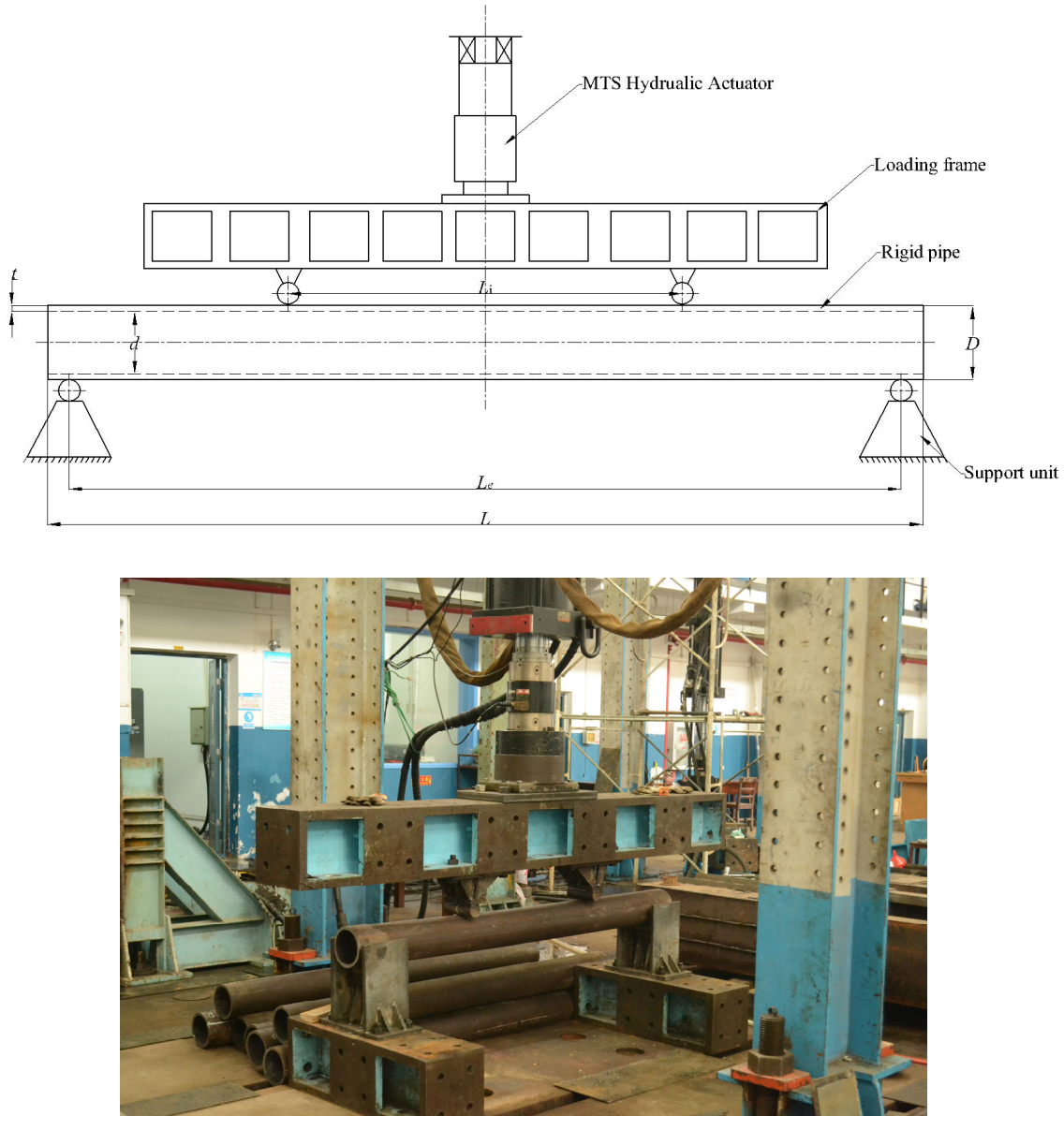

Figure 3.14. Four-point bending test set-up: the schematic and specimen configuration is shown in the upside; actual test set-up is shown in the downside

All the fatigue tests are conducted at room temperature and air environment under load control condition. The loading frequency for pipe bending test is set as 2.5 Hz. The stress ratio R maintained 0.1 for the crack growth of all tests. The crack growth process is recorded by beach marking technique by means of changing the stress ratio R to 0.5 and cycle for 5,000 times, as described in Figure 3.15.

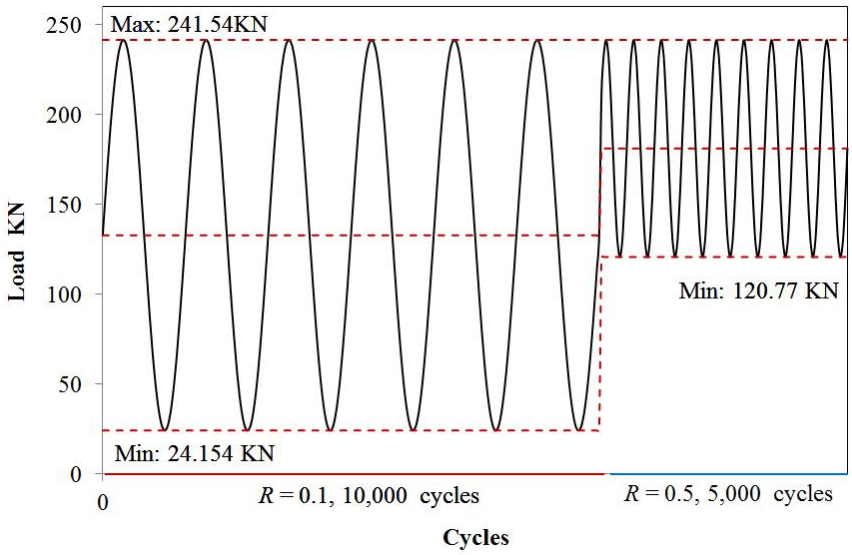

Figure 3.15. The load spectrum and beach mark generating procedure

3.4.3 Experimental results and validation of the analytical method

After each test, the cross-section of bending specimen has been sampled around the cracked area by oxy-acetylene cutting. Then the beach marks recorded on the cross-section were obtained, as shown in Figure 3.16. The crack growth between each adjacent beach marks represents 10,000 cycles; therefore, the cyclic number corresponding to each crack size was recorded, and then measured by an electronic reading microscope. Figure 3.16 clearly demonstrates multiple initiations of surface cracks along the notch front, and surface crack continually propagates as a semi-elliptical shape until the crack penetrates the pipe wall. The fatigue tests results are shown in Table II.2 in Appendix II, all the units of a and c are in mm.

The test results of crack depth and its corresponding cyclic numbers of the specimens with the same notch size were modified to start from a given starting point, in order to identify the repeatability of the results. Then the surface crack growth of each category was estimated: the SIFs of each scenario were calculated by the corresponding proposed analytical method, and the crack growth rate was then estimated using the Paris law. In this part, the material constant C is 3.98×10^{-13} (ΔK in MPa/mm$^{1/2}$), and m is 2.88, provided by BS 7910 [20] and API 579-1/ASME FFS-1 [19]. Figure 3.17 to Figure 3.19 shows the comparison of surface crack growth predicted by the analytical method and the test results. In addition, those results were compared with the results evaluated by Newman-Raju's method [141]. It should be noted that the stress ratio for all external loads herein examined is equal to R = 0.1.

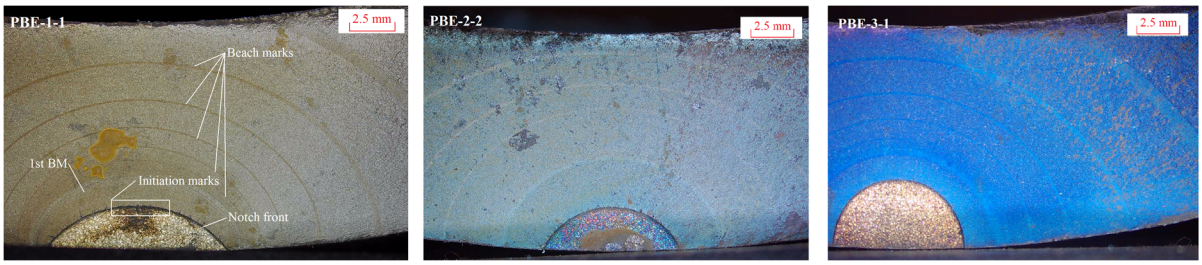

Figure 3.16. Beach marks on the cross-section of three pipe bending specimens

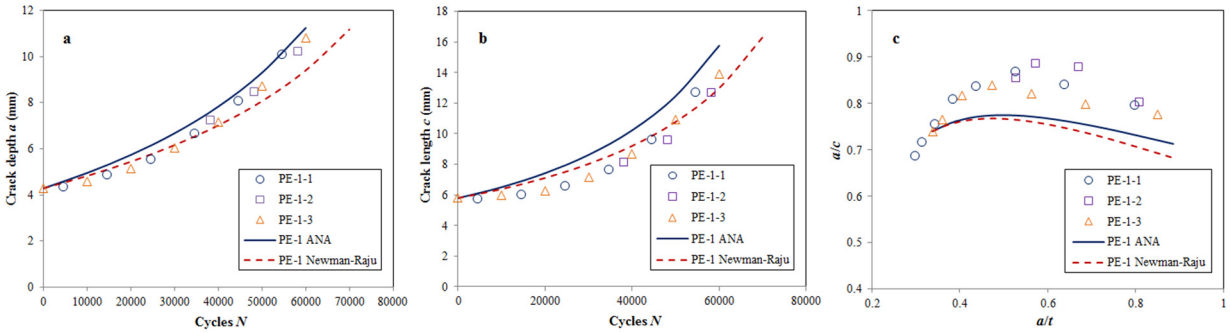

Figure 3.17. The results comparison of PE-1. a) crack growth along depth direction; b) crack growth along length direction; c) crack aspect ratio variation

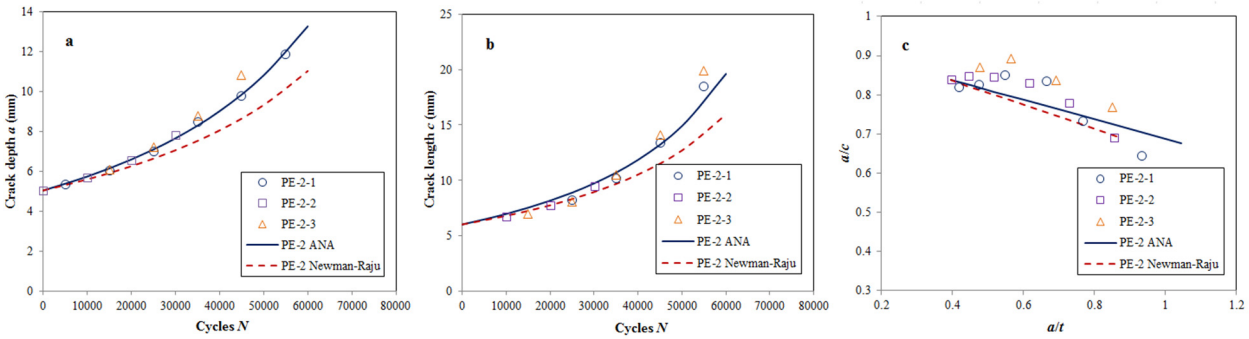

Figure 3.18. The results comparison of PE-2. a) crack growth along depth direction; b) crack growth along length direction; c) crack aspect ratio variation

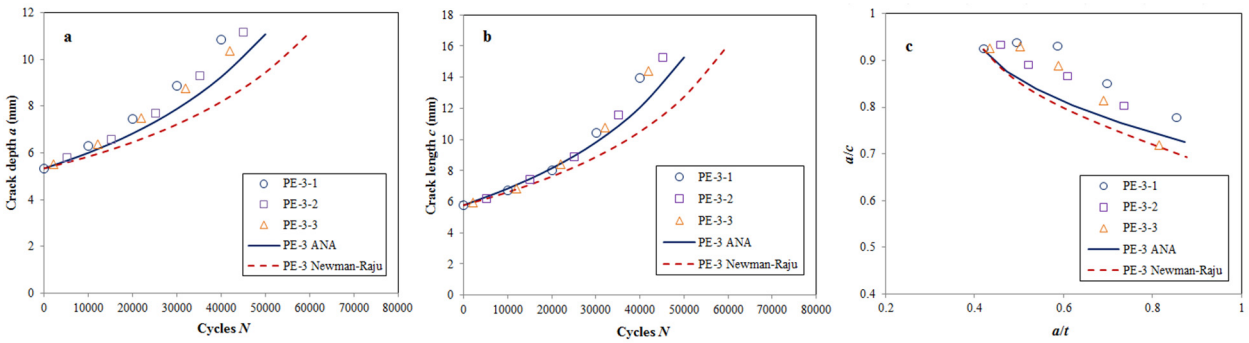

Figure 3.19: The results comparison of PE-3. a) crack growth along depth direction; b) crack growth along length direction; c) aspect ratio variation

It is clearly indicated from Figure 3.17 to Figure 3.19 that the experimental results of external surface crack growth in pipes subjected to bending have a good repeatability. The results estimated by the proposed analytical formula, i.e., PE-1 ANA, PE-2 ANA, and PE-3

ANA, agree well with the experimental results, which perform better than the Newman-Raju's method [86]. In addition, rather than underestimating the crack growth rate, the proposed analytical method stands on the conservative side for the case of PE-1 and PE-2, which might be safer for usage. Similar to the Newman-Raju's method, the *a*/*c* versus *a*/*t* ratio have been underestimated by the proposed analytical method (see in Figures 3.17c, 3.19c and 3.20c). The reason might be that the Paris constant *C* of the surface point and deepest point are different due to a larger plastic zone around the surface point [62]. However, the analytical results agreed better with the experimental data for the *a*/*c* versus *a*/*t* ratio, owing to the proposed bending correction factor *G*.

The analytical method of estimating the SIFs of internal surface cracks in pipes subjected to bending is validated by three groups of available experimental data from Ref. [52], with different *t*/*D* and initial *a*/*c* ratio, as given in Table 3.4. The results of *a*/*c* versus *a*/*t* ratio are shown in Figure 3.20a, which illustrates that the analytical method can predict the variation of the crack profile during the fatigue process more accurately than the Newman-Raju's method. In addition, the fatigue lives of the three specimens predicted by the analytical method, which is the cycles of the crack propagate from the initial size till penetrating the wall, match well with the experimental data, only with an maximum error of 4.79% for PI-2, as shown in Figure 3.20b.

Table 3.4. Detailed information related to geometries, loading and material parameters for the specimens with internal surface crack

Specimen	Initial geometry parameters (mm)				Load condition (kN)		Material constant	
	c	*a*	*D*	*t*	Max	Min	*C*	*m*
PI-1	6.0	3.0	102	8.1	28.92	2.89	3.2×10^{-10}	3.72
PI-2	6.0	6.0	102	12.7	30.30	3.03	3.2×10^{-10}	3.72
PI-3	6.0	3.0	102	12.7	35.95	3.60	3.2×10^{-10}	3.72

Note: Unit for d*a*/d*N* and d*c*/d*N* are mm/cycle.

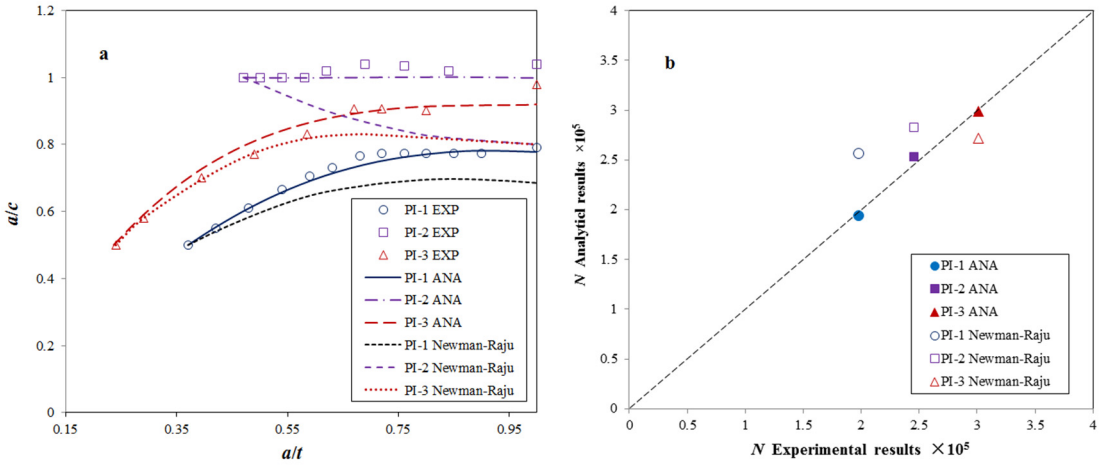

Figure 3.20. The results comparison of internal surface crack specimens of the experimental results (EXP) [52], the analytical method and Newman-Raju's method: a) a/c versus a/t ratio; b) fatigue life cyclic numbers

3.5 Numerical verification of circumferential surface cracked metallic pipes subjected to fatigue tension and bending

Both bending and tension loads generate Mode-I normal stress on the metallic substrate, which can be mathematically superposed [41], such as the Newman-Raju' law for surface cracked plate subjected to tension and bending [92]. Thus, Eq. (3.7) can be modified to

$$K_{\mathrm{I}} = (\sigma_{\mathrm{t}} + G \cdot \sigma_{\mathrm{b}}) \cdot \sqrt{\pi \frac{a}{Q}} \cdot F \tag{3.28}$$

where σ_{t} is the tensile normal stress.

Table 3.5. Pipe geometry and loading conditions

Pipe length	External diameter	Tension loads	Bending moment
2000 mm	200 mm	200 MPa	200 kN · m

Then the analytical method is verified by the FEM. The pipe geometry and the loading condition are listed in Table 3.5. The verification is conducted in a rigid pipe under combined tensile and bending loads. The size, meshing method, material properties of the FE model are the same with the FE model in Section 3.1. Then the bending moment is applied on side of the pipe model, while the other side of the pipe model is fixed supported, as shown in Figure 3.21.

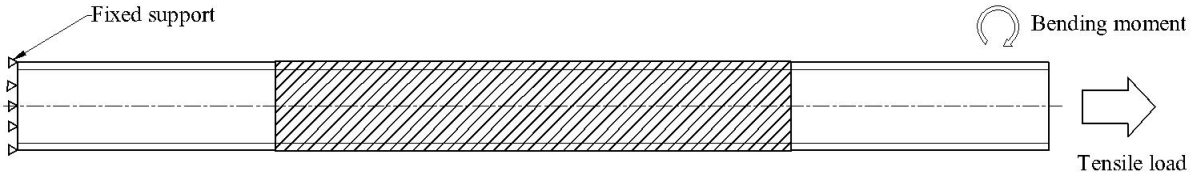

Figure 3.21. The sketch diagram of the pipe subjected to combined bending and tension

Different pipe dimensions and crack dimensions represented by *t*/*D*, *a*/*c*, and *a*/*t* ratios are verified, as shown from Figures 3.22 to 3.24. For a typical thin-wall pipe of *t*/*D* = 0.04, Figure 3.22 shows that when *a*/*t* = 0.4, *a*/*c* = 0.5, 1.0, 1.5, the analytical formula can well predict the SIFs, within 2% error band. For a typical thick-wall pipe of *t*/*D* ratio equals to 0.1, the analytical equation offers a reasonably prediction of SIFs along the internal surface crack, when *a*/*t* = 0.4, *a*/*c* = 0.5, 1.0, and 1.5 respectively, within a 2% error band as well, as is shown in Figure 3.23. In addition, for some ultra-deep water scenarios, the pipe wall can be very thick. Therefore the case of *t*/*D* = 0.15 is also validated through the FEM, which is illustrated from Figure 3.24 that the analytical equation reasonable estimate the SIFs along the surface crack front as well, within 4% error band. Thus, the verification indicates that the analytical method, i.e., Eq. (3.28), is an appropriate to evaluate the SIF of the surface cracked pipe subjected to combined tension and bending loads.

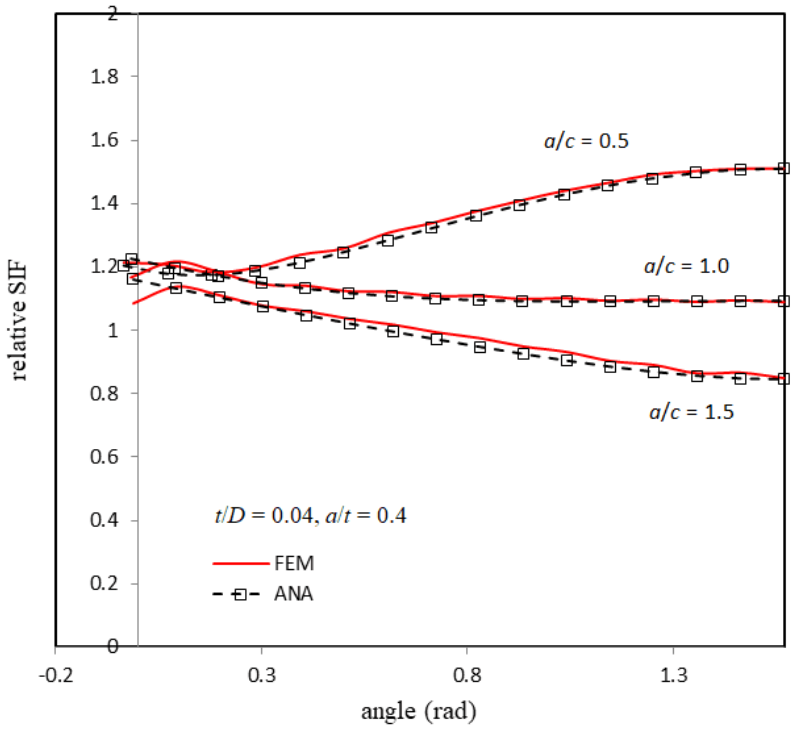

Figure 3.22. The relative SIFs along half internal surface cracks front (t/D = 0.04, a/t = 0.4) of a/c= 0.5, 1.0, and 1.5 of FEM and analytical results

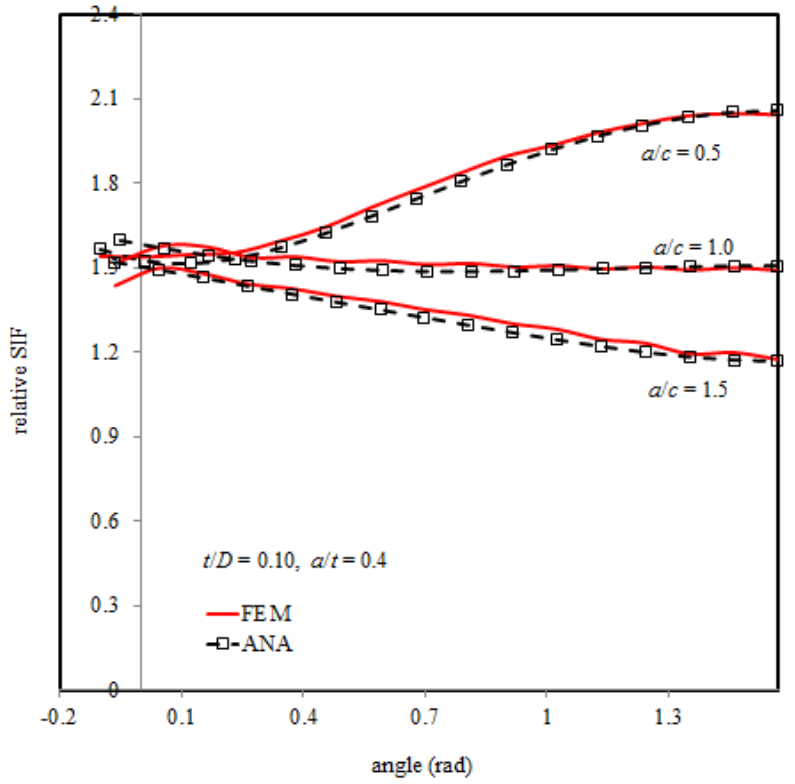

Figure 3.23. The relative SIFs along half internal surface cracks front (t/D = 0.10, a/t = 0.4) of a/c= 0.5, 1.0, and 1.5 of FEM and analytical results

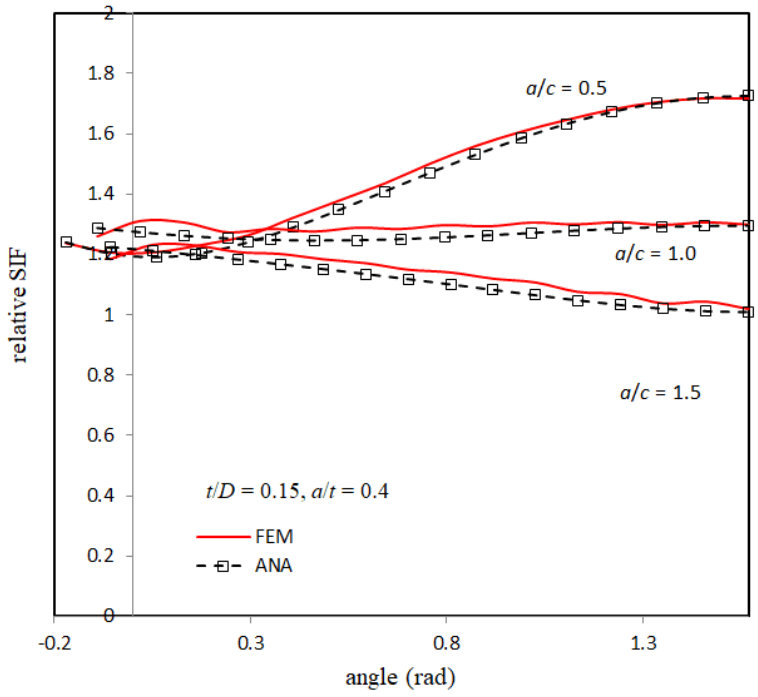

Figure 3.24. The relative SIFs along half internal surface cracks front (t/D = 0.15, a/t = 0.4) of a/c= 0.5, 1.0, 1.5 of FEM and analytical results

3.6 Conclusions

In this chapter, an analytical method to evaluate the SIFs of circumferential surface cracks in metallic pipes subject to bending and tension has been proposed by introducing the bending correction factor G, and the geometry correction factor f_c. The bending correction is deduced in light of bending stress gradient; while the geometry correction factor is determined by a FE-based parametric study. Owing to a large data set requirement by the parametric studies, three-dimensional FE models of evaluating SIFs of circumferential surface cracks are developed and validated.

The proposed analytical method is verified by means of the API recommended analytical method. The SIF results evaluated by the proposed analytical method match well with the results from the recommended analytical method. In addition, the proposed analytical method is not restricted to the limited tabulated t/R_i, a/c, and a/t ratios, which is capable of continually evaluating the SIF along the surface crack front during the surface crack growth process.

Fatigue experimental investigations have been conducted on external surface cracked API 5L X65 pipes to validate the analytical method for external surface crack growth; while available experimental data were employed to validate the analytical method for internal surface crack growth. The SIF results evaluated by the proposed analytical method matched well with the API recommended analytical method. The prediction of surface crack growth by combing the proposed analytical method and the Paris' law matched well with the experimental results, provided a more accurate prediction than the Newman-Raju's method. The results of a/c versus a/t ratio were underestimated by the analytical method. The reason

might be that the Paris constant C of the surface point and the deepest point might be different due to a larger plastic zone around the surface point. In conclusion, the analytical method is appropriate to evaluate the SIF of circumferential surface cracks in metallic pipes subjected to bending, which can be utilize for practical purposes to evaluation circumferential surface crack growth and predict residual fatigue life of cracked metallic pipes.

Chapter 4 Surface cracked metallic plates reinforced with FRP*

In this chapter, the surface crack growth in metallic plates reinforced with FRP subjected to cyclic tension is studied. The purpose is to pave the way for the study on the composite reinforced surface cracked metallic pipes by eliminating potential influences from the pipe geometry and the bending load. This study, which is conducted on a simpler plate geometry, intends to understand the mechanism of the surface crack growth reinforced with FRP, as well as indicating the failure modes of the reinforcement system. In addition, developing the FE model of the metallic plate whose scale is much smaller than the pipe model, is beneficial to identify the necessary modelling parameters, meshing conditions and the connection setup between the CRS and the metallic substrate.

The main purpose of employing the plate specimen before the study on pipes is to eliminate potential influences from the pipe geometry and the bending load. In this chapter, surface crack growth behaviour, possible failure modes were studied by means of experimental and numerical approaches. The structure of this chapter is assigned as follow: Section 4.1 conducted an experimental investigation on the surface crack growth in metallic plates reinforced with FRP to identify the failure models and to record the surface crack growth data. Section 4.2 analyses the possible failure modes by employing the cohesive zone modelling. In Section 4.3, in order to further analyse the composite reinforcement on the surface cracked metallic plate, a three-dimensional FE model is developed. Successively, the FE model is validated by the experimental results. Then in Section 4.4, on account of the

* This chapter is based on the published journal articles—[142] Z. Li, X. Jiang, H. Hopman, L. Zhu, Z. Liu, and W. Tang, "Experimental investigation on FRP-reinforced surface cracked steel plates subjected to cyclic tension," *Mechanics of Advanced Materials Structures,* vol. 27, pp. 1-15, 2020., and [143] Z. Li, X. Jiang, H. Hopman, L. Zhu, and Z. Liu, "Numerical investigation on the surface crack growth in FRP-reinforced steel plates subjected to tension," *Theoretical and Applied Fracture Mechanics,* vol. 108, p. 102659, 2020.

validated FE model, a parametric study is conducted to identify the optimum reinforcement schemes and the key influential parameters of the composite reinforcement. Finally the conclusions of this chapter are stated in Section 4.5.

4.1 Experimental investigation on surface crack growth in metallic plates reinforced with FRP

In this section, the experimental investigation on the surface crack growth in metallic plate reinforced with FRP subjected to tension was conducted. The main purpose is to analyse the effect of composite reinforcement on the crack growth, as well as indicating the failure modes and analysing their effects on the surface crack growth. In addition, the experimental results will be used to validate the FE model in Section 4.2.

4.1.1 Specimen preparation

Specimen preparation is an important step for the sake of achieving ideal experimental results. The preparation of the FRP-reinforced surface cracked metallic plate specimens required a certain number of steps: the selection of four different materials, i.e., metallic substrate, adhesive, GFRP, and CFRP; notch manufacturing; pre-cracking and composite reinforcement. The quality of each constituent part is needed to be guaranteed. In this section, the preparation procedures are step-by-step introduced.

4.1.1.1. Material properties

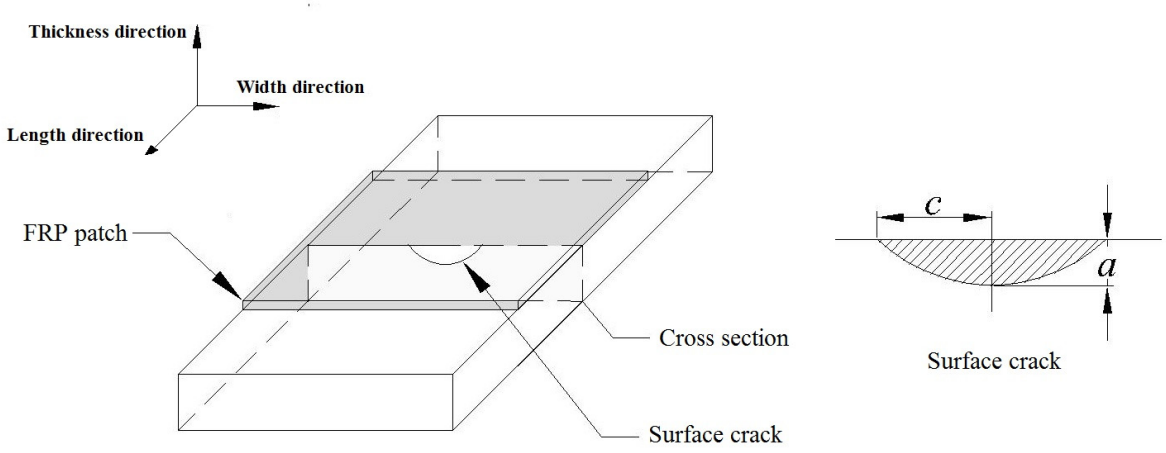

Figure 4.1. The sketch diagram of the single-side FRP-reinforced surface cracked specimen

The sketch diagram of the single-side FRP-reinforced surface cracked specimen is shown in Figure 4.1. The specimens contained four materials: the metallic substrate, GFRP, CFRP, and adhesive. Stainless steel of 907A for subsea scenarios conforming to GJB 6055-2007 code [144] has been used as the steel substrate. The steel material has yield strength of 390 MPa, and tensile strength of 530 MPa. In light of the galvanic corrosion between CFRP laminates and steel substrate, one layer of GFRP laminate was adopted as the contact inhibitor between

the steel substrate and CFRP laminates. The GFRP laminate applied the E-glass fibre weave fabric while the CFRP laminate used the T700S series unidirectional fabric. Their material properties are listed in Table 4.1 and Table 4.2 respectively. The adhesive adopted the resin epoxy conforming to the code GB/T 2567-2008 [145] and its material properties are listed in Table 4.3. Note the material properties of the steel, FRP and adhesive are all provided by each manufacturer.

Table 4.1. Material properties of GFRP

E_1 (Pa)	E_2 (Pa)	T (Pa)	G_{13} (Pa)	G_{23} (Pa)	Nu
72×10^9	72×10^9	1.1×10^9	4.7×10^9	3.5×10^9	0.33

Table 4.2. Material properties of the CFRP material

E_1 (Pa)	E_2 (Pa)	T (Pa)	G_{13} (Pa)	G_{23} (Pa)	Nu
230×10^9	25×10^9	4.9×10^9	5.5×10^9	3.9×10^9	0.3

Table 4.3. Material properties of the resin epoxy

E (Pa)	T (Pa)	G (Pa)	Nu
2.8×10^9	70×10^6	1.4×10^9	0.35

4.1.1.2. Specimen manufacturing

The detailed manufacturing procedures of the specimens are introduced in Appendix I. The Procedures are indicated in Figure 4.2.

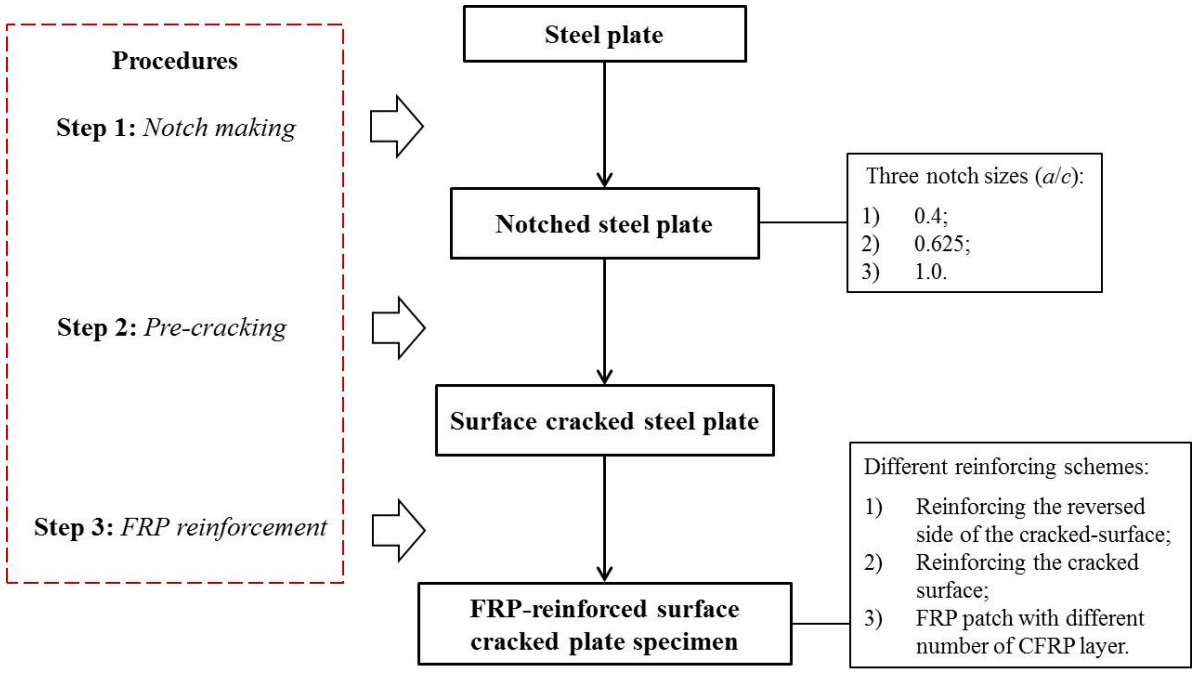

Figure 4.2. The procedure of specimen preparation

4.1.1.3. Specimens configurations

The steel plate is 400 mm long and 60 mm wide, with an approximately 12.30 mm thickness. The width of each GFRP and CFRP laminate equals to the width of steel specimen,

while the length of the FRP patch is 150 mm. The thickness of each layer of GFRP and CFRP laminate are 0.35 mm. Each composite reinforced specimen applies one layer of GFRP as the first layer, and several layers of CFRP laminate on top of that, as shown in Figure 4.3. The configuration of the specimens and reinforcement details are shown in Table 4.4. In total, nine groups of 23 specimens were prepared. Group 1, 2, and 3 are three controlling group of three different groups of initial surface crack sizes without composite reinforcement. Group 4 is using FRP to reinforce the reversed side of the cracked surface, while Group 5, 6, and 7 are using FRP to reinforce the cracked surface with different crack sizes. Most groups have three repetitive specimens except Group 8 & 9 which have only one specimen each. The name of the specimens in Table 4.4 represents the notch configuration, composite reinforcement scheme and its repetitive number. Take 'SE-1-R(1)' as an example, 'S' means steel plate, 'E' represents reinforcing the steel plate on the cracked surface, 'R' means reinforcement, the first '1' stands for the first type of notch, and the second '1' means the No. of the repetitive specimen.

Table 4.4. Specimens' configuration and reinforcement details

Group	Specimen	Notch category	b (mm)	t (mm)	a_0 (mm)	c_0 (mm)	The reinforced surface	No. of CFRP layer
	S-1(1)	1	59.86	12.39	1.90	5.00	/	/
1	S-1(2)	1	59.95	12.33	1.86	5.00	/	/
	S-1(3)	1	59.86	12.36	1.92	4.98	/	/
	S-2(1)	2	59.87	12.32	1.96	3.15	/	/
2	S-2(2)	2	59.43	12.36	1.90	3.15	/	/
	S-2(3)	2	59.87	12.36	1.96	3.14	/	/
	S-3(1)	3	59.80	12.39	3.98	4.00	/	/
3	S-3(2)	3	59.78	12.43	3.96	3.98	/	/
	S-3(3)	3	59.69	12.45	3.95	3.98	/	/
	SI-1-R(1)	1	59.45	12.30	1.96	5.00	The reversed side	4
4	SI-1-R(2)	1	59.92	12.28	1.86	4.95	The reversed side	4
	SI-1-R(3)	1	59.85	12.34	1.86	4.95	The reversed side	4
	SE-1-R(1)	1	59.79	12.41	1.90	5.02	The cracked surface	4
5	SE-1-R(2)	1	59.67	12.34	1.90	4.86	The cracked surface	4
	SE-1-R(3)	1	60.02	12.36	1.88	4.99	The cracked surface	4
	SE-2-R(1)	2	60.01	12.41	1.91	3.10	The cracked surface	4
6	SE-2-R(2)	2	59.52	12.42	1.86	3.13	The cracked surface	4
	SE-2-R(3)	2	59.96	12.43	1.90	3.08	The cracked surface	4
	SE-3-R(1)	3	59.95	12.47	3.90	3.89	The cracked surface	4
7	SE-3-R(2)	3	60.13	12.38	3.90	3.94	The cracked surface	4
	SE-3-R(3)	3	59.84	12.22	3.89	3.94	The cracked surface	4
8	SE-1-R2(1)	1	60.07	12.30	1.95	4.95	The cracked surface	2
9	SE-1-R6(1)	1	60.04	12.40	1.91	5.00	The cracked surface	6

Note: The parameters, i.e., b, t, a_0, c_0 are measured based on each specimens, each of which is the weighted average of three measurement locations.

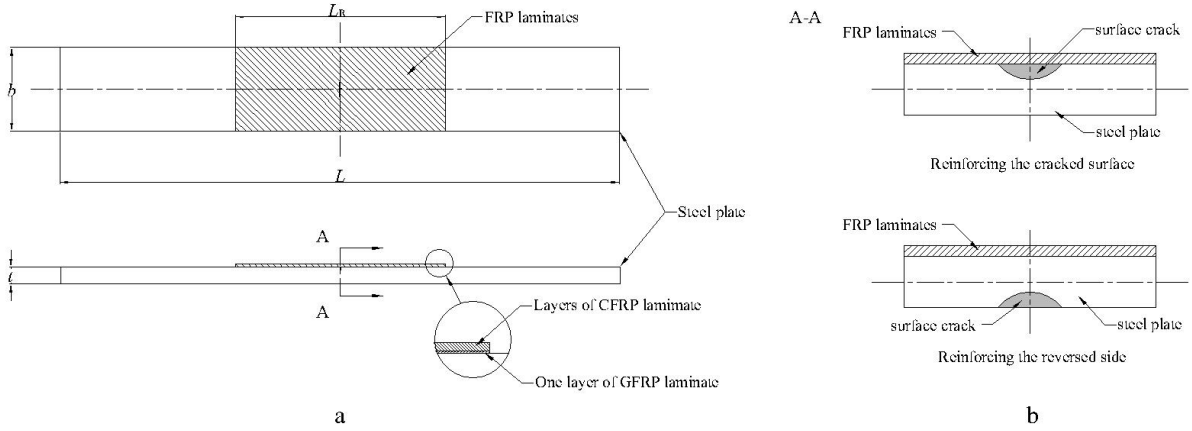

Figure 4.3. The configuration of specimens: a) a composite reinforced steel plate; b) the location of a surface crack in a steel plate

4.1.2 Test set-up

The fatigue tests were carried out under constant amplitude sinusoidal cyclic loading, generated by MTS Hydraulic Actuator, which has a capacity of 250 kN. The schematic of test setup and the real test setup is shown in Figure 4.4. Two edges of each tensile specimen were clamped by a pair of hydraulic clamps, positioned horizontally on the fatigue machine. The load was applied in tension condition to ensure a pure tension statue for the plate specimen. Note that the fatigue test follows the code of ASTM E647 [57].

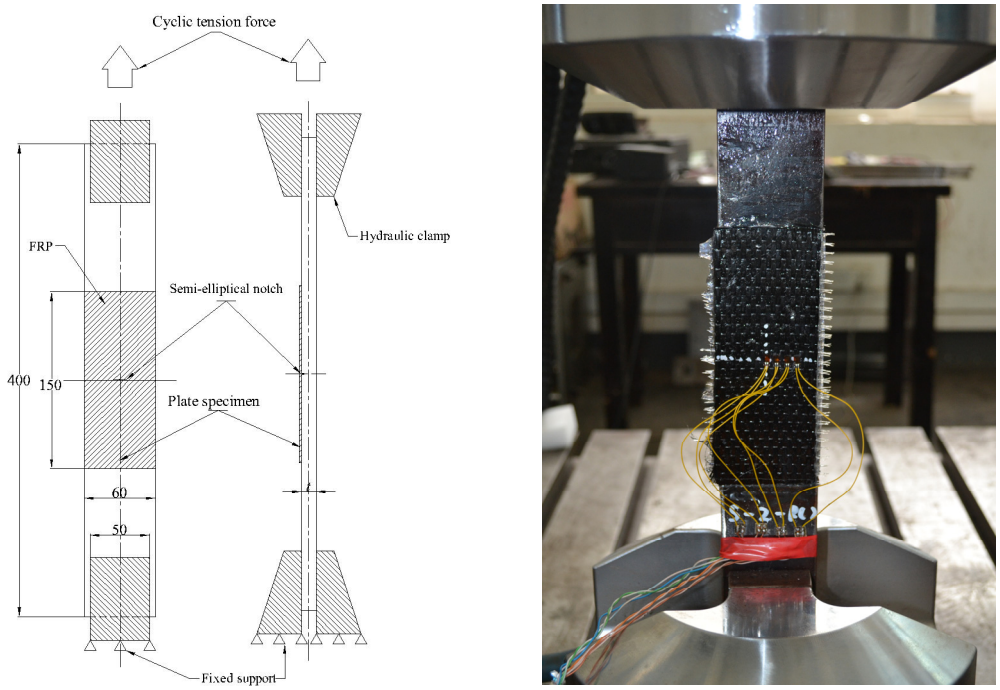

Figure 4.4. Specimen installation: a) the schematic; b) the actual specimen installation

During the fatigue test, the strain on the external CFRP laminate along the crack propagation path was monitored, as shown in Figure 4.5a. Four strain gauges were installed along the middle line, as indicated in Figure 4.5b. The size of each strain gauge is 4.0 mm × 4.0 mm, and the distance between each adjacent strain gauge is 3.0 mm. Therefore the gauge matrix can cover 25.0 mm × 4.0 mm of the right middle area on the external CFRP laminate. Then the gauges were connected to the dynamic strain indicator TMR™-300, which was set to record the strain data for 60 seconds of every 10,000 cycles until the end of the fatigue test. These data would help us to trace the crack-induced debonding during the fatigue test [129]. Note that the strain monitoring was not conducted for the specimens in Group 7.

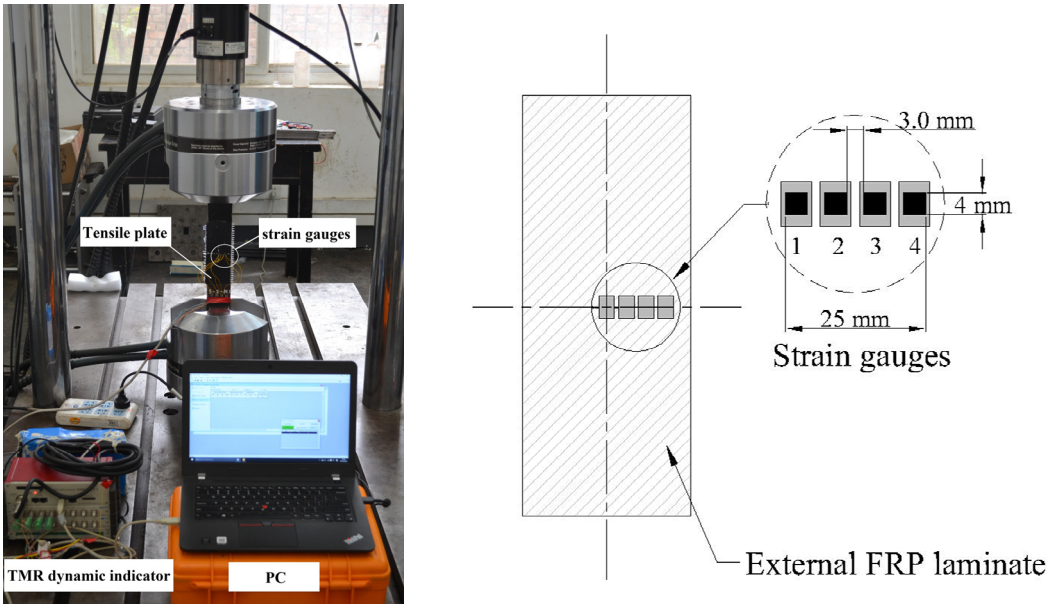

a b

Figure 4.5. a) Actual fatigue test set-up; b) strain gauges distributed on the external FRP laminate

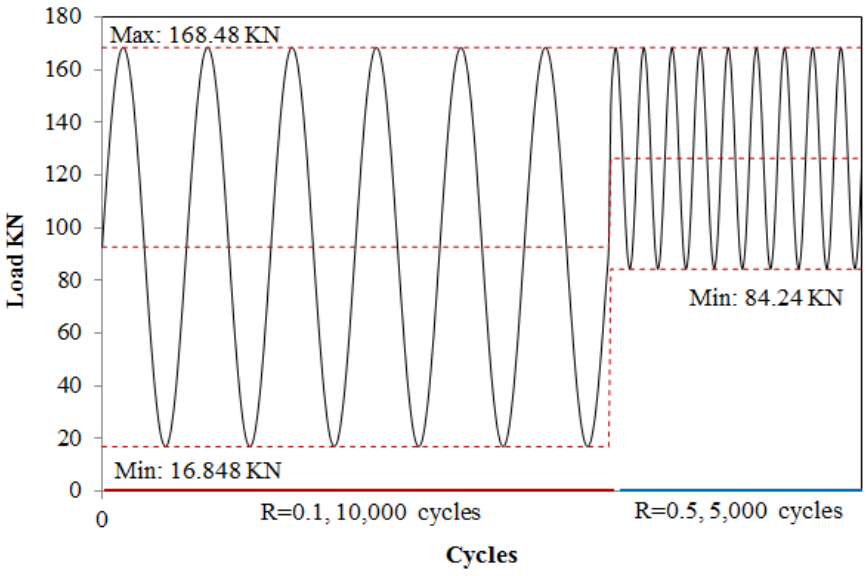

Figure 4.6. The load spectrum and beach mark generating procedure

All the fatigue tests were conducted at room temperature and air environment under load control condition. The loading frequency was set as 12.0 Hz. The load ratio *R* maintained 0.1 for the crack growth process of all tests. The crack growth process was recorded by Beach Marking technique by means of changing the load ratio *R* to 0.5 and cycle for 5,000 cycles, as described in Figure 4.6. Each test ended automatically once the tensile specimen fractured and trigger the displacement limiter of the fatigue machine.

4.1.3 Test results

Possible failures might occur when using CFRP to reinforce structures subjected to tension, including interfacial failures, cohesive failures, FRP delamination, and FRP ruptures [22]. In this section, the failure modes during and after each fatigue test, and the surface crack growth behaviour & results of each specimen were presented.

4.1.3.1 Failure modes during the fatigue test

The failure modes of all composite reinforced specimens during each fatigue tests are listed in Table 4.5. During the fatigue test, failures including cohesive failures, FRP delamination, and FRP ruptures did not occur on all specimens. After the fatigue test, along with the fracture of the steel plate, the FRP patch entirely debonded from the steel substrate of each specimen. Besides, during the fatigue test, edge debonding failures between the FRP patch and the steel substrate were observed. In total, four out of 14 specimens have encountered the edge debonding failure. These debonding failures happened either at the beginning (e.g., SE-1-R(1)) or later during the fatigue test (e.g. SE-1-R(2)), as shown in Figure 4.7.

Table 4.5. Failure modes during the fatigue tests

Specimen	Edge debonding	*N* when optical failure occurs	Crack-induced debonding	*c* when crack-induced debonding occurs
SI-1-R(1)	No	/	No	/
SI-1-R(2)	No	/	No	/
SI-1-R(3)	No	/	No	/
SE-1-R(1)	**Yes**	Between 30,000~40,000	**Yes**	Between 9.4 and 11.39 mm
SE-1-R(2)	**Yes**	Between 60,000~70,000	**Yes**	Between 8.8 and 10.07 mm
SE-1-R(3)	No	/	No	/
SE-2-R(1)	No	/	No	/
SE-2-R(2)	No	/	No	/
SE-2-R(3)	**Yes**	Between 70,000~80,000	**Yes**	Between 8.78 and 10.52 mm
SE-3-R(1)	No	/	No	/
SE-3-R(2)	No	/	No	/
SE-3-R(3)	No	/	No	/
SE-1-R2(1)	No	/	No	/
SE-1-R6(1)	**Yes**	Between 20,000~30,000	**Yes**	Between 9.22 and 11.27 mm

Figure 4.7. Edge debonding occurred during the fatigue test

When crack-induced debonding occurred, the strain on the external layer of FRP laminates around the surface cracked area would drop dramatically, owing to the fact that there is no shear stress transfer within the debonded region [129]. Therefore, the crack-induced debonding is possible to be detected using the installed strain gauge matrix. Then strain values for each specimen of every 10,000 cycles are linked to their corresponding crack length, calibrate by the cycle-index. In this study, the strain around the cracked area on the external CFRP layer was recorded, as shown in Figure 4.5b.

The study in Ref. [129] indicated that when using FRP to reinforce through-thickness cracked steel plates, the crack-induced debonding would occur along with the crack growth. While the crack-induced debonding did not occur on the majority of the specimens in this study, based on the stable strain data variation on the external CFRP laminate around the cracked area during the fatigue test. The crack-induced debonding did occur on four composite reinforced specimens (listed in Table 4.5), indicated by the sudden drop of the strain value. The crack size recorded in Table 4.5 when the crack-induced debonding occurred indicated that the failure usually at the later stage of the fatigue tests. Besides, it often accompanied by the edge debonding.

Figure 4.8 shows an example of the strain data of one cycle recorded before, during and after the crack-induced debonding occurs of specimens SE-1-R(2). The name of the curve means the strain data of the corresponding strain gauge (e.g., G1 to G4 represent the four gauges, the ‘Be’, ‘Du’, and ‘Af’ means before, during, and after the crack-induced debonding occurred respectively). It can be seen that when the crack-induced debonding occurred, the strain monitored by the four strain gauges decreases dramatically. The monitored strain value of G1 is the smallest and the strain increases successively from G1 to G4. After the crack-induced debonding occurred, the FRP patch around the middle of the steel plate completely lost the bond to the steel substrate, resulting in the almost zero micro strain value.

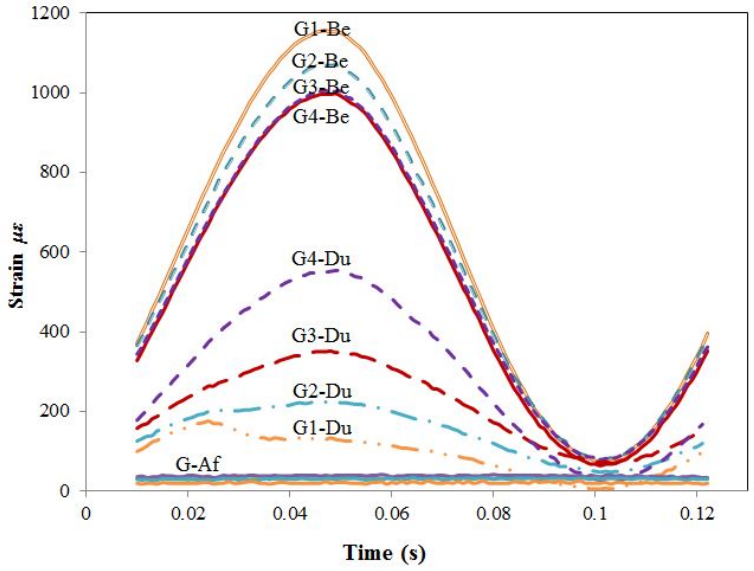

Figure 4.8. Strain monitoring data of before, during, and after crack-induced debonding occurs of specimen SE-1-R(2). Note that the 'Be', 'Du', and 'Af' means before, during, and after the crack-induced debonding occurred respectively

4.1.3.2 Failure modes after the fatigue test

Necking phenomenon appeared at the end of the fatigue test after the surface crack penetrated the wall, as shown in Figure 4.9a. Then the crack growth entered the rapid growth stage because of the limited effective sectional area, indicated by the rough cross-section surface, as shown in Figure 4.9b. Eventually after the fatigue test, the FRP patch debonded from the steel substrate uniformly, as shown in Figure 4.9c. No cohesive failure or FRP delamination, or FRP rupture were observed for all specimens.

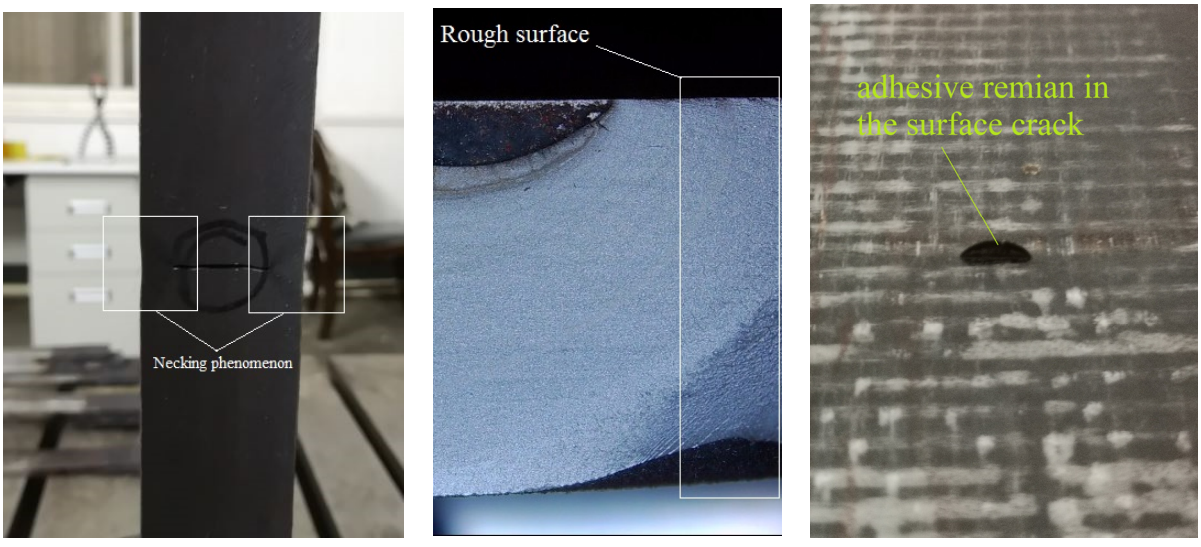

a b c

Figure 4.9. Failure modes after the fatigue tests: a) necking phenomenon appeared at the end of the fatigue test; b) rough fracture surface of the specimens after the fatigue test; c) uniform debonding after the fatigue test

4.1.3.3 Surface crack growth behaviour and crack growth results

The crack growth behaviour was recorded by the Beach Marking technique using an electronic reading microscope, as shown in Figure 4.10. One random specimen was selected from each repetitive three specimens to show the crack shape variation during the fatigue test. The cycle index between each two adjacent beach marks is 10,000. The figures clearly demonstrate the multiple initiations along the notch fronts, and the surface cracks continually propagated as a semi-elliptical shape until the crack penetrated the pipe wall. The results of crack depth and length, corresponding to the cycle-index are listed in the Table II.1 in Appendix II.

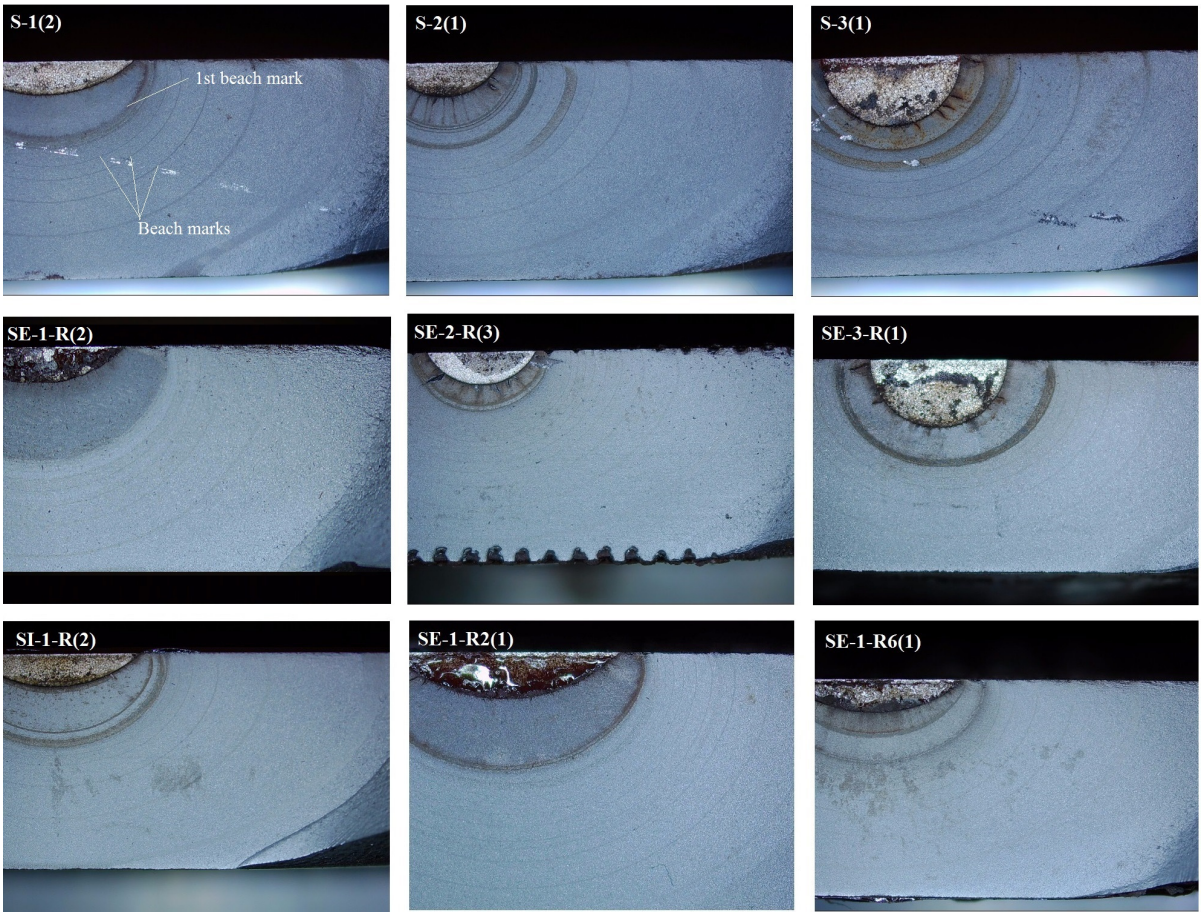

Figure 4.10. Beach marks on the cross-section of the steel plate specimens

4.1.4 Discussion on the crack growth results

In this section, the crack growth results of all specimens were discussed and analysed. Because of the individual difference between each repetitive specimen in each group, after the pre-cracking procedure, the notches have propagated to different sizes. This made it impossible to directly compare the crack growth between different specimens with the same notch sizes. To facilitate the analysing of surface crack growth, the results of crack growth along the depth/length direction versus cycle-index are modified by the interpolation method to follow the same starting crack depth. The results therefore are shown by the curves of crack

growth along the depth/length direction versus the cycle index. In addition, since debonding failure may have a negative influence on the FCGR, the response of FCGR of each specimen was analysed.

4.1.4.1. Using FRP to reinforce the reversed side of the cracked surface of the steel plates

In certain situations, directly reinforcing the cracked surface in a metallic structure is not feasible. In such case, reinforcing the reversed side of the cracked surface might be an alternative. In this section, the results of using FRP patch to reinforce the reversed side of the cracked surface of the steel plates are analysed. The results of *a*-*N* & *c*-*N* and d*a*/d*N*-*a* & d*c*/d*N*-*c* of the reinforced specimens are compared with the un-reinforced specimens.

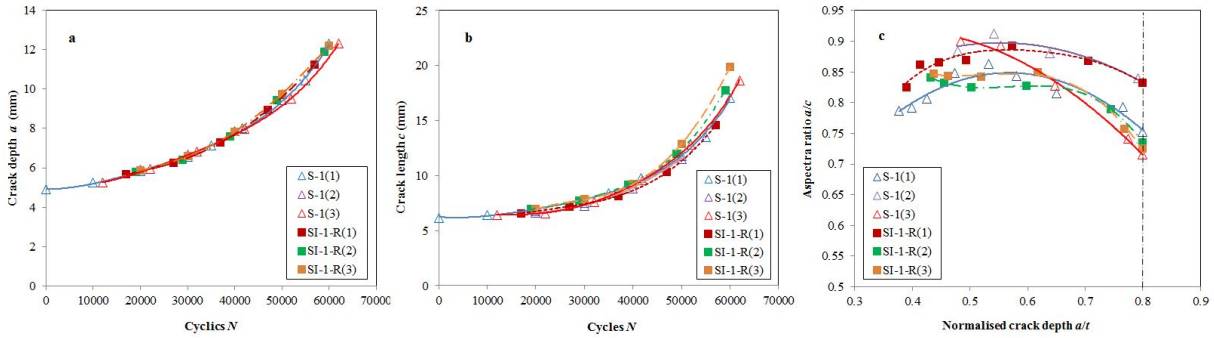

Figure 4.11. The experimental results of S-1 and SI-1-R: a) crack growth along depth direction; b) crack growth along length direction; c) a/c versus a/t ratio. Note that the name of the specimens has been explained in Sub-section 4.1.1.3

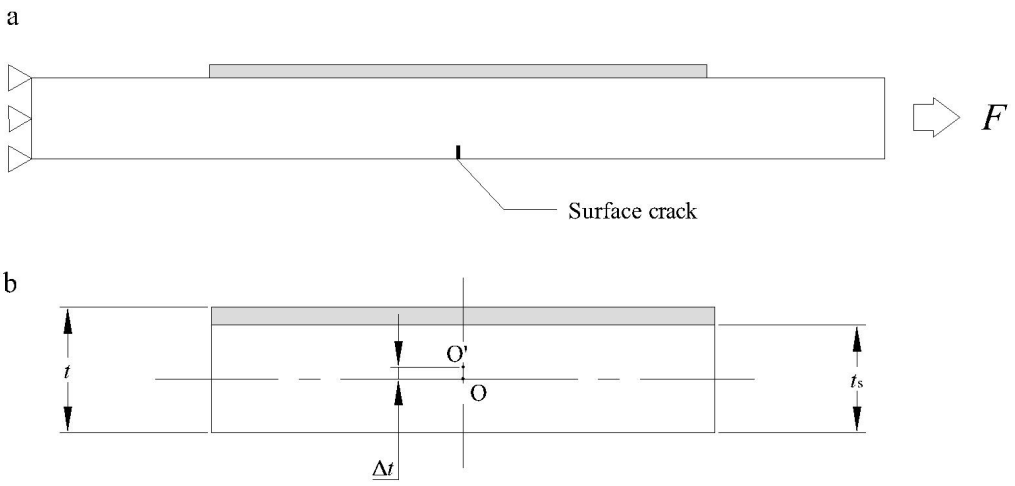

Figure 4.12. Gradient stress distribution in composite reinforced steel plate caused by out-of-plane bending: a) composite reinforced steel plates under pure tension; b) parameters of the CRS

The results of surface crack growth of using FRP to reinforce the reversed side of the cracked surface are shown in Figures 4.11a and 4.11b. The results of S-1 and SI-1-R are consistent with each repetitive specimen respectively. However, rather than prolonging the residual fatigue life, the composite reinforcement slightly shortened the fatigue life. The reason is that besides the positive effects in terms of decreasing the stress distribution, the

composite reinforcement have generated an out-of-plane bending moment on the steel plate owing to the asymmetric reinforcing geometry, as indicated in Figure 4.12. Eventually it let the stress value—combined the tensile stress and bending stress on the un-reinforced surface—become higher than the un-reinforced steel plates, resulting in a larger SIF and a higher FCGR. The mechanism will be further studied by means of the theoretical analysis in Section 3.

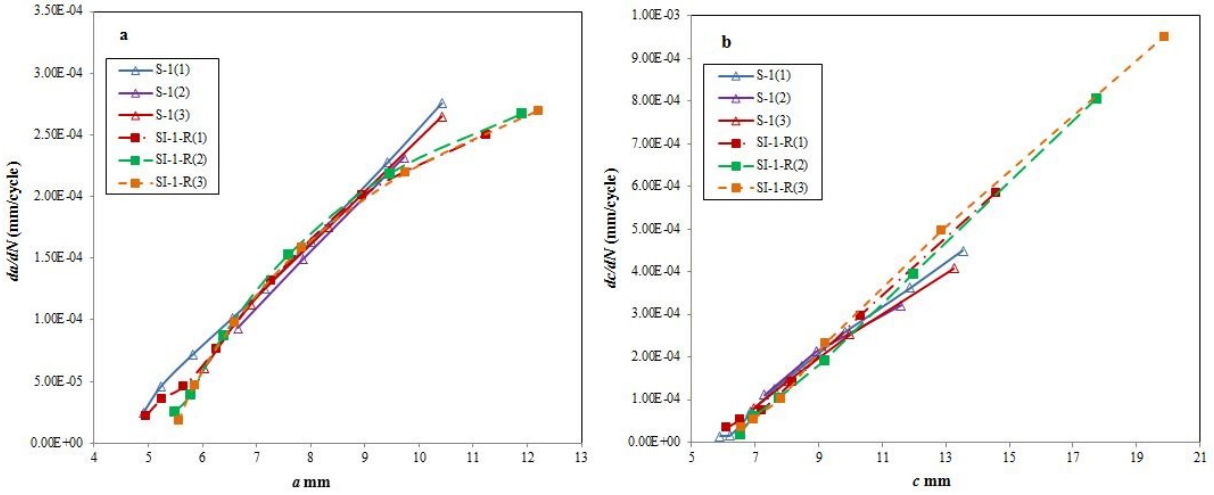

Figure 4.13. The FCGR of S-1 and SI-1-R of using four layers of CFRP: a) along the depth direction; b) along the length direction

The increasing of the surface crack growth rate is further explained by the variation of the *da*/*dN*-*a* curve in Figure 4.13a and *dc*/*dN*-*c* curve in Figure 4.13b. The d*a*/d*N*-*a* and d*c*/d*N*-*c* relations are determined from the *a*-*N* and *c*-*N* results. The method is first evaluating the differential coefficient of the *a*-*N* and *c*-*N* curves, and then calculating each values of the d*a* and d*c* based on each corresponding *a* and *c*. The *da*/*dN* of SI-1-R first increased to a higher value than the non-reinforced specimens, but then decreased evidently due to the decreasing stress (see in Figure 4.13b). While the *dc*/*dN* of SI-1-R were always higher than the *dc*/*dN* of S-1 specimens, owing to the higher stress value on the cracked surface caused by the out-of-plane bending moment. In addition, since there was no direct contact between the surface crack and the composite reinforcement, the crack-bridging effect did not contribute to the decreasing of the SIF of the surface point; hence the composite reinforcement did not evidently influence the preferred aspect ratios of the surface cracks, as shown in Figure 4.13c.

4.1.4.2 Composite reinforcement on the cracked surface of the steel plates with different notch sizes

In this part, the results of composite reinforcement on the cracked surface of specimens with three different crack sizes are analysed. The results of *a*-*N* & *c*-*N* and d*a*/d*N*-*a* & d*c*/d*N*-*c* of the reinforced specimens are compared with the un-reinforced specimens. The abnormal crack growth behaviour, i.e., the sudden growth of crack growth rate, is explained by the failure modes during the fatigue tests.

The surface crack growth results of the specimens in Group 5 by using the FRP patch to reinforce the cracked surface, i.e., SE-1-R, is shown in Figure 4.14. It demonstrated that there are two diverse results among the three reinforced specimens: the composite reinforcement of SE-1-R(2) and SE-1-R(3) have significantly prolonged the residual fatigue life approximately around 130%, while only around 20% for SE-1-R(1) due to the early occurred edge debonding failure. The possible reason of the edge debonding failures is due to the overlarge stress concentration caused by the imperfect bond condition, i.e., surface treatment, non-uniform of adhesive thickness. Note that in this chapter, the fatigue life is the cyclic index till the crack penetrating the wall thickness. In addition, when the crack penetrated the thickness, the specimens with effective reinforcement had shorter crack length. Finally the preferred aspect ratio (*a*/*c* when *a*/*t* equals to 0.8) of the composite reinforced specimen is larger than the preferred aspect ratio of the un-reinforced specimens (in between 0.7 to 0.8), as shown in Figure 4.14c. The preferred aspect ratio of SE-1-R(3), which no failure occurred, is around 1.0 owing to the composite reinforcement; while the aspect ratio of SE-1-R(2) is larger than the unreinforced specimens but much smaller than the SE-1-R(3) due to the edge debonding and crack-induced debonding occurred the later stage. Since SE-1-R(1) has encountered serious edge debonding and crack-induced debonding at the beginning, its preferred aspect ratio is identical with the unreinforced specimens.

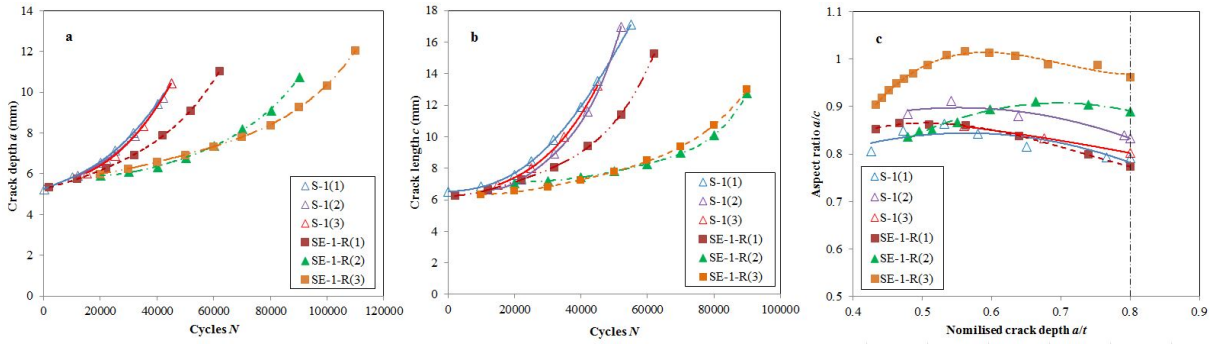

Figure 4.14. The experimental results of S-1 and SE-1-R of using four layers of CFRP: a) crack growth along depth direction; b) crack growth along length direction; c) a/c versus a/t

Figure 4.15 illustrates that the FCGR of SE-1-R(1) is higher than the SE-1-R(2) and SE-1-R(3), due to the edge debonding failures occurring at the beginning of the fatigue tests (indicated in Table 4.5). Thus the less bonding area became not effective enough to decrease the SIF. Figure 4.15 also shows that an obvious rising trend of *da*/*dN* and *dc*/*dN* have been appeared on SE-1-R(2), induced by the edge debonding happened when *a* and *c* became larger than about 9.0 mm (in between 60,000 to 70,000 cycles). The edge debonding further triggered the crack-induced debonding, monitored by the strain gauges matrix (see in Figure 4.8 and in Table 4.5). Expect that, the composite reinforced SE-1-R(3) had averagely decreased the FCGR along the depth direction of around 6.69×10^{-5} mm/cycle, while 1.25×10^{-4} mm/cycle along the length direction. Therefore the FCGR along the length direction decreases more significantly than along the depth direction, which eventually resulting in the increasing the preferred aspect ratio.

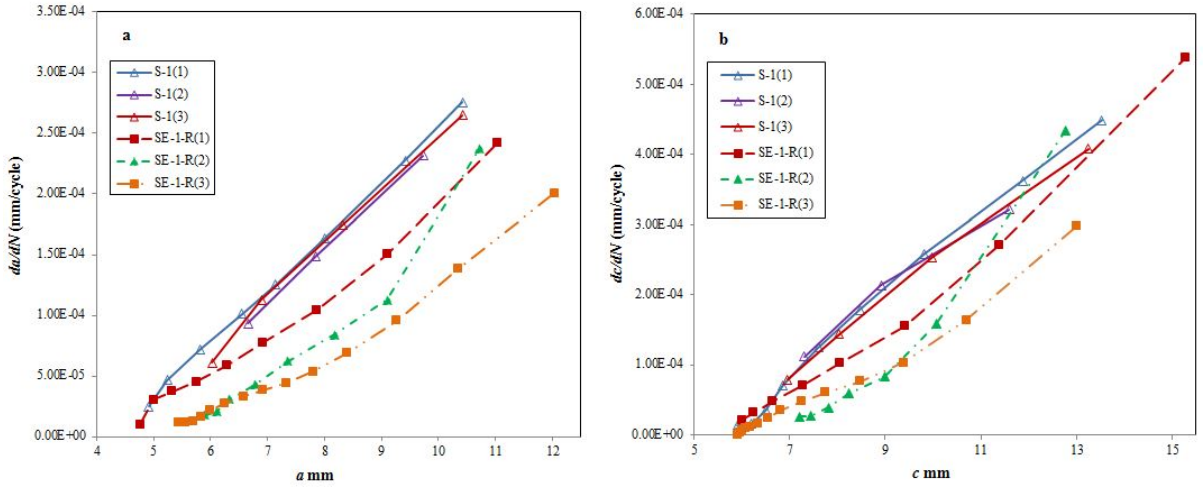

Figure 4.15. The FCGR of S-1 and SE-1-R of using four layers of CFRP: a) along the depth direction; b) along the length direction

The specimens of SE-2-R has the same initial notch depth (a = 2.0 mm) with the specimens of SE-1-R, but a shorter notch length. The results in Figure 4.16 illustrate that the results of SE-2-R repetitive specimens have good agreement with each other. Similar to SE-1-R(2), the composite reinforcement have significantly prolonged the residual fatigue life. The specimen of SE-1-R(1) encountered a sudden increase at the later stage during the fatigue test, triggered by the edge debonding and crack-induced debonding. However, since the debonding failures occurred at the later stage, they did not cause considerable influence on the surface crack growth—specimen SE-2-R(1) had only around 3.5% less residual life than the other two reinforced specimens.

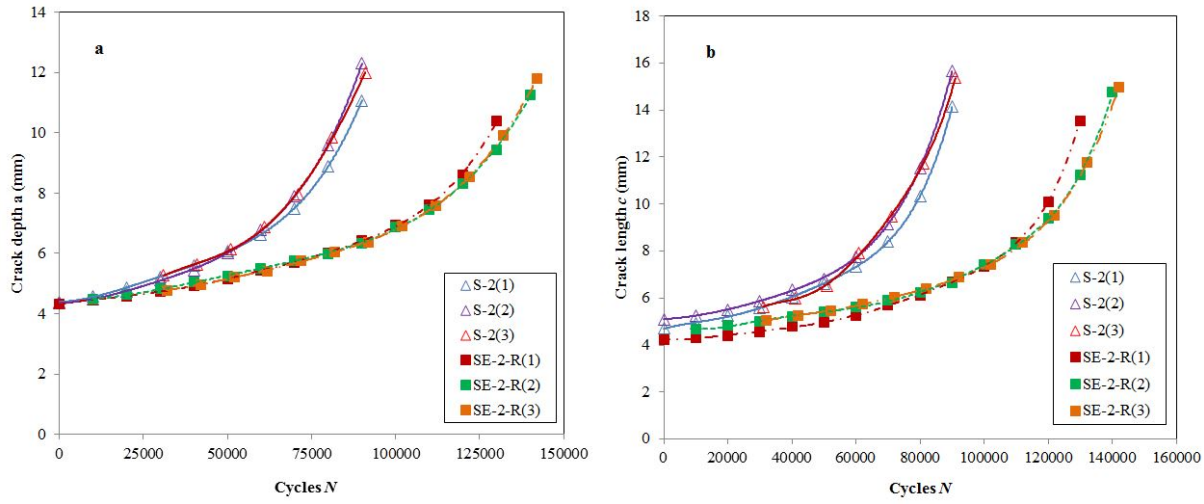

Figure 4.16. The experimental results of S-2 and SE-2-R: a) crack growth along depth direction; b) crack growth along length direction

The *da*/*dN*-*a* and *dc*/*dN*- *c* curve in Figure 4.17 illustrates that the crack growth rates of SE-2-R(1) is higher than the SE-1-R(2) and SE-1-R(3) when c reached around 8.5 mm (in between 70,000 to 80,000 cycles), due to the occurrence of the edge debonding and the crack-induced debonding (indicated in Table 4.5). Except that, the composite reinforcement has

averagely decreased the FCGR (e.g., SE-2-R(2)) along the depth direction of 8.94×10^{-5} mm/cycle, 1.50×10^{-4} mm/cycle along the length direction.

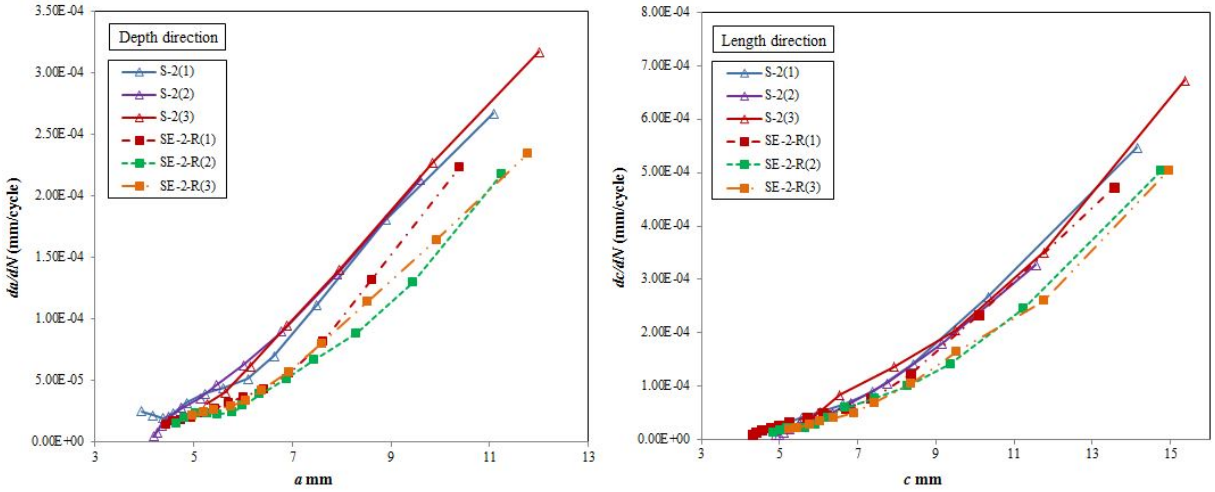

Figure 4.17. The FCGR of S-1 and SE-1-R of using four layers *of CFRP: a) along the depth direction; b) along the length direction*

However, using the FRP patch to reinforce large surface cracks was not as efficient as reinforcing smaller cracks. The reinforcement only had a minimal effect on reducing the FCGR of the specimens SE-3-R when the crack has already penetrated around half of the wall thickness, with only around 15%, as shown in Figure 4.18. The reason is not due to the absolute decreasing value of the FCGR, but the relative decreasing value. Thus the small relative decreasing FCGR eventually resulted in a limited extension of the fatigue life. Therefore, composite reinforcement on surface cracked steel plates should be implemented as early as possible.

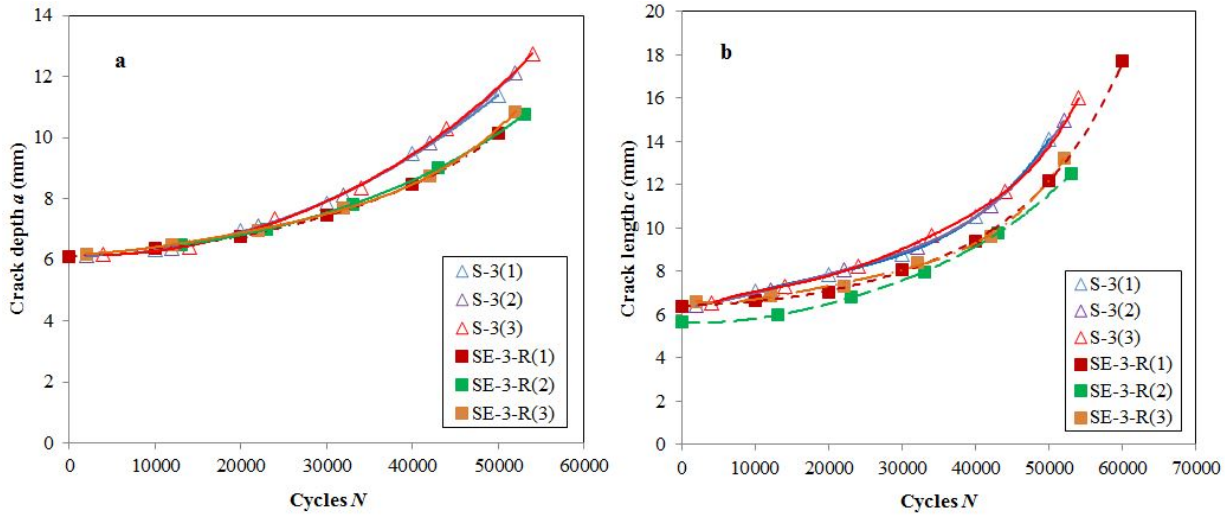

Figure 4.18. The experimental results of S-3 and SE-3-R: a) crack growth along depth direction; b) crack growth along length direction

4.1.4.3 Composite reinforcement on the cracked surface of the steel plates using different number of CFRP layers

As is commonly acknowledged, applying more numbers of composite laminates can promote the reduction the FCGR of the through-thickness cracks [146]. This has not yet been investigated on reinforcing the surface cracks. In this section, three different layers of CFRP, i.e. two layers, four layers, and six layers, are used in order to identify the influence of the number of CFRP layer on surface crack growth. Note that because of the limited number of specimens, only one specimen is prepared for the cases of using two layers and six layers.

The d*a*/d*N*-*a* and d*c*/d*N*-*c* curves in Figure 4.19 show that FCGR of SE-1-R6(1) is higher than the other two composite reinforced specimens shortly after the beginning of the test, due to the early occurred edge debonding failure. Despite the sudden FCGR increasing of specimen SE-1-R(2) when *a* and *c* reached about 9.0 mm, there is no big difference of the FCGR between the specimens using two layers of CFRP laminates and four layers of CFRP laminates. That indicates using more numbers of CFRP laminates of the single-side FRP patch might not be able to promote the effectiveness on reducing the FCGR of surface cracks.

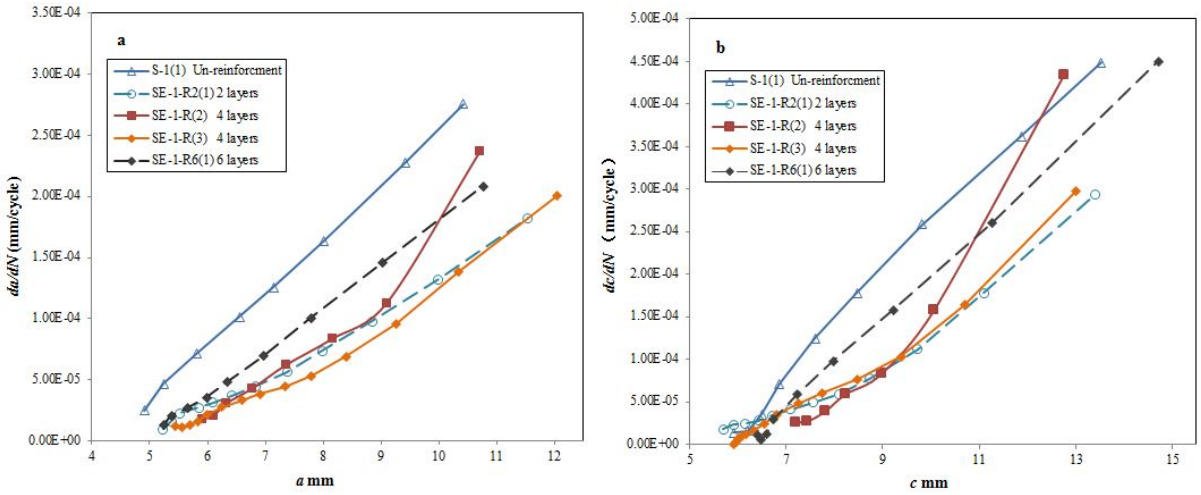

Figure 4.19. The FCGR of S-1 and SE-1-R of using different layers of CFRP: a) along the depth direction; b) along the length direction

4.1.5 Summary

The single-side composite reinforcement on the cracked surface has significantly decreased the FCGR and prolonged the residual fatigue life, owing to the crack-bridging effect as well as the effect of the out-of-plane bending moment. Indicated by the experimental study, the reinforcement has maximally prolonged the residual fatigue life of around 130%. In addition, the FCGR along the length direction decreased more significantly than along the depth direction, resulting in a higher preferred aspect ratio.

When using FRP to reinforce metallic structures, extra attention is needed on the failures during the test which might influence the crack growth, such as cohesion failures, FRP delamination, and interfacial debonding. In this study, during the fatigue test, the majority of the specimens (10 out of 14) did not encounter with any failures during the fatigue test—the FRP laminates were perfectly bonded on the steel substrate. The edge debonding occurred on

two specimens at the beginning and two specimens at the later stage respectively. The early occurred edge debonding has largely weakened the effectiveness of composite reinforcement, resulting in a minimal prolongation of the fatigue life of around 20%. The imperfect bond condition might be the culprit that has largely weakened the bond strength under the high load condition, which should be avoided by improving the surface treatment of the steel substrate.

The concerned interfacial failure, i.e., crack-induced debonding, which is a serious threat of the composite reinforcement system on repairing through-thickness cracks in steel plate, did not occur on the majority of the specimens. It means that when using FRP to reinforce surface cracked steel plates under cyclic tension, once the quality of the bond condition between the composites laminates and steel substrate is guaranteed, the crack-induced debonding is not a threat to the composite reinforcement on the surface cracked plate. In addition, even if the crack-induced debonding occurs, its negative influence on the FCGR was not serious, with only around 3.5% less residual life extension than the repetitive specimens on which no crack-induced debonding occurred.

4.2 Analysis on the possible interfacial failures by using cohesive zone model

In this section, the possible interfacial failures, i.e., crack-induced debonding and edge debonding, are analysed by using the cohesive zone model. First, the cohesive zone model is developed through the FEM, and then validated by available experimental results. Thereafter, based on the FE model, possible interfacial failures of the surface cracked plate within different crack sizes are analysed.

4.2.1 Cohesive zone modelling

4.2.1.1 Material properties in the cohesive zone model

The FE model contains four different materials, i.e., the metallic substrate, GFRP, CFRP, and adhesive, which material properties are conforming to the test materials. The interface between the metallic substrate and the FRP laminates is simulated by applying the bilinear traction-separation cohesive zone model, as indicated in Figure 4.20. Within in Figure 4.20, τ_0 is the shear strength, δ is the displacement when interfacial failure occurs, δ_0 is the displacement corresponding to τ_0, k is the shear stiffness, G_c is the energy release rate. Based on the FRP-to-steel traction-separation model [147], G_c is evaluated as

$$G_c = 31\left(\frac{T}{G}\right)^{0.56} {t_a}^{0.27}. \tag{4.1}$$

The shear strength is estimated as

$$\tau_0 = 0.8 \cdot T, \tag{4.2}$$

and δ_0 is calculated as

$$\delta_0 = \frac{t_a \tau_0}{G}, \tag{4.3}$$

where t_a is the adhesive thickness, and G is the shear modulus of the adhesive. δ is calculated as

$$\delta = \frac{2G_c}{\tau_0}, \tag{4.4}$$

The slope of the ascending part is equated to the shear stiffness of the adhesive layer, which is

$$k = \frac{\tau_0}{\delta_0}; \tag{4.5}$$

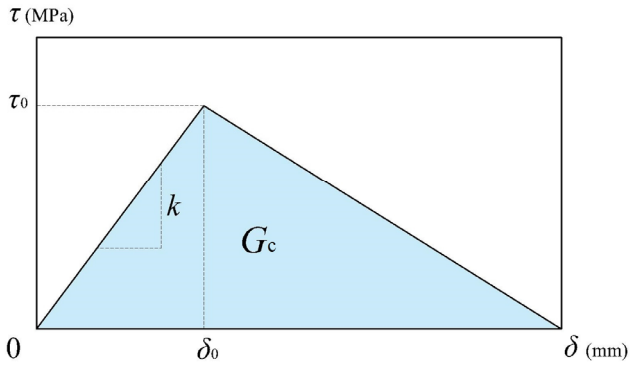

Figure 4.20. The bi-linear traction-separation law

4.2.1.2 Modelling strategy

Figure 4.21 shows a quarter-FE model, boundary condition, and the mesh conditions. The FE model constitute of three parts: the metallic plate, adhesive layer, and FRP laminates. The metallic plate and the FRP laminates were modelled by using the 8-node linear brick element C3D8R, while the adhesive layer is modelled by using the 8-node three dimensional cohesive element COH3D8.

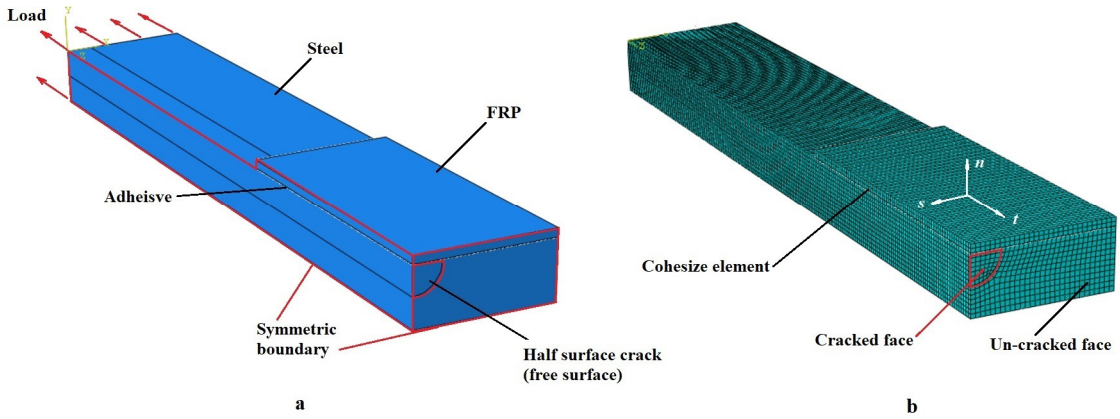

Figure 4.21. a) A quarter-FE model and boundary conditions; b) meshing conditions of the FE model

Conforming to the test specimens, the thickness of each layer is 0.35 mm. The thickness of the adhesive is 0.1 mm. The constraints of FRP-adhesive-steel interactions are set as tie.

Then a half semi-elliptical surface crack is modelling within the steel plate. Symmetric boundaries are set on the quarter-FE model on two surfaces, a tension load was applied on the edge face of the steel. While the boundary condition of the cracked surface is set as free. Sweep meshing method is applied on the FE model. The global mesh size is set as 1.0 mm in order to ensure robust evaluations.

A bi-linear traction-separation behaviour between the steel substrate and the composite laminates was assumed before the initiation of the interfacial failures

$$\begin{Bmatrix} \tau_t \\ \tau_s \\ \sigma_n \end{Bmatrix} = \begin{bmatrix} k_{tt} & & \\ & k_{ss} & \\ & & k_{nn} \end{bmatrix} \begin{Bmatrix} \delta_t \\ \delta_s \\ \delta_n \end{Bmatrix} \tag{4.5}$$

where τ_t and τ_s are two in-plane shear tractions; and σ_n is the normal traction. The corresponding separations are δ_t, δ_s, and δ_n. For cracked plate reinforced with FRP subjected to tension, only in-plane traction and separations were considered [129]. The failure mechanism at the interface consists of a damage initiation criterion and a damage evolution model. Damage is assumed when the traction stress reaches τ_0, which is indicated by the SDEG result in ABAQUS when its value is larger than 0. The completely failure of the interface, i.e., debonding, is indicated when the SDEG value reaches 1.0.

4.2.2 Analysis of the possible interfacial failures

Based on the validated FE model, the interfacial failures of the composite reinforced surface cracked steel plate subjected to tension with different crack sizes were analysed. The crack sizes adopted the experimental results of specimen of SE-1-R(1). The parameters of the cohesive model are $\tau_0 = 56$ MPa, $\delta_0 = 0.004$ mm, $\delta = 0.035$ mm, $G_c = 0.98\ \text{MPa} \cdot \text{mm}^{0.5}$, $k = 14000\ \text{MPa} \cdot \text{mm}^{-1}$. The results of the stiffness degradation in different models are shown in Figure 4.22.

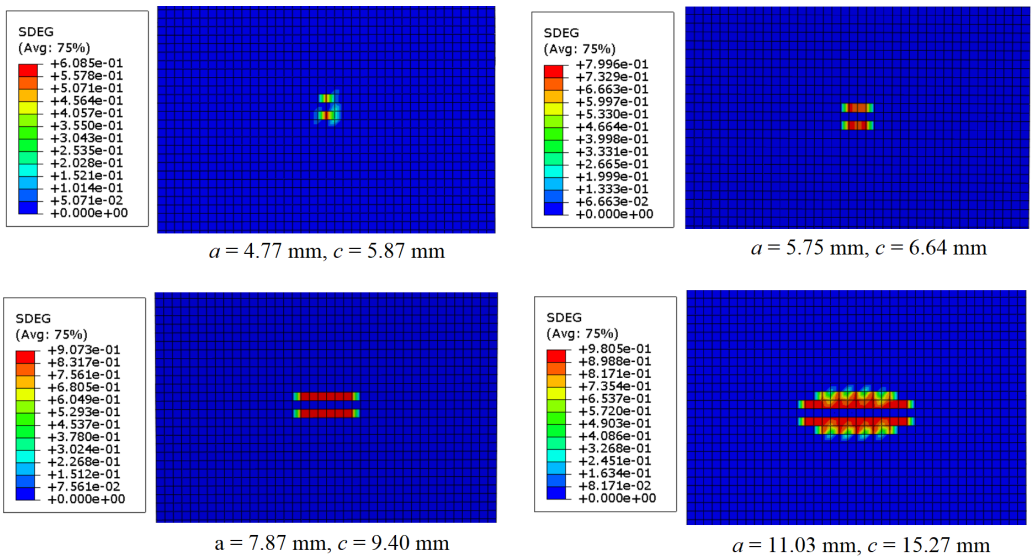

Figure 4.22. a) A quarter-FE model and boundary conditions; b) meshing conditions of the FE model

Figure 4.22 shows the results of the stiffness degradation of the interface between the steel substrate and the FRP laminates, indicated by the SDEG value. The value of SDEG represents the degree of the stiffness degradation, and the interfacial debonding occurred when SDEG equals to 1.0. Therefore, along with the surface crack growth from a relatively small size to a large size, the degree of the degradation increases, indicated by the size of the stiffness degradation area and the SDEG value. Since the SDEG did not reached 1.0 for all crack sizes, indicating the FRP laminates adequately bonded on the steel substrate. However, the increasing stiffness degradation might result in the reduction of the reinforcement effectiveness on the crack growth along the length direction.

4.3 Numerical investigation on surface crack growth in steel plates reinforced with FRP

The numerical investigation is conducted to further analyse the composite reinforcement on surface cracked steel plate. In this section, a three-dimensional FE model is developed to calculate the SIF along the surface crack front reinforced with FRP. Then the FE model is validated by the experimental results. By means of this analysis, the modelling parameters, meshing conditions and the connection setup between the CRS and the steel substrate are determined.

4.3.1 FE model

The FEM is an efficient method to evaluate the SIF of surface cracks in metallic structures reinforced with composite patches. In this section, a three-dimensional FE model is developed to calculate the SIF of the surface crack in composite reinforced steel plates.

4.3.1.1. Materials in the FE model

The FE model contains four different materials: the steel substrate, GFRP, CFRP, and adhesive. Conforming to the experimental study, the material properties of the GFRP, CFRP and adhesive are listed in Tables 4.1 to 4.3 respectively.

4.3.1.2. Configuration of the FE models

The FE model of composite reinforced surface cracked plate conforms to the experimental specimens, whose sketch diagram is shown in Figure 4.1. While different from the experimental specimens, besides the single-side composite reinforcement on the cracked surface or the reversed surface, the double-side reinforcement on both sides is investigated as well.

On account of the experimental results indicating the no delamination failures within the FRP laminates occurred during the fatigue test, and the overall patch thickness is around 1.85 mm, different layers of FRP laminates are modelled as a whole, by merging the bodies together while remain their own material properties and fibre directions. The initial sizes of

the surface cracks are conforming to the experimental specimens in Section 4.1, together with the reinforcement details, the specimen configurations are listed in Table 4.6.

Table 4.6. The configurations of the FE models

FE model	Crack size (mm)		Reinforcement scheme	Reinforced surface	No. of CFRP layer
	Crack	Crack			
S-1 FE	5.24	6.50	no reinforcement	/	/
S-2 FE	4.48	4.70	no reinforcement	/	/
S-3 FE	5.40	5.78	no reinforcement	/	/
SE-1-R FE	6.25	6.33	single-side reinforcement	cracked surface	4
SE-2-R FE	4.48	4.68	single-side reinforcement	cracked surface	4
SE-3-R FE	6.11	6.40	single-side reinforcement	cracked surface	4
SI-1-R FE	5.66	6.54	single-side reinforcement	reverse surface	4
SE-2-RD FE	4.48	4.68	double-side reinforcement	double sides	8

4.3.1.3. FE modelling strategy

The modelling strategy (e.g., element type, meshing method, element size, contours around the crack front and their divisions) has been discussed through the sensitivity analysis in Chapter 3 to ascertain that the FE model is able to rationally predict the SIF. The FE model adopts 20-node solid element 'solid 186'. Two different meshing methods are applied to the steel plate: the middle part where the crack is located adopts the tetrahedral meshing method; while the other two parts apply the sweep meshing method with hexahedron element. The sweep method is applied for the FRP laminates as well. To ensure a robust and accurate evaluation, a 3.0 mm body element size is used for the area around the surface crack and the adhesive layer, while 5.0 mm edge size is used for the rest parts of the steel plate, as well as the FRP patch, as shown in Figure 4.23.

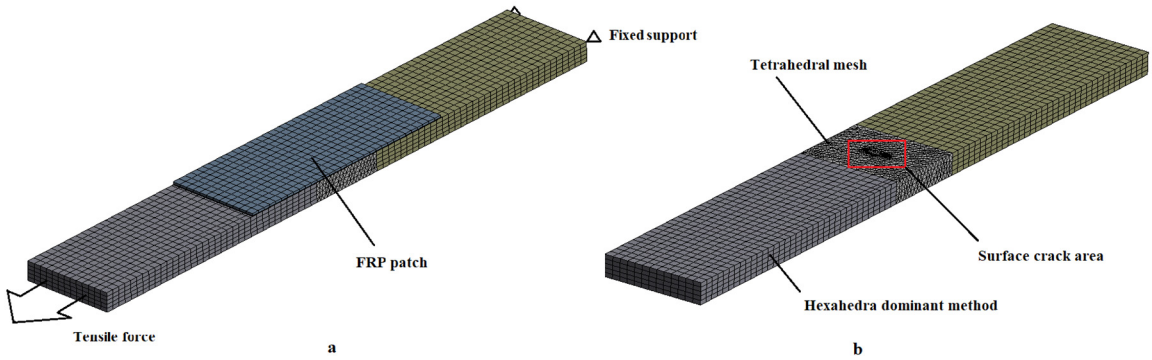

Figure 4.23. FE model: a) global meshing condition and boundary condition; b) the surface cracked area and different meshing methods

The semi-elliptical surface crack is modelled by the *Semi-elliptical Crack* module in ANSYS workbench 19. Six concentric contours with eight divisions of each are modelled around the surface crack front, as shown in Figure 4.24a. Then the surface crack is meshed using hexahedra dominant method, as shown in Figure 4.24b. The size of the external contour is 1.0 mm, thus the element size around the crack front is controlled as less than 0.2 mm.

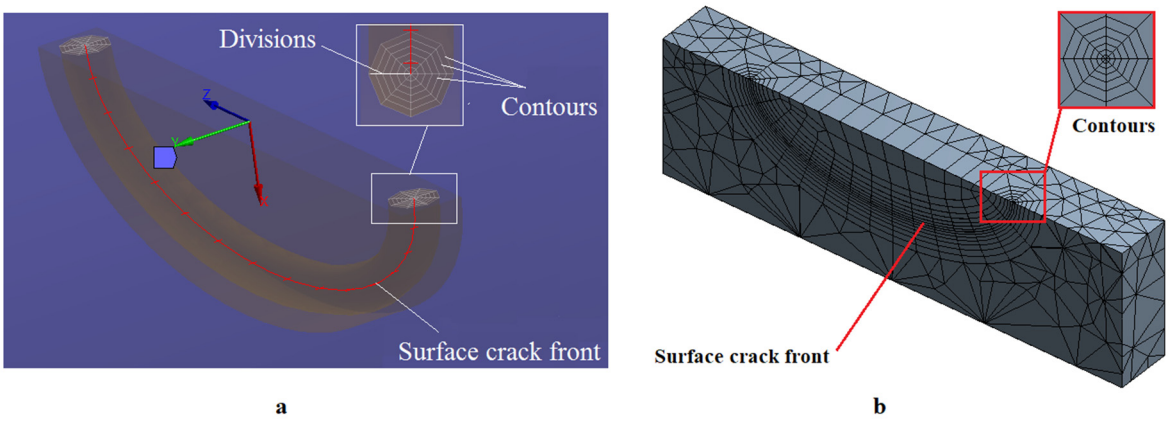

Figure 4.24. a) Surface crack modelling module; b) the mesh around the surface crack

Since the FRP laminates are modelled as a whole, setting the contact condition between the adjacent FRP layers is not necessary. While based on the results in Section 4.2 that the FRP laminates were adequately bonded on the steel, the bond constraint is set at the interface between the steel substrate and the adhesive layer, and at the interface between the adhesive layer and the GFRP laminate. Then the model is set to be subjected to tension—one side is fixed supported, while tensile load is applied on the other side. The amplitude of the tensile load is 168.48 kN, identical to the experimental set-up. Finally, the SIF along the crack front is calculated by means of the contour integral method.

4.3.1.4. FE results

In this sub-section, the FE results of the global and local stress distribution, as well the SIF along the surface crack front are presented. The results demonstrate the effectiveness of the composite reinforcement on the decreasing of stress distribution and the SIF along the surface crack front preliminarily, while further validation of the FE results will be presented in Section 4.3.2.

- Global and local stress distribution in the steel plate

The global equivalent stress distribution on the steel plate of ‘S-1’ and ‘SE-1-R’ models are shown in Figure 4.25. It illustrates that under the composite reinforcement, the stress decreases dramatically, especially in the area covered by the FRP. The maximum stress has dropped from 2876.4 MPa to 1239.2 MPa, of 56.92%. Figure 4.26 indicates that the stress concentrates around the surface cracked area where the maximum point located at the surface point. Owing to the composite reinforcement, the stress concentration zone around the surface crack, represented as the butterfly zone, becomes smaller.

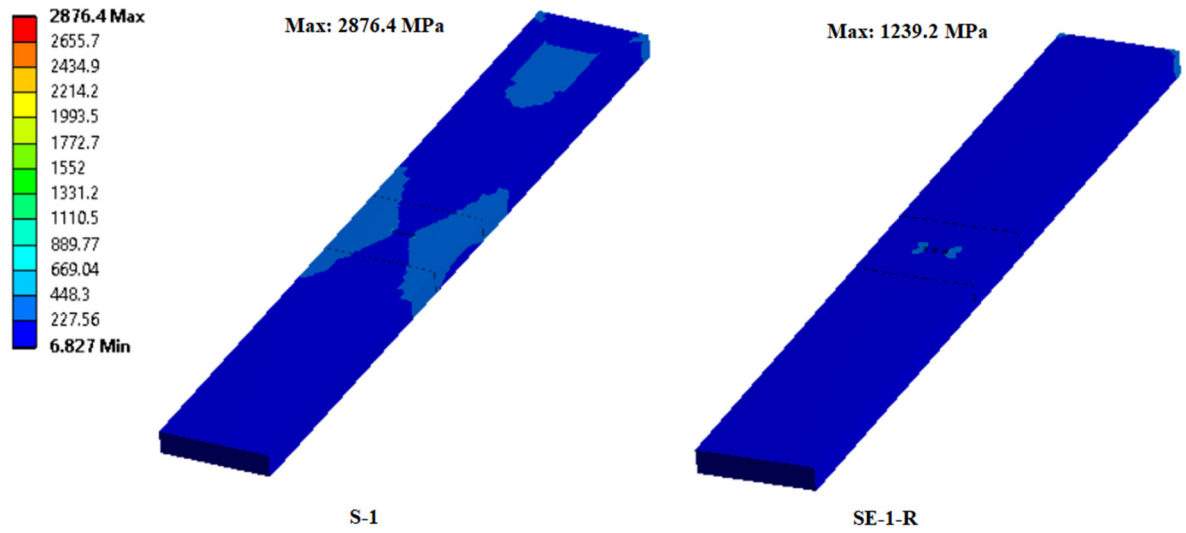

Figure 4.25. The global equivalent stress distribution of the plate including the un-reinforced plate and the composite reinforced specimen

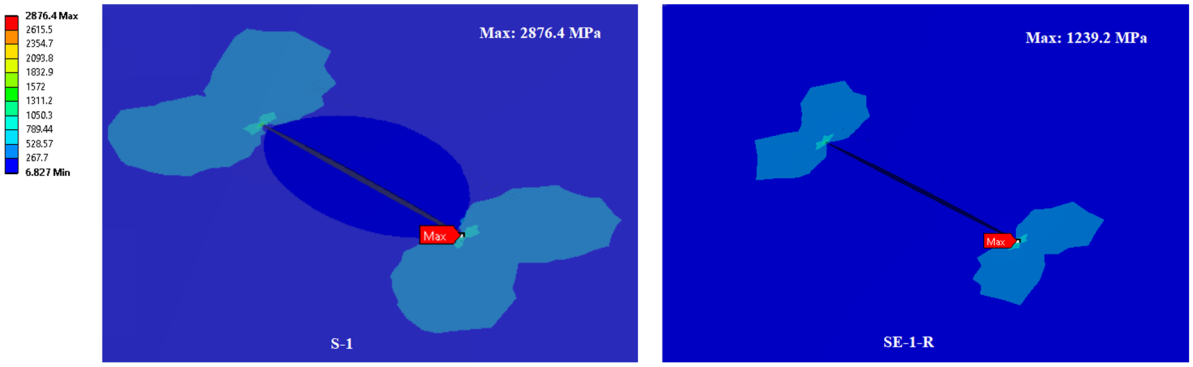

Figure 4.26. The equivalent stress distribution around the surface crack on the cracked surface

- SIF along the surface crack front

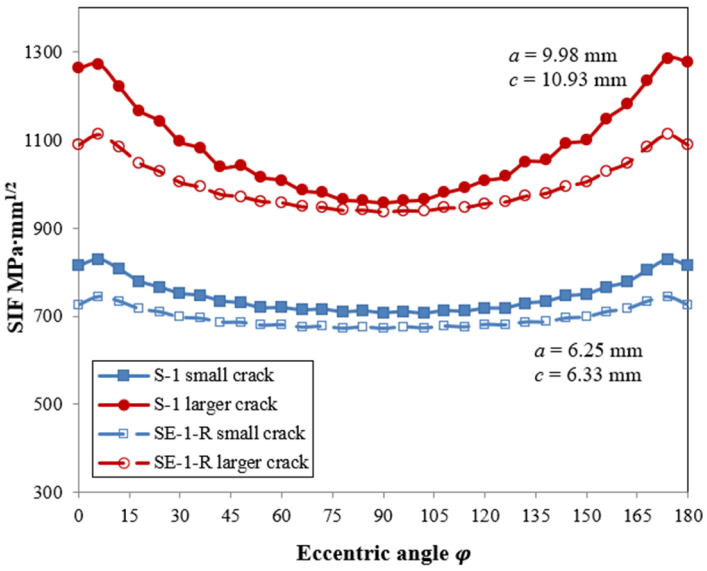

Figure 4.27. The SIF distributions along the crack front

Further on, the results of the SIF along the surface crack front of both the un-reinforced and composite reinforced specimens are shown in Figure 4.27. The SIFs along the crack front of a small crack of a = 6.25 mm, c = 6.33 mm, and a large crack of a = 9.98 mm and c = 10.93 mm are investigated. Note that these two crack sizes are derived from the FE model of SE-1-R from the start and the later stage respectively. It clearly shows that the composite reinforcement decreases the SIF at both stages, but the effectiveness is different: for the small crack, the SIFs of the surface crack depth point and the deepest point decrease 10.20% and 4.93% respectively; while for the large crack, the SIFs of the surface crack depth point and the deepest point decrease 12.46% and 2.24% respectively. Hence it indicated that: 1) composite reinforcement is more effective on the surface point than on the deepest point, which might be owing to the crack-bridging effect; 2) along with the crack propagation, the effectiveness of the composite reinforcement increases on the surface point while decreases on the deepest point.

- Stress distribution in the adhesive layer

The results of the equivalent stress distribution in the adhesive layer adjacent to the steel substrate with a small crack of a = 6.25 mm, c = 6.33 mm, and a large crack of a = 9.98 mm and c = 10.93 mm are shown in Figure 4.28. It demonstrates that the stress concentration mainly occurs at two areas—the edge area and the central area. Besides, the stress concentration with a large surface crack is more serious than with a small surface crack in terms of the area and maximum stress value. Therefore, along with the surface crack growth, the local stress concentration at the edge and the central area might be the potential safety hazard of the edge debonding and the crack-induced debonding respectively.

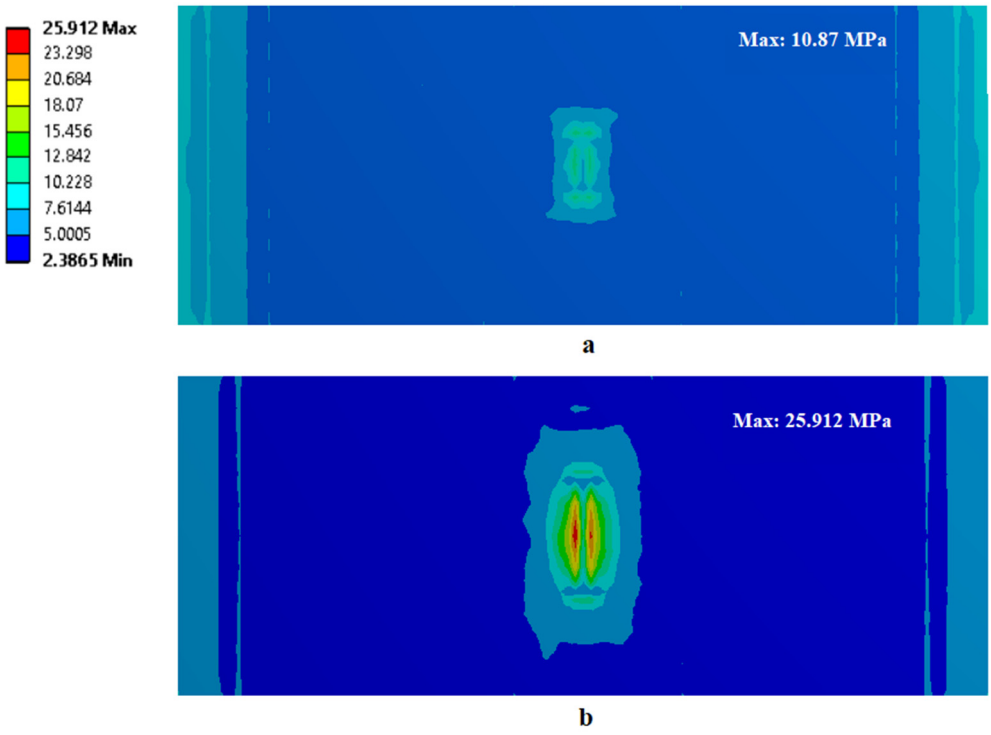

Figure 4.28. The equivalent *stress distribution of the adhesive layer: a) small crack; b) large crack*

4.3.2 Validation

In this sub-section, the experimental results of surface crack growth and FE results are compared and analysed. First, the Paris' constants are calibrated on account of the experimental results. Then, the FE model is validated by the experimental results.

4.3.2.1 Paris' constant calibration

The SIFs of the surface crack in the models without composite reinforcement are calculated by means of Newman-Raju's equation [92], which is

$$K_{\mathrm{I}} = \sigma_{\mathrm{t}} \cdot \sqrt{\pi \frac{a}{Q}} \cdot F\left(\frac{a}{t}, \frac{a}{c}, \frac{c}{b}, \varphi\right), \tag{4.6}$$

where σ_{t} is the tension normal stress, Q is an approximation factor, $F(a/t, a/c, c/b, \varphi)$ is the boundary correction factor. Then incorporating with the Pairs' law, the surface crack growth rate along the depth direction and length direction are predicted by Eq. (3.2) and Eq. (3.3). In this chapter, the values of *C* and *m* were calibrated by from the experimental results, as shown in Figure 4.29.

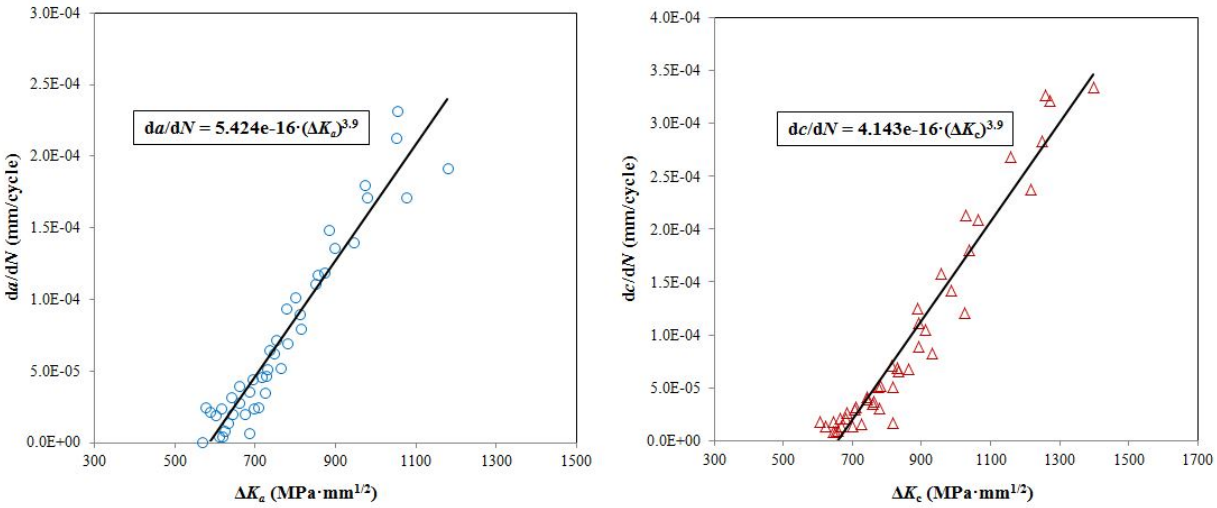

Figure 4.29. Evaluation of the Paris' constants (C and m) from da/dN versus ΔK_{Ia}, and dc/dN versus ΔK_{Ic}

Figure 4.29 illustrated that the *C* for crack growth along the depth direction and the length direction are different, while the *m* is the same for crack growth along the two directions [62]. Therefore C_a and C_c are used as the constants for the depth and length direction respectively, where C_a equals to 5.424×10^{-16} and C_c equals to 4.143×10^{-16}. The *m* equals to 3.9 for both directions. Note that the unit for SIF in this chapter is $\mathrm{MPa} \cdot \mathrm{mm}^{1/2}$.

4.3.2.2. Experimental validation

In this sub-section, the FE models are validated by the experimental results of surface crack growth. Take 'SE-1-R(1)' as an example, 'S' means steel plate, 'E' represents reinforcing the

steel plate on the cracked surface, 'R' means reinforcement, the first '1' stands for the first type of notch, and the second '1' means the No. of the repetitive specimen.

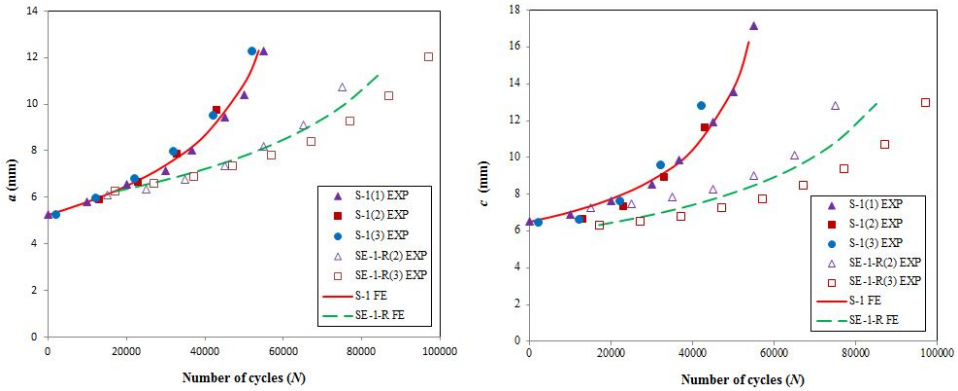

Figure 4.30. The comparison of FE results and experimental results on S-1 and SE-1-R specimens

The SIF of the surface crack in the steel plate reinforced with FRP is calculated by means of the FEM. Then the crack growth rate is evaluated by using the Paris' law. The procedure of evaluating the surface crack growth along the depth direction and length direction is indicated by Figure 2.9. Eventually the results of surface crack growth evaluated by the FE model and the Paris' law are compared with the experimental results. Hence, the FE model of evaluating the SIF is validated by the experimental results.

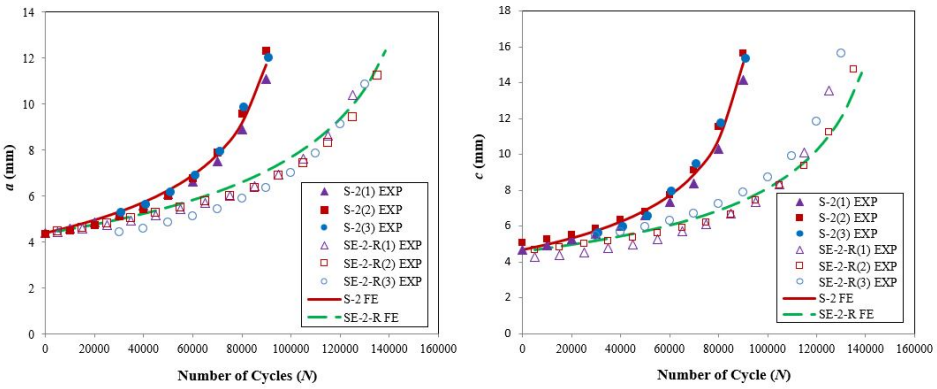

Figure 4.31. The comparison of FE results and experimental results on S-2 and SE-2-R specimens

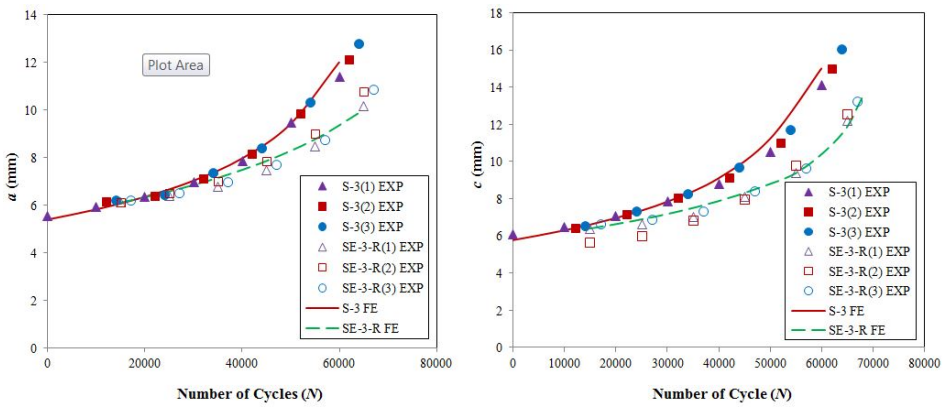

Figure 4.32. The comparison of FE results and experimental results on S-3 and SE-3-R specimens

The comparison between the FE results and the experimental results of surface crack growth of three different specimens categories are shown from Figures 4.30 to 4.32. The figures indicate that the FE results match well with the experimental results when using FRP to reinforce the cracked surface of the steel plates, which means that the FE model can accurately evaluate the SIF of surface cracks reinforced with the sing-side FRP patch. In addition, the results indicate that composite reinforcement has significantly decreased the surface crack growth and prolonged the fatigue life of specimens.

In addition to the validation of the SIF evaluation, the FE results of the strain data at the central of the external CFRP laminate are compared with the experimental results, in order to further validate the mechanical transmission within the FE model. The strain on the central point along the force direction of the specimen of 'SE-1-R(2)' under the maximum load of 167.48 kN is 1058.18 uε, and the FE result is 1024 uε, with around 3.23% errors. It indicate that the FE result of strain at the central point on the external CFRP laminate agrees well with the experimental results, which means the FE model has rationally evaluated the mechanical transmission from the steel substrate through each FRP laminates to the external layer of the CFRP laminate.

4.3.3 Summary

The FEM is able to accurately evaluate the SIF along the surface crack in the composite reinforced steel plate subjected to tension. The experimental validation has proved the feasibility of the FE model and confirmed that the contact setup between the FRP laminate and the steel substrate is perfectly bonded.

The FE results also confirmed the finding of the experimental study that the single-side composite reinforcement performs better on the crack growth along the length direction than along the depth direction, owing to the effect of the out-of-plane bending moment, as well as the crack-bridging effect. This results in the increasing of the preferred aspect ratio of the composite reinforced surface cracks.

4.4. Parametric study

In previous studies, researchers investigated the influential parameters on through-thickness crack growth in composite reinforced steel plates [148]. However, their effects on surface cracked steel plates are unclear. In this regard, the parametric study is conducted by means of the FE model, and their effects has been quantitatively analysed.

4.4.1. Different reinforcement schemes

In this sub-section, three different reinforcement schemes, i.e., single-side composite reinforcement on the cracked surface of the specimens or on the reversed side, and the double-side composite reinforcement, are analysed and discussed. Note that four layers of CFRP laminates are applied for all single-side composite reinforced specimens, while four

layers of CFRP laminates are applied on both of the surfaces when using the double-side composite reinforcement.

4.4.1.1. Single-side reinforcement on the reverse surface

Using the FRP to reinforce the cracked surface of a metallic structure may not be always feasible. In such situation, alternative reinforcement methods, such as reinforcing the reversed side of the cracked surface, might be an option. Therefore this sub-section discussed the effectiveness of single-side composite reinforcement on the reverse side on the surface crack growth rate and the prolongation of fatigue life. The FE model is built on accordance with the test specimens. Then the FE results, as well as the comparison with the experimental results, are shown in Figure 4.33.

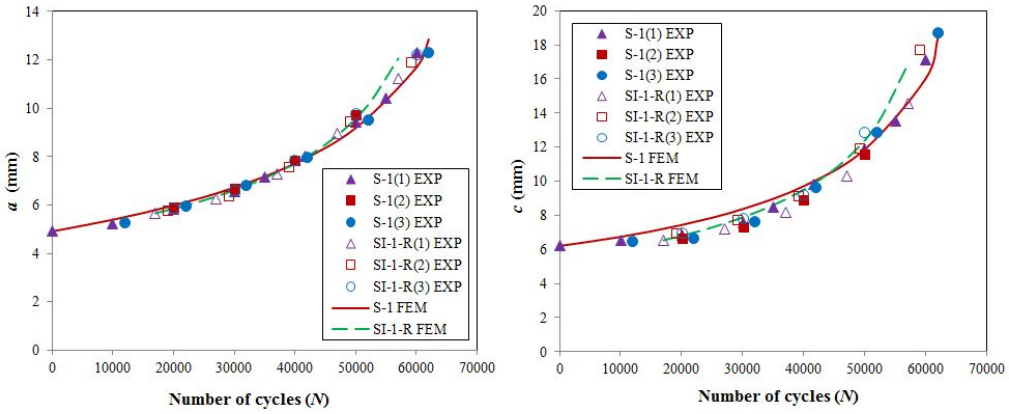

Figure 4.33. The comparison of FE results and experimental results on S-1 and SI-1-R specimens

As a result, the composite reinforcement slightly increases the FCGR rather than decreasing the FCGR, owing to the out-of-plane bending moment on the steel plate generated by the asymmetric reinforcing geometry, as indicated in Figure 4.34. Figure 4.34a illustrates that the composite reinforcement has caused a bending deformation on the steel specimen where the surface crack located (when a = 5.66 mm, and c = 6.54 mm). Therefore, the stress distribution around the cracked area reinforced with FRP, of which especially closing to the cracked surface, is higher than the non-reinforced steel plates (228.3 MPa), as indicated in Figure 4.34b. The higher stress concentration eventually results in higher SIF along the crack front.

Figure 4.34b also explains the SIF results shown in Figure 4.27 when using the FRP to reinforce the surface cracks with different crack sizes. When the surface crack grows deeper, the stress concentration around the deepest point increases correspondingly due to the bending stress. Thus the reinforcement on the deeper crack does not performed as efficient as on the crack with a smaller crack depth. In addition, since the composite reinforcement is invariably efficient on the cracked surface around the surface point, the SIF decreasing on the surface point is more significant than on the deepest point, regardless of the crack size.

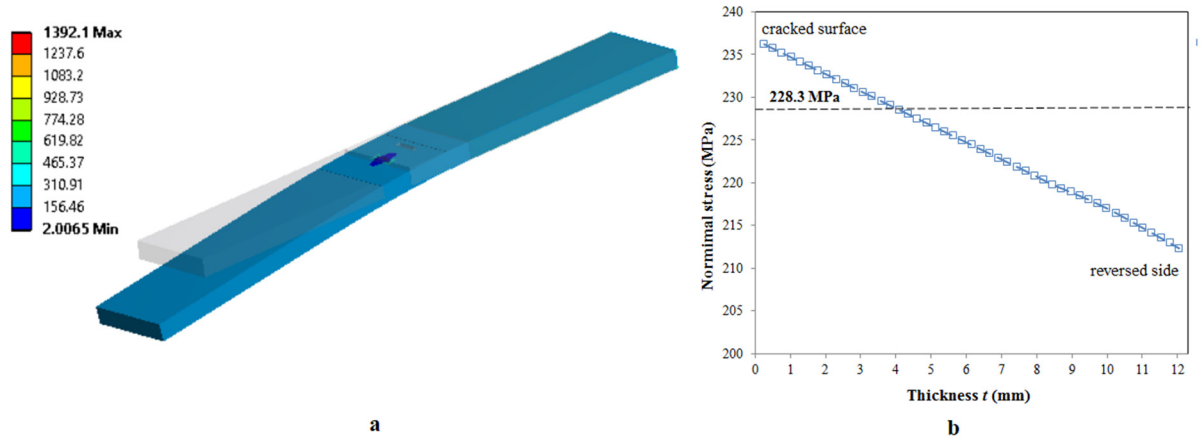

Figure 4.34. Stress distribution of the SI-1-R model: a) global stress distribution and deformation (90 times of the true scale); b) normal stress distribution of the path in the centre along the wall-thickness direction (exclude the surface crack)

4.4.1.2. Double-side reinforcement on both surfaces

Double-side reinforcement is more efficient on reinforcing the through-thickness cracked steel plates [149]. While its applicability on surface cracked plate remains unknown. In this part, double-side reinforcement is compared with the single-side reinforcement by means of the FEA. FE model of SE-2-R is chosen as the single-side reinforcement which applies one layer of GFRP and four layers of CFRP laminate on the cracked surface. While the double-side reinforcement applies one layer of GFRP and four layers of CFRP laminate on both sides, named as SE-2-RD. The FE results and their comparison are shown in Figure 4.35.

Interestingly, the SE-2-RD which applies more FRP laminates performs less effectiveness than the single-side reinforcement on prolonging the fatigue life, especially on the crack growth along the length direction (see in Figure 4.35b), results in a smaller preferred aspect ratio (a/c when a/t = 0.8), as illustrated by Figure 4.35c. The reason of single-side reinforcement preforming the best can be explained by the out-of-bending bending (see in Figure 4.34) as well. In contrast with reinforcing the reversed side, the bending stress in this case facilitate the stress decreasing around the surface crack. However, the out-of-plane bending effect on the surface crack growth has been eliminated by the double-side composite reinforcement, resulting in a less efficient performance on decreasing the surface crack growth.

Figure 4.36 further shows the effect of composite reinforcement on the SIF along the surface crack with two different sizes of either using the single-side composite reinforcement on the cracked surface or double-side composite reinforcement on both surfaces. The SIFs along the surface crack front under the single-side reinforcement are slightly smaller than those SIFs under the double-side reinforcement with a smaller crack (when a = 4.48 mm, c = 4.68 mm). While for the large crack (when a = 10.23 mm, c = 11.33 mm), the double-side composite reinforcement performs slightly better than the single-side reinforcement on the deepest point but it performs worse on the surface point. Hence, since the crack growth is an

accumulate process, the slower FCGR owing to the single-side reinforcement on a smaller crack finally facilitate the prolongation of the fatigue life.

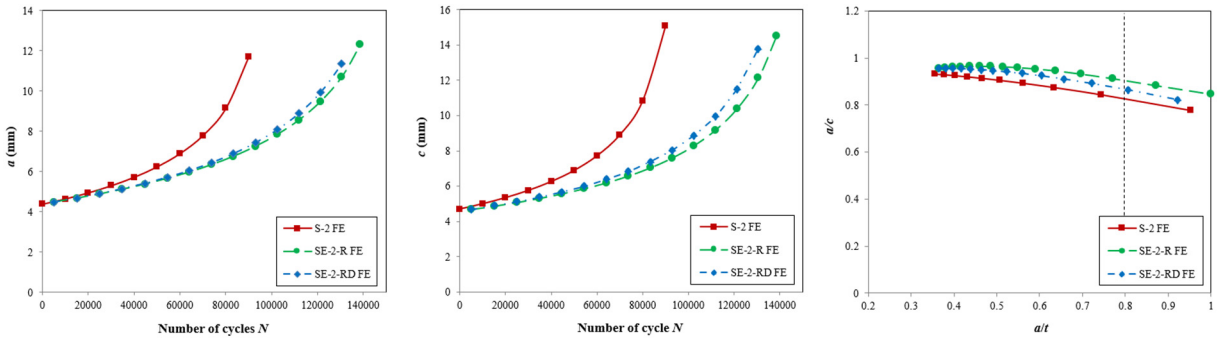

Figure 4.35. The comparison of FE results on SE-2-R and SD-2-R models

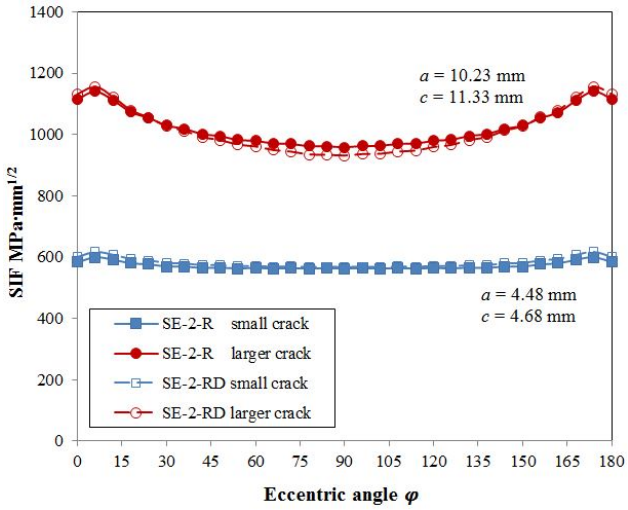

Figure 4.36. FE results comparison of SIF along the surface crack between using single-side reinforcement on the cracked surface and the double-side reinforcement

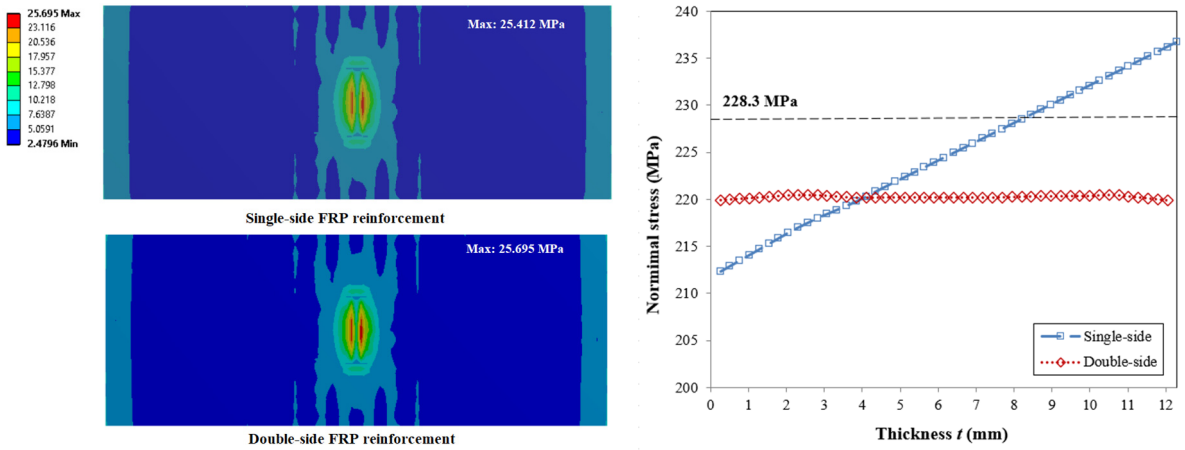

a b

Figure 4.37. The comparison between the single-side reinforcement and double-side reinforcement on stress distribution: a) stress concentration in the adhesive layer; b) normal stress distribution of the path in the centre along the wall-thickness direction (exclude the surface crack)

The comparison of the stress distribution in the adhesive layer using the single-side composite reinforcement and the double-side composite reinforcement (when a = 10.23 mm, c = 11.33 mm) is shown in Figure 4.37. Figure 4.37a indicates that the stress using the double-side composite reinforcement is basically identical but slight higher than using the single-side composite reinforcement, owing to the fact that there is no bending effect on the double-side reinforced steel plate. In addition, owing to the out-of-plane bending effect, the stress value on the steel surface adjacent to the composite reinforcement of using single-side reinforcement is smaller than using the double-side reinforcement. While the stress value gradually increases along the thickness direction and at around t = 4 mm, the stress value surpass the double-side reinforcement. In general, as shown in Figure 4.35, the single-side reinforcement preforms slightly better on decreasing the FCGR. The reasons might be that the stress distribution is always smaller around the surface point, which reduces the crack growth along the length direction, which reduces the crack growth along the depth direction to some extend as well.

In summary, among the three reinforcement method, the single-side composite reinforcement on the cracked surface performs the best on decreasing the FCGR of the surface cracks. The double-side composite reinforcement performs well on decreasing the FCGR, while there is no obvious advantage over the single-side composite reinforcement such as decreasing the stress distribution in the adhesive layer. Hence in light of the doubled cost and reinforcement time, the double-side composite reinforcement is not suggested in practical situations.

4.4.2. Influential parameters

4.4.2.1 Bond length of the FRP patch

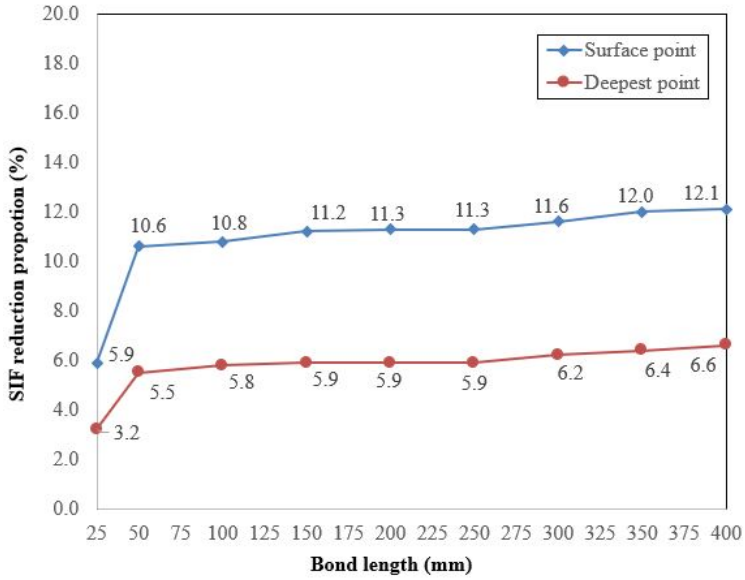

Figure 4.38. The SIF reduction results of the deepest point and the surface point with different bond length

The bond length is one of the easiest parameters to be changed in practice which could affect the budget and time-consuming of the project. In addition, it might significantly influence the reinforcement effectiveness. The main purpose of this section is to find a sound and cost-effective bond length for practical usage. In this sub-section, the effect of bond length ranging from 25 mm to cover the full length of the steel plate, which is 400 mm are analysed.

From this sub-section to sub-section 4.4.7, the SIFs along the crack front of different models are calculated based on the crack size of a = 5.33 mm, c = 5.90 mm, which is the starting size of FE model 'SE-1-R'. The SIF reduction results of the FE models by applying different bond lengths, compared to the unreinforced FE model, is shown in Figure 4.38. It clearly shows that a sufficient bond length is necessary, as the bond length of 25 mm only has a minor effect on the reduction of the SIF. Then increasing the bond length can further decrease the SIF of the surface crack, while the added effect is minimal. In addition, reinforcing the cracked steel plate is not only account for the SIF reduction, but the stress distribution in the adhesive as well, in order to prevent the potential bond failures. The stress distribution within the adhesive layer of using different bond lengths from 50 mm to 400 mm is shown in Figure 4.39, which indicates that the maximum stress value which located in the middle area decreasing rapidly when increasing the bond length from 50 mm to 150 mm and then remains stable despite the further increasing of the bond length. Therefore, in light of both the SIF reduction and the stress distribution within the adhesive layer, the optimum bond length is 150 mm.

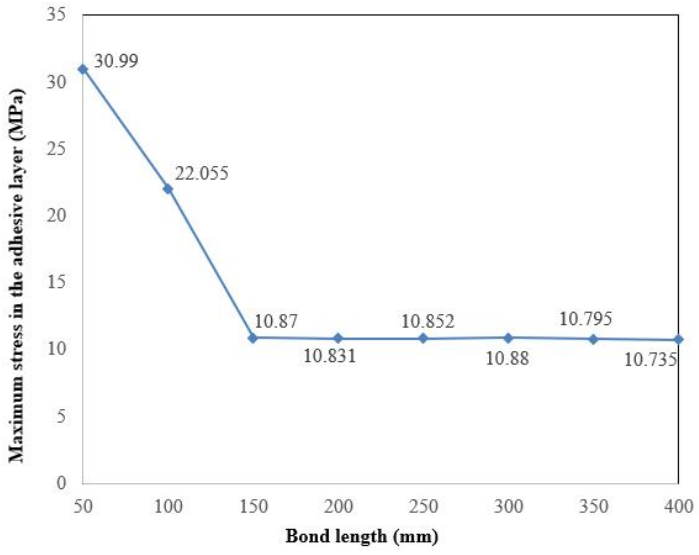

Figure 4.39. The SIF reduction results of the deepest point and the surface point with different bond length

4.4.2.2. Numbers of bond layer

Applying more layers of CFRP laminates is another practical approach that might affect the reinforcement effectiveness, since the study on composite reinforced through-thickness cracked steel plates subjected to tension has indicated its efficiency [150]. In this sub-section, the influence on surface crack growth is investigated, by applying six different numbers of

CFRP layer, ranging from one to six. Note that the one layer of GFRP is always applied as the first layer in between the steel substrate and the CFRP laminates. In addition, the bond length of 150 mm is chosen for all FE models in the following sub-sections.

Figure 4.40 shows that similar to the bond length, increasing the numbers of bond layer does not always decrease the SIF of the surface crack. In fact, there exist an optimum number of bond layers on the 12.3 mm thickness steel plate—two layers of CFRP laminates (0.7 mm), while beyond that, the effectiveness of the composite reinforcement start to reduce. The FE results are agreed well with the experimental results, as shown in Figure 4.41, by simulating the surface crack growth reinforced with two layers or four layers of CFRP laminates respectively. In addition, there only has a minor difference of the results between using two layers of CFRP and four layers of CFRP laminates.

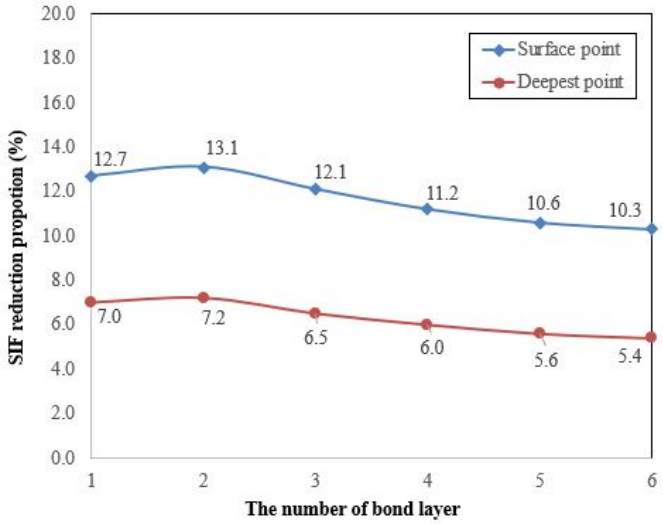

Figure 4.40. The SIF reduction results of the deepest point and the surface point with different number of bond layer

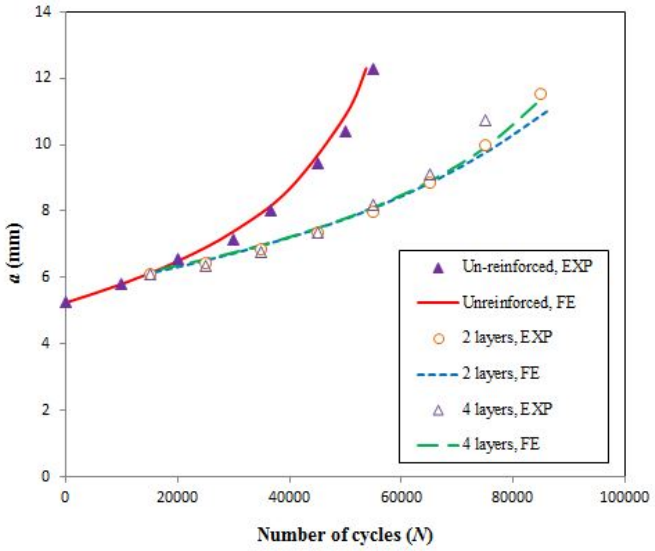

Figure 4.41. The FE and experimental results of the cracked plate by using two layers and four layer of CFRP respectively

As is indicated in Figure 4.41, two layers of CFRP laminate is the optimum for the plate whose thickness equals to 12.3 mm, while whether it is the optimum for different thickness steel plates is uncertain. Given that, a sensitivity study is conducted on steel plates with thickness from 8 mm to 16 mm with 2 mm interval. The results of the SIF reduction of the surface point are shown in Figure 4.42, surprisingly indicating that two layers of CFRP laminate is the optimum for all different thickness steel plates. The reason is that the optimum bond layer (bond thickness) shares the maximum displacement and stress from the tensile steel plate. While applying more layers of CFRP laminates would not promote for the effect on the SIF reduction.

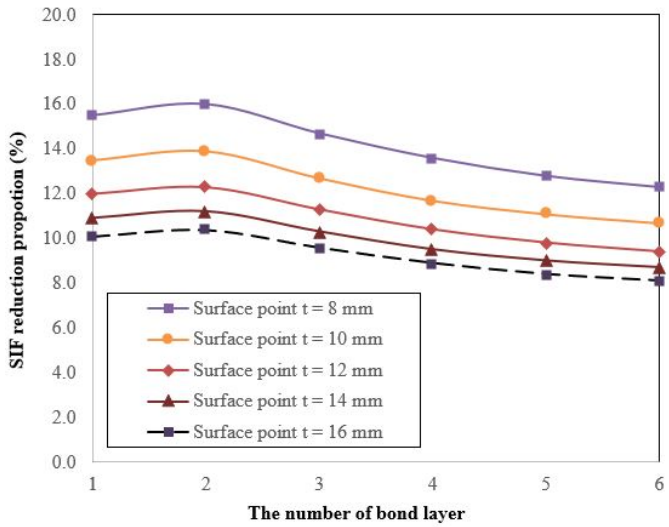

Figure 4.42. The SIF reduction results of the surface point on steel plates with different thickness by using different numbers of bond layer

4.4.2.3. CFRP tensile modulus

The rapid development of material technology has led an increasing on the material properties of the CFRP laminates. The tensile modulus is one of its most important property. At present, there is a variety of CFRP materials in the global market. In this sub-section, three representative CFRP materials with the tensile modulus of 150, 230, and 552 GPa respectively are studied. For all FE models, the SIF is transformed into the normalised SIF K_{nor} to better illustrate the effect of the influential parameters on the SIF, which is the quotient of the SIF along the crack front K and the SIF of the deepest point of the surface crack K_{Ic} (the largest SIF for this crack), calculated as

$$K_{\mathrm{nor}} = K/K_{Ic}. \tag{4.8}$$

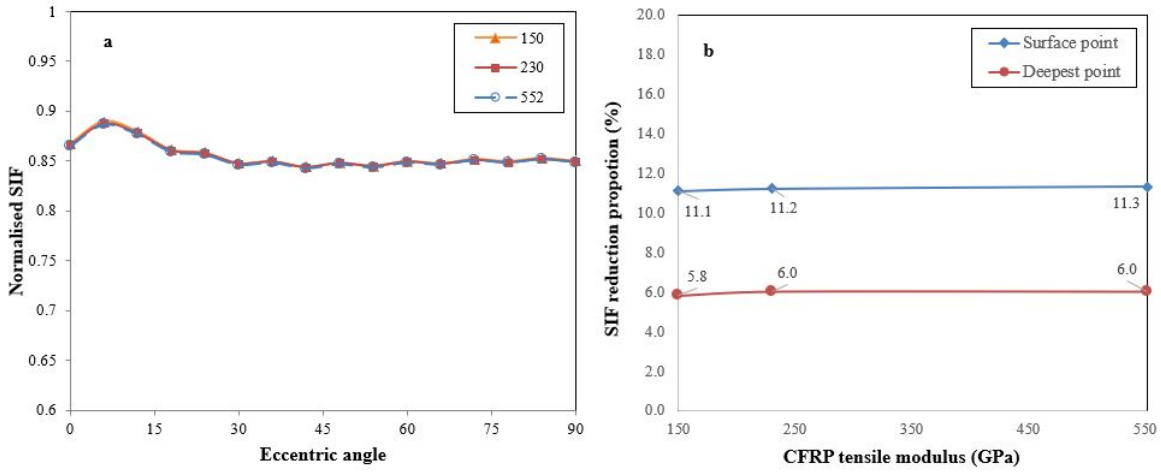

Figure 4.43. The SIF response of the FE models with different CFRP tensile modulus: a) the normalised SIF result along the crack front; b) the SIF reduction proportion of the deepest point and the surface point

It is surprising to see that the tensile modulus of CFRP laminate has a minor influence on the SIF reduction of the surface crack, as indicated in Figure 4.43a. Note the SIF values has been normalised to better illustrate the effect on the SIF, which is the quotient of the SIF along the crack front and the SIF of the deepest point of the surface crack (the largest SIF along the crack front). Figure 4.43b further illustrated that by showing the SIF reduction proportion. The CFRP with the tensile modulus of 230 GPa indeed performs better than the CFRP with the tensile modulus of 150 GPa, while the improvement of the effectiveness by further increasing the tensile modulus becomes negligible. Therefore, in practical situations, choosing CFRP material with high tensile modulus is not suggested from the economic perspective.

4.4.2.4. Adhesive thickness

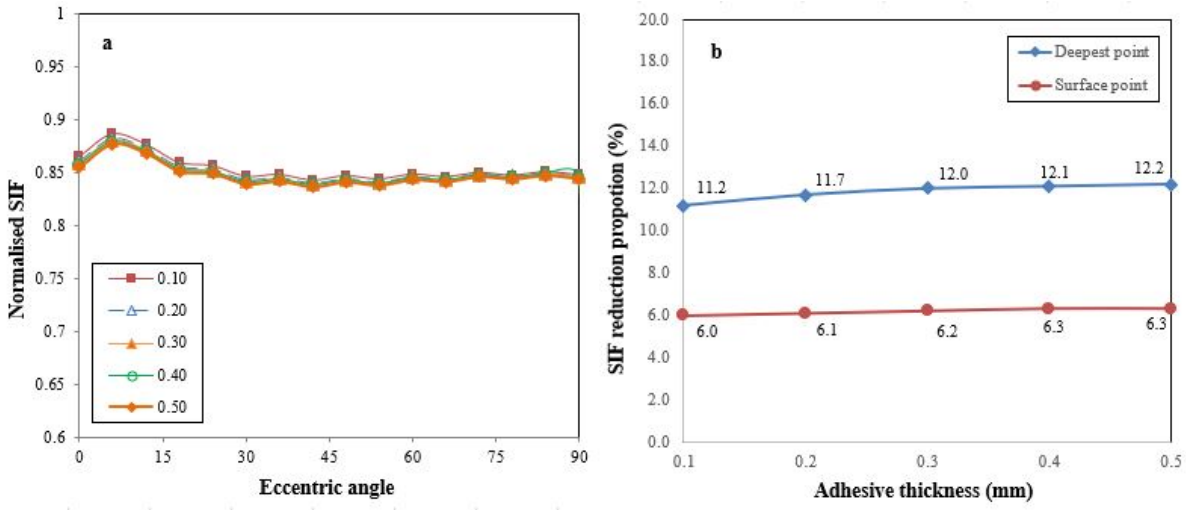

Figure 4.44. The SIF response of the FE models with different adhesive thickness: a) the normalised SIF result along the crack front; b) the SIF reduction proportion of the deepest point and the surface point

The adhesive layer is the intermediary between the steel substrate and the FRP laminates, which is the weakest layer in the reinforcement system. In this sub-section therefore, both the reinforcement effectiveness and the stress distribution in the adhesive layer by using different adhesive thicknesses are investigated. Five ranges of the adhesive thickness from 0.1 to 0.5 mm are adopted.

Figure 4.44 shows that increasing the adhesive thickness insignificantly contributes to the SIF reduction. However, the stress distributed in the adhesive layer is very sensitive to the thickness of the adhesive, especially when increasing the adhesive thickness from 0.1 mm to 0.3 mm, as indicated in Figure 4.45. For all FE models, the maximum stress occurs around the cracked area. Although the stress slightly decreased with the adhesive thickness of 0.5 mm, overall speaking, the maximum stress increases within the increasing of the adhesive thickness. Thus, in this case, the adhesive thickness needed to be controlled as a relatively thin level in order to avoid adhesion failure.

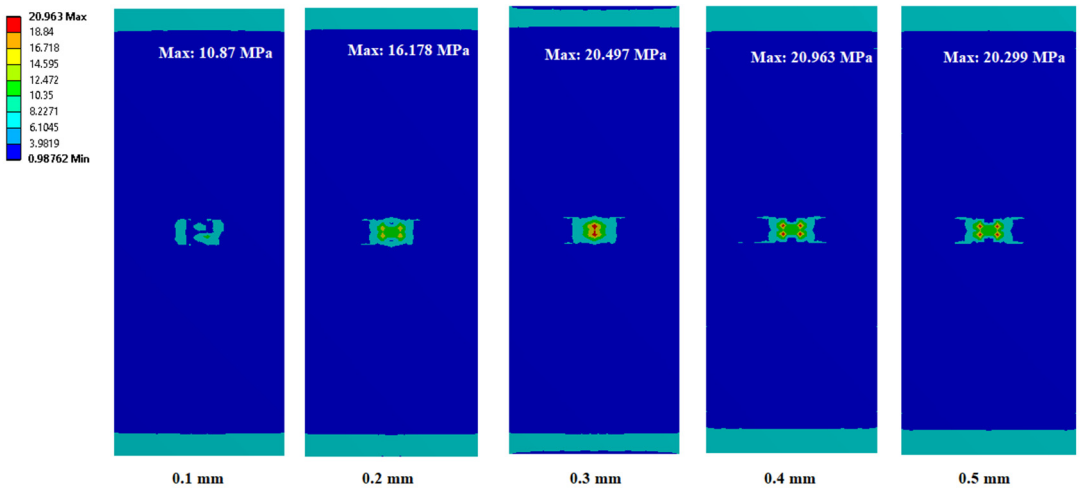

Figure 4.45. The stress distribution in the adhesive layer with different thickness

4.4.2.5 Crack aspect ratio

Since the causes of surface cracks in steel structures are various, the aspect ratio of surface crack can be diverse as well. In this section, the SIF reduction response to the crack aspect ratio is analysed. Six sets of surface cracks with different aspect ratio, ranging from 0.25 to 2.0 have been arranged. Table 4.7 shows the detailed crack sizes of each FE model, as well as the SIF reduction results of the deepest point and the surface point respectively.

Table 4.7. Specimen configuration of steel plates with different aspect ratios

Model No.	*a* (mm)	*c* (mm)	*a*/*c*	SIF reduction of the deepest point	SIF reduction of the surface point
1	3.0	12.0	0.25	8.8%	10.6%
2	3.0	6.0	0.5	7.3%	9.9%
3	4.5	6.0	0.75	6.2%	10.3%
4	6.0	6.0	1.0	4.9%	10.3%
5	6.0	4.5	1.5	3.9%	9.7%
6	6.0	3.0	2.0	3.2%	9.2%

Clearly, Table 4.7 illustrates that within the increase of the crack aspect ratio, the SIF reduction of the deepest point is decreasing, while the SIF reduction of the surface point is insensitive to the crack aspect ratio. In light of Model No. 4 to No. 6, which has the same crack depth, the SIF reduction proportion reduces from 4.9% to 3.2% of the deepest point. These results in Table 4.7 indicate that composite reinforcement is more efficient on reducing the SIF on the deepest point of surface cracks with a small aspect ratio.

4.4.2.6 Crack dimensions

In sub-section 4.4.6 which indicated that composite reinforcement preforms better on the surface crack with small aspect ratio, but in fact, the aspect ratio is changing constantly during the fatigue process. Therefore, in this section, the effectiveness of the composite reinforcement on the SIF reduction during the fatigue cracking process is analysed. The FE model SE-1-R is adopted, starting from the crack size of a = 5.33 mm, and c = 5.90 mm till a = 9.98 mm, and c = 10.93 mm.

As shown in Figure 4.46, it is interesting to see that the trends of the surface point and the deepest point along with the crack growing process are diverse—the SIF reduction of the surface point becomes more significant, whereas the SIF reduction on the deepest point becomes insignificant. The reason for the decreasing of the SIF reduction proportion on the deepest point is owing to the out-of-plane bending moment that when the crack grows deeper, the stress around the deepest direction becomes higher. While the reason for the increasing of the SIF reduction proportion on the surface point is owing to the decreasing of the stress around the surface point along with the increasing of the crack length. Therefore, in consideration of that preventing surface crack growth from penetrating the wall thickness is of great importance, reinforcing the surface crack as early as possible is suggested, in order to achieve the optimum fatigue life extension.

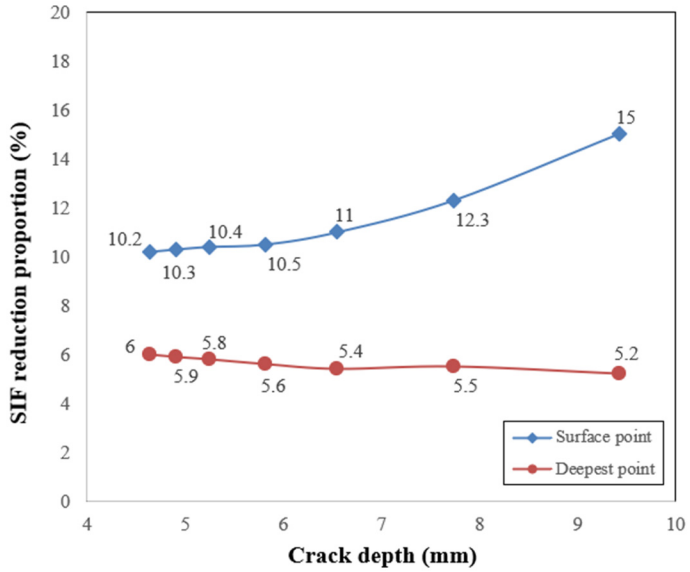

Figure 4.46. The SIF reduction results of the deepest point and the surface point with different crack dimensions along with the crack growing process

4.4.3 Summary

The parametric study indicates that among the three reinforcement method, single-side composite reinforcement on the cracked surface performs the best on decreasing the FCGR and prolonging the fatigue life. The double-side reinforcement performs slightly less effective with doubled cost and time. Nevertheless, only reinforcing the reversed side of the cracked surface is not an appropriate reinforcement method, because the stress distribution around the surface crack has been increased by the out-of-plane bending moment.

The parametric study also indicates that there exist an optimum bond length and numbers of bond layer. While the SIF is less sensitive to influential parameters such as the CFRP tensile modulus, and adhesive thickness. In practical situations, overall considering the effects on the SIF and the stress concentration in the adhesive layer, as well as the reinforcement cost and time, two layers of normal tensile modulus CFRP laminates with the bond length of 150 mm is suggested, and the adhesive layer is needed to be controlled as a relatively thin level. Besides, the parametric study indicates the composite reinforcement is more efficient on reducing the SIF of surface cracks with a small aspect ratio. Along with the crack growing process, the composite reinforcement becomes more effect on decreasing the SIF of the surface point, while less efficient on the deepest point. Therefore, it is suggested to reinforce the surface crack as early as possible, in order to achieve the optimum fatigue life extension before the crack penetrating the wall thickness.

4.5. Conclusions

In this chapter, the composite reinforced surface cracked metallic plate reinforced with FRP was investigated by experimental and numerical approaches. First, nine groups of 23 specimens were tested. The effectiveness of composite reinforcement on surface cracks with different aspect ratio, different reinforcement schemes are investigated. Then two three-dimensional FE models were developed to identify the bond condition of the interface between the steel substrate and the composite laminates respectively using the cohesive modelling, and to evaluate the SIF of the surface crack, respectively. By means of the FEM, three different reinforcement schemes were studied. Finally, a FE-based parametric has been conducted to determine the key influential parameters of the composite reinforcement. The conclusions can be drawn:

- The experimental data and the FE results indicate the single-side reinforcement on the cracked surface can significantly decrease the FCGR and prolong the residual fatigue life. The major contribution comes from the out-of-plane bending moment on the steel plate owing to the asymmetric reinforcing geometry.
- The cohesive analysis indicated that along with the surface crack growth, the degree of stiffness degradation of the interface increased. While interfacial failure did not occur during the surface crack growing stage, indicating the FRP bonded adequately on the steel substrate.

- The FEM of evaluating the SIF of the surface crack determined that the single-side composite reinforcement on the cracked surface is the most efficient method, owing to the out-of-plane bending moment. The crack-bridging effect might play an impartment role as well, especially for the crack growth along the length direction, indicated by the increased crack aspect ratio.

This chapter aims to pave the way of the investigation on composite reinforcement on surface cracked metallic pipes. The experimental design, surface crack growth behaviour, possible failure modes, FE modelling strategy, cohesive analysis have a reference value for the following investigations.

Chapter 5 Internal surface cracked metallic pipes reinforced with CRS*

In this chapter, CRS is applied to repair the circumferential internal surface cracked metallic pipes subjected to bending, while the study on external surface cracks is arranged in the next chapter. The reason of separating the studies was due to the different interfacial bond behaviour between the composite laminates and the metallic substrate—composite laminates directly contact with the external cracked substrate, which was not the case for internal surface cracked pipes. Besides, conducting the study on internal surface cracked pipes at first can pave the way for the experimental design on reinforcing the external surface cracked pipes.

A three-dimensional FE model is developed at first to quantitatively analyse the SIF of the internal surface crack reinforced with CRS. Besides, the crack growth rate is predicted by using the Paris' law. Then the FE model is proved that it can accurately predict the SIF of the composite reinforced internal surface cracked metallic pipes by a two-phase validation process. Afterwards, a parametric study is performed in order to guide the optimization design of composite reinforcement accounting for multiple influential factors, as well as paving a way for the experimental design and the analysis towards the study on reinforcing the external surface cracked metallic pipes.

The structure of this chapter is assigned as follow: in Section 5.1, a three-dimensional FE model is developed to evaluate the SIF of circumferential internal surface cracks in metallic pipes reinforced with CRS. The FE model is then validated by means of available experimental results from literature. In Section 5.2, in light of the validated FE model, a case

* This chapter is based on the published journal article—[151] Z. Li, X. Jiang, and H. Hopman, "Numerical analysis on the SIF of internal surface cracks in steel pipes reinforced with CRS subjected to bending," *Ships and offshore structures,* vol. 14, p. 1, 2019.

study is conducted to analyse the effect of composite reinforcement on surface crack growth. In Section 5.3, a parametric study is launched to identify the key influential parameters of the CRS in order to guide an optimization design of composite reinforcement. Finally, the conclusions are drawn in Section 5.4.

5.1 Numerical modelling

The FEM is a well-recognised method to evaluate the SIF of surface cracks (Branco et al., 2015) and the mechanical response of composite reinforced steel structures (Haedir et al., 2009, Kabir et al., 2016). In this section, a three-dimensional FE model is built for the purpose of evaluating the SIF of the circumferential internal surface crack in steel pipes reinforced with CRS. The pipe models are subjected to bending, which is a major load case for offshore steel pipes. In order to guarantee its accuracy, the FE model is validated by experimental results from literature (Yoo and Ando, 2000, Kabir et al., 2016).

5.1.1 FE modelling strategy

The model conforming to the experimental setup of the studies by Kabir et al. (2016) and Yoo and Ando (2000) subjected to four-point bending are developed for the validation purpose. The FE model includes the cracked steel pipe, CRS on the steel pipe, load and supports units. The steel pipe is horizontally positioned, supported by two semi-roller units whose bottoms are fixed supported, as shown in Figure 5.1. Three layers of CFRP laminates are wrapped around the pipe specimen. The contact surfaces of different layers (e.g., between steel and adhesive layer, adhesive layer and CFRP, and different CFRP laminates) are bonded—no sliding or separation is allowed. The contact of load units to pipe/CFRP and pipe to support units adopts the no separation contact which do not allow penetration or separation of contact surfaces but allows sliding in the tangent. A pair of symmetrical vertical forces is applied on the load units, generating a bending moment on the pipe model. The size of the pipe and composite, and their material properties will be introduced in sub-section 5.1.2, because these parameters are complying with the test specimens from two different studies.

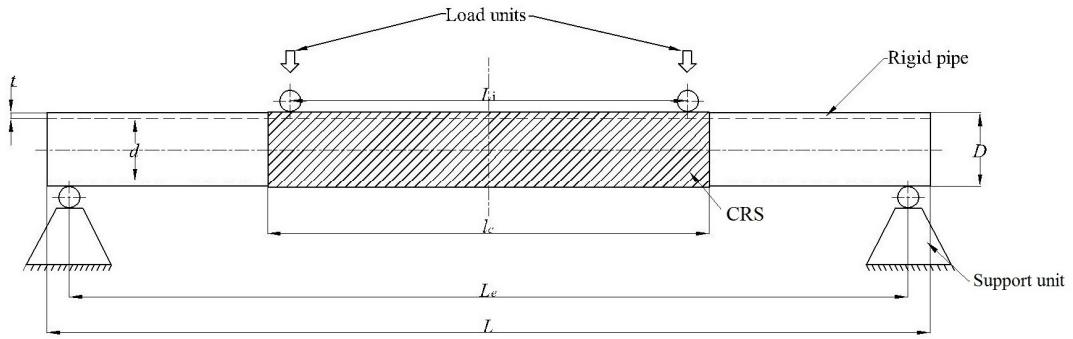

Figure 5.1. The schematic of the FE model and the 4-point bending setup

The internal surface crack is introduced to the bottom mid-span of the pipe, as shown in Figure 5.2. The surface crack is circumferentially oriented in the cross-section plane, as a semi-elliptical shape. The profile of the surface crack is determined by the crack depth a, and the half crack length c. The eccentric angle φ is adopted to define different point along the crack front. Note that in this chapter, the value of φ can be smaller than 0 or larger than π due to the inner curved pipe surface.

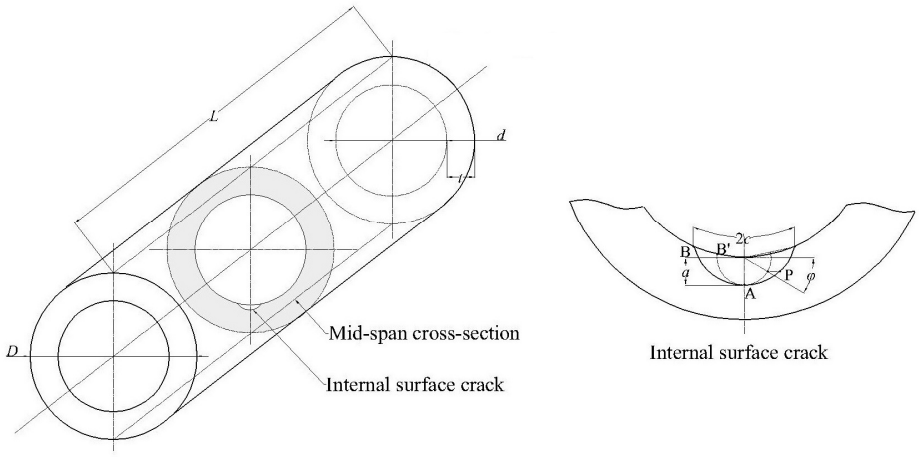

Figure 5.2. The location of the surface crack and the parameters of the surface crack

A sensitivity study has been conducted in a Chapter 3 to determine the appropriate modelling strategy (e.g., element type, meshing method and size, modelling contours and divisions around crack tip) in order to ensure the accuracy of SIF evaluation. Figure 5.3a shows the FE mode and the global meshing condition. The 20 nodes solid element 'solid 186' is adopted to build the FE model. Two different meshing strategies are applied to the pipe: tetrahedral meshing method is used for the middle part where the crack is located; while sweep meshing method is applied for the other two parts. Sweep meshing method is used for the FRP laminates, and the support/load units as well. In this chapter, to ensure a robust and efficient evaluation, a 5.0 mm body element size is used for the areas of the pipe around the surface cracks and the CRS laminates, a 15.0 mm edge size is used for the rest of the pipe model. For the CRS reinforcing laminates, a 4.0 mm body element size is adopted for the adhesive layer, and a 5.0 mm body element size for the CRS laminates.

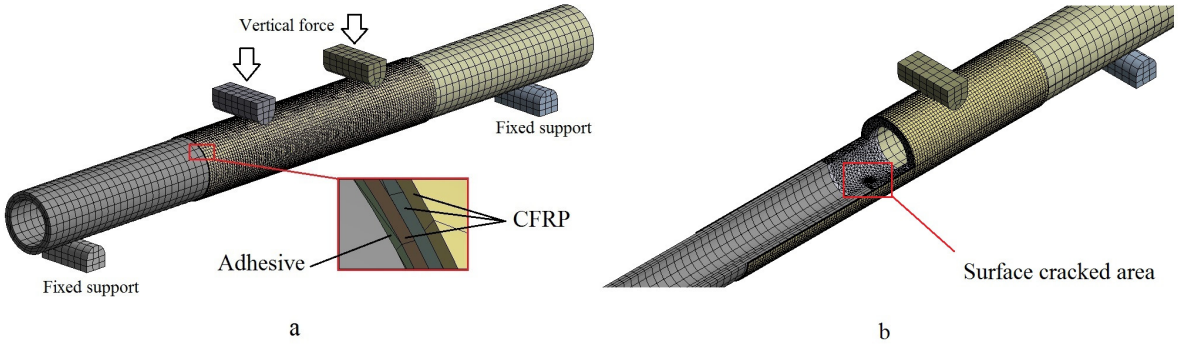

Figure 5.3. a) Global mesh of the FE model and the composite reinforcement; b) illustration of the surface cracked area by splitting the pipe

The surface crack is modelled by deploying the *Semi-elliptical Crack* module [152] in ANSYS workbench, as shown in Figure 5.4a. Six contours with eight divisions for each contour are modelled around the crack tip to ensure an accurate prediction of the SIF. The diameter of the largest contour is 1.0 mm, which makes the element size around the crack front smaller than 0.2 mm. The meshing condition around the internal surface crack adopts the tetrahedral meshing method, while around the surface crack front (e.g., the contour around the crack front) employs hexahedra dominant meshing method to form well-ordered concentric contours, in order to achieve a rational prediction of the SIF.

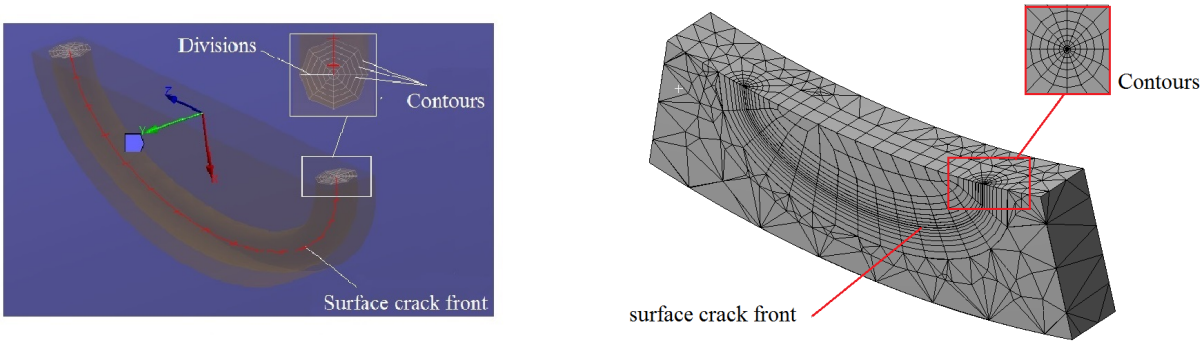

Surface crack modelling module
a

Mesh of and around the surface crack
b

Figure 5.4. a) Surface crack modelling module; b) the mesh around the surface crack

5.1.2. Validation of the numerical method

On account of the fact that it is hard to find available experimental/numerical data of surface crack growth in pipe reinforced with CRS subjected to bending in open documents, the FE model is validated in two phases by using experimental data of intact pipe reinforced with CRS and surface crack growth in steel pipes respectively. The two phases separately validate the pipe mechanical response of the pipe owing to composite reinforcement, and the SIF evaluation of surface cracks in pipe subjected to bending, as the two key components, in order to ensure the accuracy of the FE model. It should be noted that the validation is based on the assumption that no interfacial failures or adhesion failures will occur to the FE model. Therefore, the investigations and analysis towards the SIF response owing to composite reinforcement are based on this assumption.

5.1.2.1. Validation of phase one: intact pipe reinforced with CRS subjected to bending

The aim of phase one is to validate the mechanical transmission between the pipe and the composite layers. Three groups of experimental results (conforming to the specimens ‘B2_US’, ‘S5B-1’, and ‘S6B-2’ in the referred study) of intact pipes reinforced with CRS subjected to bending from the study by Kabir, et al. [27] are applied, as listed in Table 5.1. The FE models include one intact pipe without reinforcement, and two composite reinforced steel pipes using different CFRP wrapping scheme. The pipe steel has an elastic modulus of 214 GPa, and its yield strength and tensile strength are 327 MPa and 383 MPa respectively. The material properties of CFRP and adhesive are listed in Table 5.2. Note that a uniaxial

CFRP laminate has been used in the investigations throughout the dissertation. The thickness of the each CFRP laminate is 0.6 mm, while the thickness of the adhesive layer is 0.35 mm, as shown in Figure 5.1a. Notice that all the setup and material properties in phase one are conforming to the research by Kabir, et al. [27].

Table 5.1. Detail information of the phase one FE models

Index	D	t	L_e	L_i	Wrapping scheme (see in Figure 5.5)
P	101.6	4.0	1200	500	\
P-R1	101.6	4.0	1200	500	L-H-L
P-R2	101.6	4.0	1200	500	L-L-H

Note: 'P' is the unreinforced pipe model. 'P-R1' and 'P-R2' are two composite reinforced pipes by two different wrapping schemes. The 'L' and 'H' of the wrapping scheme mean longitudinal wrapping and hoop wrapping respectively. For instance, 'L-H-L' stands for longitudinal wrapping for the first and third layer, while hoop wrapping for the second layer. All units in this table are in 'mm'.

Table 5.2. Material properties of the adhesive and CFRP [27]

Material	E_1 (Pa)	E_2 (Pa)	G_{12} (Pa)	G_{13} (Pa)	G_{23} (Pa)	T (Pa)	Nu
Adhesive	2.86×10^9	2.86×10^9	\	\	\	46×10^6	0.35
CFRP	205×10^9	25×10^9	1	1	3.0×10^9	4.9×10^9	0.33

Note: E_i is the elastic modulus of fibre along the i direction, G_{ij} is the shear modulus, Nu is the Passion's ratio.

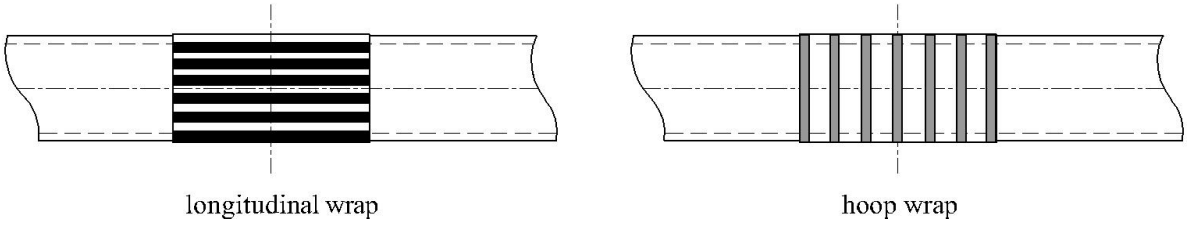

Figure 5.5. Wrapping pattern including longitudinal direction (L) and hoop direction (H)

Two vertical loads are applied on the loading units of the FE models under displacement control condition at a constant rate, as shown in Figure 5.1. Then the mid-span displacement is calculated by means of the FEM, and the results of load-displacement curves are compared with the experimental data.

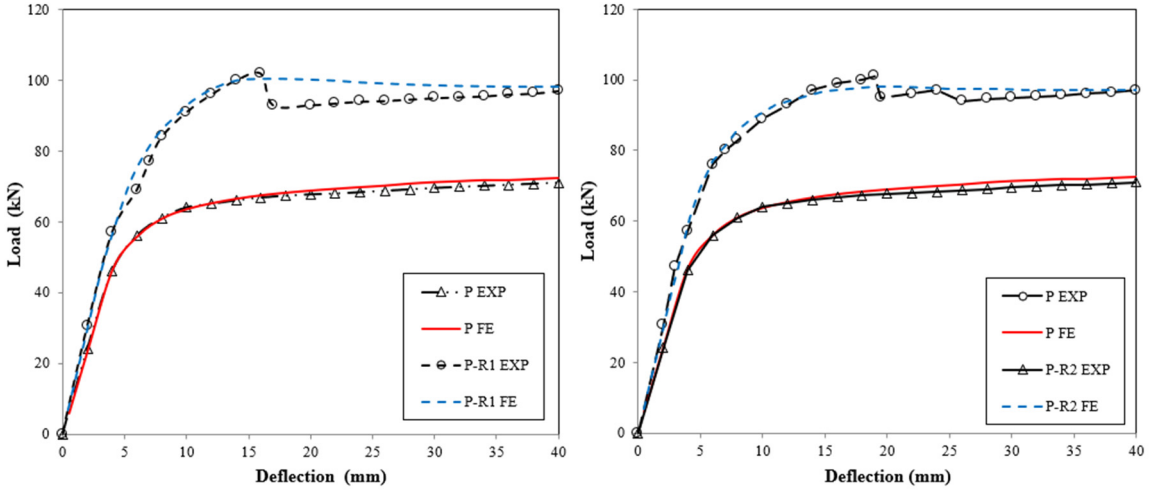

Figure 5.6. Numerical and experimental [27] load-displacement response of P, and (a) P-R1, (b) P-R2

Figure 5.6 shows the numerical and experimental load-displacement responses for the bare pipe models and the composite reinforced pipe models. It shows that the FE results match well with the experimental data until the load reaches the peak value. Then the load suddenly decreases due to debonding, which is not predicted by the FE models because interfacial failure is not considered. However, in the linear-elastic zone for crack growing under high-cycle fatigue condition, the FEM is able to accurately predict the load-displacement response for both bare and composite reinforced pipes. It means that the FE model is appropriate to simulate mechanics transmission within the composite layers and the steel pipes subjected to bending.

5.1.2.2. Validation of phase two: circumferential internal surface crack growth in pipe subjected to bending

The purpose of phase two is to validate the feasibility of the FE model to evaluate the SIF of circumferential internal surface cracks in steel pipes subjected to bending. The FE model is validated by six groups of experimental results from the research by Yoo and Ando [52], as listed in Table 5.3. In this phase, only pipe material is considered. Its elastic modulus is 200 GPa, yield stress is 227 MPa and tensile strength is 406 MPa. Note that the setup and material properties in phase two are conforming to the research by Yoo and Ando [52].

Table 5.3. Detail information of phase two FE models

Index	D (mm)	t (mm)	c (mm)	a (mm)	L_i (mm)	L_e (mm)	σ_{max} (MPa)	σ_{min} (MPa)
PI-1	102.0	8.1	22.75	4.5	245	1000	200.0	20.0
PI-2	102.0	8.1	6.0	3.0	245	1000	210.0	21.0
PI-3	102.0	8.1	5.0	5.0	245	1000	325.0	32.5
PI-4	102.0	8.1	18.25	3.0	245	1000	200.0	20.0
PI-5	102.0	12.7	6.0	6.0	245	1000	220.0	22.0
PI-6	102.0	12.7	6.0	3.0	245	1000	261.0	26.1

Since the reference by Yoo and Ando [52] provides the data of the maximum stress of the pipe subjected to bending (see $\sigma_{\max}$ in Table 5.3), therefore the maximum value of the fatigue load applied on the load units P is determined as

$$P = \frac{\sigma_{max} \cdot \frac{\pi \cdot D^3}{32} \cdot \left(1 - \frac{d^4}{D}\right)}{L}. \quad (5.1)$$

The calculated P is applied on the load unit to generate a bending moment to the bare pipe, and the SIF of the deepest point and surface point of internal surface cracks are calculated by the FE models, using the contour integral method. Incorporating with the Paris' law, surface crack growth rate along the depth and length direction are predicted by Eq. (3.2) and Eq. (3.3). C and m are 3.2×10^{-10} and 3.72 respectively (unit in MPa/m$^{1/2}$) [52], ΔK_{Ia} and ΔK_{Ia} are the SIF range of the deepest point and the surface point of the crack. Afterwards, by assuming a small amount of cycles, the increments of the crack length and depth are calculated. Eventually, it is possible to trace the surface crack growth along the two directions. The detailed procedure of evaluating surface crack growth is indicated in Figure 2.9.

The FE results are compared with the experimental data of *a*/*c* versus *a*/*t* ratio and fatigue life of the specimens, as shown in Figure 5.7. The comparisons of *a*/*c* versus *a*/*t* ratio in Figure 5.7a show that the FEMs are able to predict the crack shape variation during the crack growth process. The good agreement of fatigue life predictions between the experimental and FEM in Figure 5.7b illustrated that the FEM is able to accurately evaluate the residual fatigue life. Therefore, the validation illustrates that the FE models provide reasonable SIF evaluations of circumferential internal surface cracks in steel pipes subjected to bending.

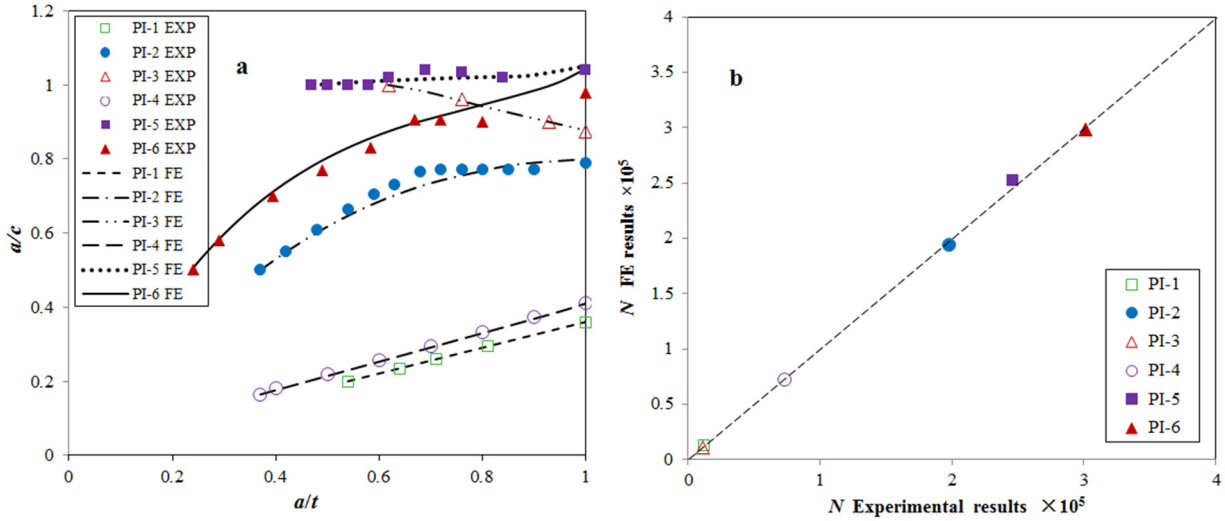

Figure 5.7. Comparison between the experimental results [52] and FE results: a) a/c versus a/t ratio; b) fatigue life

In summary, the two phases' validation indicated that the FEM is able to accurately evaluate the mechanics response of composite reinforced steel pipe in linear-elastic zone and the SIF response of circumferential internal surface cracks in steel pipe. Therefore, since the surface cracks do not contact the composite layers and assuming no interfacial failures and adhesion failures, the combined FE model—circumferential internal surface crack in steel pipes reinforced with CRS subjected to bending—is able to rationally predict the SIF.

5.2 Case studies

In this section, two case studies of composite reinforcement were conducted on the internal surface cracked steel pipes subjected to two different load cases, i.e., bending and tensile, respectively. Both of the studies are conducted based on the validated FE model.

5.2.1 Composite reinforcement on internal surface cracked steel pipes subjected to bending

The CRS material and reinforcing scheme (e.g., layers, wrapping orientation) in sub-section 5.1.2.1 are adopted to reinforce the surface cracked steel pipe in sub-section 5.1.2.2. The material properties and model size are identical to the corresponding models in sub-section 5.1.2. The geometry, model setup and material properties of the steel pipes are identical to FE

model ‘PI-6’, while the material properties of CFRP and adhesive are identical to the FE model of ‘P-R1’. The 600 mm long CFRP material was used to reinforce the internal cracked steel pipe with the ‘L-L-H’ wrapping scheme (as the same as model ‘P-R2’). The new FE model is named as ‘PI-R’ and its SIF is calculated through the validated FE model. Afterwards, combined with the procedure of evaluating the surface crack growth rate, the surface crack growth rate of both ‘PI-6’ and ‘PI-R’ is predicted. Then assuming a small amount of cyclic numbers, the crack extension value along the length direction and the depth direction are calculated. Note that the stress ratio is assumed to be $R = 0.1$ for the evaluation of the crack growth rate.

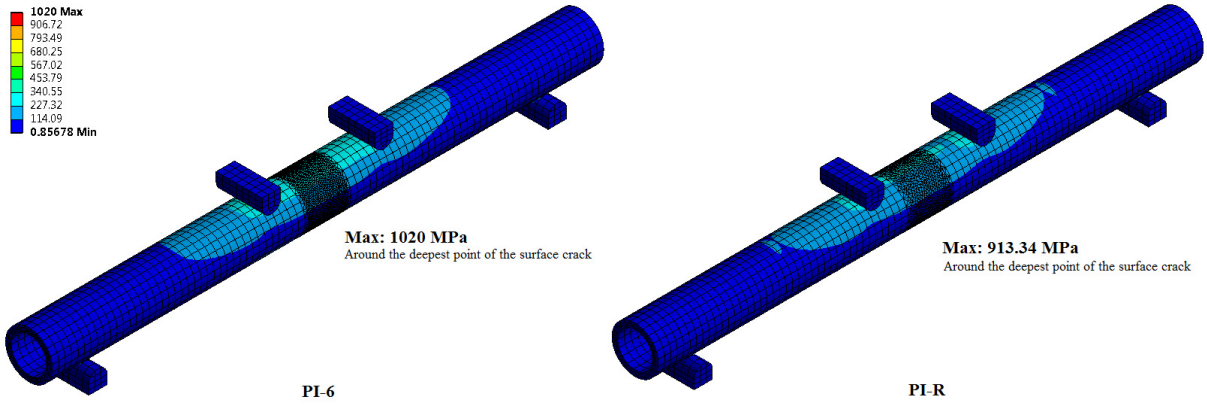

Figure 5.8. The global equivalent stress distribution of the pipe subjected to bending

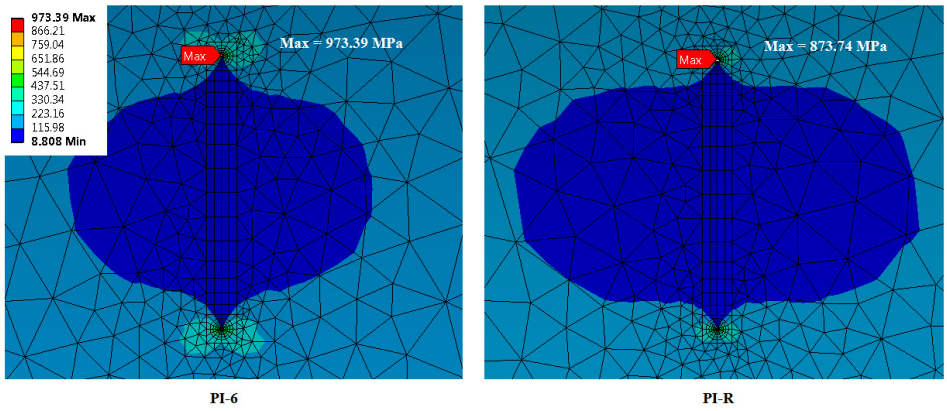

Figure 5.9. The equivalent stress distribution around the surface crack on the pipe internal surface when the pipe subjected to tension

Figure 5.8 shows the global equivalent stress of the steel pipe of ‘PI-6’ and ‘PI-R’. More detailed, the equivalent stress distributed around the internal surface crack on the pipe internal surface as a butterfly shape is shown in Figure 5.9. It illustrates that by means of CRS, the stress concentration around the internal surface crack decreases significantly. Particularly, the stress concentration area around the two surface points of the surface crack, i.e., point B in Figure 5.2, becomes smaller owing to the CRS.

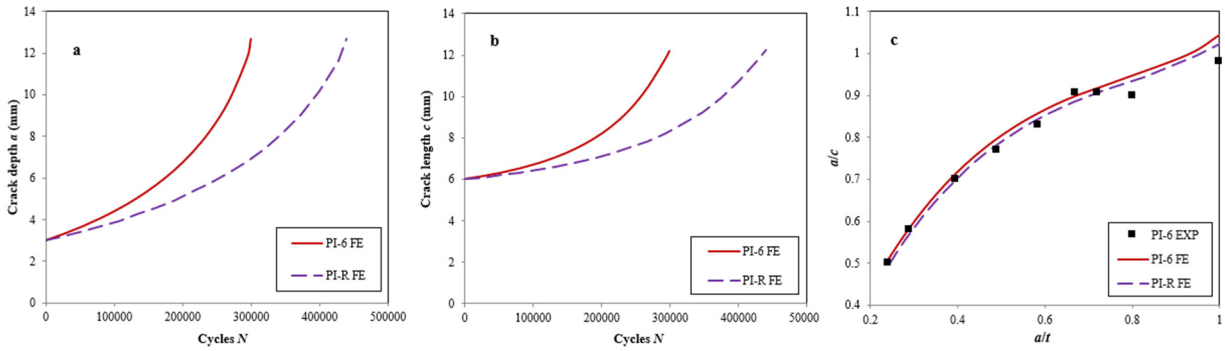

Figure 5.10. The comparison results between the un-reinforced FE model 'PI-6' and the composite reinforced FE model 'PI-R': a) crack growth rate along depth direction; b) crack growth rate along length direction; c) a/c versus a/t ratio

Figure 5.10 shows the crack growth results of 'PI-R' and its comparison with 'PI-6'. It demonstrates that the CRS significantly decreased the crack growth rate of the internal surface crack along both depth direction (see Figure 5.10a) and length direction (see Figure 5.10b). Thus, the CRS increased the fatigue life of the cracked steel pipes. The fatigue life of the unreinforced steel pipe 'PI-6', i.e., the cycles when the surface crack penetrating the pipe wall, predicted by the FEM is 298,869, matching well with the experimental results of 287,500 cycles (3.95% error). Owing to the CRS, the fatigue life increased to 439,448, or 47.04%. When the surface crack penetrates the wall, the crack length 2*c* of 'PI-R' is approximately the same with the crack length of 'PI-6', indicating that the composite reinforcement did not change the crack profile. It is also illustrated in Figure 5.10c that the variation of aspect ratio *a*/*c* of 'PI-R' kept the same as the aspect ratio variation of 'PI-6'. The reason is that CRS decreases the crack growth rate approximately equally along the depth direction and the length direction.

5.2.2 Composite reinforcement on internal surface cracked steel pipes subjected to tension

In this sub-section, a case study of composite reinforcement on the internal surface cracked steel pipes subjected to tension is conducted. The FE model is converted from the FE model in sub-section 5.2.1 by changing the load case from bending to tension, as shown in Figure 5.11. The load units and support units has been removed while the pipe model, crack modelling, and meshing conditions are identical to the models in sub-section 5.2.1. Tensile load is applied on the transverse plane at one edge of the pipe model, while fixed supported is set on the other edge. The tensile load on the transverse plane is 616.38 kN, generating a 173 MPa normal stress on the pipe model, which is identical to the stress value around the internal surface cracks in the pipe model subjected to bending. Within the same methods of calculating the SIF and evaluating the crack growth rate, the crack extension value under the load ratio $R = 0.1$ is analysed. Here, the unreinforced cracked pipe model is named as 'PTI-6', while the reinforced model is named as 'PTI-R'.

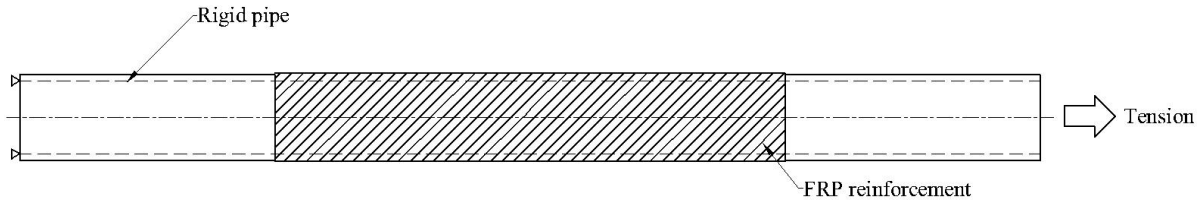

Figure 5.11. The schematic of the FE model subjected to tension

The equivalent stress distribution around the internal surface crack on the pipe internal surface as a butterfly shape are shown in Figure 5.12. Similar to the cracked pipe under bending, the stress concentration around the internal surface crack decreases significantly owing to the reinforcement. However, unlike the pipe under bending, the maximum stress value located at the surface point rather than at the deepest point, owing to the fact that tension did not generate a gradient effect.

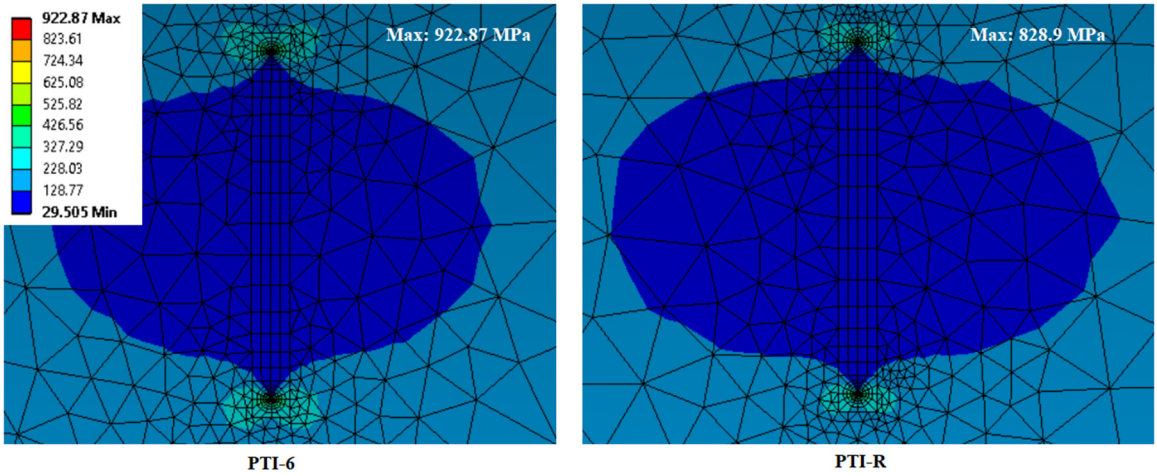

Figure 5.12. The equivalent stress distribution around the surface crack on the pipe internal surface when the pipe subjected tension

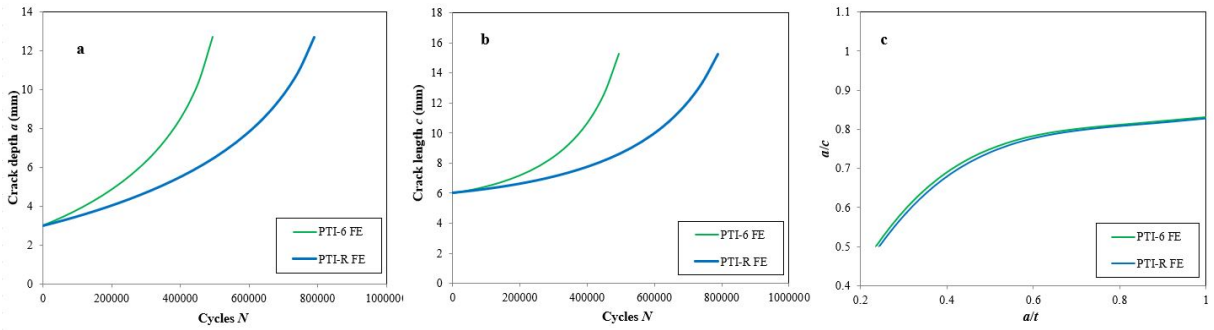

Figure 5.13. The comparison results between the un-reinforced FE model 'PI-6' and the composite reinforced FE model 'PI-R': a) crack growth rate along depth direction; b) crack growth rate along length direction; c) a/c versus a/t ratio

Figure 5.13 shows the crack growth results of 'PTI-R' and its comparison with 'PTI-6'. Similar to the model subjected to bending, the CRS significantly decreased the crack growth rate along both the depth and the length direction respectively. The composite reinforcement

has prolonged the fatigue life of PTI-6 from 493,550 cycles to 789,231 cycles, of 59.91%, which performs better than the CRS on the FE model subjected bending. In addition, the CRS on 'PTI-R' does not change the variation of the aspect ratio a/c from 'PTI-6'. While when penetrating the pipe wall, the crack length on the pipe under tension (15.27 mm) is larger than the crack length under bending (12.22 mm). The reason is that the stress distribution within the pipe subjected to tension does not have the gradient effect caused by the bending moment. The aspect ratio when a/t = 1 equals to 0.83, which is much smaller than the aspect ratio of the crack in the pipe under bending, whose aspect ratio equals to 1.04.

5.3 Parametric study

In a previous study, researchers indicated that influential parameters of composite reinforcement, i.e., bond length, numbers of composite layer, CFRP tensile modulus, adhesive thickness, types of adhesive, CFRP wrapping orientation, and pipe dimensions may affect the strength of the reinforced pipes [27]. However, the understanding of their effects on the SIF of circumferential internal surface cracks is lacking. Regarding this, a range of parametric study has been conducted using the validated FE model to quantitatively analyse their effects. The parametric study is conducted on the FE model in sub-section 5.2.1 with the initial crack size of a = 3.0 mm and c = 6.0 mm, except the study on analysing the effect of the dimension of the pipe on the SIF reduction. Employing the model subjected bending is because in practical situations, cyclic bending is the dominant load case. The reinforcement scheme follows the 'L-L-H' wrapping pattern except the study on analysing the effect of CRS wrapping orientation, and the study on analysing the effect by adding one GFRP layer. It should be noted that a hoop orientated CRS is always applied as the outer layer in light of practical application, because the hoop orientated composite laminate may help to compress the inner layers thus providing a more robust adhesion condition for the composite reinforcement system. For all FE models, the SIF is transformed into the normalised SIF K_{nor} to better illustrate the effect of the influential parameters on the SIF, which is the quotient of the SIF along the crack front K and the SIF of the deepest point of the surface crack K_{Ia} (the largest SIF for this crack), calculated as

$$K_{nor} = K/K_{Ia}. \tag{5.2}$$

- CRS bond length

The CRS bond length is one of the easiest parameters to be changed in practice which affects the budget and time-consuming of the project. In addition, it can significantly influence the reinforcement effectiveness. The main purpose of this sub-section is to find a sound and cost-effective bond length for practical usage. The bond length will be applied for further parametric studies as well. In this study, besides the 600 mm bond length, the bond length ranging from 50 mm to 600 mm was investigated. The FE models therefore are named as 'PI-R-L50', 'PI-R-L100', 'PI-R-L150', 'PI-R-L200', 'PI-R-L400', and 'PI-R-L600' respectively. The number in their names represents the bond length.

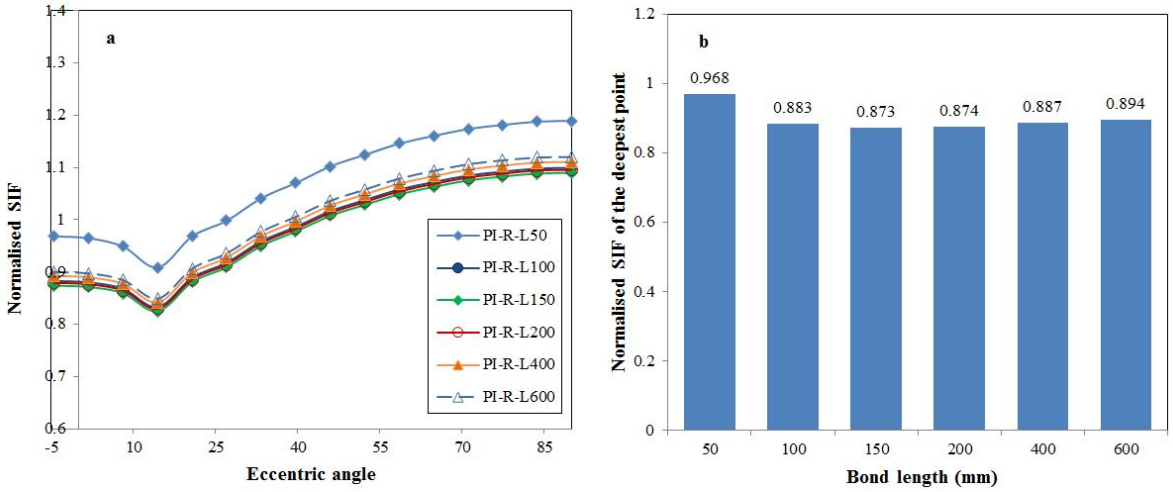

Figure 5.14. The normalised SIF result of FE models with different bond length: a) normalised SIF along the crack front; b) normalised SIF of the deepest point

Table 5.4. Specimen configuration of steel pipes with various diameters and thickness, and the SIF decrease

External diameter (mm)	**102.0**			**168.3**			**219.1**				**273.0**			
Bond length (mm)	100	**150**	200	100	**150**	200	100	150	**200**	300	100	150	**200**	300
SIF decrease (%)	11.7	**12.7**	12.6	7.6	**11.6**	11.0	5.3	9.3	**10.4**	9.9	3.4	7.9	**9.6**	9.0

Note: The percentage of SIF decrease is the reduction of each model towards the corresponding model without CRS.

Figure 5.14a shows the results of normalised SIF along the crack front of the FE models using different bond length. The SIF of 'PI-R-L50' is remarkably larger than the other FE models. The possible reason is the lack of effective bond length. The SIF decreases within the increasing of the bond length until it reaches 150 mm. Then the normalised SIF basically remains constant within the increasing of bond length. The reason is that once the bond length reaches a sufficient value, the bending moment remains basically stable within the increasing of the bond length, thus its effect on the SIF reduction is negligible. Overall, the SIF along the crack front of the FE models with the bond length from 100 mm to 600 mm do not have significate differences, as illustrated in Figure 5.14b. The FE model 'PI-R-L150' has the smallest SIF; therefore 150 mm bond length is selected as a most efficiency and cost-effective bond length, which is applied in the following parametric studies.

Besides the pipe in this FE model, which has an external diameter of 102 mm, the possible relation between the optimum bond length and the external diameter of the pipe is discussed. The diameter ranging from 102 mm to 273 mm as some of the common used offshore pipeline specifications [39] of the FE models are listed in Table 5.4. The thickness of the pipes is kept constant as 12.7 mm. It shows that the optimum bond length for pipes with larger external diameter has been increased. For instance, the optimum bond length for the pipe with the diameter of 102 mm is approximately 150 mm, as well as for the pipe with diameter of 168.3 mm. While for pipe diameter of 219.1 mm and 273.0 mm, the optimum length increases to 200 mm. When reinforcing steel pipes with larger diameter, the bond

length needs to be increased correspondingly. The optimum bond length for a specific steel pipe should be further determined by means of a sensitive study based on its dimension.

- Numbers of composite layer

Changing the numbers of composite layer is another practical way to affect the budget, time-consuming and reinforcement effectiveness. In this section, the influence of composite layers by using four different ranges of longitudinal CFRP layers is analysed. CRS bond length of 150 mm is chosen based on the study CRS bond length. The FE models are named as 'PI-R-LH', 'PI-R-LLH', 'PI-R-LLLH', and 'PI-R-LLLLH'.

Figure 5.15a shows that the normalised SIFs decrease equally along the crack front by increasing the numbers of composite layer of longitudinal CFRP. Figure 5.15b shows that SIF of the deepest point decreases by increasing the numbers of composite layer. Theoretically, the SIF is able to be decreased to a smaller value than the threshold value. In practical situations, users are able to design the numbers of composite layer based on requirement of the life extension. In this case, adding one layer of longitudinal CFRP from 'PI-R-LLH' to 'PI-R-LLLH' deceased the SIF approximately 6%.

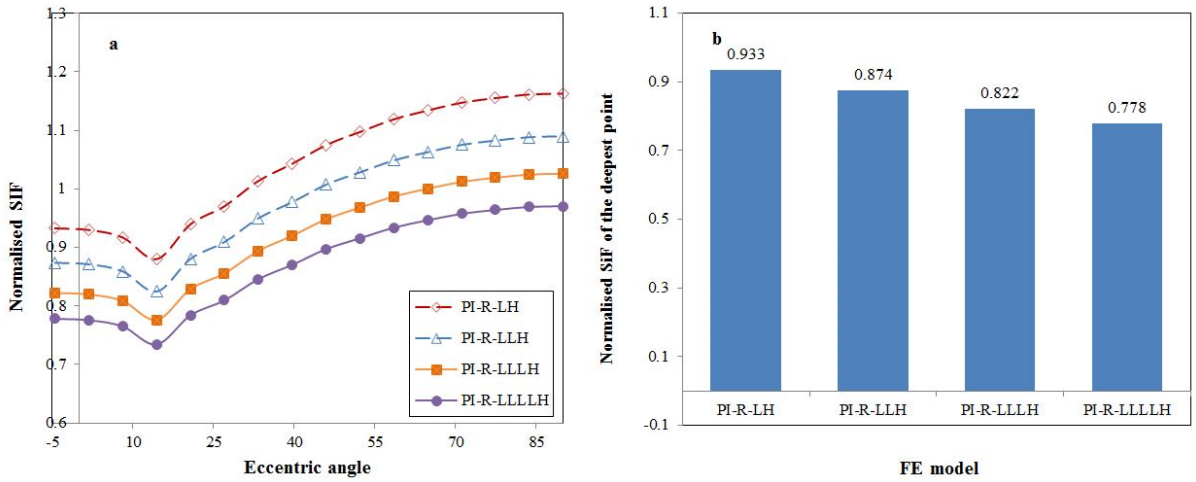

Figure 5.15. The normalised SIF result of FE models with different numbers of composite layer: a) normalised SIF along the crack front; b) normalised SIF of the deepest point

- CFRP tensile modulus

The material properties of CFRP have been rapidly developed thanks to the development of material technology. One of the most important material properties of CFRP is the tensile modulus. To date, the global market provides CFRP materials with different tensile modulus. This sub-section investigated three different CFRP materials with the tensile modulus of 150, 210 and 552 GPa respectively. The FE models are named as 'PI-R-C150', 'PI-R-C210' and 'PI-R-C552'.

Figure 5.16a shows that using the CFRP with higher tensile modulus have enhanced the effectiveness of the composite reinforcement. Compared to the normal CFRP with tensile

modulus of 205 GPa which decrease the SIF of 12.6%, the SIF of 'PI-R-C150' decreases 9.8%, while the SIF of 'PI-R-C552' decreases 25.9%, as shown in Figure 5.16b. Therefore, high tensile modulus CFRP can be applied as an alternative of using more composite layers, in order to avoid adding excessive dead weight.

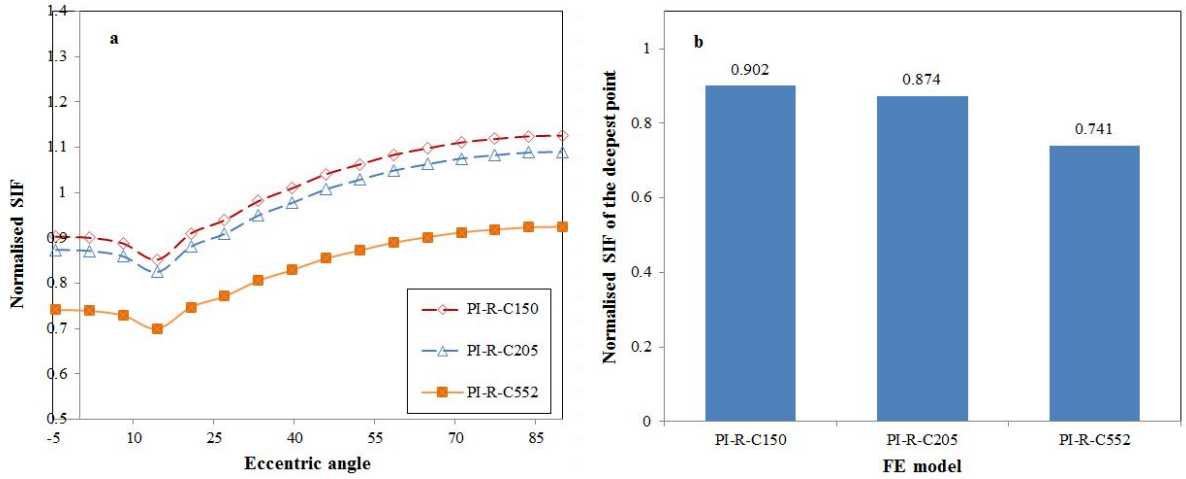

Figure 5.16. The normalised SIF result of FE models with different CFRP modulus: a) normalised SIF along the crack front; b) normalised SIF of the deepest point

- Adhesive thickness

The adhesive layer acts as intermediary between different layers of the CRS, particularly between the steel pipe and the first composite layer. In addition, the adhesive layer is the weakest layer in the reinforcement system. In practice, changing adhesive thickness might influence the reinforcement effectiveness. In this sub-section, three different ranges of adhesive thickness are analysed, 0.2, 0.35 and 0.5 mm.

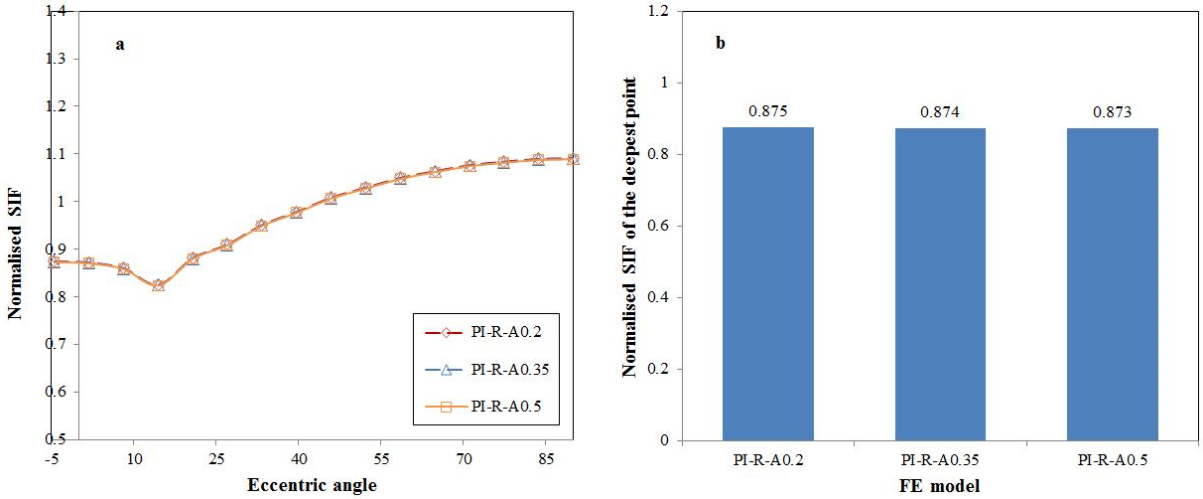

Figure 5.17. The normalised SIF result of FE models with different adhesive thickness: a) normalised SIF along the crack front; b) normalised SIF of the deepest point

Figure 5.17 illustrated that the effect on the SIF of surface cracks by changing the thickness of the adhesive layer is negligible. However, increasing the thickness decreases the

stress concentration in the adhesive layer, particularly at the edge of the bond, as indicated in Figure 5.18. The maximum stress value of the adhesive layer in model 'PI-R-A0.2' is larger than the yield stress of adhesive material, which instantly leads to edge debonding failure. A minimum thickness should be identified to avoid such failure. The maximum stress decreases when increasing the adhesive layer thickness, which is helpful to avoid unexpected edge debonding failures.

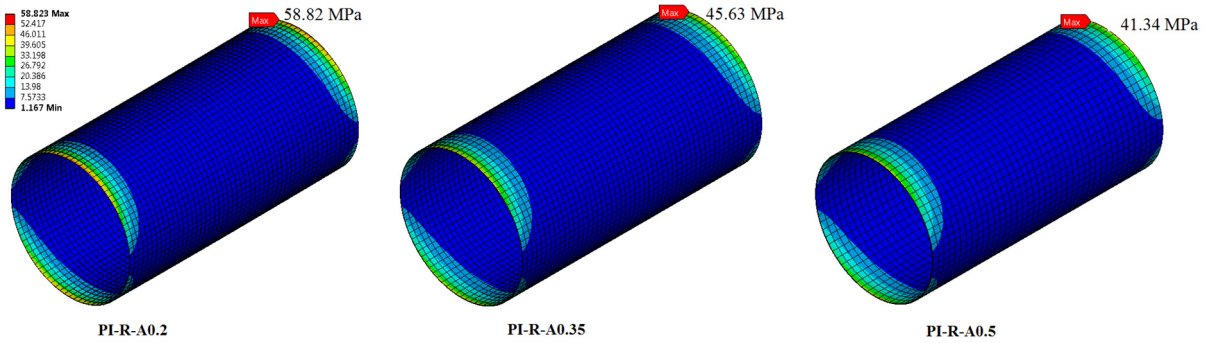

Figure 5.18. The stress distribution in the adhesive layer with different thickness

- Type of adhesive

Table 5.5. Material properties of different type of adhesive [27]

Adhesive type	*E* (Pa)	*T* (Pa)
MBrace saturant	2.86×10^9	46×10^6
Araldite K630	6.50×10^9	33×10^6
Sikadur 330	4.82×10^9	31.28×10^6

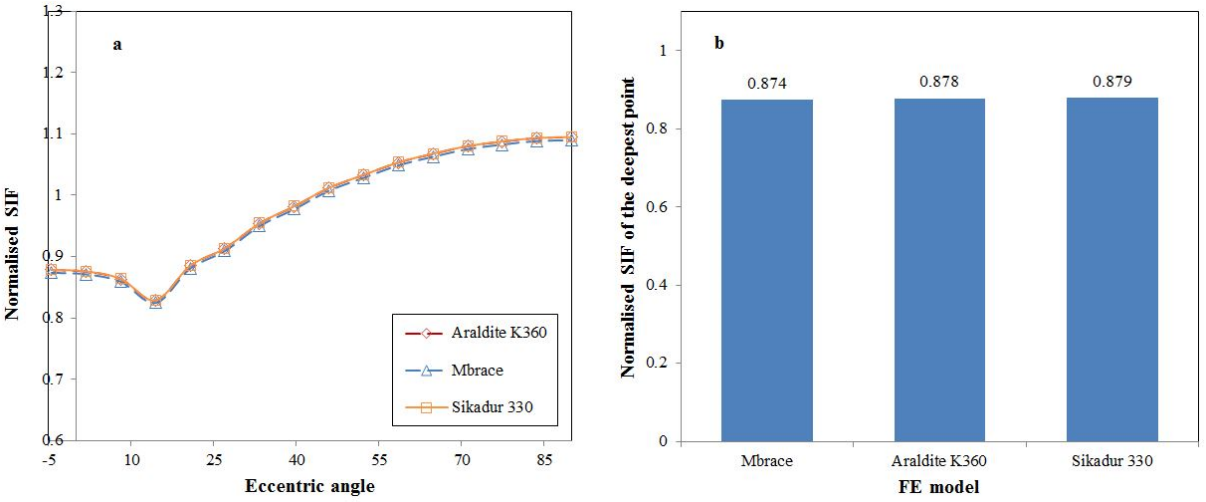

Figure 5.19. The normalised SIF result of FE models by using different types of adhesive: a) normalised SIF along the crack front; b) normalised SIF of the deepest point

In global market, various types of adhesive are available. In accordance with the research by Kabir, et al. [27], in this part, three types of adhesive are chosen for this study. The types of adhesive and their material properties are shown in Table 5.5. The thickness of all adhesive types is set as 0.35 mm. The SIF results of the FEMs using three different types of adhesive

are shown in Figure 5.19. It shows that the material properties of adhesive have a minor influence on the SIF of the surface cracks. However, the maximum stress of the adhesive layer using 'Araldite K630' and 'Sikadur 330' have reached 62.84 MPa and 56.03 MPa respectively (see in Figure 5.20). Edge debonding will be triggered. Therefore the 'MBrace saturant' adhesive, which has a lower elastic modulus and higher yield strength, is suggested for usage in terms of its lower stress concentration around the edge of the reinforcement.

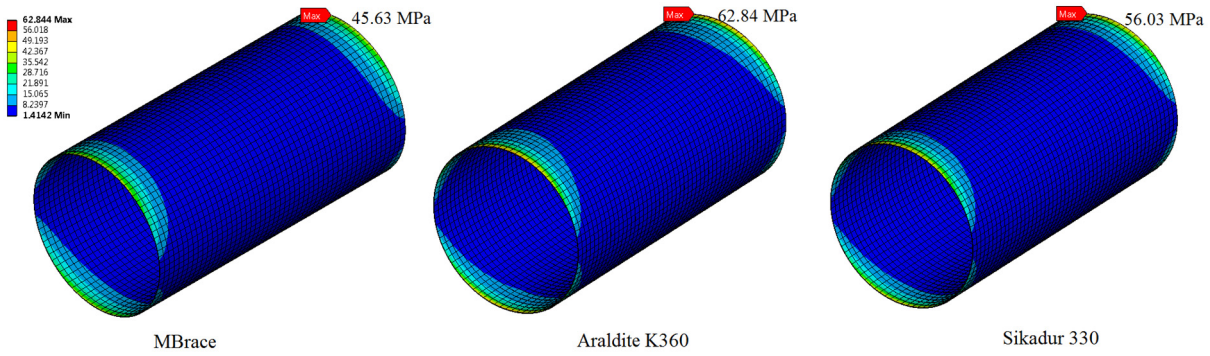

Figure 5.20. The stress distribution in the adhesive layer using different types of adhesive

- CFRP wrapping orientation

Normally in market, the principle direction of unidirectional CFRP is the longitudinal direction. However, in practice, longitudinal wrapping is difficult to be employed, especially for underwater scenario and for pipes with large external diameter. In this sub-section, the 'L-L-L-H' wrapping pattern with an inversely diagonal wrapping pattern, i.e., 45°-135°-45°-135° wrapping, and L-H-L-H wrapping pattern, are compared, as shown in Figure 5.21. The FE models are named as 'PI-R-LLLH', 'PI-R-In.' (inversely diagonal wrapping pattern), and 'PI-R-LHLH' correspondingly. In addition, the results of these FE models are also compared with 'PI-R-LLH' as the control model.

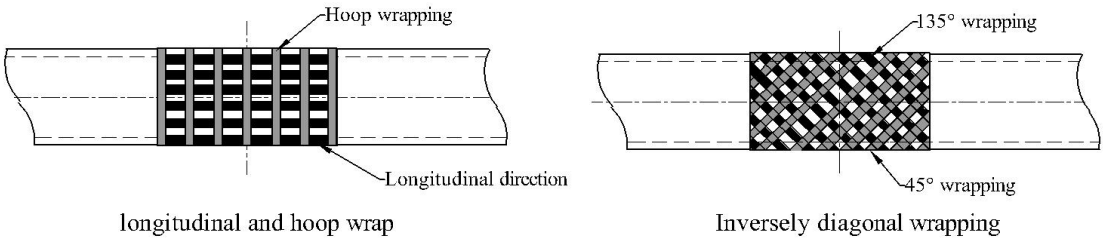

Figure 5.21. Wrapping scheme: 1) longitudinal and hoop wrapping; 2) inversely diagonal wrapping pattern

The SIF results in Figure 5.22 show that using longitudinal CFRP is the most effective way to reduce the SIF of the internal surface crack. The comparison between 'PI-R-LHLH' and 'PI-R-LLH' in Figure 5.22b illustrated that adding one hoop oriented CFRP has a minor effect on the reduction of the SIF. It shows that the SIF of 'PI-R-In.' model preforms slight better than the 'PI-R-LHLH' model. In practical situations when longitudinal wrapping is difficult to be implemented, using the inversely diagonal wrapping pattern is an alternative.

However, considering the remarkable SIF reduction, longitudinal orientated CFRP is recommended for practical usage. In global market, it is possible to acquire CFRP material with user-design fibre direction, in order to guarantee CFRP wrapping orientation during the reinforcement, as well as ensure the feasibility of construction.

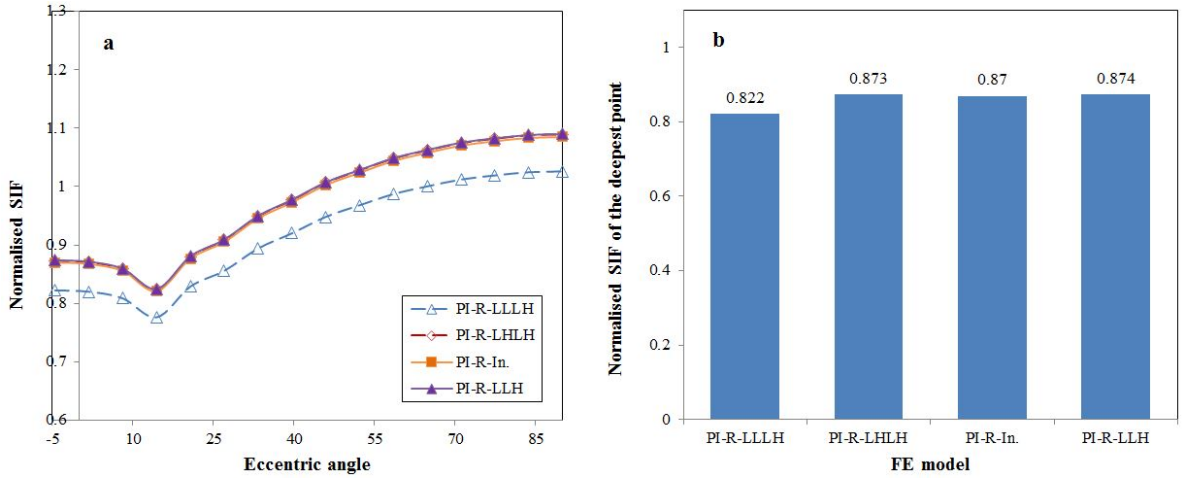

Figure 5.22. The normalised SIF result of FE models with different CFRP wrapping orientation: a) normalised SIF along the crack front; b) normalised SIF of the deepest point

- Crack aspect ratio

Table 5.6. Specimen configuration of steel pipes with different aspect ratios

Model No.	*a* (mm)	*c* (mm)	*a*/*c*	SIF decrease
1	3.0	12.0	0.25	13.15%
2	3.0	6.0	0.5	12.98%
3	4.5	6.0	0.75	12.92%
4	6.0	6.0	1.0	13.22%
5	6.0	4.5	1.5	13.13%
6	6.0	3.0	2.0	13.10%

Surface cracks are commonly induced by mechanical damage, corrosion pitting, and welding defects. They frequently appear on steel pipes with various profiles, mainly represented by their aspect ratios. In this sub-section, the SIF response of internal surface cracks in steel pipes with six different aspect ratios from 0.25 to 2.0 reinforced with CFRP are analysed. Table 5.6 shows the crack profile of the specimens, and the results of SIF decrease after reinforcement. The composite reinforcement continually adopts the scheme of 'PI-R-LLLH'. The results indicate that all the SIF of surface cracks with different aspect ratio from 0.25 to 2.0 decreases around 13% owing to the composite reinforcement.

- One added GFRP layer

In practical situation, when using CFRP to repair metallic structures, one layer of GFRP is generally applied in between the metallic substrate and the CFRP laminates in order to prevent the galvanic corrosion. In this part, both the GFRP and CFRP are employed to reinforce the internal cracked steel pipe, named as 'PI-R-GLLH'. The GFRP uses E-glass fibre from the material library of ANSYS workbench, and its properties are listed in Table 5.7.

The thickness of the GFRP is 0.35 mm. The SIF is evaluated by means of the FEM and then compared to the results of specimen 'PI-R-LLH' and 'PI-R-LLLH'. The results are shown in Figure 5.23, which indicates that adding one GFRP layer is rather effective to reduce the SIF of the surface crack. Comparing to 'PI-R-LLH', the SIF of the deepest point decreases 1.6%. Therefore, one-layer GFRP is recommended mainly because of its galvanic corrosion resistance.

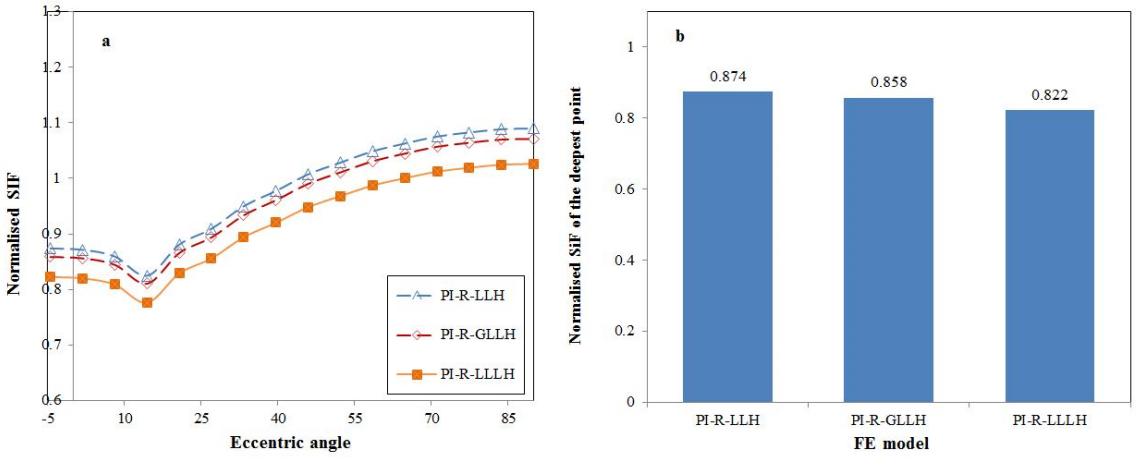

Figure 5.23. The normalised SIF result of FE models by using on one layer of GFRP laminate: a) normalised SIF along the crack front; b) normalised SIF of the deepest point

Table 5.7. Material properties of the GFRP material

Fibre type	E_1 (Pa)	E_2 (Pa)	G_{12} (Pa)	G_{13} (Pa)	G_{23} (Pa)	T (Pa)	Nu
GFRP	35×10^9	35×10^9	4.7×10^9	3.5×10^9	4.7×10^9	1.1×10^9	0.33

- Dimension of the steel pipe

In this sub-section, eight different pipe dimension with various D/t ratios of API 5L offshore steel pipes, conforming to the code [39] are studied using the FEM. Table 5.8 lists the configuration of the composite reinforced steel pipes with various diameter and wall thickness. Diameter of steel pipes from 168.3 mm to 323.8 mm pipes are adopted with five different pipe wall thickness from 10.97 mm to 21.95 mm: five incremental pipe wall thickness has been discussed within the external diameter of 168.3 mm, while four incremental external diameter has been analysed within the pipe wall thickness of 12.7 mm. These pipe dimensions can represent the frequently used steel pipeline in the offshore industry. The reinforcing scheme applies the optimum choices in all parametric analysis. Therefore, the bond length of all pipes is 150 mm. CRS wrapping scheme adopts 'G-L-L-L-L-H', the CFRP laminates adopt the high tensile modulus of 552 GPa, while the adhesive material chooses the 'MBrace saturant', with the thickness of 0.35 mm. The crack size of a = 3.0 mm and c = 6.0 mm is applied for this study.

The results in Table 5.8 illustrates that within the same external diameter, the reinforcement effectiveness (represented by the SIF decrease percentage) decreases with the increasing of wall thickness, and within the same wall thickness, the reinforcement

effectiveness decreases with the increasing of pipe external diameter as well. Therefore, when repairing surface cracks in steel pipes with larger external diameter and thicker wall thickness, high elastic modulus CFRP and more CFRP layers are suggested in order to achieve a satisfying decrease of crack growth rate.

Table 5.8. Specimen configuration of steel pipes with various dimensions, and the results of the SIF decrease

Model No.	*D* (mm)	*t* (mm)	*D*/*t*	SIF decrease
1	168.3	10.97	15.34	23.58%
2	168.3	12.70	13.25	22.70%
3	168.3	14.27	11.79	19.55%
4	168.3	18.26	9.22	16.16%
5	168.3	21.95	7.67	13.89%
6	219.1	12.70	17.25	18.63%
7	273.0	12.70	21.50	15.71%
8	323.8	12.70	25.40	13.64%

5.4 An analytical approach of evaluating the SIF of the internal surface cracked metallic pipes reinforced with CRS

Section 5.3 indicates that the key influential parameters includes the number of bond layer, CFRP tensile modulus, the dimension of the pipe. Adding one layer of GFRP can improve the reinforcement as well. These influential parameters are hence considered in the analytical analysis to predict the SIF of the internal surface cracks in metallic pipes. In this section, the CRS is regarded as an additional wrap on the external surface of the cracked metallic pipe, which decreases the overall deflection of the pipe, resulting in the reducing the stress around the surface crack.

5.4.1 Mathematical model

In this section, an analytical method of evaluating the SIF of the internal surface crack in metallic pipes reinforced with CRS is proposed. Since the internal surface crack did not contact with the composites, the decreasing of the SIF mainly owes to the reduction of the pipe deflection. First, the bending stress of the pipe is identified by proposing an equivalent stiffness. As shown in Figure 5.24, the composite reinforced pipe is subjected to tension (Figure 5.24a) and bending load (Figure 5.24b). Since the composite reinforced pipe is regarded as a whole, the strain of the different layers at the mid-span area are assumed as equal; therefore,

$$E_{\mathrm{eq}} \cdot \varepsilon_{\mathrm{eq}} \cdot A = \sum_{i=1}^{n} E_i \cdot \varepsilon_i \cdot A_i, \tag{5.3}$$

where E_{eq} and ε_{eq} are the equivalent tensile modulus and the strain value of the composite reinforced pipe along the pipe length direction, A is the whole area of the cross-section, E_i, ε_i, A_i are the tensile modulus, strain value, and the cross-section area of each area, including the metallic pipe, the GFRP and several layers of CFRP. The strain of different layers are assumed as equal, as

$$\varepsilon_{\mathrm{eq}} = \varepsilon_i. \tag{5.4}$$

Therefore,

$$E_{\mathrm{eq}} \cdot A = \sum_{i=1}^{n} (E_i \cdot A_i), \tag{5.5}$$

where

$$A_i = \pi[(R_i + t_i)^2 - R_i^2] = \pi(t_i^2 + 2t_i \cdot R_i), \tag{5.6}$$

$$A = \pi[t_{\mathrm{crs}}^2 + 2 \cdot t_{\mathrm{crs}} \cdot R_i], \tag{5.7}$$

in which t_{crs} is the thickness of the CRS, including all layers of FRP laminates.

When the pipe is under pure bending moment, the bending stress therefore can be calculated as:

$$\sigma_{\mathrm{b}} = M \Big/ \frac{\pi \cdot (R + t_{\mathrm{crs}})^3}{4} \cdot \left(1 - \left(\frac{r}{R + t_{\mathrm{crs}}}\right)^4\right). \tag{5.8}$$

Then the equivalent stress at the interface between the CRS and the metallic pipe (see in Figure 5.25) is

$$\sigma_{\mathrm{eq}} = \sigma_b \cdot \frac{R}{R + t_{\mathrm{crs}}}. \tag{5.9}$$

Thus the corresponding equivalent strain is

$$\varepsilon_{\mathrm{eq}} = \frac{\sigma_{\mathrm{eq}}}{E_{\mathrm{eq}}}. \tag{5.10}$$

Since all adjacent layer share the same value at the interface, the stress at the external surface of the metallic pipe is

$$\sigma_{\mathrm{s}} = E_{\mathrm{s}} \cdot \varepsilon_{\mathrm{eq}}, \tag{5.11}$$

Then incorporating with the analytical method—Eq. (3.7) proposed in Chapter 3, as well as the bending correction factor of Eq. (3.8) and the geometry correction factor of Eq. (3.17), the SIF of the internal surface crack reinforced with CRS can be evaluate.

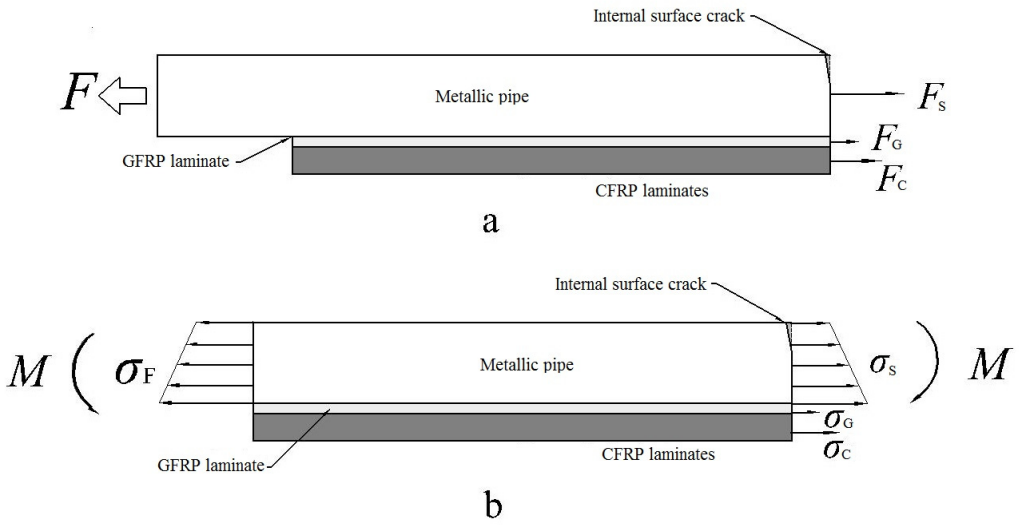

Figure 5.24. The stress analysis of a circumferential internal surface cracked pipe reinforced with CRS under bending

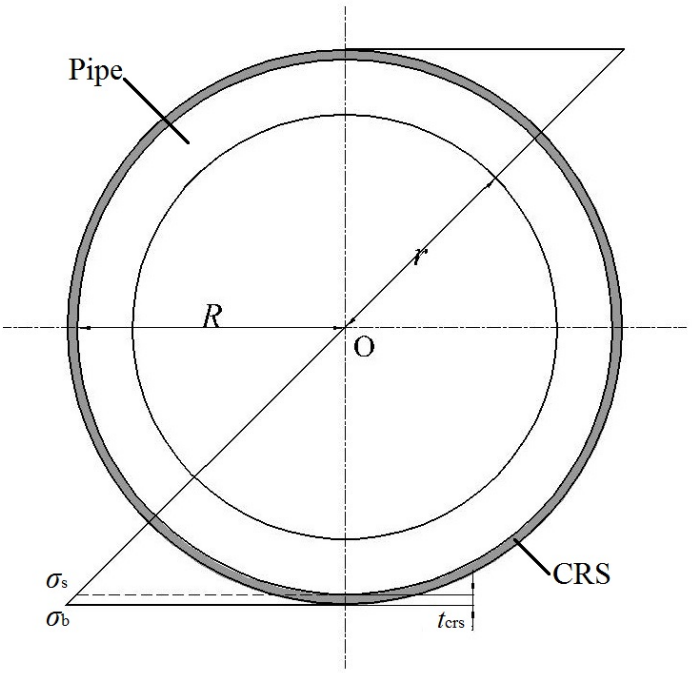

Figure 5.25. The bending stress in a pipe reinforced with CRS

5.4.2 Verification of the analytical method by using the FEM

The analytical method in this sub-section is verified by means of the FEM. First, the SIF results along the crack front evaluated by the analytical method is compared with the FE results. The pipe dimension, meshing method, material properties, and reinforcement method are identical to the FE model in Section 5.2. While combined tensile and bending loads are applied on the model, as shown in Figure 3.22 in Chapter3. Here three crack dimensions with the same crack length while different crack depth were adopted. The comparison results between the FE model and the analytical method is shown in Figure 5.26.

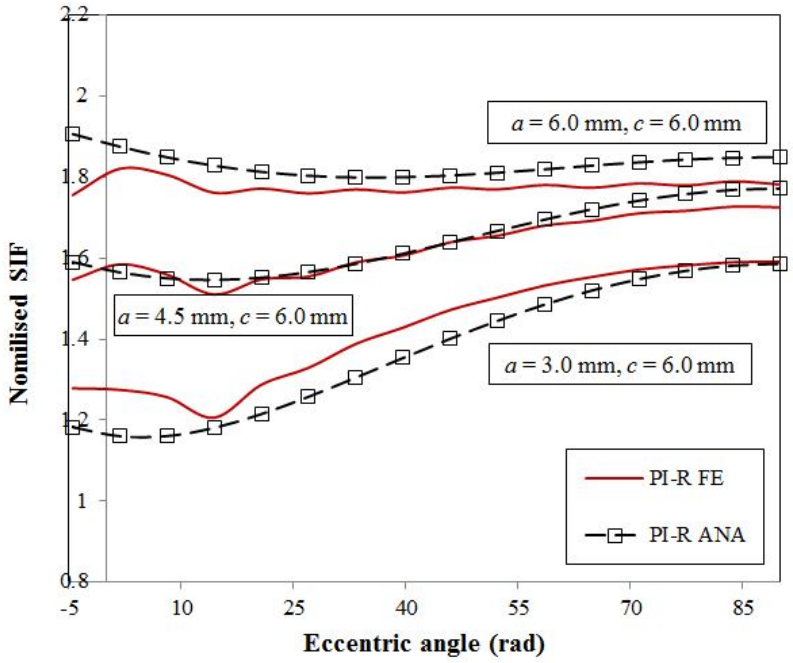

Figure 5.26. The relative SIFs along half internal surface cracks front of FEM and analytical result

The comparison in Figure 5.26 indicates that the analytical method can rationally predict the SIFs along the internal crack front in the metallic pipes reinforced with CRS subjected to combing tension and bending loads. In those cases, the average error of 2.8%, and the maximum error is 8.98% (near the surface point).

5.5 Conclusions

Circumferential internal surface crack growth is a serious threat to the structural integrity of offshore metallic pipes. Critical surface cracks need to be repaired instantly in order to avoid oil and gas leakage. In this chapter, CRS is applied to repair the circumferential surface cracked metallic pipe subjected to bending. The SIF of the surface crack growth has been evaluated by means of the FEM. Based on the FEM, a parametric study has been conducted. The conclusions are drawn:

- CRS is an efficient and cost-effective method for repairing internal surface cracked steel pipes. Its effects on crack growth reduction and fatigue life extension are remarkable. For instance, using 'L-L-H' wrapping pattern, which is the specimen 'PI-R-LLH', has prolonged the fatigue life of the cracked steel pipe with 47.04%.
- CRS decreases the internal crack growth rate along the depth direction and length direction approximately equal. It means CRS will not change the variation of the crack profile (represented by the variation of the crack aspect ratio) during the crack growth process.
- The parametric study indicates the key influential parameters significantly affects the SIF of the composite reinforced surface crack, including the CRS bond length, numbers of composite layer, CFRP tensile modulus, wrapping orientation, and pipe dimensions. In

practical situation, users need to achieve a balance among the fatigue life extension requirement, budget and the dead weight.

- The parametric study also indicated that adhesive thickness and adhesive types have negligible influences on the SIF reduction. However, increasing the adhesive thickness and using low elastic modulus adhesive material have reduced the stress concentration at the edge of the adhesive layer. Therefore, users need to apply appropriate thickness and type of adhesive layer in order to avoid unexpected edge debonding failure. CRS has an approximately identical effect on the SIF decrease of surface cracks with different aspect ratio between 0.25 and 2.0. One layer of GFRP as the first layer is recommended for preventing galvanic corrosion between the CFRP laminate and the steel substrate. The added layer of GFRP has a minor effect on reducing the SIF of the surface crack.
- The proposed analytical method can rational predict the SIFs along the crack front in the composite reinforced metallic pipe subjected to combined tension and bending loads.

Chapter 6 External surface cracked metallic pipes reinforced with CRS*

Following the previous chapter, in this chapter, composite reinforcement on the external surface cracked steel pipes has been analysed. The adhesive layer has a direct contact with the cracked surface, which leads to a more complex situation than composite reinforcement on internal surface cracked pipes. In this sense, identifying the possible failure modes and their influence on surface crack growth is significant. In addition, besides the indirect effect of the composite reinforcement on reducing the SIF, the crack-bridging effect might have a positive effect on decreasing the surface crack growth rate. Therefore, the mechanism of composite reinforcement on the external surface cracked pipes is needed to be investigated, in order to propose appropriate rational methods of predicting the surface crack growth.

Following the investigations on the flat plates in Chapter 4 and the internal surface cracked pipes in Chapter 5, first, an experimental study is designed and conducted in order to identify the test phenomenon and collect test results, as arranged in Section 6.1. Then a three-dimensional FE model is developed to evaluate the SIF of the external surface cracks reinforced with CRS, arranging in Section 6.2. The FEM is validated by the experimental results. Besides, the potential interfacial failure is discussed. Then in Section 6.3, a parametric study is conducted to indicate the influential parameters and their effects on the surface crack growth. On account of the parametric study, an analytical method of evaluating the external surface crack growth reinforced with CRS is proposed in Section 6.4. Finally, the conclusions of this chapter are presented in Section 6.5.

* This chapter is based on the published journal articles [153] Z. Li, X. Jiang, H. Hopman, L. Zhu, and Z. Liu, "External surface cracked offshore steel pipes reinforced with composite repair system subjected to cyclic bending: An experimental investigation," *Theoretical and Applied Fracture Mechanics,* vol. 109, p. 102703, 2020., and Li, Z., Jiang, X., Hopman, H., Zhu, L. and Liu, Z., 2020. External surface cracked offshore steel pipes reinforced with CRS subjected to cyclic bending: A numerical investigation. Submitted to a journal.

6.1 Experimental investigation on external surface cracked steel pipes reinforced with CRS

In this section, the composite reinforced external surface cracked steel pipes subjected to cyclic bending was investigated. The main purpose is to analyse the composite reinforcement effect on the crack growth, as well as indicating the potential failure modes. In addition, the experimental results will be used to validate the FE model in Section 6.2.

6.1.1 Specimen preparation

Specimen preparation is an important step for the sake of achieving ideal experimental results. The quality of each constituent part is needed to be guaranteed. In this sub-section, the preparation procedures including material properties, specimens manufacturing, and specimens configurations are introduced successively.

6.1.1.1 Material properties

The sketch diagram of the composite reinforced external surface cracked steel pipe specimen is shown in Figure 6.1. Four materials were used to manufacture the specimens: steel substrate, GFRP, CFRP, and adhesive. Stainless steel *API 5L X65* for subsea scenarios conforming to API SPEC 5L code [39] has been used as the steel substrate, which has a yield strength of 448 MPa, and a tensile strength of 530 MPa. The adhesive and FRP materials are identical to the materials in Chapter 4, as listed in Tables 4.1 to 4.3.

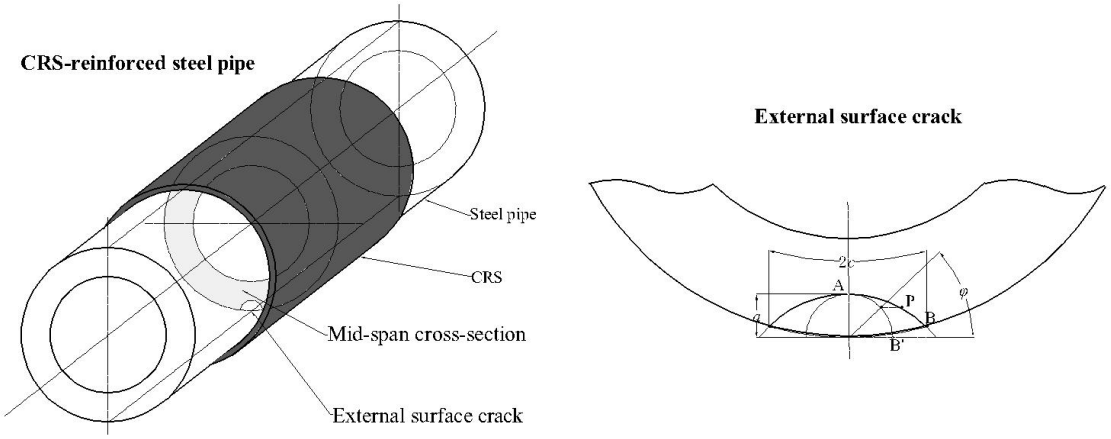

Figure 6.1. The sketch diagram of the composite reinforced surface cracked pipe specimens

6.1.1.2. Specimen manufacturing

The detailed manufacturing procedures of the specimens are introduced in Appendix I.

6.1.1.3. Specimens configurations

The sketch diagram of the composite reinforced cracked specimen is shown in Figure 6.2, and the dimensions of the specimens are listed in Table 6.1, including the pipe length *L*, pipe

external diameter D, wall thickness of the pipe specimens t, and the depth & half length of the notch a_0 and c_0. The thickness of each layer of GFRP and CFRP laminate are 0.35 mm. In total, nine groups of 27 specimens were prepared. Group 1, 2, 3 are three controlling groups without composite reinforcement. The difference between Groups 1 to 3 is lying in their notch sizes. Groups R1 to R3 are the corresponding groups of Groups 1 to 3 respectively, using the default reinforcement scheme: four layers of CFRP laminates, the 'L-L-L-H' wrapping pattern (L represents longitudinal wrapping pattern, while H represents hoop wrapping pattern) shown in Figure 6.3a, and 1,000 mm bond length. The specimens in Groups R4 and R5 applied the same wrapping pattern of Group R1, while using a different bond length L_c and number of bond layers respectively. The difference between Group R6 and Group R1 is that R6 applied the inversely diagonal wrapping method, as indicated in Figure 6.3b. Table 6.1 summarised the configuration and reinforcement details of all specimens. The name of the specimens represents the notch category, composite reinforcement scheme, CFRP wrapping pattern, and their repetitive number. Take 'PE-1-R(1)' as an example, 'P' means steel pipe, 'E' represents external surface crack, the '1' stands for the notch category 1, R means reinforcement, and the '(1)' means the No. of the repetitive specimen.

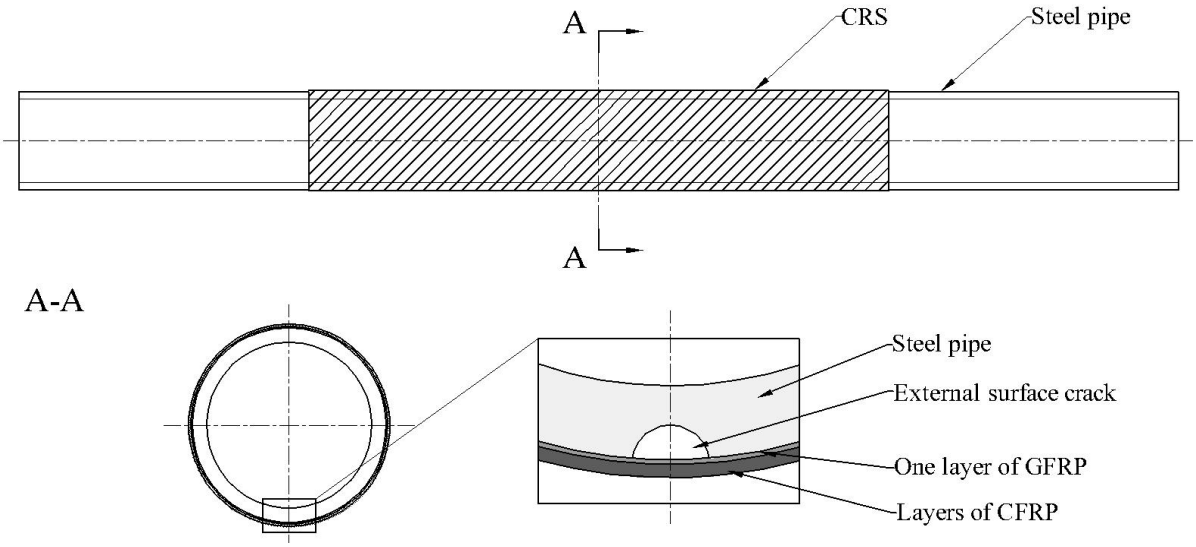

Figure 6.2. The configuration of composite reinforced steep pipe specimens

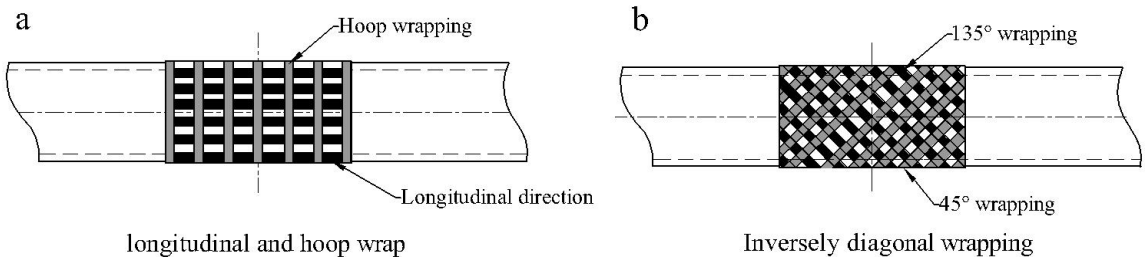

Figure 6.3. Wrapping scheme: a) the longitudinal and hoop wrapping pattern; b) the inversely diagonal wrapping pattern

Table 6.1. Specimens' configuration and reinforcement details

Group	Specimen	Notch category	L (mm)	D (mm)	t (mm)	a_0 (mm)	c_0 (mm)	L_c (mm)	CFRP wrapping
	PE-1(1)	1	2,000	168.3	12.76	2.31	4.94	\	\
1	PE-1(2)	1	2,000	168.3	12.81	2.48	5.04	\	\
	PE-1(3)	1	2,000	168.3	12.77	2.44	4.89	\	\
	PE-2(1)	2	2,000	168.3	12.70	2.39	3.99	\	\
2	PE-2(2)	2	2,000	168.3	12.74	2.44	3.82	\	\
	PE-2(3)	2	2,000	168.3	12.68	2.39	3.99	\	\
	PE-3(1)	3	2,000	168.3	12.61	3.99	4.00	\	\
3	PE-3(2)	3	2,000	168.3	12.73	3.96	3.98	\	\
	PE-3(3)	3	2,000	168.3	12.84	3.92	3.97	\	\
	PE-1-R(1)	1	2,000	168.3	12.63	2.31	4.94	1,000	L-L-L-H
R1	PE-1-R(2)	1	2,000	168.3	12.78	2.48	5.035	1,000	L-L-L-H
	PE-1-R(3)	1	2,000	168.3	12.76	2.44	4.885	1,000	L-L-L-H
	PE-2-R(1)	2	2,000	168.3	12.71	2.50	3.95	1,000	L-L-L-H
R2	PE-2-R(2)	2	2,000	168.3	12.68	2.53	3.90	1,000	L-L-L-H
	PE-2-R(3)	2	2,000	168.3	12.78	2.47	4.445	1,000	L-L-L-H
	PE-3-R(1)	3	2,000	168.3	12.66	4.03	4.02	1,000	L-L-L-H
R3	PE-3-R(2)	3	2,000	168.3	12.47	3.95	3.955	1,000	L-L-L-H
	PE-3-R(3)	3	2,000	168.3	12.65	4.02	3.97	1,000	L-L-L-H
	PE-1-R600(1)	1	2,000	168.3	12.62	2.47	5.25	600	L-L-L-H
R4	PE-1-R600(2)	1	2,000	168.3	12.69	2.46	4.92	600	L-L-L-H
	PE-1-R600(3)	1	2,000	168.3	12.74	2.48	4.93	600	L-L-L-H
	PE-1-R8(1)	1	2,000	168.3	12.77	2.56	5.09	1,000	L-L-L-H-L-L-
R5	PE-1-R8(2)	1	2,000	168.3	12.72	2.56	4.90	1,000	L-L-L-H-L-L-
	PE-1-R8(3)	1	2,000	168.3	12.63	2.48	5.15	1,000	L-L-L-H-L-L-
	PE-1-R45(1)	1	2,000	168.3	12.74	2.46	4.95	1,000	Inversely
R6	PE-1-R45(2)	1	2,000	168.3	12.70	2.50	4.875	1,000	Inversely
	PE-1-R45(3)	1	2,000	168.3	12.79	2.52	4.87	1,000	Inversely

Note: The parameters, i.e., D, t, a_0, c_0 were measured based on each specimens, each of which is the weighted average of three measurement locations. The three notch categories represent the three different notch sizes shown in Figure 6.2, i.e., aimed aspect ratio of 0.5, 0.625, and 1.0.

6.1.2 Test set-up

The fatigue tests followed the code of ASTM E647 [57]. All tests were carried out under constant amplitude sinusoidal cyclic loading, generated by MTS Hydraulic Actuator, which has a capacity of 1,000 kN. The schematic and the real test set-up are shown in Figure 6.4 and Figure 6.5 respectively. The load was applied in four-point bending condition to ensure a pure bending statue around the cracked location within the inner span. Note that the inner span L_i is designed as 800 mm, which is more than four times larger than the pipe diameter, in order to eliminate potential negative effects from the loading cells. The external span L_e is designed as 1,800 mm, leaving the bending arm equals to 500 mm.

All the fatigue tests were conducted at room temperature and air environment under load control condition. The amplitude of the applied force, namely 241.54 kN, produced a

maximum stress value of 268.8 MPa, accounting for 60% of the yield strength of the steel substrate. Such selection is based on the fact the normal stress at the critical zones of a steel lazy-wave riser can reach 240 MPa or even higher [60], as well as considering to adequately reducing the test period. The loading frequency was set as 2.5 Hz. The load ratio R maintained 0.1 for the crack growth process of all tests. The crack growth process was recorded by beach marking technique by means of changing the load ratio R to 0.5 and cycled for 5,000 cycles, as indicated in Figure 6.6. Each test ended automatically once the pipe specimen fractured and trigger the displacement limiter of the fatigue machine.

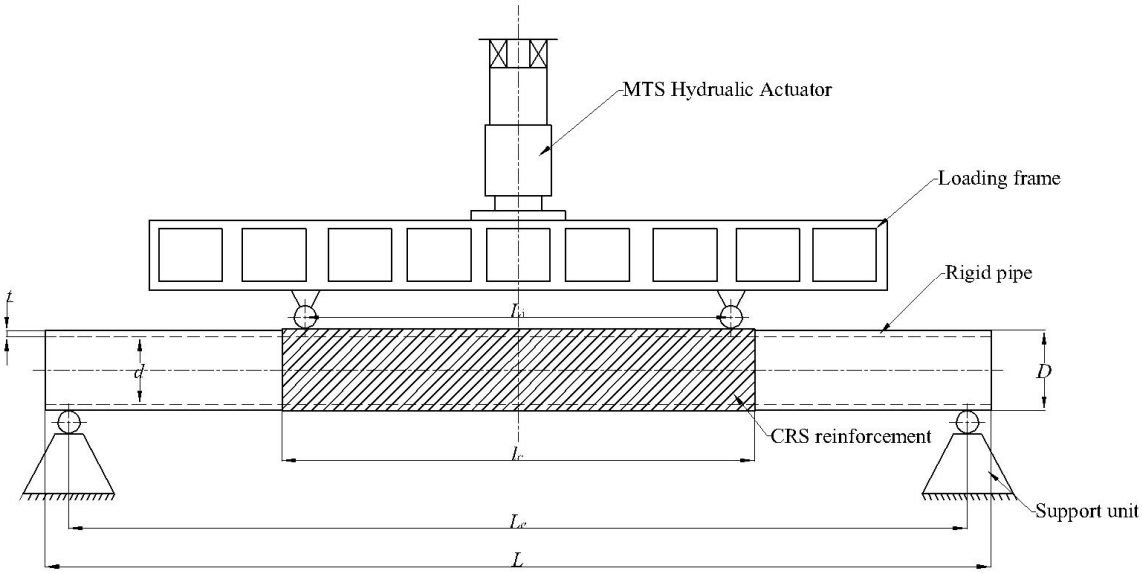

Figure 6.4. The schematic of the four-point bending test set-up

Figure 6.5. Specimen and instruments installation

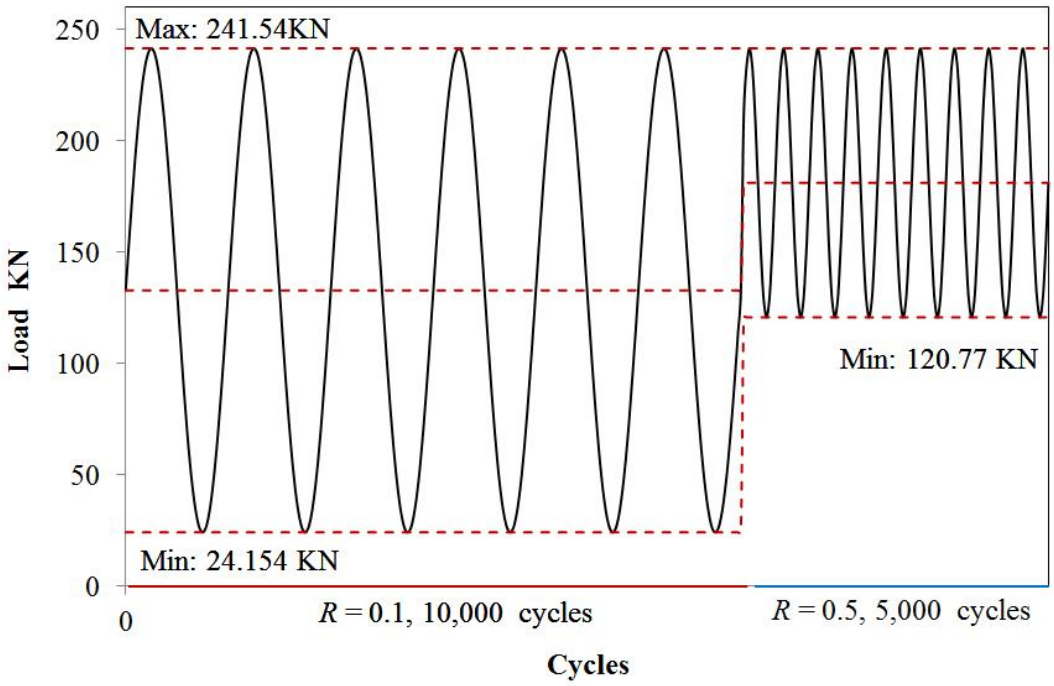

Figure 6.6. The load spectrum and beach mark generating procedure

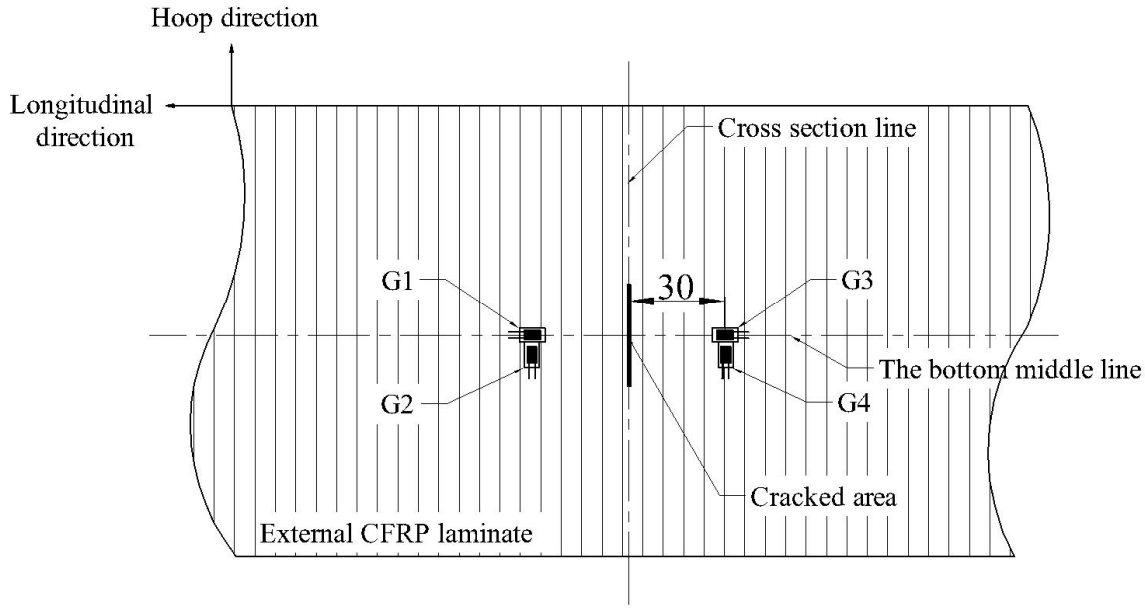

Figure 6.7. The installation of strain gauges on the external CFRP laminate around the cracked area

During the fatigue test, the strain on the external CFRP laminate around the middle bottom was monitored. Four strain gauges were installed on each composite reinforced specimens on the external CFRP laminate along the bottom middle line, as shown in Figure 6.7. G1 and G3 were axial symmetry installed by the surface crack along the bottom middle line, so as G2 and G4. The gauges of G3 and G4 were acting as the substitutions for G1 and G2 respectively. The distance between G1 and the middle cross-section of the pipe is 30 mm,

while G2 was installed adjacent to G1. Then the gauges were connected to the dynamic strain indicator to monitor the strain data for 60 seconds of every 10,000 cycles.

Three dial indicators were installed at the bottom side of the specimens as well, each of them was positioned at the one fourth of the external span of the four-point bending (Points B, C and D), connecting to the static indicator, as shown in Figure 6.5 and Figure 6.8. Point A and E are the points where the steel pipes contacted with the support units, thus their displacement during the test remained zero. During the test, the displacement results of point B, C, and D were recorded for every 10,000 cycles, from 0 kN to the amplitude of the bending load of 241.54 kN.

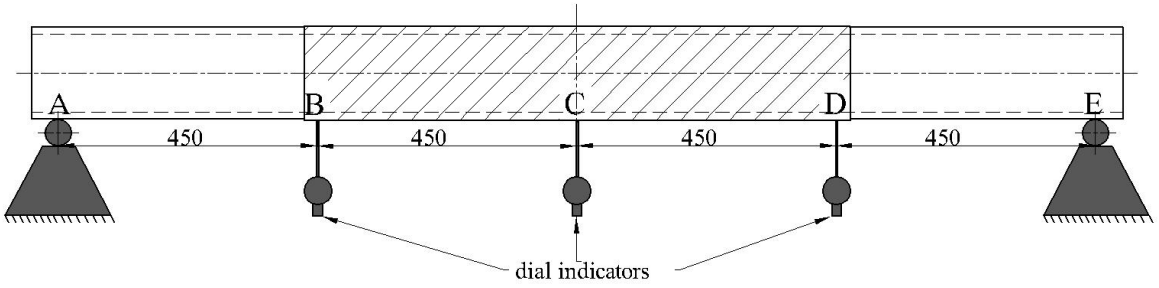

Figure 6.8. The dial indicators installed underneath the specimens

6.1.3 Results and discussion

In this sub-section, the test results, including failure modes, the surface crack growth results, as well as the strain data around the mid-bottom of the specimens and the load-displacement data of the specimens along the bottom middle line, are presented and analysed.

6.1.3.1 Failure modes

Within the surface crack growing stage, no failures were observed for all specimens, including interfacial failure, composite delamination, cohesion failures or composite rupture. The CRS was adequately bonded on the steel pipes during the fatigue tests before the crack penetrating the pipe wall. When approaching the end of each test, the crack has already propagated to larger through-thickness cracks, a clearly sound of debonding at the mid-bottom was captured for each composite reinforced specimen.

6.1.3.2 Surface crack growth behaviour and crack growth results

After each test, the cross-sections of bending specimens were sampled around the cracked area by the oxy-acetylene cutting. Then the crack growth behaviour was recorded by the beach marking technique using an electronic reading microscope. Then the crack sizes corresponding to each additional 10,000 cycles under R = 0.1 were measured by using an electronic reading microscope. One random specimen of the repetitive three specimens is selected to show the crack shape variation during the fatigue test, as shown in Figure 6.9. The cycle-index between each two adjacent beach marks is 10,000. The figures demonstrate the

multiple initiations from the notch fronts, and the surface crack continually propagated as a semi-elliptical shape until the crack penetrated the pipe wall. In addition, the photographs show that the beach marks on the composite reinforced specimens are denser than on the un-reinforced specimens. Especially, the beach marks of specimens PE-1-R8(2) is significantly denser than PE-1(1), indicating that the FCGR was dramatically reduced by using eight layers of CFRP laminates. The detailed results of crack depth (a) and half crack length (c), corresponding to the cycle-index are listed in the Table II.2 in Appendix II.

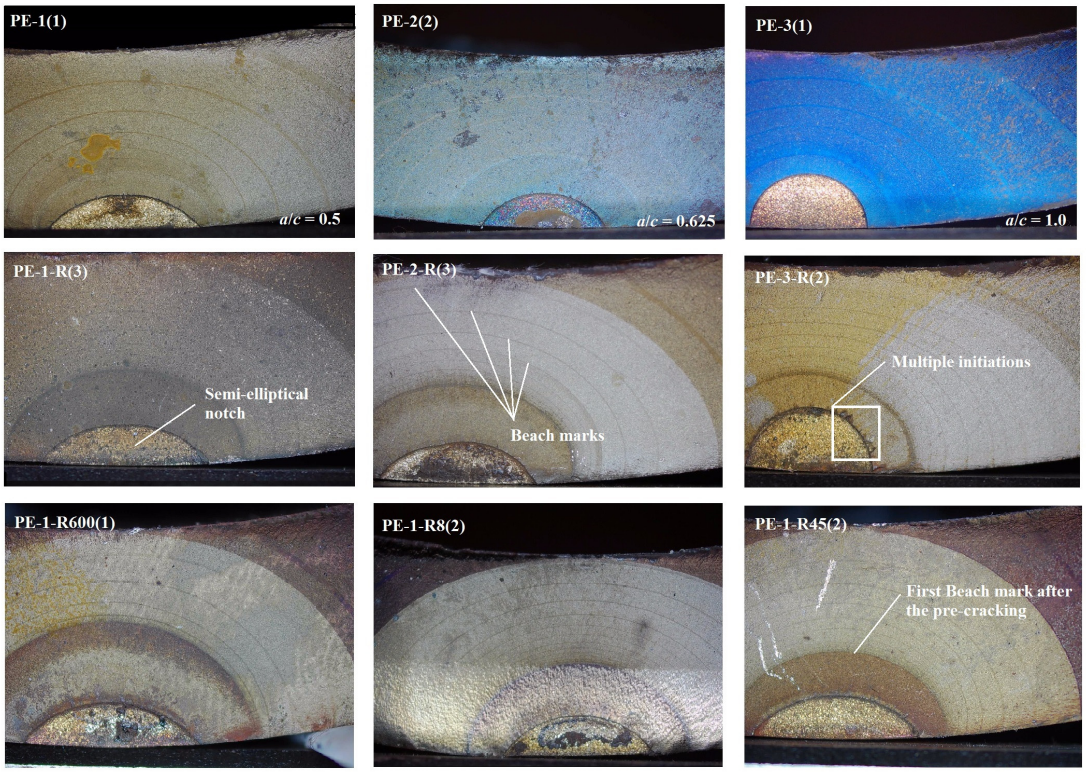

Figure 6.9. Beach marks on the cross-section of the steel pipe specimens

- *Composite reinforcement on the cracked steel pipes with different crack size*

It is clearly indicated from Figures. 10 to 12 that the experimental results have a good repeatability. The results of crack growth along the depth direction in Figure 6.10a shows that starting from a = 5.81 mm (when N is around 25,000 cycles), the CRS prolonged the residual fatigue life from around 65,000 cycles to 110,000 cycles, or approximately 110%. Note that in this chapter, the residual fatigue life is defined as the cycle-index from the initiation crack till the crack penetrating the pipe wall. Figure 6.10b illustrated that between 30,000 and 60,000 cycles, the cracks barely grew along the length direction. The crack aspect ratio (a/c) variation results in Figure 6.10c shows that the a/c of the composite reinforced specimens were always higher than the non-reinforced specimens during the test. Finally, the preferred aspect ratios (a/c when a/t equals to 0.8) of the composite reinforced specimens reached around 0.9, which is larger than the un-reinforced specimens of 0.8. This indicates that the CRS is more effective on crack growth along the length direction, which might be owing to the crack-bridging effect.

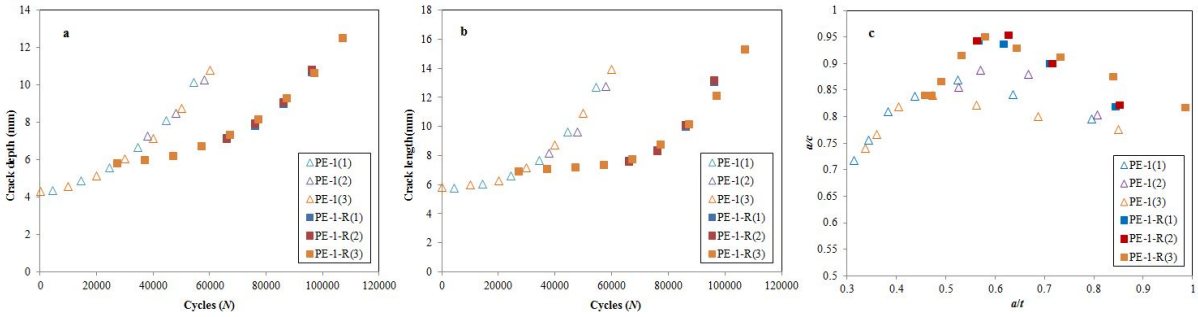

Figure 6.10. The experimental results of PE-1 and PE-1-R of using the default reinforcement scheme: a) crack growth along depth direction; b) crack growth along length direction; c) aspect ratio variation: a/c versus a/t curves

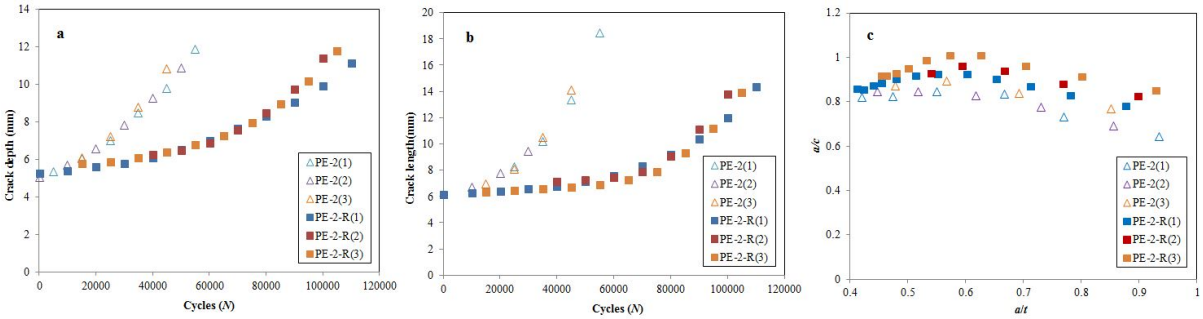

Figure 6.11. The experimental results of PE-2 and PE-2-R of using the default reinforcement scheme: a) crack growth along depth direction; b) crack growth along length direction; c) aspect ratio variation: a/c versus a/t curves

The results in Figure 6.11 and Figure 6.12 of using CRS to reinforce the specimens with different crack sizes show similar trends with the results in Figure 6.11 in terms of the repeatability, fatigue life prolongation, and aspect ratio variation. Figure 6.11 indicates that the residual fatigue life has prolonged from 58,000 cycles to 120,000 cycles, of around 110%, and Figure 6.12 shows that the residual fatigue life was prolonged around 120%. Besides, the crack of PE-2-R and PE-3-R barely grew along the length direction before the crack length *c* reached around 7.0 mm. Thus the CRS has a similar effect on surface crack with different crack aspect ratios.

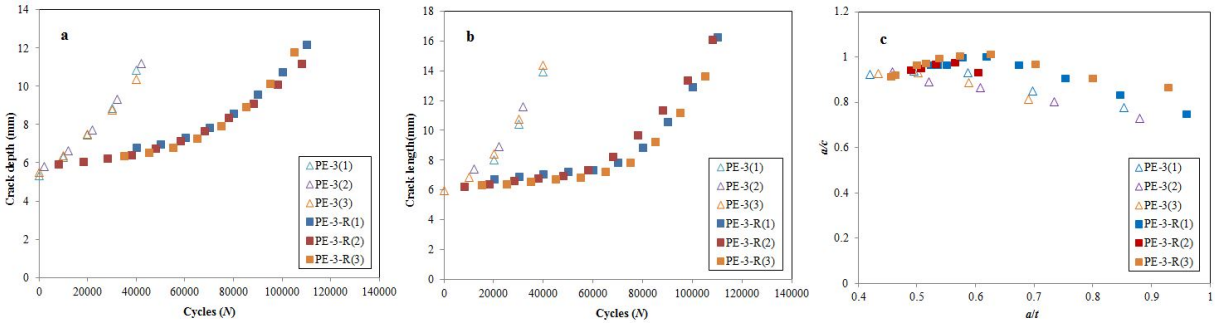

Figure 6.12. The experimental results of PE-3 and PE-3-R of using the default reinforcement scheme: a) crack growth along depth direction; b) crack growth along length direction; c) aspect ratio variation: a/c versus a/t curves

- *Composite reinforcement on the cracked steel pipes using different bond length*

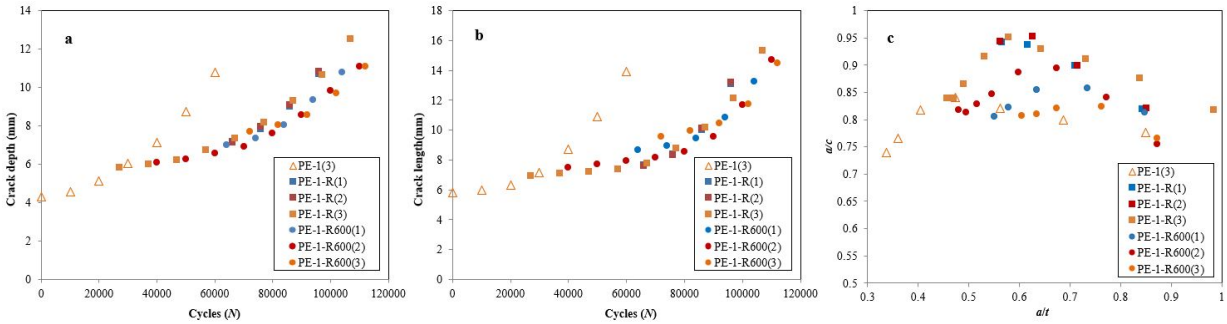

Figure 6.13. The experimental result comparison between 1000 mm bond length (PE-1-R) and 600 mm bond length (PE-1-R600) method: a) crack growth along depth direction; b) crack growth along length direction; c) aspect ratio variation: a/c versus a/t curves

When using composite materials to enhance the strength and stiffness of intact steel pipes, an effective bond length exists: once the bond length has reached a certain value, the effectiveness increases minimal when increasing of the bond length [27]. In this sub-section, crack growth behaviour of the composite reinforced steel pipes by using different bond length were discussed and analysed. Besides the default length which is 1,000 mm, the less bond length of 600 mm is applied. Figure 6.13 illustrates that there is no evident difference of the crack growth between the specimens using the bond lengths of 600 mm and 1,000 mm. This is further illustrated by the da/dN-a and dc/dN-c curves (see in Figure 6.22) that the FCGR along the depth/length direction of PE-1-R and PE-1-R600 are similar. Note that da/dN and dc/dN are the crack growth rate along the depth direction and the length direction respectively. In this sense, there might be an effective bond length for reinforcing the surface cracked steel pipes as well, which could be less than 600 mm.

- *Composite reinforcement on the cracked surface using different number of layers*

In Chapter 5, the SIF of internal surface cracked steel pipes reinforced with CRS by using different amount of bond layers has been discussed. The results indicated that the SIF has staged decreased when applying more layers of CFRP. In this sub-section, crack growth behaviour of the composite reinforced steel pipes by using different numbers of bond layer is discussed. Besides the default number of CFRP laminates which is four layers, eight layers is used by doubling the CFRP layers of PE-1-R (see specimens PE-1-R8 in Table 6.1). Figure 6.14a illustrates that the residual fatigue life prolonged dramatically when applying eight layers of CFRP. Starting from 25,000 cycles when a is around 5.8 mm, PE-1-R prolonged the residual fatigue life from 65,000 to 110,000 cycles of 110%, while the PE-1-R8 prolonged the residual fatigue life further to 150,000 cycles, of around 280%. Figure 6.14b shows that before the half crack length c reached around 8.0 mm, the increments of crack length of specimens PE-1-R8 are minimal, while the final crack lengths are similar with the specimens of PE-1-R. The aspect ratio variation of PE-1-R8 specimens did not have an evident difference with the PE-1-R specimens, as shown in Figure 6.14c.

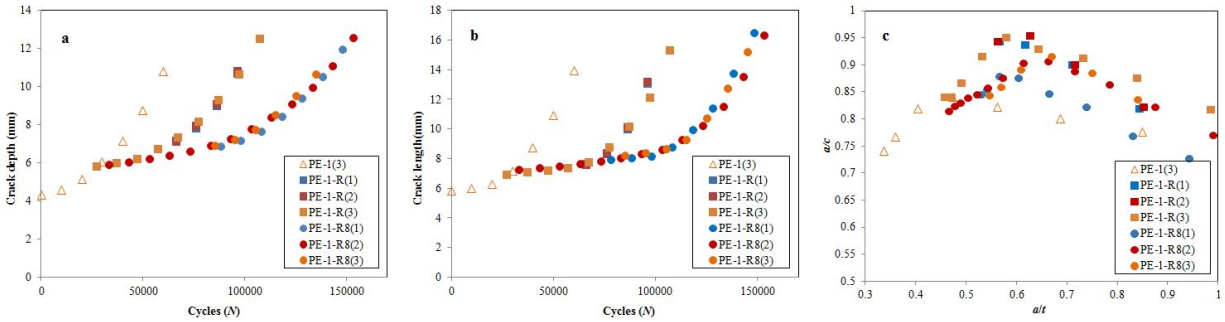

Figure 6.14. The experimental result comparison between using four layers of CFRP (PE-1-R) and eight layers of CFRP (PE-1-R8): a) crack growth along depth direction; b) crack growth along length direction; c) aspect ratio variation: a/c versus a/t curves

- *Composite reinforcement on the cracked surface using different wrapping orientation*

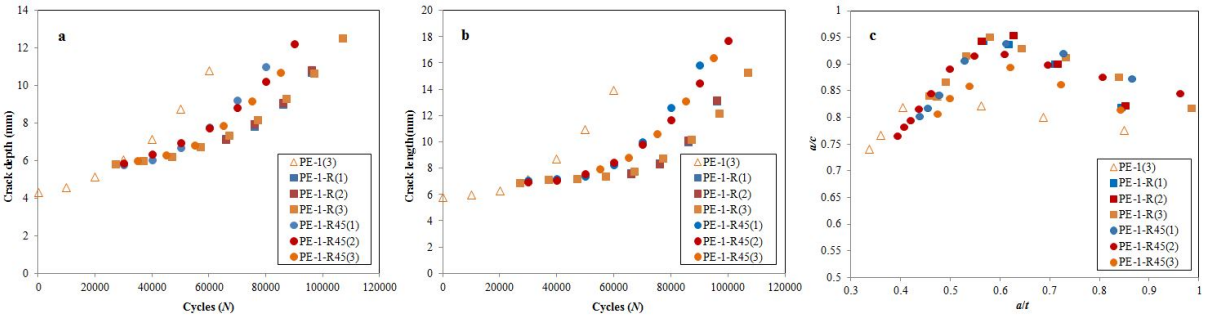

Figure 6.15. The experimental result comparison between using L-L-L-H CFRP wrapping (PE-1-R) and inversely diagonal wrapping (PE-1-R45) method: a) crack growth along depth direction; b) crack growth along length direction; c) aspect ratio variation: a/c versus a/t curves

In light of the practical situation of applying CRS to repair the surface cracked offshore steel pipes, that the wrapping construction will be taking place under water, the longitudinal wrapping in some cases might be difficult to be implemented. In this sub-section, the default wrapping pattern 'L-L-L-H' is compared with an inversely diagonal wrapping pattern (see in Figure 6.3). Figure 6.15a and Figure 6.15b illustrates that the inversely diagonal wrapping pattern performed less effective than the 'L-L-L-H' wrapping pattern, which prolonged the residual fatigue life of around 66.7%. Figure 6.15c shows that there is no evident difference of the aspect ratio variation between the PE-1-R and PE-1-R45 specimens.

6.1.3.3. Strain data

Figure 6.16 shows the strain data recorded by G1 and G2 gauges for using different schemes to reinforce the first type of crack at the beginning stage (Beg.), middle stage (Mid.) and the last stage (Las.). It is clearly shown that there is no evident difference of the strain results among the beginning, middle, and the last stage for all specimens. The maximum strain value of G1 for PE-1-R(1), PE-1-R8(1) and PE-1-R45(1) are all around 1300 με, while the maximum strain for PE-1-R45(1) is around 1120 με, as shown in Figure 6.17. The possible reason is that PE-1-R600 has a shorter bond length, the load cells therefore contacted with the steel substrate rather than the CFRP laminates (as shown in Figure 6.18), thus the stress were transferred from the steel pipes to the CFRP laminates, resulting in smaller strain values. The

strain value of PE-1-R8(1) is slightly higher than the PE-1-R(1), owing to the larger external diameter by the doubled layers of CFRP laminates.

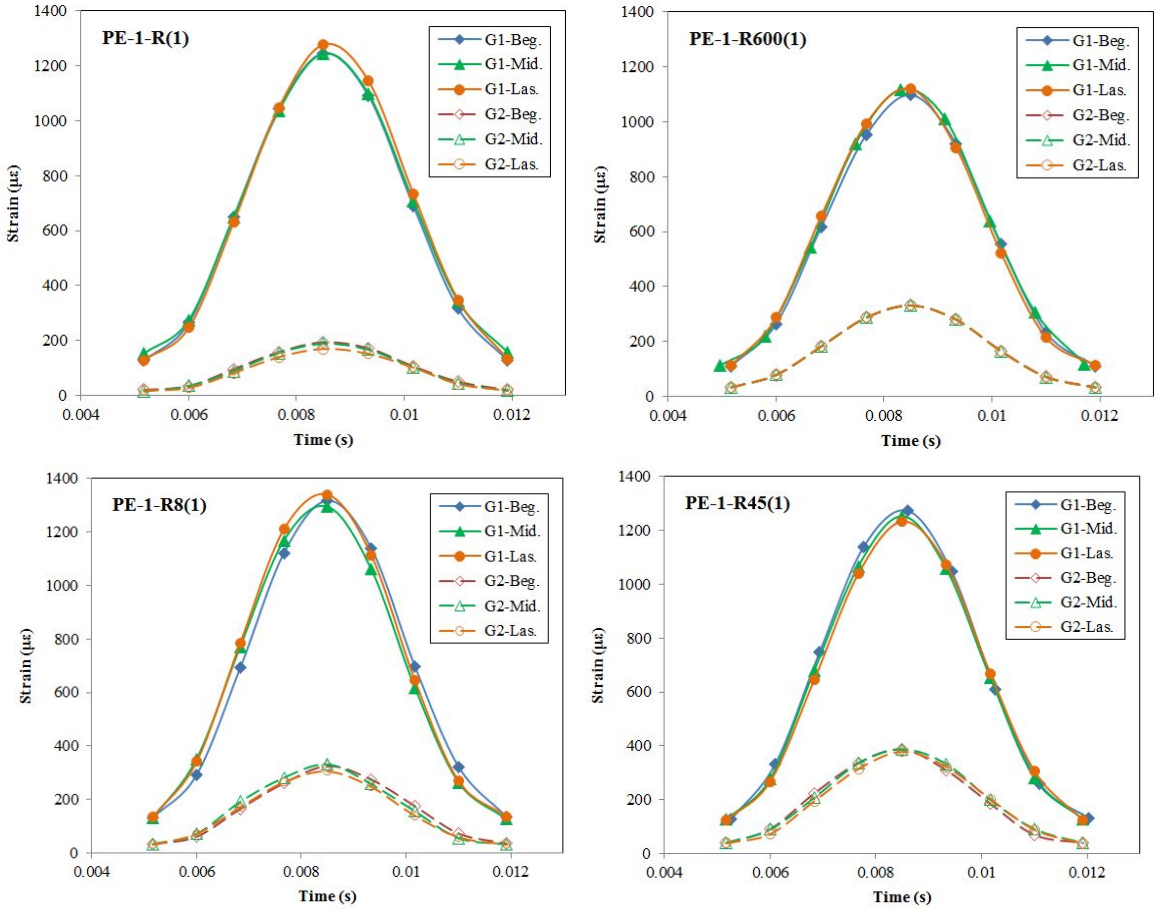

Figure 6.16. The strain data of using different scheme to reinforce the type one crack

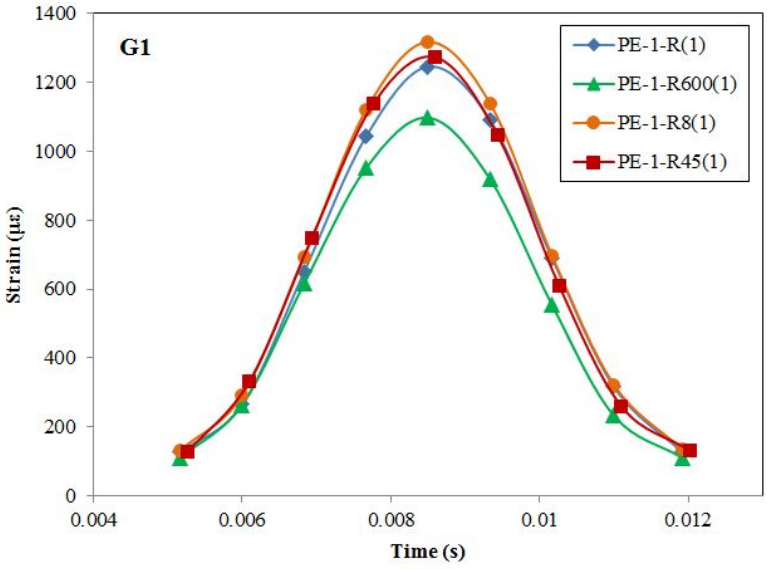

Figure 6.17. The strain data at the beginning of each test of using different schemes to reinforce the type one crack

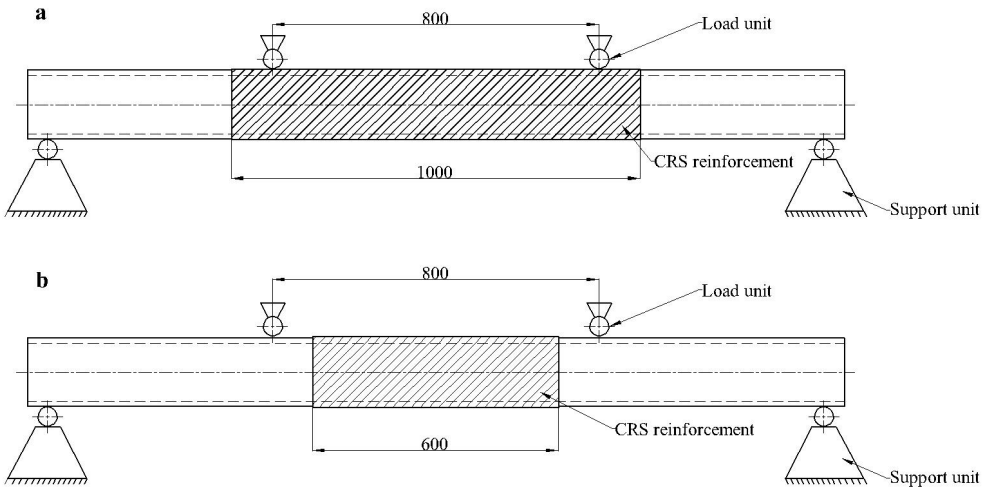

Figure 6.18. Loading position of specimens using different bond length: a) PE-1-R and b) PE-1-R600

6.1.3.4. Displacement of the specimens

Figure 6.19 shows the load-displacement response of the composite reinforced specimens of using different reinforcement schemes, which clearly illustrates that the displacement response at the beginning stage (Beg.), the middle stage (Mid.), and the last stage (Las.) remained identical.

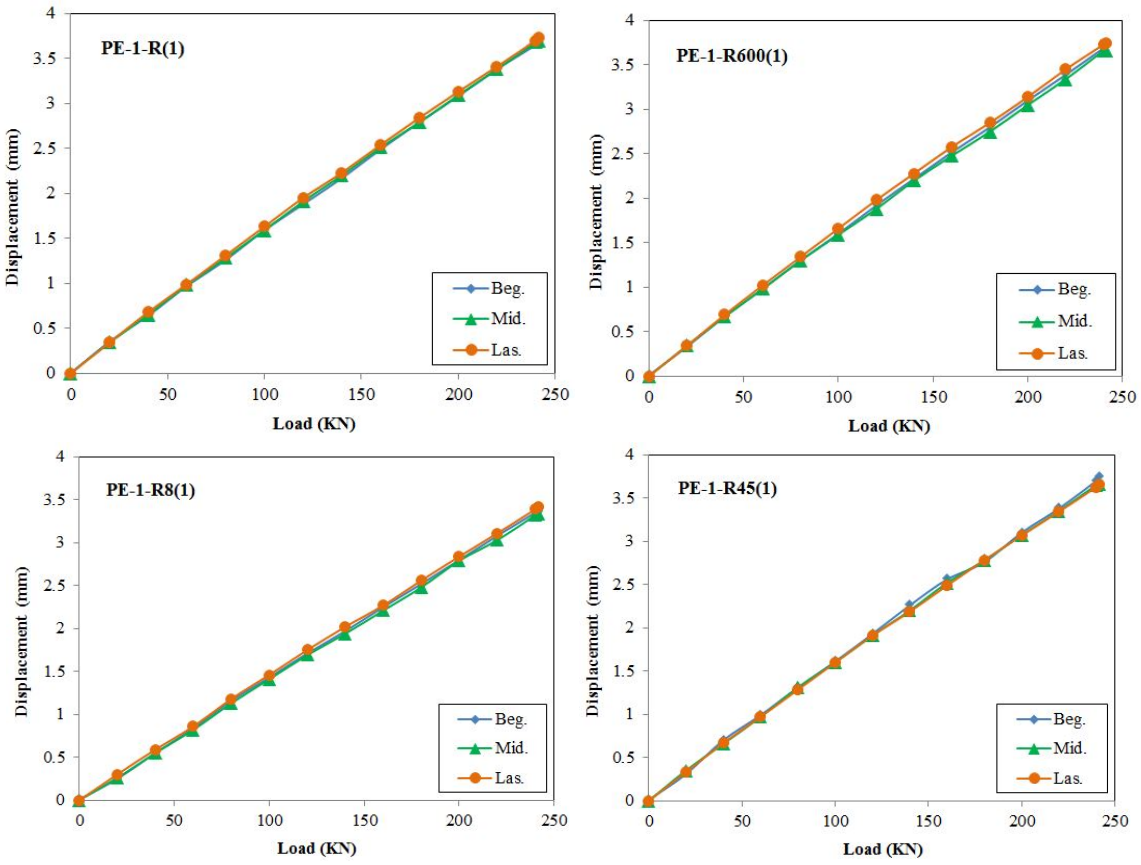

Figure 6.19. The displacement data at point C (mid-span displacement) subjected to load from 0 to 241.54 KN

The results indicate that the strength of the composite reinforced pipes was insensitive to the growth of the surface crack. The comparison of the load-displacement response of different specimens was shown in Figure 6.20. The deflection at point C of PE-1-R(1) has decreased by 4.7%, from 3.87 mm to 3.69 mm. PE-1-R45(1) has the largest deflection, of 3.82 mm, which is slightly larger than PE-1-R(1) of 3.69 mm and PE-1-R600(1) of 3.72 mm. Specifically, the deflection of PE-1-R8(1), which is 3.36 mm, is dramatically smaller than the rest of the specimens – 13.18% smaller than the unreinforced specimen PE-1(1) and 8.94% smaller than PE-1-R(1). Therefore, increasing the amount of composite layers of CFRP had effectively increased the stiffness of the cracked steel pipe.

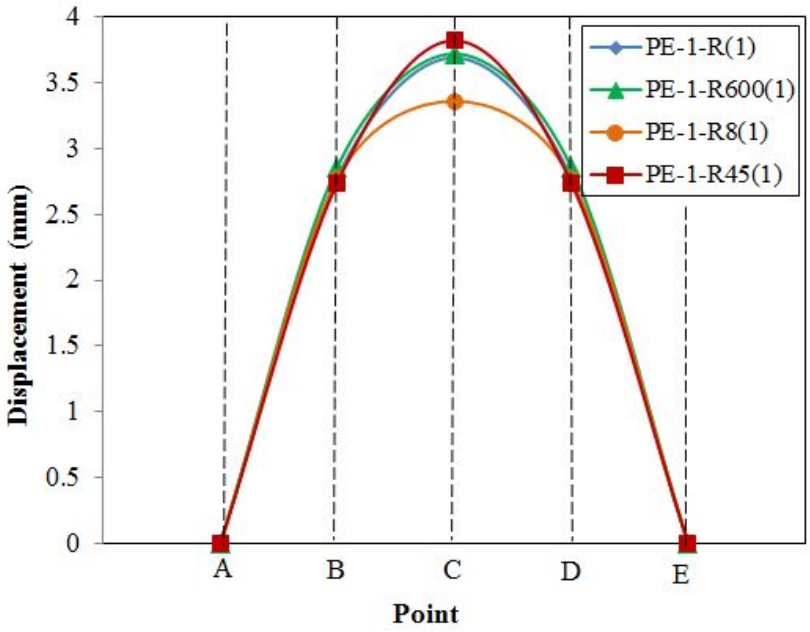

Figure 6.20. The displacement data when reaching the amplitude of the fatigue load (241.54 kN)

6.1.4. Summary of using different reinforcing schemes

In this section, the results in terms of the crack growth, the strain on the external CFRP laminate adjacent to the cracked area, and the load-displacement response are presented and analysed. Figure 6.21 summaries the effectiveness of using different reinforcement schemes on the surface crack growth. It shows that there is no evident difference between the specimens of PE-1-R(3) and PE-1-R600(2). Using the inversely diagnose wrapping method is less efficient, while applying eight layers of CFRP laminates preforms the best among the reinforcement methods.

Figure 6.22 further displayed the performance of using different reinforcement methods by the $da/dN - \Delta K_a$ and $dc/dN - \Delta K_c$ curves in Figure 6.22. Note that ΔK_a and ΔK_c are the range of the SIF of the deepest point and the surface point along the surface crack front respectively, which are calculated by the analytical method proposed in Chapter 5, assuming the surface cracks were not reinforced with CRS. Along the depth direction, PE-1-R(3) and PE-1-R600(2) decreased the FCGR along the depth direction approximately 8.3×10^{-5}

mm/cycle, while PE-1-R45(2) decreased FCGR around 6.7×10^{-5} mm/cycle, PE-1-R8(2) have significantly reduced the FCGR of 1.22×10^{-4} mm/cycle. The decrease of crack growth along the length is more evident than along the depth direction (see in Figure 6.22b), resulting in a shorter crack length when the crack penetrating the pipe wall, illustrated by the larger aspect ratios of the composite reinforced specimens (see in Figure 6.21c).

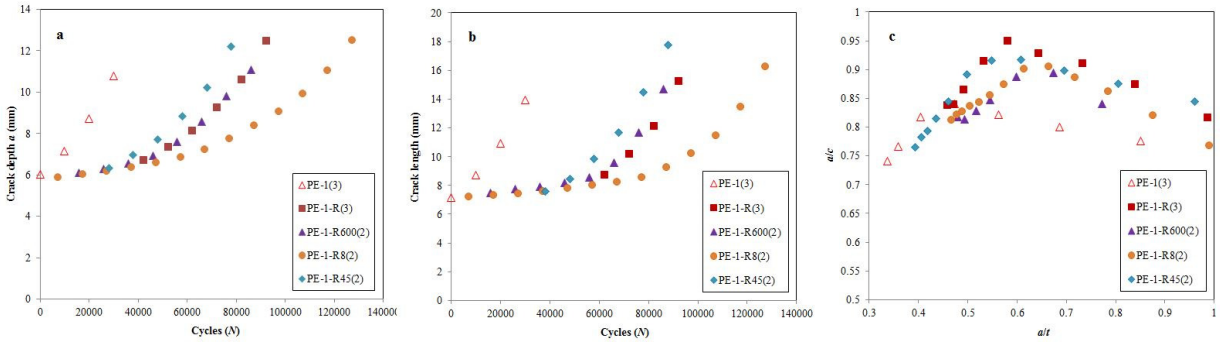

Figure 6.21. The experimental result comparison of using different reinforcement schemes

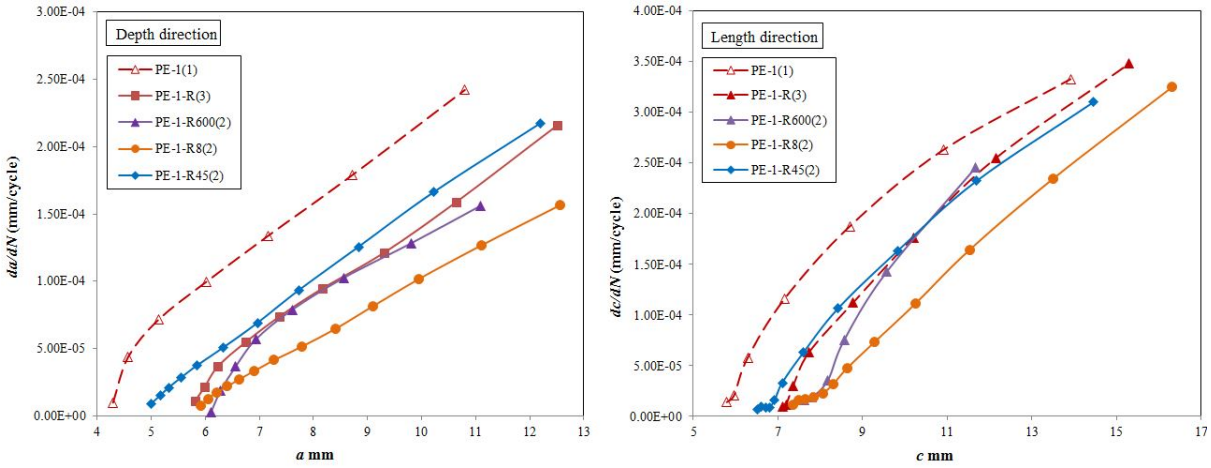

Figure 6.22. The experimental *result of FCGR comparison of using different reinforcement schemes*

The results also indicate that the strain and the displacement were insensitive to the surface crack growth. In addition, the load-displacement response of the specimens had a similar pattern with the crack growth reduction response: 1) the specimens of PE-1-R and PE-1-R600 had minimal difference in the crack growth rate, so did the load-displacement response; 2) the specimens of PE-1-R45 had the largest displacement when the load reached the amplitude, the FCGR of PE-1-R45 specimens were the largest as well; 3) the specimens of PE-1-R8 had significantly reduced the FCGR, so did the reinforcement of using eight layers of CFRP on decreasing the vertical deformation.

6.2 Numerical investigation on external surface cracked steel pipes reinforced with CRS

The numerical investigation is conducted to further analyse the composite reinforcement on surface cracked steel pipes. In this section, a three-dimensional FE model is developed to calculate the SIF along the surface crack front reinforced with CRS. Then the FE model is validated by the experimental results. Afterwards, on account of the validated FE model, a parametric study is developed, in order to guide the optimization design of composite reinforcement accounting for multiple influential parameters.

6.2.1 FE model

In this sub-section, the FE model of external surface cracked metallic pipe reinforced with CRS subjected to bending was developed. The configuration of the model and boundary condition of the four-point bending confirms to the test specimens and experimental set-up.

6.2.1.1 Materials

Consistent to the experimental study, the same four materials have been used for the specimens: steel substrate, GFRP, CFRP, and adhesive. The FE models of composite reinforced surface cracked pipe are conforming to the test specimens as well. The adhesive layer adopts the resin epoxy. In addition, a cohesive zone model is incorporated into the adhesive layer to simulate the interfacial bond condition, using the bi-linear traction-separation law, as shown in Figure 4.20. The interfacial properties calculated by Eqs. (4.1-4.5) are listed in Table 6.2. The interfacial stiffness starts to degrade when the value of the peeling stress exceeds τ_0. The degree of the degradation is represented by the SDEG value from 0 to 1, and debonding failure happens when SDEG reaches 1.

Table 6.2 Properties of traction-separation model

E (Pa)	T (Pa)	G (Pa)	Nu	τ_0 (MPa)	δ_0 (mm)	δ (mm)	K (MPa/mm)	G_c (N/mm)
2.8×10^9	70×10^6	1.4×10^9	0.35	56	0.008	0.134	7000	3.75

6.2.1.2 Modelling strategy

The FE modelling and analysis are conducted in ABAQUS 2019 [154]. The FE model and its global meshing condition is shown in Figure 6.23a. The size of the model conforms to the test specimens in the previous experimental study. The length, diameter and thickness of the steel pipe are 2000 mm, 168.3 mm, and 12.7 mm respectively. The thickness of each composite layer is 0.35 mm, and the thickness of the adhesive is 0.2 mm. A semi-elliptical surface crack [155] is modelled at the mid-button, as shown in Figure 6.23b of a 1/4 crack model, orienting circumferentially on the X-Y plane. A bending moment of 6.0385×10^7 kN · m is applied on the pipe, which is identical to the bending moment of experimental study by applying the four-point bending set-up.

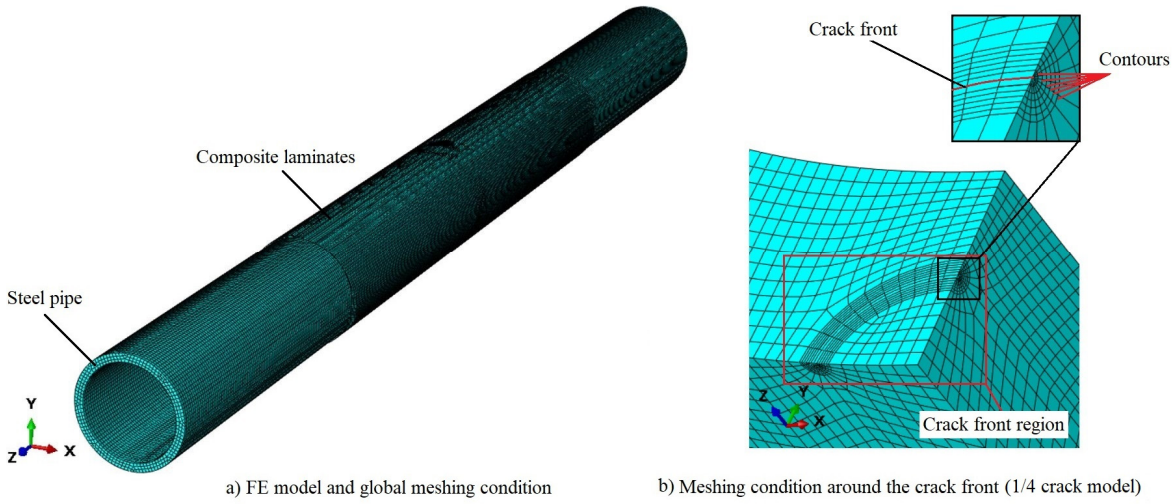

Figure 6.23. The FE model and the meshing condition of the global (a), and around the crack front (b)

Table 6.3. The configurations of the FE models

FE model	Crack size (mm)		CFRP wrapping scheme	Wrapping length
	Crack depth *a*	Crack length *c*		
PE-1	4.29	5.795	\	\
PE-2	5.34	6.53	\	\
PE-3	5.34	5.78	\	\
PE-1-R	5.98	7.12	L-L-L-H	1,000
PE-2-R	5.24	6.13	L-L-L-H	1,000
PE-3-R	5.92	6.235	L-L-L-H	1,000
PE-1-R600	6.1	7.465	L-L-L-H	600
PE-1-R8	5.92	7.28	L-L-L-H-L-L-L-H	1,000
PE-1-R45	4.99	6.525	Inversely diagonal	1,000

The FE model is composed by the steel pipe, the composite laminates, and the adhesive layer. The composite laminates, including one layer of GFRP and several layers of CFRP, are modelled as one part. While each laminate remains its own material properties and orientation. One layer of adhesive is modelled between the CFRP laminates and the steel substrate through the cohesive zone modelling. The steel pipe excludes the crack front region, as well as the composite laminates, apply the 20-node quadratic brick element C3D20R, while the crack front area adopts the 15-node quadratic triangular prism element C3D15. The adhesive layer applies the 8-node cohesive element COH3D8. Different meshing methods are adopted to ensure a robust and accuracy evaluation. The FE model excluded the crack front region and the adhesive layer adopt the hexahedron element by the structural meshing method. While the crack front region and the adhesive layer applies the sweep meshing methods, using wedge element and hexahedron element, respectively. Under the premise of accuracy evaluation, different element sizes are assigned in different areas of the FE model to reduce the computation time. The size of the wedged elements in the crack front region is controlled by the six concentric contours and 24 divisions on each of those, as indicated in Figure 6.23b. The diameter of the external contour is 1.0 mm, and the crack front has been divided into 22 pieces. The size of the area in the steel pipe adjected to the crack front area, as well as the

adhesive layer and the composite laminates are set as 1.0 mm, while the size of the pipe away from the crack front area is set as 5.0 mm. Here, we use three different sizes of surface cracks and four different reinforcement methods, for the validation purpose. The specimen configurations are listed in Table 6.3.

6.2.2 Results and discussion

6.2.2.1 Interfacial bond condition

Three sizes of surface cracks including a small (a = 5.98 mm, c = 7.12 mm), a medium (a = 8.16 mm, c = 8.78 mm), and a large surface crack (a = 10.64 mm, c = 12.15 mm) are modelled, to identify the bond condition during different cracking stages. Note the sizes of the surface crack are extracted from the test specimen PE-1-R(3). The results indicate that the stiffness degradation only occurs at the interface of the FE model with the large surface crack.

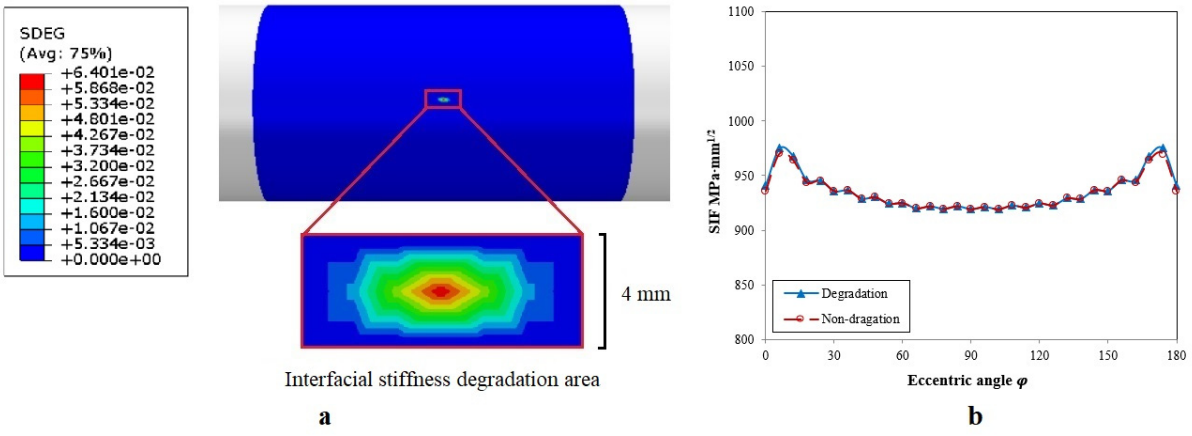

Figure 6.24. The results of the interfacial bond condition when a = 10.64 mm and c = 12.15 mm (a), and the SIFs along the surface crack front (b)

Figure 6.24a shows the area and the degree of the stiffness degradation at the interface of the FE model when a = 10.64 mm and c = 12.15 mm. The area of the stiffness degradation is small comparing to the 24.30 mm long surface crack. In addition, the maximum SDEG value only reaches 0.064, indicating the interface still provides a considerable bond between the composite and the steel substrate.

6.2.2.2 SIF results

The results of SIFs along the crack front of two models with a large surface crack are shown in Figure 6.24b. One more has considered the stiffness degradation, while the other one hasn't. The results indicate that even if the surface crack propagates to a large size, the effect of the stiffness degradation on the SIFs is insignificant, causing only about 2.5% raise of the SIF at the surface point, while causing no effect at the deepest point. Together with the consideration that the large crack is already at the very late stage of the cracking process, it is reasonable to ignore the effect of the interfacial stiffness degradation on the surface crack growth.

Further on, the SIF results of the unreinforced model and the reinforced model using the default reinforcing method are shown in Figure 6.25, indicating the different effective of composite reinforcement on different crack sizes: composite reinforcement decreases the SIFs of a small crack at the deepest point and the surface point of 18.37% and 27.32% respectively, while decreases 17.74% and 35.68% respectively for a large crack. Hence it indicated that: 1) composite reinforcement is more effective on the surface point than on the deepest point, which might be owing to the crack-bridging effect; 2) along with the crack propagation, the effectiveness of the composite reinforcement increases on the surface point while remain on the deepest point.

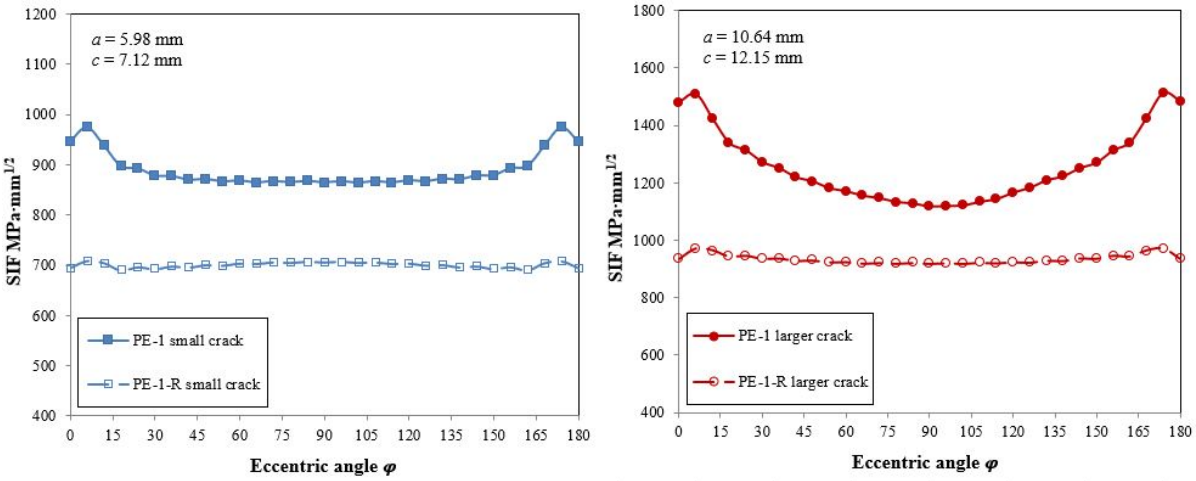

Figure 6.25. The SIF distributions along the crack front of a small crack (left) and a large crack (right)

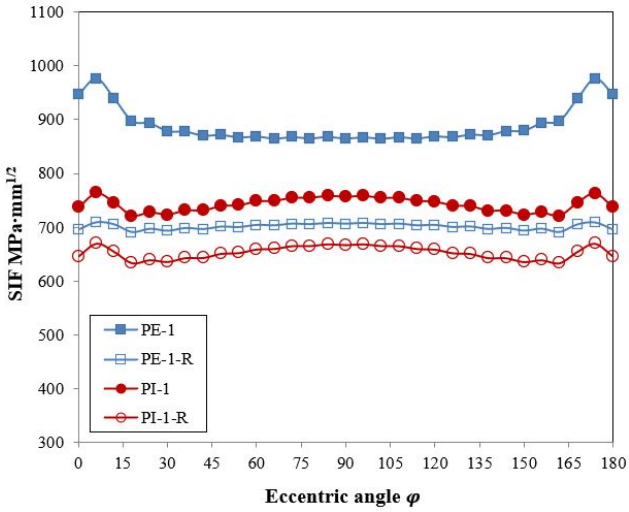

Figure 6.26. The comparison of the SIF results between the external surface crack and the internal surface crack reinforced with CRS

The effect of composite reinforcement on internal surface cracks in steel pipes has been investigated in Chapter 5. While its effect on external surface cracks is different from its effect on internal surface cracks. Figure 6.26 shows the SIF results of two surface cracks with the same crack size (a = 5.98 mm, c = 7.12 mm), of either on the external surface (PE-1-R) or the internal surface (PI-1-R) of a steel pipe. The composite reinforcement has evenly

decreased the SIFs along the internal surface crack front of around 12%. While the reinforcement performs significantly more efficient on the external surface crack, decreasing the SIF at the deepest point and the surface point of 18.4% and 27.3% respectively. Particularly, the reinforcement performs more significantly on decreasing the SIF at the surface point.

6.2.3 Experimental validation

In this sub-section, the experimental results of surface crack growth and FE results are compared and analysed. First, the Paris' constants are calibrated on account of the experimental results. Then, the FE model is validated by the experimental results.

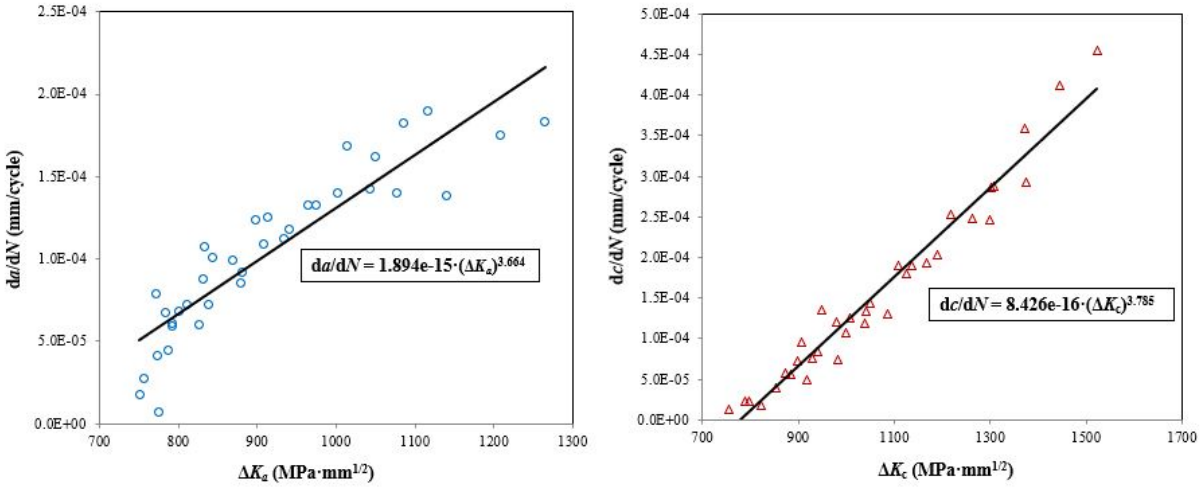

Figure 6.27. Evaluation of the Paris' constants (C and m) from da/dN versus ΔK_{Ia}, and dc/dN versus ΔK_{Ic}

The SIFs of the surface crack in the models without composite reinforcement are calculated by means of the validated FE model, then the surface crack growth rate along the depth direction and length direction are predicted by Eq. (3.2) and Eq. (3.3) in Chapter 3. In this chapter, the value of C and m are calibrated from the experimental results, as shown in Figure 6.27. It illustrated that the C for crack growth along the depth direction and the length direction are different, while the m is the same for crack growth along the two directions. Therefore C_a and C_c are used as the constants for the depth and length direction respectively, where C_a equals to 1.894×10^{-15} and C_c equals to 8.462×10^{-16}. The m_a equals to 3.664 and m_c equals to 3.785.

The SIF of the surface crack in the steel plate reinforced with CRS is calculated by means of the FEM. Then the crack growth rate is evaluated by using the Paris' law. Eventually the results of surface crack growth evaluated by the FE model and the Paris's law are compared with the experimental results. Hence, the FE model of evaluating the SIF is validated by the experimental results. The comparison between the FE results and the experimental results of surface crack growth are shown from Figures 6.28 to 6.33. The figures indicate that the FE results match well with the experimental results when using CRS to reinforce the cracked

surface of the steel plates, which means that the FE model can accurately evaluate the SIF of surface cracks reinforced with CRS. In addition, the results indicate that composite reinforcement has significantly decreased the surface crack growth and prolonged the fatigue life of specimens.

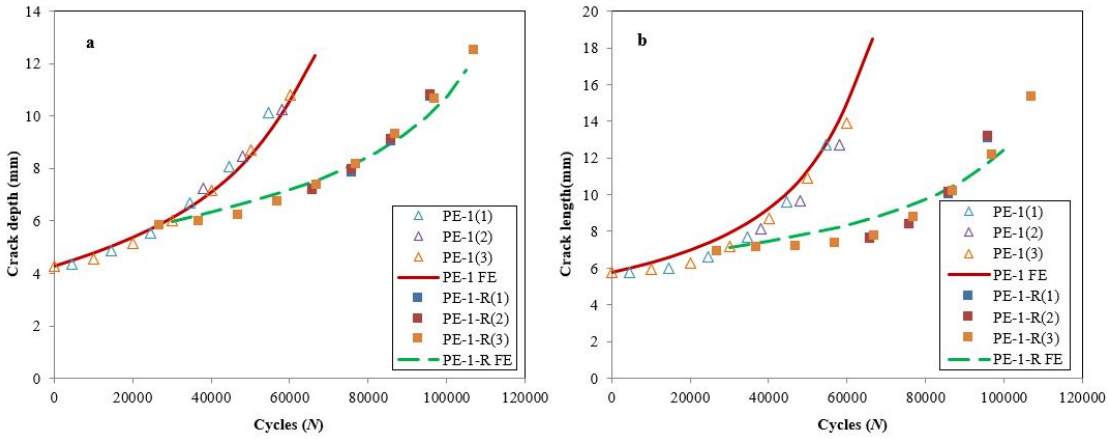

Figure 6.28. The comparison of FE results and experimental results on PE-1 and PE-1-R specimens

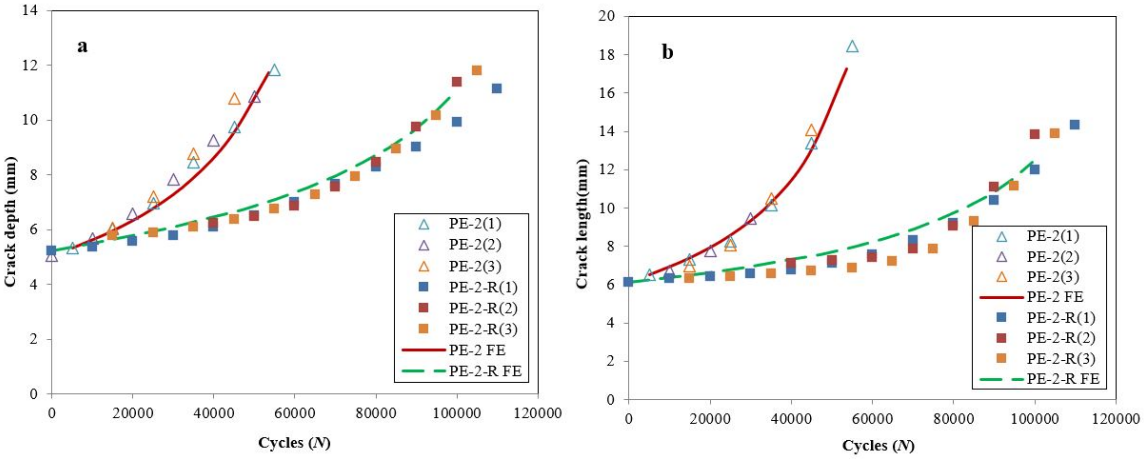

Figure 6.29. The comparison of FE results and experimental results on PE-2 and PE-2-R specimens

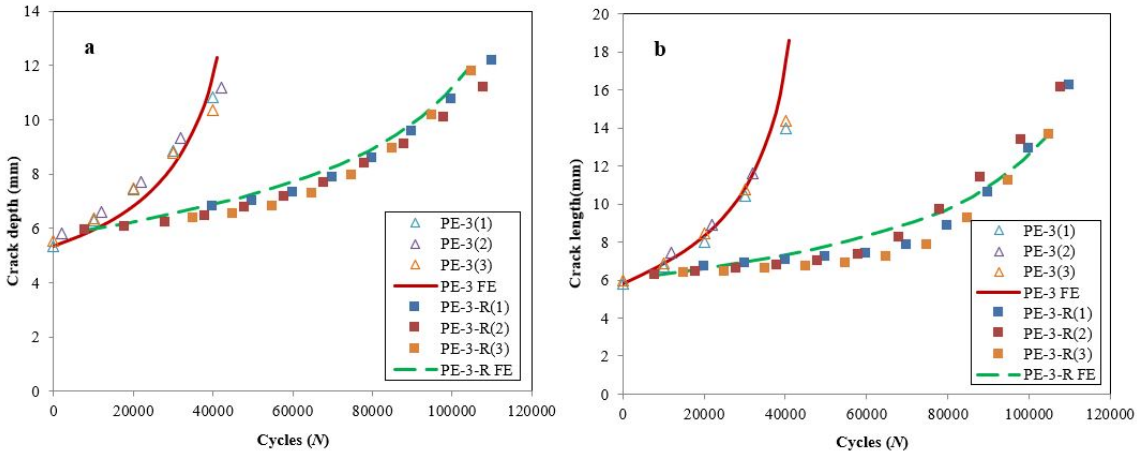

Figure 6.30. The comparison of FE results and experimental results on PE-3 and PE-3-R specimens

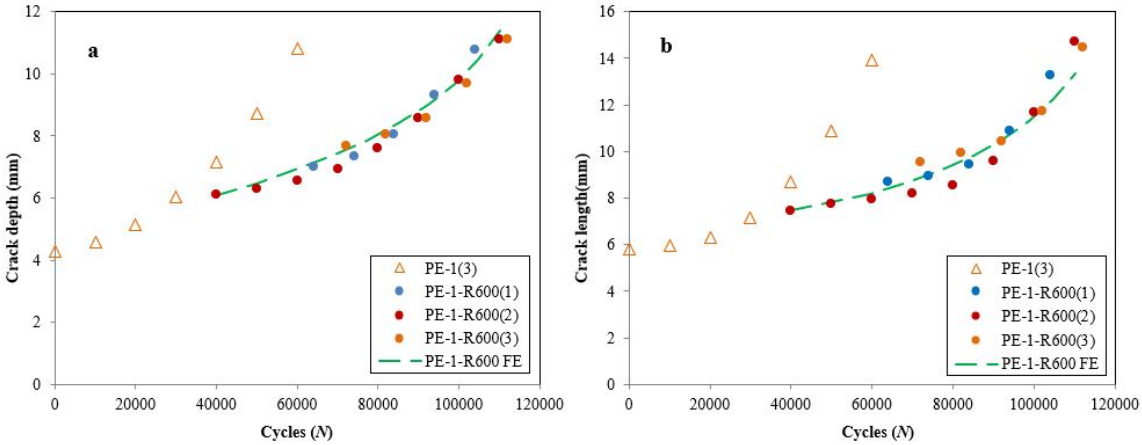

Figure 6.31. The comparison of FE results and experimental results on PE-1 and PE-1-R600 specimens

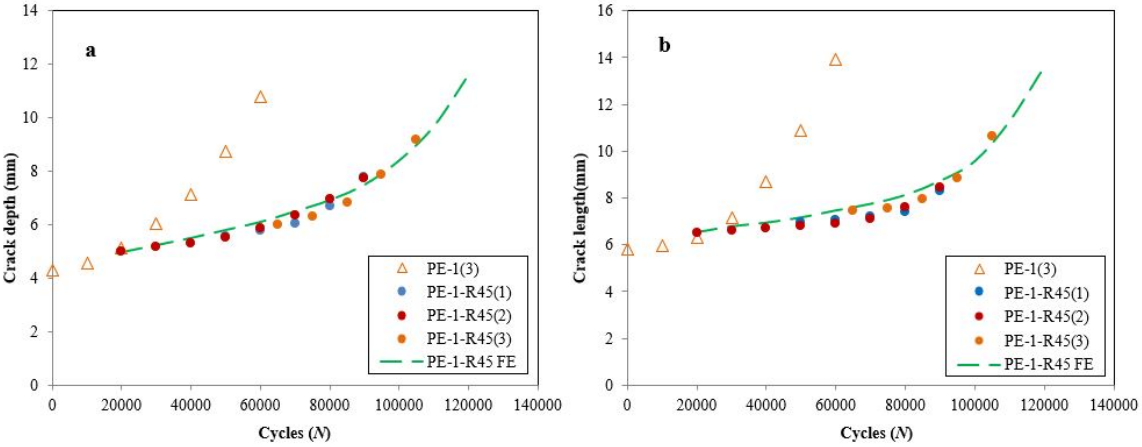

Figure 6.32. The comparison of FE results and experimental results on PE-1 and PE-1-R45 specimens

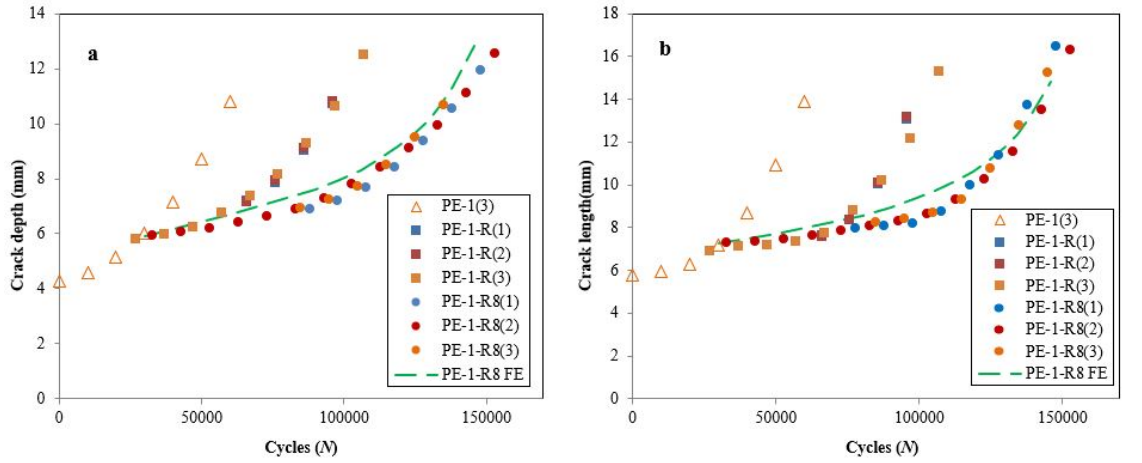

Figure 6.33. The comparison of FE results and experimental results on PE-1 and PE-1-R8 specimens

6.3 Parametric study

In Chapter 5, we investigated the influential parameters on internal surface cracked steel pipes reinforced with CRS. However, their direct effect on the external surface cracks is unclear. In this regard, the parametric study is conducted by means of the FE model, and their effects has been quantitatively analysed. The SIFs along the crack front of different models are calculated based on the crack size of a = 5.98 mm, c = 7.12 mm, which is the starting size of FE model 'PE-1-R'.

- Bond length of the CRS

The CRS bond length is one of the easiest parameters to be changed in practice which affects the budget and time-consuming of the project. In addition, it can significantly influence the reinforcement effectiveness. The main purpose of this sub-section is to find a sound and cost-effective bond length for practical usage. The bond length will be applied for further parametric studies as well.

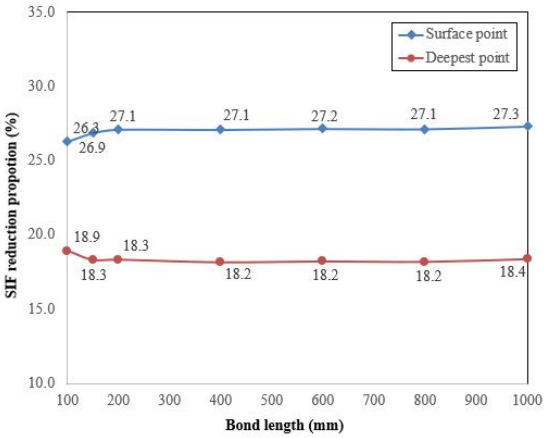

Figure 6.34. The SIF reduction results of the deepest point and the surface point with different bond length

Here, besides the 1000 mm bond length, we investigate another six ranges of bond length, namely 100 mm, 150 mm, 200 mm, 400 mm, 600 mm, and 800 mm. The results of the SIF reduction proportion of using different bond lengths is shown in Figure 6.34. It indicates that, similar to reinforcing the internal surface crack, there exists an optimum bond length. When the bond length is longer than 200 mm, the SIF becomes insensitive to the increase of the bond length. Thus 200 mm bond length is chosen as the optimum bond length in terms of the material and time cost.

- Numbers of bond layers

Changing the numbers of composite layer is another practical way to affect the budget, time-consuming and reinforcement effectiveness. In this sub-section, the influence of longitudinal composite layers by using six different ranges of longitudinal CFRP layers is analysed. Note that the reinforcement always applies an additional circumferential CFRP layer as the external

layer of the CRS. The CRS bond length of 150 mm is chosen based on the study of the bond length.

Figure 6.35 shows that the SIF reduction proportion has a positive correlation with the number of longitudinal bond layers, which is identical to the experimental results shown in Figure 6.33. While the relation between the numbers of bond layers and the SIF reduction proportion is not linear. With the increase of the bond layers, the increment of the SIF reduction decreases. This means the SIF may not decrease below the threshold value if only applying more number of bond layers. Nevertheless, adding the bond layer is a high effective method to improve the reinforcement effectiveness.

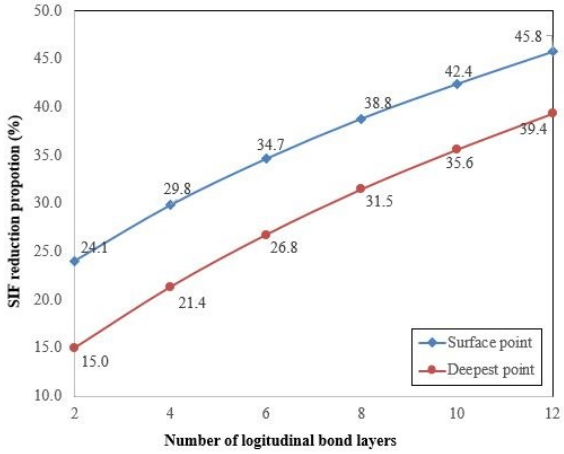

Figure 6.35. The SIF reduction results of the deepest point and the surface point with different number of bond layer

- CFRP tensile modulus

The material properties of CFRP have been rapidly developed thanks to the development of material technology. One of the most important material properties of CFRP is the tensile modulus. To date, the global market provides CFRP materials with different tensile modulus. In this section, besides the CFRP material used in Sections 2&3 which has a 230 GPa tensile modulus, another two different CFRP materials were investigated: a low tensile modulus CFRP of 150 GPa and a high tensile modulus CFRP of 552 GPa. Figure 6.36 shows that the SIF reduction proportion has a positive correlation with the CFRP tensile modulus. Therefore, high tensile modulus CFRP can be applied as an alternative of using more composite layers, in order to avoid adding excessive dead weight.

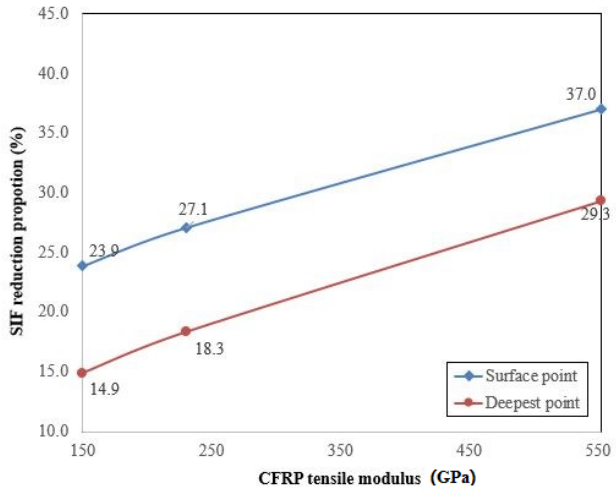

Figure 6.36. The SIF response of the FE models with different CFRP tensile modulus: a) the normalised SIF result along the crack front; b) the SIF reduction proportion of the deepest point and the surface point

- Adhesive thickness

The adhesive layer is the weakest layer in the reinforcement system. It acts as the intermediary between different layers of the composite laminates, particularly between the steel substrate and the first composite layer. The interfacial bond condition might be sensitive to the adhesive thickness. In this section, five different thicknesses ranging from 0.1 to 0.5 mm with a 0.1 mm interval are analysed.

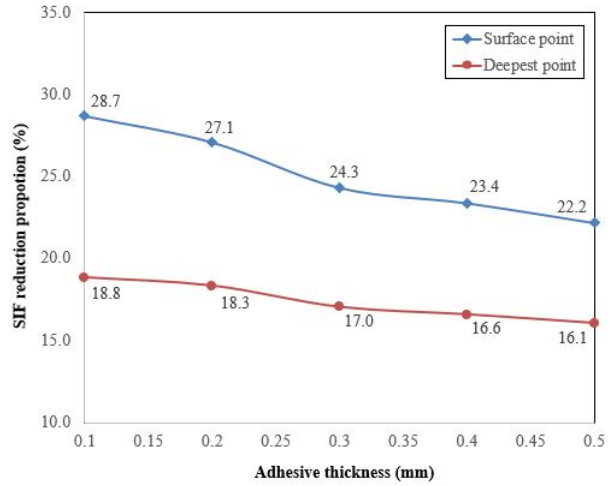

Figure 6.37. The SIF response of the FE models with different adhesive thickness: a) the normalised SIF result along the crack front; b) the SIF reduction proportion of the deepest point and the surface point

Fig. 6.37 shows that unlike reinforcing the internal surface cracks, the SIF reduction proportion of the external surface crack has a negative correlation with the adhesive thickness. In addition, the SIF of the surface point is more sensitive the deepest point. The results suggest when reinforcing the external surface crack using CRS, the thickness of the adhesive layer should be controlled relatively thin.

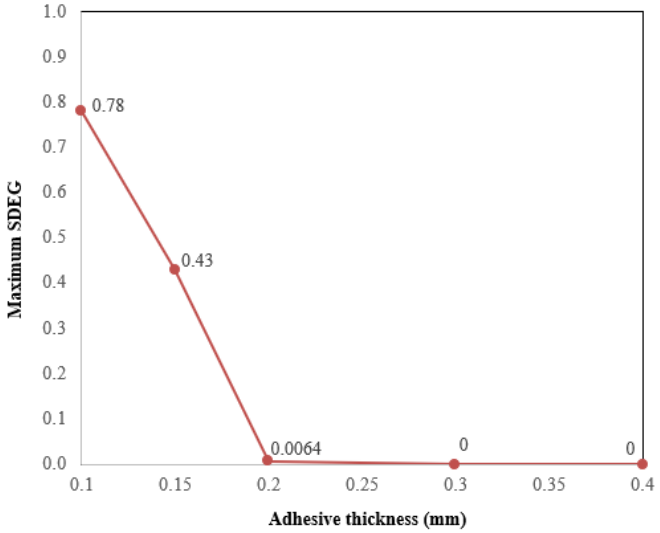

Figure 6.38. The interfacial stiffness degradation (SDEG) of the FRP-to-steel interface when using different adhesive think

However, as indicated in Fig. 6.38 of the maximum SDEG value, the adhesive thickness has a significant influence on the stiffness degradation at the FRP-to-steel interface. In addition to the five sets of the thickness, 0.15 mm is added, while 0.5 mm is excluded because the SDEG value when thickness equals to 0.4 mm has already become 0. The maximum SDEG value reaches 0.78 when the adhesive thickness is 0.1 mm. It decreases to 0.43 when using 0.2 mm adhesive thickness, and continuously decreases with the increasing of the adhesive thickness. Therefore, in practical situations, selecting the adhesive thickness should reach a compromise between the reinforcement effectiveness and the bond condition. In the case within this research, the adhesive thickness is chosen as 0.2 mm.

- Crack aspect ratio

In this sub-section, the SIF response of composite reinforced external surface cracks with six different aspect ratios ranging from 0.25 to 2.0 are analysed. The detailed crack sizes of each FE model, as well as the SIF reduction results of the deepest point and the surface point respectively are shown in Table 6.4. It illustrates that within the increase of the crack aspect ratio, the SIF reduction of the deepest point is decreasing. While there is no clear trend of the SIF response along the surface point. In light of the models from No.2 to No.4 which have the same crack length, the SIF reduction proportion increases within the increasing of the surface depth. From the model No. 4 to No.6 which have the same crack depth, the SIF reduction proportion also has a positive correlation with the crack length. Generally speaking, since the crack growth along the depth direction has a special significance in terms of preventing the pipe leakage, the composite reinforcement is more efficient on surface cracks with smaller aspect ratio.

Table 6.4. Specimen configuration of steel plates with different aspect ratios

Model No.	*a* (mm)	*c* (mm)	*a*/*c*	SIF reduction of the deepest point	SIF reduction of the surface point
1	3.0	12.0	0.25	21.9%	20.8%
2	3.0	6.0	0.5	18.4%	23.2%
3	4.5	6.0	0.75	17.8%	26.4%
4	6.0	6.0	1.0	16.9%	27.8%
5	6.0	4.5	1.25	14.8%	22.9%
6	6.0	3.0	2.0	12.3%	20.8%

- Dimension of the steel pipe

Eight different pipe dimensions with various *D*/*t* ratios of API 5L offshore steel pipes, conforming to the code [39] are analysed. Table 6.5 lists the configuration of the composite reinforced steel pipes with various diameter and wall thickness. Diameter of steel pipes ranging from 168.3 mm to 323.8 mm pipes are adopted with five different pipe wall thickness from 10.97 mm to 21.95 mm: five incremental pipe wall thickness has been discussed within the external diameter of 168.3 mm, while four incremental external diameter has been analysed within the pipe wall thickness of 12.7 mm. These pipe dimensions can represent the frequently used steel pipeline in the offshore industry.

Table 6.5. Specimen configuration of steel pipes with various dimensions, and the results of the SIF decrease

Model No.	*D* (mm)	*t* (mm)	*D*/*t*	SIF reduction of the deepest point	SIF reduction of the surface point
1	168.3	10.97	15.34	20.1%	29.5%
2	168.3	12.70	13.25	18.4%	27.3%
3	168.3	14.27	11.79	17.3%	26.0%
4	168.3	18.26	9.22	15.3%	23.8%
5	168.3	21.95	7.67	14.1%	22.6%
6	219.1	12.70	17.25	17.5%	28.2%
7	273.0	12.70	21.50	16.4%	25.3%
8	323.8	12.70	25.40	14.7%	24.6%

The results illustrates that within the same external diameter, the reinforcement effectiveness (represented by the SIF decrease percentage) decreases with the increasing of wall thickness. In light of the models from No. 2, and No. 6 to No.8, within the same wall thickness, the reinforcement effectiveness decreases with the increasing of pipe external diameter as well. Therefore, the composite reinforcement is less effective on offshore pipes with larger external diameter and thicker wall thickness. In such cases, high elastic modulus CFRP and more CFRP layers are suggested in order to achieve a satisfying decrease of crack growth rate.

6.4 An analytical method of evaluating the SIF of the external surface cracked metallic pipes reinforced with CRS

In this section, an analytical method of evaluating the SIF of the external surface cracks in metallic pipes reinforced with CRS is proposed.

6.4.1. The analytical method of evaluating the SIF at the deepest point of the external surface crack

Similar to the composite reinforcement on internal surface cracked pipes, the key influential parameters are the number of bond layers and the composite tensile modulus, as indicated in Section 6.3. In addition, based on the comparison results of the composite reinforcement on the internal surface cracked pipe and the external surface cracked pipes, the effectiveness of decreasing the SIF at the deepest point of the crack are equal of both the internal surface crack and the external surface crack. That means the crack-bridging effect has a negligible influence on the SIF at the deepest point of the external surface crack. Therefore, the SIF at the deepest point ($\varphi = \pi/2$) can be evaluated by incorporating the analytical method—Eq. (3.7) proposed in Chapter 3, as well as the bending correction factor of Eq. (3.9) and the geometry correction factor of Eq. (3.24).

6.4.2. Evaluating the SIF at the surface point of the external surface crack

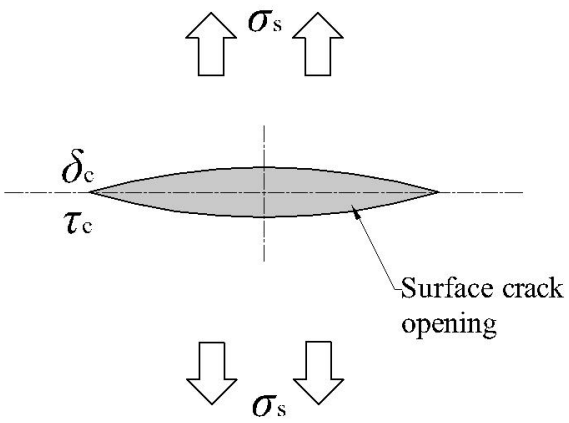

Figure 6.42. The crack-bridging effect on the external surface crack

Unlike the deepest point of the surface crack, the cracked surface directly contact with the CRS laminates. As a result, the surface crack growth along the length direction decreases more efficiently than along the depth direction, owing to the crack-bridging effect. In this sub-section, a simple analytical model is proposed to evaluate the SIF at the surface point of the external surface crack.

As shown in Figure 6.42, the crack is constrained by the crack-bridging effect. Hence, a local stress σ_c is assumed to directly applied on the crack tip (at the surface point). In such

situation, since the local displacement at the crack tip is defined as the COD, which can be calculated under the plane stress condition [156], as

$$\delta_c = \frac{4K_{Ic}^2}{\pi \cdot E \cdot \sigma_y}. \tag{6.1}$$

where σ_y is the yield strength of the steel. Then the traction stress around the crack tip is calculate using the bilinear traction-separation law indicating in Figure 4.20 in Chapter 4, as

$$\tau_c = \begin{cases} k \cdot \delta_c & (\delta_c \le \delta_0) \\ -\frac{\tau_0}{\delta - \delta_0} \cdot (\delta_c - \delta_0) + \tau_0 & (\delta_0 < \delta_c < \delta). \\ 0 & (\delta_c \ge \delta) \end{cases} \tag{6.2}$$

Since the crack-bridging effect promote the decreasing of the SIF at the surface point, τ_c is incorporating into the evaluation method of Eq. (3.7), where the overall stress is calculated as

$$\sigma_b = \sigma_s - \tau_c. \tag{6.3}$$

Thus,

$$K_{Ic} = G \cdot (\sigma_s - \tau_c) \cdot \sqrt{\pi \frac{a}{Q}} \cdot F. \tag{6.4}$$

By Eq. (6.4), K_{Ic} at the surface point therefore can be calculated. Since K_{Ic} exists in the right-hand side of the equation as well, in order to simply the calculation, the value of K_{Ic} calculated using the previous crack size is used to evaluate the τ_c in Eq. (6.4).

6.4.3. Validation of the analytical method

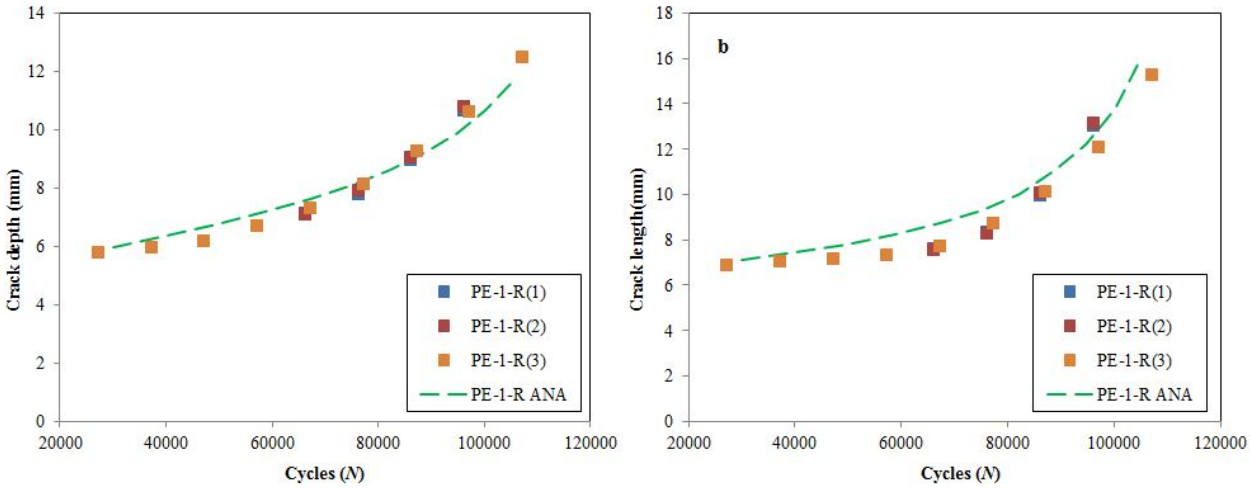

Figure 6.43. Validation of the analytical method on PE-1-R

In this sub-section, the analytical method is validated by the experimental results of PE-1-R and PE-1-R8 specimens, as shown in Figure 6.43 and Figure 6.44. The analytical prediction agrees well with the experimental results, indicating the analytical method can rationally

predict the crack growth of external surface crack in metallic pipes subjected to cyclic bending. Based on the superposition principle, the analytical method is regarded as an appropriate method in tensile loading condition as well.

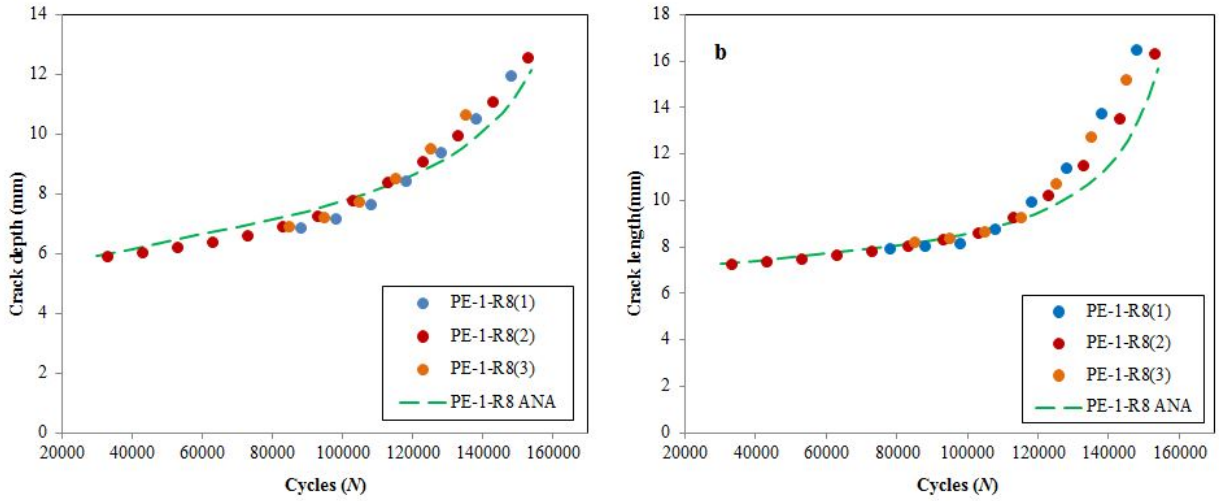

Figure 6.44. Validation of the analytical method on PE-1-R8

6.5 Conclusions

In this chapter, composite reinforcement on circumferential surface cracked steel pipe subjected to bending was investigated, by means of experimental, numerical and analytical approaches, respectively. First, nine groups of 27 specimens were tested. The effectiveness of composite reinforcement on surface cracks with different aspect ratio, different reinforcement schemes in terms of bond length, numbers of bond layer, wrapping orientation has been discussed. Then a three-dimensional FE model was developed to evaluate the SIF of the composite reinforced external surface crack, which is thereafter validated by the experimental results. After that, based on the FEM, a parametric study is conducted to determine the key influential and their influence on the SIF. Finally, an analytical method is proposed to evaluate the SIF at the deepest point and the surface point of the composite reinforced external surface crack. The conclusions of this chapter can be drawn:

- The CRS has significantly decreased the FCGR of the surface crack and thus prolonged the residual fatigue life. In the experimental study, under D/t = 13.25 and L_c/L = 0.5, applying the default reinforcing scheme reduced the FCGR along the depth direction of 8.3×10^{-5} mm/cycle, and prolonged the residual fatigue life of around 110%, while using eight layers of CFRP laminate have maximally decreased the FCGR along the depth direction of 1.22×10^{-4} mm/cycle, thus it prolonged the residual fatigue life of approximately 280%.
- Different from reinforcing internal surface cracks in steel pipes subjected to bending, the CRS performed more efficiently on reducing the FCGR along the length direction than along the depth direction, resulting in the increase of the preferred aspect ratio, owing to the crack-bridging effect.

- The analysis on the FRP-to-steel interfacial bond condition indicates the interfacial stiffness degradation only happened at a later stage of the cracking process. Its minor influence on the SIF suggests that it is reasonable to ignore the effect on the surface crack growth.
- The parametric study indicates the SIF is sensitive to the influential parameters including the number of bond layers, and the CFRP tensile modulus. While the SIF is less sensitive to the bond length and the adhesive thickness. The interfacial stiffness degradation is sensitive to the adhesive thickness. Thus, an adequate minimum thickness is necessary to prevent potential interfacial bond failures.
- An analytical method has been proposed by considering the overall deflection of the pipe owing to the CRS and the crack-bridging effect on the crack opening surface. The validation indicated that it can rationally predict the crack growth of external surface cracks in metallic pipes reinforced with CRS.

Chapter 7 Conclusions

This dissertation proposes a protocol of using CRS to repair surface cracked offshore metallic pipe. The main purpose is to understand the mechanism of composite reinforcement, in order to develop/improve the associated CRS standards. The proposed reinforcement method enables to decrease the crack growth rate and prolong the residual fatigue life of the cracked pipes effectively. The developed FE and analytical methods are able to evaluate the SIF of the surface crack adequately, which can be used for CRS design and surface crack growth evaluation in the offshore piping industry. The main conclusions and answers to research questions are addressed in Section 7.1. Section 7.2 discusses the remaining limitations and proposes possible future research.

7.1 Main conclusions

The main objective of this dissertation is to answer the main research question:

What is the mechanism of CRS on decreasing the surface crack growth in metallic pipes subjected to cyclic bending/tension loads?

To address this question, a composite repairing protocol on surface cracked metallic pipes has been proposed. Two investigation approaches, i.e., experimental study and numerical analysis, were employed. First, circumferential surface crack growth in metallic pipes subjected to cyclic bending/tension loads were conducted to pave a way for investigations on composite reinforced surface crack growth. Then, in light of the potential influential factors due to pipe geometry and load type, an experimental study was first conducted on an composite reinforced surface cracked plate. By this approach, the possible failure modes and surface crack growth behaviour reinforced with FRP were determined in simpler small-scale specimens. Thereafter, an FE model was developed based on the specimens and validated by the experimental results, which is able to rationally evaluate the SIF of the surface crack

reinforced with FRP. In Chapter 5 and Chapter 6, based on the previous investigations on surface cracked pipe and composite reinforced surface cracked plates, the investigations on surface cracked metallic pipes reinforced with CRS were conducted by experimental and numerical approaches. The mechanism of CRS on decreasing the surface crack growth has been identified; then based on of the mechanism, an analytical method was proposed, which is able to rationally evaluate the SIF of the surface crack in metallic pipes reinforced with CRS.

More specifically, the key questions that related to the main research question are answered as follows.

1) *What are the available methods of evaluating the SIF of circumferential surface cracks in pipes subjected to bending/tension?*

This question needs to be answered from two perspectives, in terms of the numerical and analytical approaches. The numerical studies, as listed in Table 2.2, has been employed to evaluate the SIF of the circumferential surface crack in metallic pipes in the past two decades. They were able to rationally predict the SIF of the circumferential surface crack, as well as determining influential parameters such as D/t, a/c and a/t ratios. The modelling strategy can be referred for developing the FE model in this dissertation.

The analytical methods of evaluating the SIF of circumferential surface cracks in metallic pipes, as reviewed in Sub-section 2.1.2.3, are employed by relevant standards such as BS 7910 and API 579-1/ASME-FFS-1. These methods are able to evaluate the SIF, yet either not accurate or not practical enough, as indicated in Sub-section 2.1.3.3. In order to predict the surface crack growth along with the Paris' law, an analytical method which can accurately evaluate the SIF of the surface crack with continuous of a/c and a/t values is still in great demand, in order to pave the way for the analytical method of evaluating the SIF of surface cracks reinforced with CRS.

2) *What are the key influential parameters in a prediction method of evaluating the surface crack growth in different scenarios?*

The key influential parameters of a prediction method to evaluate the surface crack growth in different scenarios, such as the profile of a surface crack (e.g., aspect ratio, the relative crack depth), different geometers (e.g., pipe, plate) under different load cases (e.g., tension, bending, or combined loads), can be implemented by the geometry correction factor and the load correction factor. An analytical equation for evaluating the SIF of surface cracks in different scenarios, generally contains a core component, which is the equation of evaluating the SIF in a standard semi-elliptical crack in a finite plane plate under tensile load. Then the equation were integrated by influential parameters to provide rational evaluations. Those influential parameters were generally determined by the numerical simulation method or the weight function method, by using curve-fitting method or based on engineering experience.

In this dissertation, the purpose of accurately evaluate the SIF of circumferential surface cracks lay in the pipe geometry, load case (e.g., bending), and the crack profile in a pipe

surface. Therefore, the bending correction factor was deduced and the geometry correction factor was determined by means of the numerical analysis.

3) *What are the research gaps of using composite reinforcement on the surface cracked metallic pipes?*

CRS has been applied in repairing damaged pipes in the offshore industry for decades, and it has been introduced as an efficient method in relevant maintenance standards or recommended practice documents. However, available investigations on the mechanism and the reinforcement effect on surface crack growth is seriously lacking in open documents. The existing research gaps are induced by the deficiencies in the corresponding research: (1) the mechanism of composite reinforcement on decreasing the surface crack growth rate is unclear. The effect of composite reinforcement on surface cracks might be similar to composite reinforcement on through-thickness cracks in terms of decreasing the local stress around the crack, and the crack-bridging effect. However, since surface cracks propagate as a more complex semi-elliptical shape, the effectiveness of composite reinforcement on the surface crack growth along different directions is insufficient in research. (2) Possible failure modes on the composite reinforced metallic pipes under cyclic loads are unclear. Those failures might generate considerable negative influence on the composite reinforcement. The failure modes, as well as their effect on the surface crack, are needed to be determined.

4) *What are the differences of using composite reinforcement on the surface cracked pipes and surface cracked plate under tension?*

Although composite reinforcement on plates and pipes share certain commonalities, the differences are derived from their geometries and load types. Composite reinforcement on cracked plates will generate an out-of-plane moment on the plate, resulting in a combination of tension and bending onto the cracked plate. The gradually distributed stress in the thickness direction affects the SIF along the crack front. While there is no such concern on the out-of-plane issue in regards to composite reinforced pipes, whose stress distribution around the surface crack is determined by the bending gradient effect.

The differences are implemented by their key influential parameters as well. For example, increasing the tensile modulus of the composite and the number of bond layers have significantly enhanced the reinforcement effectiveness on cracked pipes, while their influences on reinforced plates are entirely different. Other influential parameters have a diverse effect on two cases as well.

5) *What is the difference between employing composite reinforcement on internal surface crack and the external surface crack of metallic pipes?*

The main difference is derived from the interaction between the composite laminates and the surface crack. Internal surface cracks do not contact with the composite laminates; therefore, the decreasing of crack growth rate owes to the decreasing of stress distributed around the surface crack. The decreasing of the crack growth rate of the external surface crack benefits from the stress decreasing as well. Moreover, the composite reinforcement has generated a

crack-bridging effect on the cracked surface, especially at the surface point of the surface crack, which significantly decreased the crack growth rate along the length direction. While the crack-bridging effect has a negligible influence on the surface crack at the deepest point. As a result, the crack-bridging effect performed more efficiently on reducing the FCGR along the length direction than along the depth direction, implemented by the increasing value of the preferred aspect ratio.

Another difference is implemented by the possible failure modes. Since composite laminates do not contact with internal cracked surfaces, the bond condition between composite laminates and the steel substrate can be regarded as perfect. While for the external surface cracked pipes, in light of their direct contact, the bond condition cannot be regarded as perfect; but as adequately bonded. The reason is, although crack-induced debonding would not occur during the surface crack growing process, the stiffness degradation of the interface has weakened the effect on decreasing the SIF of the surface point, which is needed to be taken into account.

6) *What are the possible failure modes of composite reinforced surface cracked metallic pipes, and how would they influence the crack growth behaviour?*

The experiments of composite reinforcement on surface cracked plates indicated that the edge debonding and crack-induced debonding have occurred on four specimens. While these debonding failures were not occurred on the rest ten specimens, indicating interface failures could be avoided by improving the lay-up technique and introducing advanced technique for the surface quality. In contrast to the plate specimens, the CRS was adequately bonded on all pipe specimens—interfacial failures did not occur.

However, even though no failures occurred during the surface crack process in a macroscopic scale, the degree of stiffness degradation has weakened the effect on decreasing the SIF at the surface point of the surface crack. Owing to this, the surface crack growth along the length direction has been directly influenced, which will indirectly influence the crack growth along the depth direction.

7) *How to appropriately reinforce the surface cracked metallic pipes, in order to achieve the desired reinforcement effect?*

The parametric studies in Chapter 5 and 6 conclude that the number of bond layers and the tensile modulus of the CFRP are the key influential parameters. Besides, controlling the adhesive thickness at a low level is recommended to ensure the reinforcement effectiveness. The proposed analytical method for evaluating SIF of the surface crack reinforced with CRS has taken those key influential parameters into account. Practitioners can evaluate the surface crack growth rate and predict the residual fatigue life using the analytical method. On the other hand, the analytical method is an efficient tool to determine the reinforcement parameters for a desired prolongation of the residual fatigue life.

In summary, a brief answer to the main research question is presented as follows:

The composite reinforcement decreases the surface crack growth through two approaches: (1) decreasing the stress magnitude distributed adjacent to the surface crack, and (2) the crack-bridging effect on the crack opening. Both effects are effective when using CRS to reinforce the external surface cracks, while only effect (1) is effective on the internal surface cracks.

The composite laminate were adequately bonded on the cracked metallic substrate with no interfacial failures during the surface crack growth process. While, the interfacial stiffness degraded along with the crack growth, resulting in the weakening of crack-bridging effect at the surface point of the surface crack. The proposed analytical method has taken this issue into account, which is able to rationally predict the surface crack growth reinforced with CRS.

7.2 Recommendations for future research

In this dissertation, a composite repairing protocol for surface cracked metallic pipes subjected to cyclic loads is proposed, aiming to decrease the crack growth rate and prolong the residual fatigue life. Although some achievement has been obtained, there are still issues not covered sufficiently and need further studies.

- **Recommendation on further discussion on surface crack growth in metallic pipes**

  This dissertation focused on surface crack growth in metallic pipes. There is a high probability the surface cracks initiate around girth welds. Hence, quantitative analysis on the influence of welding residual stress are necessary. The FEM, which has been used for analysing the residual stress on butt weld surface cracks, is an appropriate method for such investigations. In addition, experimental measurement and investigation of the residual stress distribution for clarification and validation, and analytical methods proposing are demanded as well.

  Surface cracked pipes subjected to major load cases such as bending and tension loads were investigated. In practical situations, complicated combined loading might applied on metallic pipes, introducing issues such as mixed-modes surface crack growth and the influence of internal/external pressure on the surface crack growth. Related discussions are required in order to promote the CRS application towards a further step. The effectiveness and accuracy of X-FEM and S-version FEM have been validated in recent years, especially for handling multiple surface cracks growth problem, while applications on offshore metallic pipes are still very limited in open documents. Further application and analysis are expected.

  Since surface cracks are approximately semi-elliptical shaped in practical situations, researchers generally applied this shape as a simplification. In fact, the shape of the surface crack can be affected by external factors such as welding residual stress, load types, and geometry. Advanced modelling method which can take these factors into account, is demanded.

In practical situations, surface crack growth frequently combined with corrosion problems such as hydrogen corrosion, often known as the corrosion-cracking problems. In many cases, offshore metallic pipes are adopted in harsh marine environment, for example, sour or sweet seawater, and low/high temperature. Further quantitative analysis of sour/sweet environment on surface crack growth is demanded. Their influence can be formulized as influential functions into analytical methods.

- **Recommendation on the durability of CRS in the marine environment**

The experimental investigations in this dissertation were conducted under laboratory conditions, thus composite durability in the marine environment was not considered. Relevant studies have been conducted on intact metallic pipes reinforcement with CRS under marine environment such as cold weather and sea water environment. Such analysis has not been conducted in composite reinforced surface cracked pipes. The long-term exposure to the marine environment might result in the degradation of the mechanical properties of the composite and the adhesive material, which could weaken the reinforcement effectiveness on decreasing the crack growth rate, or resulting in failures within the CRS. Relevant investigations are in a great demand to promote the CRS application in the offshore industry.

- **Recommendation on further studies on the failure mechanism at the FRP-to-steel interface**

In this dissertation, a bilinear traction-separation cohesive zone model was developed to analyse the bond behaviour at the FRP-to-steel interface. The results indicated that crack-induced debonding did not occur during the surface crack growth process, while the interfacial stiffness degraded along with the crack growth. The stiffness degradation resulted in weakening of the crack-induced effect. Later on, an analytical method of evaluating the composite reinforced external surface cracked pipe was proposed by taken the stiffness degradation into account.

The interfacial stiffness degradation behaviour was analysed by assuming the maximum stress was the dominate influential parameters [129], hence fatigue at the interfacial was not considered. Researchers have indicated the interfacial properties might degrade under cyclic loads [157]. In this regard, further in-depth research is demanded to identify its mechanism. Experimental investigation on the traction-separation of the FRP-to-steel interface on surface cracked specimens subjected to cyclic loads might be a possible solution.

- **Recommendation on the practical issues of CRS application in the offshore industry**

This dissertation proposed a prototype of using CRS to repair the surface cracked offshore metallic pipes. Practical issues are needed to be determined to remove the obstacles from practical applications. The first issue is to remove the obstacle of underwater wrapping operation. Prototypes of automatic wrapping have been designed and tested, which was learned from the automatic wrapping machine of pressure vessels, are expected to be

applied in practical application in the near future. The second issue is the underwater packaging technique, because of the significant negative effect of the harsh marine environment on the crack growth and CRS durability. The GFRP's function on isolating seawater from metallic pipes is effectively but might not be sufficient. For a future study, an underwater packaging technique that can completely isolate seawater from composite reinforced metallic pipes is expected.

Appendix I Specimens manufacturing

The manufacturing of the specimens contains three main steps: manufacturing notches, pre-cracking, and the CRS reinforcement, as indicated in Figure A.1. For plate specimens, the semi-elliptical notches located in the middle of the steel plates, orienting perpendicular to the length direction of the steel plate; while for pipe specimens, the semi-elliptical notches located in the mid-bottom of the steel pipes. They were made by Micro-Electric Discharging Machining (Micro-EDM) suggested by ASME E2899 in order to achieve the user designed notch profile and to avoid the thermal residual stress [158]. The aimed aspect ratio of the notches on the plates are 0.4, 0.625, and 1.0, representing some common seen surface cracks in metallic structures in practical situations [69, 71], while the aimed aspect ratio of the notches on pipes are 0.5, 0.625, and 1.0, representing the range of common seen shapes of surface cracks in offshore metallic pipes in practice [159]. The width and half-length of all notches are controlled as 0.35 mm. The shape of the notches guaranteed that the surface cracks would propagate as semi-elliptical shaped during the fatigue tests.

Then, a pre-cracking procedure was conducted on the notched steel pipes, in order to initiate fatigue cracks from the notches [57]. The procedure was conducted on the fatigue machine, which contained two stages: the first stage adopted 80% yield stress of the steel as the amplitude of the constant amplitude sinusoidal cyclic loading, while the second stage adopted 60% yield stress. Note that both of the two stages were under the load ratio equals to R = 0.1. During each stage, cyclic bending load was applied on the specimens until the surface crack initiated from the notch and propagated more than 1.0 mm. Then the size of each surface crack after the pre-cracking procedure was regarded as the initial crack size. The specimens therefore were ready for the composite reinforcement procedure.

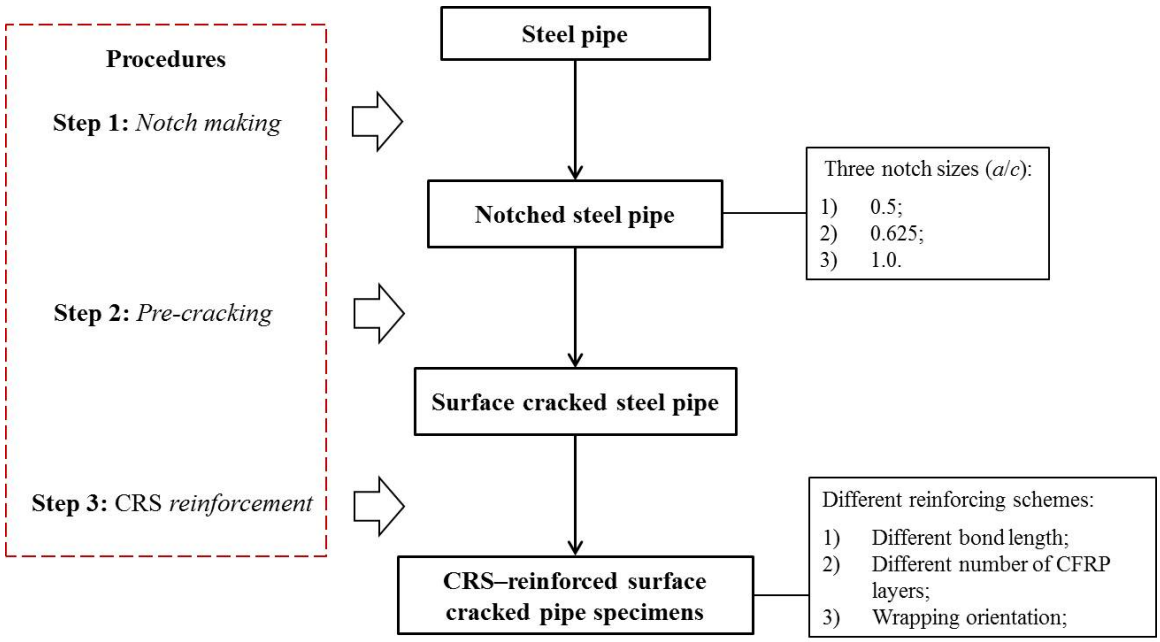

Figure I.1. The procedure of pipe specimen preparation

Afterwards, the surface cracked specimens were reinforced with composite laminates, which was implemented by professional workers using hand lay-up technique. This step contained three procedures: surface preparation, cleaning, and pasting the composite laminates. The rust cleaning and sanding process were implemented during the surface preparation procedure, trying to meet the practical situation of reinforcing the offshore metallic pipes to the maximum extent. Then the surface of the steel substrate was cleaned using acetone. During the pasting procedure, the composite laminates were bonded at the middle of the steel plates/pipes. One layer of GFRP was applied as the first layer for all the composite reinforced specimens, in order to prevent the galvanic corrosion between the CFRP laminates and the steel substrate. Then for pipe specimens, the CFRP laminates were wrapped around the cracked pipes using different reinforcement schemes. For instance, different bond lengths, CFRP orientation, number of bond layers. The composite laminates were compressed by wrapping plastic tapes around the external composite layer to squeeze redundant resin epoxy and eliminate the bubbles in the interlaminations. For plate specimens, these purposes were realized by compressing by a large mass. In this way, the composite laminates were bonded tightly onto the steel pipes. Finally the reinforced specimens were placed at room temperature for solidification of one week, in order to achieve the optimum bond condition.

Appendix II Experimental results on surface crack growth

II.1 Results of the surface crack growth on steel plates subjected to cyclic tension

Table II.1 Surface crack size in plate along the depth and the length direction corresponding to cycle-index (units of *a* and *c* are in mm)

Specimen	**S-1(1)**		**S-1(2)**		**S-1(3)**		**S-2(1)**	
Cycles	***a***	***c***	***a***	***c***	***a***	***c***	***a***	***c***
0	4.64	5.90	5.89	6.66	6.03	6.95	4.17	4.52
10,000	4.91	6.20	6.66	7.30	6.89	8.03	4.38	4.7
20,000	5.24	6.50	7.85	8.92	8.32	9.98	4.59	4.92
30,000	5.82	6.86	9.73	11.59	10.42	13.25	4.85	5.26
40,000	6.55	7.59	$> t$	16.99	/	/	5.22	5.56
50,000	7.74	9.47	/	/	/	/	5.6	6.04
60,000	9.42	12.07	/	/	/	/	6.09	6.6
70,000	11.96	15.43	/	/	/	/	6.63	7.36
80,000	/	/	/	/	/	/	7.49	8.41
90,000	/	/	/	/	/	/	8.89	10.33
100,000	/	/	/	/	/	/	11.07	14.14
110,000	/	/	/	/	/	/	$> t$	17.97

Continued Table II.1…

Specimen	**S-2(2)**		**S-2(3)**		**S-3(1)**		**S-3(2)**	
Cycles	***a***	***c***	***a***	***c***	***a***	***c***	***a***	***c***
0	4.18	4.90	5.27	5.63	5.40	5.78	6.15	6.42
10,000	4.25	4.99	5.63	5.98	5.55	6.08	6.38	7.16
20,000	4.35	5.10	6.15	6.54	5.92	6.48	7.13	8.06
30,000	4.49	5.26	6.89	7.92	6.35	7.06	8.14	9.13
40,000	4.75	5.50	7.95	9.48	6.98	7.85	9.83	11.02
50,000	5.13	5.88	9.84	11.75	7.85	8.78	12.13	14.78
60,000	5.45	6.35	12.00	15.36	9.48	10.52	/	/
70,000	6.00	6.83	/	/	11.40	14.11	/	/
80,000	6.78	7.75	/	/	/	/	/	/
90,000	7.90	9.15	/	/	/	/	/	/
100,000	9.59	11.54	/	/	/	/	/	/
110,000	12.30	15.66	/	/	/	/	/	/

Continued Table II.1…

Specimen	S-3(3)		SI-1-R(1)		SI-1-R(2)		SI-1-R(3)	
Cycles	*a*	*c*	*a*	*c*	*a*	*c*	*a*	*c*
0	5.86	5.78	4.95	6.00	5.49	6.53	5.56	6.56
10,000	5.93	6.08	5.26	6.10	5.78	6.94	5.86	6.95
20,000	6.18	6.52	5.66	6.54	6.39	7.75	6.59	7.83
30,000	6.42	7.32	6.26	7.20	7.59	9.17	7.84	9.23
40,000	7.35	8.23	7.28	8.16	9.45	11.97	9.75	12.88
50,000	8.37	9.66	8.95	10.31	11.90	17.75	12.2	19.88
60,000	10.32	11.69	11.24	14.57	/	/	/	/
70,000	12.70	16.02	/	/	/	/	/	/

Continued Table II.1…

Specimen	SE-1-R(1)		SE-1-R(2)		SE-1-R(3)	
Cycles	*a*	*c*	*a*	*a*	*c*	*a*
0	4.77	5.87	5.78	4.77	5.87	5.78
10,000	5.00	6.00	5.90	5.00	6.00	5.90
20,000	5.33	6.25	6.10	5.33	6.25	6.10
30,000	5.75	6.64	6.33	5.75	6.64	6.33
40,000	6.28	7.28	6.77	6.28	7.28	6.77
50,000	6.92	8.04	7.36	6.92	8.04	7.36
60,000	7.87	9.40	8.17	7.87	9.40	8.17
70,000	9.10	11.39	9.10	9.10	11.39	9.10
80,000	11.03	15.27	10.72	11.03	15.27	10.72

Continued Table II.1…

Specimen	SE-2-R(1)		SE-2-R(2)		SE-2-R(3)		SE-3-R(1)	
Cycles	*a*	*c*	*a*	*c*	*a*	*c*	*a*	*c*
0	4.04	4.01	3.96	4.33	4.78	5.05	5.40	5.78
10,000	4.09	4.05	4.02	4.36	4.97	5.26	5.55	6.08
20,000	4.15	4.10	4.10	4.43	5.21	5.46	5.92	6.48
30,000	4.22	4.16	4.22	4.54	5.42	5.76	6.35	7.06
40,000	4.32	4.23	4.48	4.68	5.76	6.04	6.98	7.85
50,000	4.44	4.31	4.64	4.83	6.05	6.38	7.85	8.78
60,000	4.58	4.40	4.82	5.01	6.38	6.89	9.48	10.52
70,000	4.75	4.56	5.04	5.20	6.92	7.42	11.4	14.11
80,000	4.94	4.78	5.26	5.40	7.59	8.36	/	/
90,000	5.15	4.98	5.49	5.64	8.53	9.53	/	/
100,000	5.44	5.26	5.77	5.91	9.92	11.76	/	/
110,000	5.70	5.70	5.99	6.23	11.78	14.95	/	/
120,000	6.01	6.11	6.34	6.66	/	/	/	/
130,000	6.43	6.70	6.88	7.44	/	/	/	/
140,000	6.94	7.35	7.44	8.27	/	/	/	/
150,000	7.62	8.36	8.30	9.38	/	/	/	/
160,000	8.61	10.10	9.44	11.25	/	/	/	/
170,000	10.38	13.55	11.24	14.77	/	/	/	/

Continued Table II.1…

Specimen	SE-3-R(2)		SE-3-R(3)		SE-1-R2(1)		SE-1-R6(1)	
Cycles	***a***	***c***	***a***	***c***	***a***	***c***	***a***	***c***
0	5.82	5.36	6.21	6.60	5.82	5.36	6.21	6.60
10,000	6.12	5.66	6.52	6.88	6.12	5.66	6.52	6.88
20,000	6.51	5.97	6.98	7.32	6.51	5.97	6.98	7.32
30,000	7.01	6.81	7.69	8.40	7.01	6.81	7.69	8.40
40,000	7.83	7.97	8.75	9.63	7.83	7.97	8.75	9.63
50,000	9.01	9.78	10.86	13.23	9.01	9.78	10.86	13.23
60,000	10.77	12.54	> *t*	18.66	10.77	12.54	> *t*	18.66

II.2 Results of the surface crack growth on steel pipes subjected to cyclic bending

Table II.2 Surface crack size in pipe along the depth and the length direction corresponding to cycle-index (units of *a* and *c* are in mm)

Specimen	**PE-1(1)**		**PE-1(2)**		**PE-1(3)**		**PE-2(1)**	
Cycles	***a***	***c***	***a***	***c***	***a***	***c***	***a***	***c***
0	3.79	5.51	6.69	7.82	4.29	5.80	5.34	6.53
10,000	3.99	5.56	7.25	8.17	4.57	5.96	6.03	7.33
20,000	4.36	5.77	8.48	9.64	5.14	6.29	6.98	8.24
30,000	4.87	6.02	10.24	12.74	6.02	7.17	8.47	10.16
40,000	5.55	6.62	/	/	7.15	8.71	9.77	13.38
50,000	6.67	7.67	/	/	8.720	10.91	11.86	18.46
60,000	8.09	9.62	/	/	10.80	13.92	/	/
70,000	10.11	12.01	/	/	/	/	/	/

Continued Table II.2…

Specimen	**PE-2(2)**		**PE-2(3)**		**PE-3(1)**		**PE-3(2)**	
Cycles	***a***	***c***	***a***	***a***	***c***	***a***	***a***	***c***
0	5.05	6.03	6.07	5.05	6.03	6.07	5.82	6.23
10,000	5.68	6.72	7.2	5.68	6.72	7.2	6.61	7.43
20,000	6.58	7.79	8.79	6.58	7.79	8.79	7.72	8.92
30,000	7.84	9.46	10.81	7.84	9.46	10.81	9.32	11.61
40,000	9.27	11.93	/	9.27	11.93	/	11.18	15.32
50,000	10.86	15.76	/	10.86	15.76	/	/	/

Continued Table II.2…

Specimen	**PE-3(3)**		**PE-1-R(1)**		**PE-1-R(2)**		**PE-1-R(3)**	
Cycles	***a***	***c***	***a***	***c***	***a***	***c***	***a***	***c***
0	5.52	5.96	6.64	7.15	6.47	6.92	5.81	6.92
10,000	6.38	6.86	6.85	7.22	6.72	7.15	5.98	7.12
20,000	7.48	8.43	7.19	7.63	7.15	7.58	6.23	7.20
30,000	8.76	10.77	7.83	8.355	7.95	8.34	6.74	7.36
40,000	10.35	14.4	9.01	10.015	9.09	10.11	7.36	7.74
50,000	/	/	10.71	13.075	10.82	13.18	8.16	8.78
60,000	/	/	/	/	> *t*	16.89	9.30	10.20
70,000	/	/	/	/	/	/	10.64	12.15
80,000	/	/	/	/	/	/	12.51	15.30

Continued Table II.2…

Specimen	PE-2-R(1)		PE-2-R(2)		PE-2-R(3)		PE-3-R(1)	
Cycles	***a***	***c***	***a***	***c***	***a***	***c***	***a***	***c***
0	5.24	6.13	6.24	7.12	5.78	6.325	6.53	6.73
10,000	5.38	6.3	6.49	7.27	5.88	6.425	6.64	6.89
20,000	5.59	6.42	6.87	7.43	6.1	6.575	6.79	7.05
30,000	5.78	6.56	7.55	7.86	6.37	6.725	6.98	7.24
40,000	6.09	6.76	8.48	9.04	6.76	6.865	7.33	7.36
50,000	6.52	7.13	9.76	11.12	7.28	7.235	7.86	7.85
60,000	7.00	7.59	11.4	13.82	7.95	7.885	8.56	8.87
70,000	7.65	8.3	> *t*	17.16	8.94	9.305	9.56	10.57
80,000	8.3	9.21	/	/	10.17	11.165	10.75	12.93
90,000	9.04	10.4	/	/	11.8	13.895	12.18	16.26
100,000	9.92	12	/	/	> *t*	17.025	/	/
110,000	11.14	14.32	/	/	/	/	/	/

Continued Table II.2…

Specimen	PE-3-R(2)		PE-3-R(3)		PE-1-R600(1)		PE-1-R600(2)	
Cycles	***a***	***c***	***a***	***c***	***a***	***c***	***a***	***c***
0	5.92	6.235	5.78	6.34	6.99	8.67	6.1	7.465
10,000	6.07	6.425	5.88	6.4	7.35	8.94	6.28	7.725
20,000	6.22	6.605	6.35	6.58	8.06	9.43	6.56	7.925
30,000	6.43	6.78	6.53	6.725	9.33	10.87	6.93	8.185
40,000	6.76	6.985	6.82	6.86	10.78	13.26	7.6	8.565
50,000	7.16	7.345	7.28	7.24	> *t*	16.86	8.56	9.575
60,000	7.67	8.255	7.95	7.85	/	/	9.81	11.675
70,000	8.36	9.695	8.92	9.23	/	/	11.09	14.686
80,000	9.1	11.375	10.15	11.21	/	/	/	/
90,000	10.09	13.385	11.78	13.65	/	/	/	/
100,000	11.2	16.105	> *t*	17.025	/	/	/	/

Continued Table II.2…

Specimen	PE-1-R600(3)		PE-1-R8(1)		PE-1-R8(2)		PE-1-R8(3)	
Cycles	***a***	***c***	***a***	***c***	***a***	***c***	***a***	***c***
0	7.69	9.53	6.72	7.95	5.92	7.28	6.93	8.225
10,000	8.06	9.95	6.88	8.06	6.05	7.35	7.22	8.405
20,000	8.57	10.45	7.19	8.18	6.2	7.48	7.72	8.675
30,000	9.68	11.75	7.67	8.77	6.4	7.64	8.5	9.295
40,000	11.09	14.48	8.43	9.97	6.62	7.84	9.51	10.755
50,000	> *t*	18.59	9.37	11.4	6.9	8.06	10.66	12.765
60,000	/	/	10.54	13.73	7.27	8.3	> *t*	15.215
70,000	/	/	11.96	16.47	7.79	8.63	/	/
80,000	/	/	/	/	8.41	9.28	/	/
90,000	/	/	/	/	9.09	10.25	/	/
100,000	/	/	/	/	9.95	11.53	/	/
110,000	/	/	/	/	11.1	13.51	/	/
120,000	/	/	/	/	12.56	16.32	/	/

Continued Table II.2…

Specimen	PE-1-R45(1)		PE-1-R45(2)		PE-1-R45(3)	
Cycles	***a***	***c***	***a***	***c***	***a***	***c***
0	5.56	6.93	4.99	6.525	6.01	7.45
10,000	5.76	7.05	5.16	6.60	6.32	7.57
20,000	6.06	7.2	5.32	6.705	6.83	7.96
30,000	6.7	7.4	5.54	6.795	7.88	8.82
40,000	7.77	8.28	5.85	6.925	9.16	10.64
50,000	9.22	10.02	6.33	7.105	10.68	13.13
60,000	10.98	12.58	6.96	7.605	$> t$	16.37
70,000	$> t$	15.81	7.73	8.425	/	/
80,000	/	/	8.83	9.835	/	/
90,000	/	/	10.23	11.695	/	/
100,000	/	/	12.2	14.455	/	/

References

[1] L. Wang, J. Zhang, F. Yuan, and K. Li, "Interaction between catenary riser and soft seabed: large-scale indoor tests," *Applied ocean research,* vol. 45, pp. 10-21, 2014.

[2] J. Xia, P. K. Das, and D. Karunakaran, "A parametric design study for a semi/SCR system in Northern North Sea," *Ocean Engineering,* vol. 35, no. 17-18, pp. 1686-1699, 2008.

[3] M. Rosenfeld and J. Kiefner, "Basics of metal fatigue in natural gas pipeline systems–A primer for gas pipeline operators," *Pipeline Research Council International, Houston, TX,* 2006.

[4] C. Achebe, U. Nneke, and O. Anisiji, "Analysis of oil pipeline failures in the oil and gas industries in the Niger delta area of Nigeria," in *Proceedings of The International Multi Conference of Engineers and Computer Scientists*, 2012, pp. 1274-9.

[5] M. H. Mohd and J. K. Paik, "Investigation of the corrosion progress characteristics of offshore subsea oil well tubes," *Corrosion Science,* vol. 67, pp. 130-141, 2013.

[6] P. Rajeev, D. Robert, N. Thusyanthan, and J. Kodikara, "Reliability analysis of upheaval bucking of offshore pipelines," *Australian Geomechanics Journal,* vol. 48, no. 4, pp. 137-148, 2013.

[7] E. Duesten, "Damage and incidents involving load-bearing structures and pipeline systems 2016," Petroleum Safety Authority NorwayOct. 12, 2017 2017.

[8] *DNVGL-RP-F204. Riser fatigue*, 2005.

[9] *DNVGL-RP-C205. Environmental Conditions and Environmental Loads* 2014.

[10] C. d. A. Martins, E. Higashi, and R. Silva, "A parametric analysis of steel catenary risers: Fatigue behavior near the top," in *The Tenth International Offshore and Polar Engineering Conference*, 2000: International Society of Offshore and Polar Engineers.

[11] N. O. Chibueze, C. V. Ossia, and J. U. Okoli, "On the fatigue of steel catenary risers," *Strojniški vestnik-Journal of Mechanical Engineering,* vol. 62, no. 12, pp. 751-756, 2016.

[12] G. Mansour, "The impact of the second order vessel motion on the fatigue life of steel catenary risers," in *ASME 2004 23rd International Conference on Offshore*

Mechanics and Arctic Engineering, 2004, pp. 1177-1180: American Society of Mechanical Engineers Digital Collection.

[13] Z. Li, X. Jiang, Z. Liu, and H. Hopman, "Internal Surface Crack Growth in Offshore Rigid Pipes Reinforced With CFRP," in *ASME 2018 37th International Conference on Ocean, Offshore and Arctic Engineering*, 2018, pp. V004T03A022-V004T03A022: American Society of Mechanical Engineers.

[14] D. L. Garrett, P. N. Stanton, and P. Sharma, "Dynamic Risers for Floating Production Systems API Standard 2RD," in *Offshore Technology Conference*, 2015: Offshore Technology Conference.

[15] *DNVGL-RP-F206. Riser Integrity Management*, 2008.

[16] R. Brighenti and A. Carpinteri, "Surface cracks in fatigued structural components: a review," *Fatigue & Fracture of Engineering Materials & Structures,* vol. 36, no. 12, pp. 1209-1222, 2013.

[17] *DNV-RP-F108. Assessment of flaws in pipeline and riser girth welds*, 2017.

[18] *API 570. Piping Inspection Code: In-service Inspection, Repair, and Alteration of Piping Systems*, 2016.

[19] *API 579-1/ASME FFS-1. Fitness-for-service*, 2016.

[20] *BS 7910. Guide on methods for assessing the acceptability of flaws in metallic structures*, 0580330818, 2019.

[21] V. M. Karbhari, *Rehabilitation of pipelines using fiber-reinforced polymer (FRP) composites*. Elsevier, 2015.

[22] X. Zhao and L. Zhang, "State-of-the-art review on FRP strengthened steel structures," *Engineering Structures,* vol. 29, no. 8, pp. 1808-1823, 2007.

[23] C. Alexander and B. Francini, "State of the art assessment of composite systems used to repair transmission pipelines," in *2006 International Pipeline Conference*, 2006, pp. 823-830: American Society of Mechanical Engineers.

[24] Z. Liu, K. Chen, Z. Li, and X. Jiang, "Crack monitoring method for an FRP-strengthened steel structure based on an antenna sensor," *Sensors,* vol. 17, no. 10, p. 2394, 2017.

[25] Z. Li, X. Jiang, and H. Hopman, "Numerical investigation on surface crack growth in steel plates repaired with Carbon Fiber-reinforced Polymer," in *ASME 2019 38th International Conference on Ocean, Offshore and Arctic Engineering*, 2019: American Society of Mechanical Engineers.

[26] Z. Li, X. Jiang, and G. Lodewijks, "The latest development of reinforcement techniques on tubular joints," *Progress in the Analysis and Design of Marine Structures,* pp. 783-790, 2017.

[27] M. Kabir, S. Fawzia, T. Chan, J. Gamage, and J. Bai, "Experimental and numerical investigation of the behaviour of CFRP strengthened CHS beams subjected to bending," *Engineering Structures,* vol. 113, pp. 160-173, 2016.

[28] J. Haedir, M. Bambach, X.-L. Zhao, and R. Grzebieta, "Strength of circular hollow sections (CHS) tubular beams externally reinforced by carbon FRP sheets in pure bending," *Thin-walled structures,* vol. 47, no. 10, pp. 1136-1147, 2009.

[29] S. Fawzia, R. Al-Mahaidi, X. L. Zhao, and S. Rizkalla, "Strengthening of circular hollow steel tubular sections using high modulus CFRP sheets," *Construction and Building Materials,* vol. 21, no. 4, pp. 839-845, 2007.

[30] M. V. Seica and J. A. Packer, "FRP materials for the rehabilitation of tubular steel structures, for underwater applications," *Composite Structures,* vol. 80, no. 3, pp. 440-450, 2007.

[31] A. P. Kumar and R. Senthil, "Axial behaviour of CFRP-strengthened circular steel hollow sections," *Arabian Journal for Science and Engineering,* vol. 41, no. 10, pp. 3841-3850, 2016.
[32] A. P. Kumar and R. Senthil, "Behavior of CFRP strengthened CHS under axial static and axial cyclic loading," *KSCE Journal of Civil Engineering,* vol. 20, no. 4, pp. 1493-1500, 2016.
[33] M. Kabir, S. Fawzia, T. Chan, and M. Badawi, "Numerical studies on CFRP strengthened steel circular members under marine environment," *Materials and Structures,* vol. 49, no. 10, pp. 4201-4216, 2016.
[34] A. Achour, A. Albedah, F. Benyahia, B. A. B. Bouiadjra, and D. Ouinas, "Analysis of repaired cracks with bonded composite wrap in pipes under bending," *Journal of Pressure Vessel Technology,* vol. 138, no. 6, p. 060909, 2016.
[35] M. Meriem-Benziane, S. A. Abdul-Wahab, H. Zahloul, B. Babaziane, M. Hadj-Meliani, and G. Pluvinage, "Finite element analysis of the integrity of an API X65 pipeline with a longitudinal crack repaired with single-and double-bonded composites," *Composites Part B: Engineering,* vol. 77, pp. 431-439, 2015.
[36] F. Benyahia, A. Albedah, and B. B. Bouiadjra, "Stress intensity factor for repaired circumferential cracks in pipe with bonded composite wrap," *Journal of Pressure Vessel Technology,* vol. 136, no. 4, p. 041201, 2014.
[37] *ASME B31.4. Pipeline Transportation Systems for Liquids and Slurries*, 2019.
[38] *ISO 24817. Petroleum, petrochemical and natural gas industries — Composite repairs for pipework — Qualification and design, installation, testing and inspection*, 0580330818, 2017.
[39] *API SPEC 5L:Specification for Line Pipe*, 2018.
[40] Z. Li, X. Jiang, H. Hopman, and Engineering, "Surface Crack Growth in Offshore Metallic Pipes under Cyclic Loads: A Literature Review," *Journal of Marine Science and Engineering,* vol. 8, no. 5, p. 339, 2020.
[41] H. A. Richard and M. Sander, *Fatigue crack growth*. Springer, 2016.
[42] P. S. A. Norway, "Riser Damage - Injuries and incidents from the Petroleum Safety Authority Norway's CODAM database," DNVGL, Hovik, Norway2018.
[43] Z. Li, X. Jiang, H. Hopman, L. Zhu, and Z. Liu, "An investigation on the circumferential surface crack growth in steel pipes subjected to fatigue bending," *Theoretical and Applied Fracture Mechanics,* vol. 105, p. 102403, 2020.
[44] A. M. Horn, I. Lotsberg, and O. Orjaseater, "The rationale for update of S-N curves for single sided girth welds forrisers and pipelines in DNV GL RP C-203 based on fatigue performance of more than 1700 full scale fatigue test results," in *Proceedings of the ASME 2018 37th International, Conference on Ocean, Offshore and Arctic Engineering*, 2018, no. OMAE-2018.
[45] J. Newman, "A review and assessment of the stress-intensity factors for surface cracks," in *Part-through crack fatigue life prediction*: ASTM International, 1979.
[46] P. Scott and T. Thorpe, "A critical review of crack tip stress intensity factors for semi‐elliptic cracks," *Fatigue & Fracture of Engineering Materials & Structures,* vol. 4, no. 4, pp. 291-309, 1981.
[47] D. M. Parks, "A surface crack review: elastic and elastic-plastic behavior," in *Surface-Crack Growth: Models, Experiments, and Structures*West Conshohocken, United States: ASTM International, 1990.
[48] H. Pang, "A Review of Stress of Intensity Factors for Semi-elliptical Surface Crack in a plate and Fillet Weld Joint (in Japanses)," *Weld. Inst. Rpt.,* vol. 426, 1990.

[49] R. Branco, F. V. Antunes, and J. D. Costa, "A review on 3D-FE adaptive remeshing techniques for crack growth modelling," *Engineering Fracture Mechanics,* vol. 141, pp. 170-195, 2015/06/01/ 2015.

[50] T. Shimakawa, H. Takahashi, H. Doi, K. Watashi, and Y. Asada, "Creep-fatigue crack propagation tests and the development of an analytical evaluation method for surface cracked pipe," *Nuclear engineering and design,* vol. 139, no. 3, pp. 283-292, 1993.

[51] L. Zhu, X. Tao, and L. Cengdian, "Fatigue strength and crack propagation life of in-service high pressure tubular reactor under residual stress," *International journal of pressure vessels and piping,* vol. 75, no. 12, pp. 871-877, 1998.

[52] Y. Yoo and K. Ando, "Circumferential inner fatigue crack growth and penetration behaviour in pipe subjected to a bending moment," *Fatigue & fracture of engineering materials & structures,* vol. 23, no. 1, pp. 1-8, 2000.

[53] P. Singh, K. Vaze, V. Bhasin, H. Kushwaha, P. Gandhi, and D. R. Murthy, "Crack initiation and growth behaviour of circumferentially cracked pipes under cyclic and monotonic loading," *International journal of pressure vessels and piping,* vol. 80, no. 9, pp. 629-640, 2003.

[54] P. Arora *et al.*, "Predictions for fatigue crack growth life of cracked pipes and pipe welds using RMS SIF approach and experimental validation," *International Journal of Pressure Vessels and Piping,* vol. 88, no. 10, pp. 384-394, 2011.

[55] V. Sahu, P. Ray, and B. Verma, "Experimental fatigue crack growth analysis and modelling in part‐through circumferentially pre‐cracked pipes under pure bending load," *Fatigue & Fracture of Engineering Materials & Structures,* vol. 40, no. 7, pp. 1154-1163, 2017.

[56] V. Shlyannikov, R. Yarullin, and I. Ishtyryakov, "Effect of temperature on the growth of fatigue surface cracks in aluminum alloys," *Theoretical and Applied Fracture Mechanics,* vol. 96, pp. 758-767, 2018.

[57] *ASTM E647. Standard Test Method for Measurement of Fatigue Crack Growth Rates*, 1994.

[58] *ASTM E2899. Standard Test Method for Measurement of Initiation Toughness in Surface Cracks Under Tension and Bending*, 2019.

[59] *ASTM E740. Standard Practice for Fracture Testing with Surface-Crack Tension Specimens*, 2016.

[60] S. Kim and M.-H. Kim, "Dynamic behaviors of conventional SCR and lazy-wave SCR for FPSOs in deepwater," *Ocean Engineering,* vol. 106, pp. 396-414, 2015.

[61] *Section XI. Rules for inservice inspection of nuclear power plant components*, 2001.

[62] D. L. Corn, "A study of cracking techniques for obtaining partial thickness cracks of pre-selected depths and shapes," *Engineering Fracture Mechanics,* vol. 3, no. 1, pp. 45-52, 1971.

[63] R. Branco, F. Antunes, and J. Costa, "Extent of the surface region in notched Middle Cracked Tension specimens," in *Key Engineering Materials*, 2013, vol. 560, pp. 107-127: Trans Tech Publ.

[64] G. V. Guinea, J. Planas, and M. Elices, "KI evaluation by the displacement extrapolation technique," *Engineering fracture mechanics,* vol. 66, no. 3, pp. 243-255, 2000.

[65] R. S. Barsoum, "On the use of isoparametric finite elements in linear fracture mechanics," *International journal for numerical methods in engineering,* vol. 10, no. 1, pp. 25-37, 1976.

[66] X. Lin and R. Smith, "Finite element modelling of fatigue crack growth of surface cracked plates: Part I: The numerical technique," *Engineering Fracture Mechanics,* vol. 63, no. 5, pp. 503-522, 1999.

[67] A. Sedmak, N. Savovic, and M. PAVlSlC, "ESIS recommendations for use of finite element method in fracture mechanics," in *ECF9, Varna 1992*, 1992.

[68] M. Heyder, K. Kolk, and G. Kuhn, "Numerical and experimental investigations of the influence of corner singularities on 3D fatigue crack propagation," *Engineering Fracture Mechanics,* vol. 72, no. 13, pp. 2095-2105, 2005.

[69] A. T. Diamantoudis and G. Labeas, "Stress intensity factors of semi-elliptical surface cracks in pressure vessels by global-local finite element methodology," *Engineering Fracture Mechanics,* vol. 72, no. 9, pp. 1299-1312, 2005.

[70] C. Oh, T. Song, Y. J. Kim, J. Kim, and T. Jin, "Approximate J estimates for axial part‐through surface‐cracked pipes," *Fatigue & Fracture of Engineering Materials & Structures,* vol. 30, no. 12, pp. 1127-1139, 2007.

[71] T. Meshii, T. Tanaka, and K. Lu, "T-Stress solutions for a semi-elliptical axial surface crack in a cylinder subjected to mode-I non-uniform stress distributions," *Engineering Fracture Mechanics,* vol. 77, no. 13, pp. 2467-2478, 2010.

[72] C. Li and S. Yang, "Stress intensity factors for high aspect ratio semi-elliptical internal surface cracks in pipes," *International Journal of Pressure Vessels and Piping,* vol. 96, pp. 13-23, 2012.

[73] K. Sharma, I. Singh, B. Mishra, and S. Maurya, "Numerical simulation of semi-elliptical axial crack in pipe bend using XFEM," 2014.

[74] A. Carpinteri, R. Brighenti, and S. Vantadori, "Circumferentially notched pipe with an external surface crack under complex loading," *International journal of mechanical sciences,* vol. 45, no. 12, pp. 1929-1947, 2003.

[75] S. Ligoria, G. S. Knight, and D. Ramachandra Murthy, "Three-dimensional finite element analysis of a semi-elliptical circumferential surface crack in a carbon steel pipe subjected to a bending moment," *The Journal of Strain Analysis for Engineering Design,* vol. 40, no. 6, pp. 525-533, 2005.

[76] K. P. Kou and F. Burdekin, "Stress intensity factors for a wide range of long-deep semi-elliptical surface cracks, partly through-wall cracks and fully through-wall cracks in tubular members," *Engineering fracture mechanics,* vol. 73, no. 12, pp. 1693-1710, 2006.

[77] A. Shahani and S. Habibi, "Stress intensity factors in a hollow cylinder containing a circumferential semi-elliptical crack subjected to combined loading," *International journal of Fatigue,* vol. 29, no. 1, pp. 128-140, 2007.

[78] B. Mechab, B. Serier, B. B. Bouiadjra, K. Kaddouri, and X. Feaugas, "Linear and non-linear analyses for semi-elliptical surface cracks in pipes under bending," *International Journal of Pressure Vessels and Piping,* vol. 88, no. 1, pp. 57-63, 2011.

[79] N. H. Dao and H. Sellami, "Stress intensity factors and fatigue growth of a surface crack in a drill pipe during rotary drilling operation," *Engineering fracture mechanics,* vol. 96, pp. 626-640, 2012.

[80] J. Predan, V. Močilnik, and N. Gubeljak, "Stress intensity factors for circumferential semi-elliptical surface cracks in a hollow cylinder subjected to pure torsion," *Engineering Fracture Mechanics,* vol. 105, pp. 152-168, 2013.

[81] X. Lin and R. Smith, "Direct simulation of fatigue crack growth for arbitrary-shaped defects in pressure vessels," *Proceedings of the Institution of Mechanical Engineers, Part C: Journal of Mechanical Engineering Science,* vol. 213, no. 2, pp. 175-189, 1998.

[82] N. Couroneau and J. Royer, "Simplified model for the fatigue growth analysis of surface cracks in round bars under mode I," *International Journal of Fatigue,* vol. 20, no. 10, pp. 711-718, 1998.
[83] P. Paris and F. Erdogan, "A critical analysis of crack propagation laws," *Journal of basic engineering,* vol. 85, no. 4, pp. 528-533, 1963.
[84] J. Schijve, *Fatigue of structures and materials*. Springer Science & Business Media, 2001.
[85] J. Newman and I. Raju, "Analysis of surface cracks in finite plates under tension or bending loads," *National aeronautics and space administration hampton va langley research center,* 1979.
[86] J. Newman and I. Raju, "An empirical stress-intensity factor equation for the surface crack," *Engineering fracture mechanics,* vol. 15, no. 1-2, pp. 185-192, 1981.
[87] H. Petroski and J. Achenbach, "Computation of the weight function from a stress intensity factor," *Engineering Fracture Mechanics,* vol. 10, no. 2, pp. 257-266, 1978.
[88] I. Raju and J. Newman Jr, "Stress-Intensity Factor Influence Coefficients for Internal and External Surface Cracks in Cylindrical Vessels," *Aspects of fracture mechanics in pressure vessels and piping,* pp. 37-49, 1982.
[89] I. Raju and J. Newman, "Stress-intensity factors for circumferential surface cracks in pipes and rods under tension and bending loads," in *Fracture Mechanics: Seventeenth Volume*: ASTM International, 1986.
[90] T. L. Anderson, "Developmenr of Stress Intensity Factor Solutions for Surface and Embedded Cracks in API579," *Welding Research Council Bulletin,* 2002.
[91] J. Newman Jr, "Predicting failure of specimens with either surface cracks or corner cracks at holes," 1976.
[92] J. Newman Jr and I. Raju, "An empirical stress-intensity factor equation for the surface crack," *Engineering fracture mechanics,* vol. 15, no. 1-2, pp. 185-192, 1981.
[93] A. Green and I. Sneddon, "The distribution of stress in the neighbourhood of a flat elliptical crack in an elastic solid," in *Mathematical Proceedings of the Cambridge Philosophical Society*, 1950, vol. 46, no. 1, pp. 159-163: Cambridge University Press.
[94] A. Russell, "Application of proof testing to assess k-reactor piping integrity," Douglas United Nuclear, Inc., Richland, WA (USA)1970.
[95] D. Dedhia and D. Harris, "Improved Influence Functions for Part-Circumferential Cracks in Pipes," *Circumferential Cracks in Pressure Vessels and Piping,* vol. 2, pp. 35-48.2, 1983.
[96] M. Bergman, "Stress intensity factors for circumferential surface cracks in pipes," *Fatigue & fracture of engineering materials & structures,* vol. 18, no. 10, pp. 1155-1172, 1995.
[97] J. Newman and I. Raju, "Stress-intensity factors for internal surface cracks in cylindrical pressure vessels," *Journal of Pressure Vessel Technology,* vol. 102, no. 4, pp. 342-346, 1980.
[98] E. Folias, "On the effect of initial curvature on cracked flat sheets," *International Journal of Fracture Mechanics,* vol. 5, no. 4, pp. 327-346, 1969.
[99] Y. Murakami and L. Keer, "Stress intensity factors handbook, vol. 3," *Journal of Applied Mechanics,* vol. 60, p. 1063, 1993.
[100] D. Green and J. Knowles, "The treatment of residual stress in fracture assessment of pressure vessels," *Journal of pressure vessel technology,* vol. 116, no. 4, pp. 345-352, 1994.
[101] T. Belytschko and T. Black, "Elastic crack growth in finite elements with minimal remeshing," *International journal for numerical methods in engineering,* vol. 45, no. 5, pp. 601-620, 1999.

[102] J. Fish, "The s-version of the finite element method," *Computers & Structures,* vol. 43, no. 3, pp. 539-547, 1992.
[103] ANSYS. (2019). *Semi-elliptical Crack. Defines a semi-elliptical crack based on an internally generated mesh to analyze crack fronts by use of geometric parameters.* Available: https://ansyshelp.ansys.com/account/secured?returnurl=/Views/Secured/corp/v191/wb_sim/ds_Crack_o_r.html
[104] I. Fracture Analysis Consultants, "FRANC3D ABAQUS tutorial Version 7.1," 2017, Available: http://www.fracanalysis.com/.
[105] A. J. Pachoud, P. Manso, and A. Schleiss, "Stress intensity factors for axial semi-elliptical surface cracks and embedded elliptical cracks at longitudinal butt welded joints of steel-lined pressure tunnels and shafts considering weld shape," *Engineering Fracture Mechanics,* vol. 179, pp. 93-119, 2017.
[106] *DNVGL-RP-F113. Pipeline subsea repair*, 2016.
[107] L. Djukic, W. Sum, K. Leong, and A. Gibson, "Clamp and overwrap repairs of oilfield pipelines," in *Rehabilitation of Pipelines Using Fiber-reinforced Polymer (FRP) Composites*: Elsevier, 2015, pp. 237-265.
[108] N. Saeed, H. Ronagh, and A. Virk, "Composite repair of pipelines, considering the effect of live pressure-analytical and numerical models with respect to ISO/TS 24817 and ASME PCC-2," *Composites Part B: Engineering,* vol. 58, pp. 605-610, 2014.
[109] *ASME PCC-2: Repair of Pressure Equipment and Piping*, 2015.
[110] A. A. Abd-Elhady, H. E.-D. M. Sallam, I. M. Alarifi, R. A. Malik, and T. M. El-Bagory, "Investigation of fatigue crack propagation in steel pipeline repaired by glass fiber reinforced polymer," *Composite Structures,* vol. 242, p. 112189, 2020.
[111] B. Zheng and M. Dawood, "Fatigue crack growth analysis of steel elements reinforced with shape memory alloy (SMA)/fiber reinforced polymer (FRP) composite patches," *Composite Structures,* vol. 164, pp. 158-169, 2017.
[112] M. Zeinoddini, J. Harding, and G. Parke, "Axially pre-loaded steel tubes subjected to lateral impacts (a numerical simulation)," *International journal of impact engineering,* vol. 35, no. 11, pp. 1267-1279, 2008.
[113] M. Zeinoddini, G. Parke, and J. Harding, "Axially pre-loaded steel tubes subjected to lateral impacts: an experimental study," *International Journal of Impact Engineering,* vol. 27, no. 6, pp. 669-690, 2002.
[114] J. Haedir, X.-L. Zhao, M. Bambach, and R. Grzebieta, "Analysis of CFRP externally-reinforced steel CHS tubular beams," *Composite Structures,* vol. 92, no. 12, pp. 2992-3001, 2010.
[115] J. Haedir, X.-L. Zhao, R. H. Grzebieta, and M. R. Bambach, "Non-linear analysis to predict the moment–curvature response of CFRP-strengthened steel CHS tubular beams," *Thin-walled structures,* vol. 49, no. 8, pp. 997-1006, 2011.
[116] J. Haedir and X.-L. Zhao, "Design of CFRP-strengthened steel CHS tubular beams," *Journal of Constructional Steel Research,* vol. 72, pp. 203-218, 2012.
[117] T. S. Mally, A. L. Johnston, M. Chann, R. H. Walker, and M. W. Keller, "Performance of a carbon-fiber/epoxy composite for the underwater repair of pressure equipment," *Composite Structures,* vol. 100, pp. 542-547, 2013.
[118] X. Gao, T. Balendra, and C. J. E. s. Koh, "Buckling strength of slender circular tubular steel braces strengthened by CFRP," vol. 46, pp. 547-556, 2013.
[119] M. H. Kabir, S. Fawzia, T. H. Chan, and M. Badawi, "Durability of CFRP strengthened steel circular hollow section member exposed to sea water," *Construction Building Materials,* vol. 118, pp. 216-225, 2016.

[120] M. H. Kabir, S. Fawzia, and T. H. Chan, "Durability of CFRP strengthened circular hollow steel members under cold weather: Experimental and numerical investigation," *Construction Building Materials,* vol. 123, pp. 372-383, 2016.
[121] C. Wu, L. He, E. Ghafoori, and X.-L. Zhao, "Torsional strengthening of steel circular hollow sections (CHS) using CFRP composites," *Engineering Structures,* vol. 171, pp. 806-816, 2018.
[122] T. Tafsirojjaman, S. Fawzia, D. Thambiratnam, and X.-L. Zhao, "Behaviour of CFRP strengthened CHS members under monotonic and cyclic loading," *Composite Structures,* vol. 220, pp. 592-601, 2019.
[123] M. H. Kabir, S. Fawzia, T. H. Chan, and K. Gamage, "Effects of cold weather on durability of CFRP strengthened circular hollow steel members," in *Proceedings of the 2013 Asia-Pacific Conference on FRP in Structures (APFIS 2013)*, 2013: Swinburne University of Technology.
[124] K. S. Woo, J. S. Ahn, and S. H. Yang, "Cylindrical discrete-layer model for analysis of circumferential cracked pipes with externally bonded composite materials," *Composite Structures,* vol. 143, pp. 317-323, 2016.
[125] H. Zarrinzadeh, M. Kabir, A. J. F. Deylami, F. o. E. Materials, and Structures, "Extended finite element fracture analysis of a cracked isotropic shell repaired by composite patch," vol. 39, no. 11, pp. 1352-1365, 2016.
[126] H. Zarrinzadeh, M. Kabir, and A. Deylami, "Crack growth and debonding analysis of an aluminum pipe repaired by composite patch under fatigue loading," *Thin-Walled Structures,* vol. 112, pp. 140-148, 2017.
[127] H. Zarrinzadeh, M. Kabir, and A. Deylami, "Experimental and numerical fatigue crack growth of an aluminium pipe repaired by composite patch," *Engineering Structures,* vol. 133, pp. 24-32, 2017.
[128] Z. Valadi, H. Bayesteh, and S. Mohammadi, "XFEM fracture analysis of cracked pipeline with and without FRP composite repairs," *Mechanics of Advanced Materials Structures,* pp. 1-12, 2018.
[129] B. Zheng and M. Dawood, "Debonding of carbon fiber–reinforced polymer patches from cracked steel elements under fatigue loading," *Journal of Composites for Construction,* vol. 20, no. 6, p. 04016038, 2016.
[130] C. Lam, J. Cheng, and C. Yam, "Finite element study of cracked steel circular tube repaired by FRP patching," *Procedia engineering,* vol. 14, pp. 1106-1113, 2011.
[131] M. A. Ghaffari and H. Hosseini-Toudeshky, "Fatigue crack propagation analysis of repaired pipes with composite patch under cyclic pressure," *Journal of Pressure Vessel Technology,* vol. 135, no. 3, p. 031402, 2013.
[132] J. Chen and H. Pan, "Stress intensity factor of semi-elliptical surface crack in a cylinder with hoop wrapped composite layer," *International Journal of Pressure Vessels and Piping,* vol. 110, pp. 77-81, 2013.
[133] F. Benyahia, A. Albedah, and B. Bachir Bouiadjra, "Stress intensity factor for repaired circumferential cracks in pipe with bonded composite wrap," *Journal of Pressure Vessel Technology,* vol. 136, no. 4, 2014.
[134] J. Liu, M. Qin, Q. Zhao, L. Chen, P. Liu, and J. Gao, "Fatigue performances of the cracked aluminum-alloy pipe repaired with a shaped CFRP patch," *Thin-Walled Structures,* vol. 111, pp. 155-164, 2017.
[135] D. E. Belhadri, M. Belhamiani, W. N. Bouzitouna, and W. Oudad, "Stress intensity factors analyses for external semi-elliptical crack for repaired gas-pipeline by composite overwrap under pressure," *Frattura ed Integrità Strutturale,* vol. 13, no. 49, pp. 599-613, 2019.

[136] L. Tong and X. Sun, "Nonlinear stress analysis for bonded patch to curved thin-walled structures," *International journal of adhesion adhesives,* vol. 23, no. 5, pp. 349-364, 2003.
[137] H. Okada, H. Kawai, T. Tokuda, and Y. Fukui, "Fully automated mixed mode crack propagation analyses based on tetrahedral finite element and VCCM (virtual crack closure-integral method)," *International Journal of Fatigue,* vol. 50, pp. 33-39, 2013.
[138] C. D. Wallbrink, D. Peng, and R. Jones, "Assessment of partly circumferential cracks in pipes," *International journal of fracture,* vol. 133, no. 2, pp. 167-181, 2005.
[139] A. Carpinteri, R. Brighenti, and A. Spagnoli, "Part-through cracks in pipes under cyclic bending," *Nuclear Engineering and Design,* vol. 185, no. 1, pp. 1-10, 1998.
[140] Y. Peng, C. Wu, Y. Zheng, and J. Dong, "Improved Formula for the Stress Intensity Factor of Semi-Elliptical Surface Cracks in Welded Joints under Bending Stress," *Materials,* vol. 10, no. 2, p. 166, 2017.
[141] J. Newman and I. Raju, "Stress-intensity factor equations for cracks in three-dimensional finite bodies subjected to tension and bending loads," *Computational methods in the mechanics of fracture,* vol. 2, pp. 311-334, 1986.
[142] Z. Li, X. Jiang, H. Hopman, L. Zhu, Z. Liu, and W. Tang, "Experimental investigation on FRP-reinforced surface cracked steel plates subjected to cyclic tension," *Mechanics of Advanced Materials Structures,* vol. 27, pp. 1-15, 2020.
[143] Z. Li, X. Jiang, H. Hopman, L. Zhu, and Z. Liu, "Numerical investigation on the surface crack growth in FRP-reinforced steel plates subjected to tension," *Theoretical and Applied Fracture Mechanics,* vol. 108, p. 102659, 2020.
[144] *GJB 6055-2007. Specification for 907A prefiled of military ship (in Chinese)*, 2007.
[145] *Test method for properties of resin casting boby (in Chinese)*, 2008.
[146] P. Colombi, A. Bassetti, and A. Nussbaumer, "Analysis of cracked steel members reinforced by pre‐stress composite patch," *Fatigue & Fracture of Engineering Materials & Structures,* vol. 26, no. 1, pp. 59-66, 2003.
[147] S. Xia and J. Teng, "Behaviour of FRP-to-steel bonded joints," presented at the Proceedings of the International Symposium on Bond Behaviour of FRP in Structures, Hong Kong, 7-9 December 2005, 2005.
[148] Q. Yu, X. Zhao, Z. Xiao, T. Chen, and X. Gu, "Evaluation of stress intensity factor for CFRP bonded steel plates," *Advances in Structural Engineering,* vol. 17, no. 12, pp. 1729-1746, 2014.
[149] H. Liu, R. Al-Mahaidi, and X.-L. Zhao, "Experimental study of fatigue crack growth behaviour in adhesively reinforced steel structures," *Composite Structures,* vol. 90, no. 1, pp. 12-20, 2009.
[150] H. Wang, G. Wu, and Y. Pang, "Theoretical and numerical study on stress intensity factors for FRP-strengthened steel plates with double-edged cracks," *Sensors,* vol. 18, no. 7, p. 2356, 2018.
[151] Z. Li, X. Jiang, and H. Hopman, "Numerical analysis on the SIF of internal surface cracks in steel pipes reinforced with CRS subjected to bending," *Ships and offshore structures,* vol. 14, p. 1, 2019.
[152] ANSYS, "Defines a semi-elliptical crack based on an internally generated mesh to analyze crack fronts by use of geometric parameters," 2018, vol. 2018 Available: https://ansyshelp.ansys.com/account/secured?returnurl=/Views/Secured/corp/v191/wb_sim/ds_Crack_o_r.html.
[153] Z. Li, X. Jiang, H. Hopman, L. Zhu, and Z. Liu, "External surface cracked offshore steel pipes reinforced with composite repair system subjected to cyclic bending: An experimental investigation," *Theoretical and Applied Fracture Mechanics,* vol. 109, p. 102703, 2020.

[154] ABAQUS. *SIMULIA Abaqus: Non-Linear Finite Element Analysis*. Available: https://www.simuleon.com/simulia-abaqus/

[155] Z. Li, X. Jiang, and H. Hopman, "Surface Crack Growth in Offshore Metallic Pipes under Cyclic Loads: A Literature Review," *Journal of Marine Science Engineering,* vol. 8, no. 5, p. 339, 2020.

[156] T. L. Anderson, *Fracture mechanics: fundamentals and applications*. CRC press, 2017.

[157] H. Khoramishad, A. Crocombe, K. Katnam, and I. Ashcroft, "Predicting fatigue damage in adhesively bonded joints using a cohesive zone model," *International Journal of fatigue,* vol. 32, no. 7, pp. 1146-1158, 2010.

[158] ASTM, *ASTM E2899. Standard Test Method for Measurement of Initiation Toughness in Surface Cracks Under Tension and Bending*. West Conshohocken, United States: ASTM, 2019.

[159] *Assessment of flaws in pipeline and riser girth welds*, 2017.

Summary

Metallic pipes play an irreplaceable role in the offshore industry, acting as the primary way of fluid transportation. They have been widely applied owing to the advantages of cost-effectiveness, simplicity, ease of installation and maintenance. However, metallic pipes are prone to fatigue problems. In marine environment, they bear dynamic loads long-termly. In such a situation, surface cracks frequently initiate from surface defects such as corrosion pitting, girth weld defects, or mechanical dents. Thereafter, they might continually propagate to through-thickness cracks, eventually resulting in leakage or collapse.

Surface cracks need to be repaired instantly to maintain the structural integrity of the pipeline systems towards their design service lives. The Composite Repair System (CRS) has been recognized as an efficient and advanced repairing technique in the piping industry. At present, composite repair on cracked metallic pipes conforms to standards based on either the rule of thumb or the strength-based approach, aiming to rehabilitate the load-bearing capacity of damaged steel pipes rather than decreasing the fatigue crack growth rate. The method of evaluating surface crack growth reinforced with CRS is absent from open documents. It has resulted in a lacking confidence situation, which seriously restricted the application and development of CRS.

This dissertation proposes a protocol of composite reinforcement on surface cracked metallic pipes subjected to cyclic loads, aiming to decrease the crack growth rate and prolong the residual fatigue life. The main objective of this dissertation is to reveal the mechanism of the composite reinforcement on surface crack growth in metallic pipes, in order to develop/improve the associated CRS standards. For this purpose, a series of investigations to determine the crack growth behaviour and possible failure modes have been conducted through numerical and experimental approaches. Finally, an analytical method is proposed to

evaluate the Stress Intensity Factor (SIF) of the surface crack in metallic pipes reinforced with CRS.

This research started with the literature reviews on two research topics—surface crack growth in metallic pipes and CRS reinforcement on metallic pipes, containing two main research questions: how would surface cracks grow in metallic pipes and what might be the effect of CRS on the surface crack growth? The literature survey concludes that a prediction method of evaluating the SIF of surface cracks is demanded as a basis before introducing the CRS reinforcement, and the bond behaviour of the composite-to-metallic interface is the hinge to identify the mechanism of composite reinforcement on surface cracked metallic pipes.

In Chapter 3, an analytical method to evaluate the SIF of circumferential surface cracks in metallic pipes is proposed, which is the basis of proposing an analytical method of evaluating the SIF of the CRS reinforced surface cracks. Considering the pipe geometry and bending load case, the analytical formula is raised by introducing new bending correction factors and new geometry correction factors. The bending correction factors are deduced based on the bending stress gradient, while the geometry correction factors are determined by parametric studies for internal surface cracks and external surface cracks, respectively. Owing to a large data set requirement by the parametric studies, three-dimensional finite element (FE) models of evaluating SIFs of circumferential surface cracks are developed. The FE method is validated to ensure that it could provide accurate SIF estimations. Analytical verification is conducted which shows that the SIF evaluated by the analytical method matched well with the results evaluated by the API 579-1/ASME FFS-1 recommended analytical method. Then experimental investigations of external surface crack growth in offshore steel pipe subjected to cyclic bending are implemented to further validate the analytical method of predicting surface crack growth rate. The analytical results matched well with the test results and the available experimental data from the literature, indicating that the analytical method can be used for practical purposes and facilitate the crack growth evaluation and residual fatigue life prediction of cracked steel pipes.

In Chapter 4, an investigation on composite reinforced surface crack growth is conducted on surface cracked plates, to eliminate potential influences from the pipe geometry and the bending load. In this chapter, surface crack growth behaviour and possible failure modes are studied by means of experimental and numerical approaches. The results indicated composite laminates are adequately bonded on the steel substrate during the surface cracking process, while interfacial stiffness degraded along with the crack growth. Besides, the investigations concluded the effect of composite reinforcement on surface crack growth owed to the decreasing of the stress distributed around the crack, and the crack-bridging effect. These findings pave a way for the further research on surface cracked pipes reinforced with CRS, in terms of experimental design, numerical modelling, and interfacial bonding analysis.

On the basis of previous studies on surface crack growth in metallic pipes in Chapter 3 and the composite reinforced surface crack plated in Chapter 4, the investigations of CRS reinforcement on internal and external surface cracked pipes subjected to cyclic loads are

conducted in Chapter 5 and Chapter 6, respectively. For both studies, numerical models are developed to evaluate the SIF of the CRS reinforced surface cracks. The FE model of the internal surface crack is validated by available experimental results, while the FE model of the external surface crack is validated by conducting an experimental study. Both studies conducted a parametric study based on each FE model to identify the key influential parameters and proposes the analytical method to evaluate the SIF. Particularly, the analytical method on the external surface cracked case has introduced the crack-bridging effect, as well as considering the interfacial stiffness degradation. The results of both studies indicated that the analytical methods can rationally predict the SIF, which can be used as both a prediction approach and a design tool for the CRS.

In summary, the main contribution of this dissertation lies in the quantification analysis of CRS reinforcement on the surface cracked metallic pipes. Within this research, expert knowledge is provided to guide the composite reinforcement application for the purpose of maintaining cracked pipes in practical applications. The methods of evaluating the SIF of the CRS reinforced surface cracked pipes, i.e., FE analysis and analytical method, contribute to relevant CRS standards such as ISO 24817 and ASME PCC-2. The analytical method of evaluating the SIF of surface cracks in metallic pipes subjected to bending or tension, contributes to relevant fatigue assessment standards such as BS 7910 and API 579-1/ASME FFS-1. Besides, the research methods of this dissertation could inspire investigations of composite utilization on other damaged metallic structures.

Samenvatting

Metalen pijpen zijn essentieel in de offshore industrie, als primair transportmiddel voor vloeistoffen. Ze worden algemeen toegepast wegens voordelen op het gebied van kosten, eenvoud in gebruik, installatie en onderhoud. Maar metalen pijpen zijn kwetsbaar voor vermoeiing. Ze zijn in een zeemilieu langdurig onderhevig aan dynamische belasting. Er ontstaan aan de buitenkant van de pijp dikwijls scheurtjes ten gevolge van defecten als corrosieputten, lasfouten of mechanische deuken. Scheurtjes aan de buitenkant kunnen uitgroeien tot scheuren door-en-door, en leiden tot lekkage of in elkaar klappen van de pijp.

Scheurtjes aan de buitenkant moeten direct worden gerepareerd om de structurele integriteit van de pijplijnsystemen te handhaven tot het eind van de ontwerplevensduur. CRS (Composite Repair System) wordt in de pijplijnindustrie beschouwd als een efficiente en geavanceerde reparatietechniek. Op dit moment voldoet reparatie met composieten aan normen die zijn gebaseerd op vuistregels of op treksterke, die meer bedoeld zijn om de belastbaarheid van beschadigde stalen pijpen te herstellen, dan om het groeien van de scheur tegen te gaan. Er is in de open literatuur geen methode beschikbaar voor het evalueren van de groei van een CRS-versterkte scheur. Als gevolg daarvan is er een gebrek aan vertrouwen ontstaan, die de toepassing en ontwikkeling van CRS beperkt.

In dit proefschrift wordt een protocol voorgesteld voor CRS-versterking van metalen pijpen met barsten aan de oppervlakte en die onderhevig zijn aan cyclische belasting. De versterking is bedoeld om de groei van de barst te vertragen en de residuele levensduur van de pijp te verlengen. Het hoofddoel van dit proefschrift is het mechanisme van de invloed van composietversterking op de groei van barsten aan de oppervlakte van metalen pijpen te onderzoeken en daarmee bij te dragen aan de ontwikkeling c.q. verbetering van normen voor CRS. Hiertoe is numeriek en experimenteel onderzoek gedaan om na te gaan hoe een scheur groeit en welke faaltoestanden er optreden. Er wordt een analytische methode voorgesteld

voor de evaluatie van de Stress Intensity Factor (SIF) van een barst aan de oppervlakte van CRS-versterkte metalen pijpen.

Aan het begin van dit onderzoek is een literatuurstudie gedaan naar twee aspecten: de groei van barsten aan de oppervlakte van metalen pijpen en CRS-versterking van metalen pijpen. Doel was na te gaan hoe barsten groeien en wat de invloed van CRS daar op is. Conclusie uit het literatuuronderzoek was dat er een methode nodig was voor de evaluatie van de Stress Intensity Factor van barsten aan de oppervlakte, voordat er werd begonnen aan CRS-versterking en dat de eigenschappen van de verbinding tussen composiet en metaal de sleutel zijn voor het karakteriseren van het mechanisme van CRS-versterking van gescheurde metalen pijpen.

In Hoofdstuk 3 wordt een analytische methode voorgesteld voor het evalueren van de Stress Intensity Factor van barsten aan de oppervlakte van metalen pijpen. Deze methode vormt de basis voor een analytische methode voor het evalueren van de SIF van CRS-versterkte barsten aan de oppervlakte. Rekening gehouden met de geometrie van de pijp en de buigbelasting, is een analytische uitdrukking ontwikkeld door het introduceren van nieuwe correctiefactoren voor de buiging en de geometrie. De correctiefactoren voor de buiging op grond van het verloop van de buigspanning. De correctiefactoren voor de geometrie zijn afgeleid uit parametrische studies van scheuren aan het binnenoppervlak en aan het buitenoppervlak. In verband met de grote hoeveelheid gegevens in de parametrische studies zijn er driedimensionale eindige elementen (E. Finite Element, FE) modellen ontwikkeld voor de evaluatie van SIF's van oppervlaktescheuren. De FE-modellen zijn gevalideerd om er voor te zorgen dat er accurate SIF-schattingen worden gemaakt. Er is een analytische verificatie uitgevoerd waaruit volgt dat de SIF die door de voorgestelde analytische methode wordt berekend goed overeenkomt met resultaten van de op dit moment gebruikte analytische methode. Vervolgens is experimenteel onderzoek uitgevoerd aan de groei van scheuren aan de oppervlakte van stalen pijpen voor gebruik offshore en onderhevig aan cyclische belasting. Doel was nadere validatie van de analytische methode voor het voorspellen van de groeisnelheid van oppervlaktescheuren. De analytische resultaten kwamen goed overeen met de testresultaten en met experimentele gegevens uit de literatuur. Dit geeft aan dat de analytische methode kan worden gebruikt voor praktische toepassingen en gebruikt kan worden voor de evaluatie van de groeisnelheid van de scheur en voor de voorspelling van de residuele vermoeiingslevensduur van metalen pijpen met scheuren.

In Hoofdstuk 4 wordt een onderzoek beschreven aan de groei van CRS-versterkte scheuren aan de oppervlakte van platen, zonder de mogelijke invloed van de geometrie van de pijp en de buigbelasting. In dit hoofdstuk zijn het groeigedrag en mogelijke faaltoestanden experimenteel en numeriek onderzocht. De resultaten geven aan dat het composiet tijdens het scheuren goed gehecht bleef aan het metaaloppervlak, terwijl de grensvlakstijfheid verminderde met het aangroeien van de scheur. Daarnaast is uit het onderzoek het effect vastgesteld dat composietversterking heeft op de scheurgroei door de vermindering van de spanning rond de scheur en door het scheuroverbruggend effect. Deze bevindingen maken de weg vrij voor verder onderzoek aan CRS-versterkte metalen pijpen met oppervlaktescheuren,

in termen van opzet van experimenten, numerieke modellering en analyse van de grensvlakverlijming.

Op basis van het voorafgaande onderzoek aan de groei van scheuren aan de oppervlakte van metalen pijpen in Hoofdstuk 3 en aan de composietversterkte gescheurde plaat in Hoofdstuk 4 is in de Hoofdstukken 5 en 6 onderzoek gedaan aan composietversterkte metalen pijpen met scheuren aan de binnenkant resp. aan de buitenkant. Voor beide onderzoeken zijn numerieke modellen ontwikkeld voor de evaluatie van de SIF van de CRS-versterkte scheuren. Het FE-model van de scheur aan de binnenkant is gevalideerd met beschikbare experimentele resultaten. Het FE-model van de scheur aan de buitenkant is gevalideerd door experimenteel onderzoek. In beide onderzoeken is met behulp van de FE-modellen een parametrisch onderzoek gedaan om de van invloed zijnde parameters te identificeren en wordt de analytische methode voorgesteld voor de SIF evaluatie. In het bijzonder worden in de analytische methode voor het geval met de scheur aan het buitenoppervlak het scheuroverbruggend effect geïntroduceerd en de invloed van de afname van de grensvlakstijfheid. De resultaten van de beide onderzoeken geven aan dat de analytische methoden een redelijke voorspelling kunnen geven van de SIF, hetgeen kan worden gebruikt als een voorspellend hulpmiddel en een ontwerptool voor CRS.

Samenvattend: De belangrijkste bijdrage van dit proefschrift is de kwantitatieve analyse van CRS-versterking van metalen pijpen met scheuren aan de oppervlakte. Dit onderzoek voorziet in expertkennis ten behoeve van het gebruik van composietversterking voor het onderhoud van metalen in praktische toepassingen. De methoden voor SIF-evaluatie van CRS-versterkte pijpen met scheuren aan de oppervlakte, d.w.z. FE-analyse en analytische methoden geven een bijdrage voor betreffende CRS-normen, zoals ISO 24817 en ASME PCC-2. De analytische methode voor SIF-evaluatie van scheuren aan de oppervlakte van metalen pijpen die onderhevig zijn aan buiging of spanning dragen bij aan normen voor de beoordeling van vermoeiing, zoals BS 7910 en API 579-1/ASME FFS-1. Daarnaast zouden de onderzoekmethoden in dit proefschrift ideeën kunnen geven voor onderzoek bij de toepassing van composieten op andere beschadigde metalen constructies.

Curriculum Vitae

Zongchen Li was born in March, 1990 in Rizhao, Shandong, China. He obtained the B.Sc. degree on Mechanical design, Manufacturing and Automation in 2013 and the M.Sc. degree on Mechanical Engineering in 2016, both from Wuhan University of Technology in Wuhan, China.

Starting from September 2016, Zongchen was sponsored by China Scholarship Council as a Ph.D. candidate at the Section of Transport Engineering and Logistics, Department of Maritime and Transport Technology, Delft University of Technology. In his Ph.D. project, Zongchen proposed a composite reinforcement protocol on surface cracked metallic pipes, aimed to decrease the crack growth rate under cyclic loads and prolong the residual fatigue life of damaged metallic pipes. His research interests include the design and manufacturing of composite structures, fracture mechanics, fatigue failures analysis, cohesive zone modelling.

Peer-reviewed publications

1. **Z. Li**, X. Jiang, J.J. Hopman, et al., 2020. External surface cracked offshore steel pipes reinforced with Composite Repair System subjected to cyclic bending: An experimental investigation. *Theoretical and Applied Fracture Mechanics,*109, p. 102703.

2. **Z. Li**, X. Jiang, J.J. Hopman, et al., 2020. Numerical investigation on the surface crack growth in FRP-reinforced steel plates subjected to tension. *Theoretical and Applied Fracture Mechanics,* 108, p.102659.

3. **Z. Li**, X. Jiang, J.J. Hopman., 2020. Surface Crack Growth in Offshore Metallic Pipes under Cyclic Loads: A Literature Review. *Journal of Marine Science and Engineering*, 8(5), p.339.

4. **Z. Li**, X. Jiang, J.J. Hopman, et al., 2020. Experimental investigation on FRP-reinforced

surface cracked steel plates subjected to cyclic tension. *Mechanics of Advanced Materials and Structures*, 27, pp.1-15.

5. **Z. Li**, X. Jiang, J.J. Hopman, et al., 2019. An investigation on the circumferential surface crack growth in steel pipes subjected to fatigue bending. *Theoretical and Applied Fracture Mechanics*, 105, p.102403.

6. **Z. Li**, X. Jiang & J.J. Hopman., 2019. Numerical analysis on the SIF of internal surface cracks in steel pipes reinforced with CRS subjected to bending. *Ships and Offshore Structures*, pp.1-14.

7. **Z. Li**, X. Jiang & J.J. Hopman., 2020. External surface cracked offshore steel pipes reinforced with CRS subjected to cyclic bending: A numerical investigation., submitted to a journal.

8. **Z. Li**, X. Jiang & J.J. Hopman., 2020. Composite Repair System on metallic circular hollow section structures: A literature review., submitted to a journal.

9. Z. Liu, C. Huang, **Z. Li*** & X. Jiang., 2020. An investigation on the fatigue performance of cracked steel plates repaired with FRP and a stop hole., submitted to a journal.

10. Z. Liu, K. Chen, **Z. Li** & X. Jiang., 2017. Crack monitoring method for an FRP-strengthened steel structure based on an antenna sensor. *Sensors*, 17(10), p.2394.

11. S. Zou, H. Xiao, F. Ye, **Z. Li**, et al., 2020. Numerical analysis of the effect of the scan strategy on the residual stress in the multi-laser selective laser melting. *Results in Physics*, 16, p.103005.

Conference proceedings

1. 'External surface crack growth in offshore steel pipes reinforced with CRS subjected to fatigue bending' in the *5th International Conference on Maritime Technology and Engineering* (MARTECH 2020), Nov 16-19, 2020, Lisbon, Portugal.

2. 'Numerical investigation on surface crack growth in steel plates repaired with Carbon Fibre-Reinforced Polymer' in the *38th International Conference on Ocean, Offshore and Arctic Engineering* (OMAE 2019), June 9-14, 2019, Glasgow, Scotland.

3. 'Internal surface crack growth in offshore rigid pipes reinforced with CFRP' in the *37th International Conference on Ocean, Offshore and Arctic Engineering* (OMAE 2018), June 17-22, 2018, Madrid, Spain.

4. 'Numerical investigation of external surface crack growth in rigid pipe reinforced with FRP' in the *32nd Asian-Pacific Technical Exchange and Advisory Meeting on Marine Structure* (TEAM 2018), Oct. 15-18, 2018, Wuhan, China.

5. 'The latest development of reinforcement techniques on tubular joints' in the *6th International Conference on Marine Structures* (MARSTRUCT 2017), May 8-10, 2017, Lisbon, Portugal.

TRAIL Thesis Series

The following list contains the most recent dissertations in the TRAIL Thesis Series. For a complete overview of more than 250 titles see the TRAIL website: www.rsTRAIL.nl.

The TRAIL Thesis Series is a series of the Netherlands TRAIL Research School on transport, infrastructure and logistics.

Li, Z., *Surface Crack Growth in Metallic Pipes Reinforced with Composite Repair System,* T2021/8, January 2021, TRAIL Thesis Series, the Netherlands

Gavriilidou, A., *Cyclists in Motion: From data collection to behavioural models,* T2021/7, February 2021, TRAIL Thesis Series, the Netherlands

Methorst, R., *Exploring the Pedestrians Realm: An overview of insights needed for developing a generative system approach to walkability,* T2021/6, February 2021, TRAIL Thesis Series, the Netherlands

Walker, F., *To Trust or Not to Trust? Assessment and calibration of driver trust in automated vehicles,* T2021/5, February 2021, TRAIL Thesis Series, the Netherlands

Schneider, F., *Spatial Activity-travel Patterns of Cyclists,* T2021/4, February 2021, TRAIL Thesis Series, the Netherlands

Madadi, B., *Design and Optimization of Road Networks for Automated Vehicles,* T2021/3, January 2021, TRAIL Thesis Series, the Netherlands

Krabbenborg, L.D.M., *Tradable Credits for Congestion Management: support/reject?,* T2021/2, January 2021, TRAIL Thesis Series, the Netherlands

Castelein, B., *Accommodating Cold Logistics Chains in Seaport Clusters: The development of the reefer container market and its implications for logistics and policy,* T2021/1, January 2021, TRAIL Thesis Series, the Netherlands

Polinder, G.J., *New Models and Applications for Railway Timetabling,* T2020/18, December 2020, TRAIL Thesis Series, the Netherlands

Scharpff, J.C.D., Collective Decision Making trough Self-regulation, T2020/17, November 2020, TRAIL Thesis Series, the Netherlands

Guo, W. *Optimization of Synchromodal Matching Platforms under Uncertainties,* T2020/16, November 2020, TRAIL Thesis Series, the Netherlands

Narayan, J., *Design and Analysis of On-Demand Mobility Systems,* T2020/15, October 2020, TRAIL Thesis Series, the Netherlands

Gong, X., *Using Social Media to Characterise Crowds in City Events for Crowd Management,* T2020/14, September 2020, TRAIL Thesis Series, the Netherlands

Rijal, A., *Managing External Temporal Constraints in Manual Warehouses,* T2020/13, September 2020, TRAIL Thesis Series, the Netherlands

Alonso González, M.J., *Demand for Urban Pooled On-Demand Services: Attitudes, preferences and usage,* T2020/12, July 2020, TRAIL Thesis Series, the Netherlands

Alwosheel, A.S.A., *Trustworthy and Explainable Artificial Neural Networks for choice Behaviour Analysis,* T2020/11, July 2020, TRAIL Thesis Series, the Netherlands

Zeng, Q., *A New Composite Indicator of Company Performance Measurement from Economic and Environmental Perspectives for Motor Vehicle Manufacturers,* T2020/10, May 2020, TRAIL Thesis Series, the Netherlands

Mirzaei, M., *Advanced Storage and Retrieval Policies in Automated Warehouses,* T2020/9, April 2020, TRAIL Thesis Series, the Netherlands

Nordhoff, S., *User Acceptance of Automated Vehicles in Public Transport,* T2020/8, April 2020, TRAIL Thesis Series, the Netherlands

Winter, M.K.E., *Providing Public Transport by Self-Driving Vehicles: User preferences, fleet operation, and parking management,* T2020/7, April 2020, TRAIL Thesis Series, the Netherlands

Mullakkal-Babu, F.A., *Modelling Safety Impacts of Automated Driving Systems in Multi-Lane Traffic,* T2020/6, March 2020, TRAIL Thesis Series, the Netherlands

Krishnakumari, P.K., *Multiscale Pattern Recognition of Transport Network Dynamics and its Applications: A bird's eye view on transport,* T2020/5, February 2020, TRAIL Thesis Series, the Netherlands

Wolbertus, *Evaluating Electric Vehicle Charging Infrastructure Policies,* T2020/4, February 2020, TRAIL Thesis Series, the Netherlands

Yap, M.D., *Measuring, Predicting and Controlling Disruption Impacts for Urban Public Transport,* T2020/3, February 2020, TRAIL Thesis Series, the Netherlands

Luo, D., *Data-driven Analysis and Modeling of Passenger Flows and Service Networks for Public Transport Systems,* T2020/2, February 2020, TRAIL Thesis Series, the Netherlands

Erp, P.B.C. van, *Relative Flow Data: New opportunities for traffic state estimation,* T2020/1, February 2020, TRAIL Thesis Series, the Netherlands

Zhu, Y., *Passenger-Oriented Timetable Rescheduling in Railway Disruption Management,* T2019/16, December 2019, TRAIL Thesis Series, the Netherlands

Chen, L., *Cooperative Multi-Vessel Systems for Waterborne Transport,* T2019/15, November 2019, TRAIL Thesis Series, the Netherlands

Kerkman, K.E., *Spatial Dependence in Travel Demand Models: Causes, implications, and solutions,* T2019/14, October 2019, TRAIL Thesis Series, the Netherlands